

The development and application of superhydrophilic–superhydrophobic
patterned polymer surfaces for high-density cell microarrays

Zur Erlangung des akademischen Grades eines

DOKTORS DER NATURWISSENSCHAFTEN

(Dr. rer. nat.)

Fakultät für Chemie und Biowissenschaften

Karlsruher Institut für Technologie (KIT) – Universitätsbereich

genehmigte

DISSERTATION

von

Erica Ann Boles

aus

Torrance, California, USA

Dekan: Prof. Dr. Peter Roesky

Referent: Prof. Dr. Martin Bastmeyer

Korreferent: Prof. Dr. Frank Breitling

Tag der mündlichen Prüfung: 24.10.2014

Declaration of independent work

I hereby declare that this thesis is based on my own work and was written independently by me unless stated otherwise. I have properly referenced and cited all text and figures that are not my own.



Erica Ann Boles

10.09.2014

Abstract

High-throughput cell screening of gene libraries can help determine unknown gene functions or elucidate the role of proteins in cellular processes, but performing large-scale screens usually require large quantities of expensive reagents. The miniaturized format of high-density cell microarrays provides a cost- and time-effective alternative for screening thousands of probes in parallel. In this work, the interesting and unique properties of superhydrophilic–superhydrophobic patterned surfaces were used to form high-density arrays of cells or liquids for cell screening applications. Cells seeded on the patterned surfaces preferentially adhered and grew in the superhydrophilic microspots, while the superhydrophobic barriers prevented cells from migrating between the spots. In addition, the superhydrophobic barriers confined droplets within each microspot, which precisely controlled the surface concentration of a printed solution since the spot size was independent of the droplet volume and liquid properties.

Liposomal reagents are often used in transfected cell microarrays, but their efficiency and toxicity can vary widely depending on the experimental conditions. We used one of the novel transfection reagents synthesized in our group to identify the major factors that affect reverse transfection on the superhydrophilic–superhydrophobic patterned surfaces, and a multi-variable screen was performed to improve the transfection efficiency while minimizing cytotoxicity. The surface chemistry of the superhydrophilic spot, the addition of gelatin and fibronectin to the mixture, and the ratio of pDNA to transfection reagent were found to be critical factors affecting transfection in HEK 293 cells. Ultimately, understanding the lipid structure–function relationship could allow for the rational design of transfection reagents tailored to specific cell types or nucleic acids.

The superhydrophilic–superhydrophobic micropatterned substrates were also used to create arrays of cells encapsulated in individual droplets or hydrogels in a few simple steps without the need for automated equipment. This opened up the possibility of screening chemicals or drugs printed on the patterned surfaces since the isolation of each microspot prevented mixing of the chemicals through the shared culture medium. When doxorubicin was pre-printed in the hydrophilic spots and HeLa cells were then cultured in individual hydrogels on these spots, a concentration-dependent decrease in cell viability occurred with increasing amounts of doxorubicin. This demonstrated that the drug was still active after being printed and dried on the patterned surface and that it could diffuse from the surface into the hydrogel to exert a biological effect.

Although the superhydrophobic barriers inhibited cell adhesion and migration for several days, this effect diminished with longer culture times as more proteins adsorbed on the surface and the cells became overly confluent. We improved the long-term anti-fouling performance of the surfaces by infusing the porous hydrophobic polymer with a hydrophobic liquid, which proved to be stable for at least 40 days when immersed in an aqueous solution and more efficient than a PEGylated surface, a benchmark for cell-repellent surfaces, at preventing cell adhesion.

Zusammenfassung

Hochdurchsatz-Zell-Screenings von Gen-Bibliotheken werden heutzutage eingesetzt, um die unbekannte Funktion der Gene zu erforschen oder die Rolle von Proteinen in zellulären Prozessen aufzuklären. Meist sind diese Tests kostenintensiv und benötigen eine große Menge an Analyt und Chemikalien. Diese Nachteile lassen sich durch miniaturisierte Hochdurchsatz-Zell-Screenings vermeiden, da diese tausende von Proben parallel analysieren und deutlich effizienter sind hinsichtlich der Zeit, als auch der Kosten.

In der vorliegenden Arbeit wurden eine neue Methode für Hochdurchsatz-Zell-Screenings entwickelt: basierend auf den einzigartigen Eigenschaften von superhydrophil–superhydrophob mikrostrukturierten Oberflächen konnten hochdichte Zell- oder Lipid-Arrays umgesetzt werden. Dabei adhärten und wuchsen die Zellen auf den superhydrophilen Spots des Arrays, die durch superhydrophobe Barrieren gegenüber dem nächsten Spot abgegrenzt wurden und somit eine Kreuzkontamination verhinderten. Zudem ließ sich über die superhydrophobe Barrieren die Größe der Kontaktfläche gedruckter Tropfen präzise einstellen und dadurch die Oberflächenkonzentration einer Lösung genau regeln.

Lipide werden häufig für die Transfektion von Zell-Mikroarrays eingesetzt, jedoch kann die Transfektionseffizienz und die Toxizität abhängig von der experimentellen Umgebung stark variieren. In der vorliegenden Arbeit wurde ein neues selbst-synthetisiertes Lipidreagenz genutzt, um die Machbarkeit der „reverse transfection“ unter Verwendung von superhydrophil–superhydrophob mikrostrukturierten Oberflächen zu demonstrieren. Dabei wurden HEK 293 Zellen mit Plasmide für Histon H2B-YFP als Reportergen transfektiert. Im Zuge der Arbeit konnten wichtige experimentelle Faktoren identifiziert werden, um die Transfektionseffizienz zu steigern, bei gleichzeitiger Verringerung der Zytotoxizität: dem Verhältnis von DNA und Transfektionsreagenz, also auch dem Anteil von Gelatine und Fibronectin, spielt die Oberflächenchemie der superhydrophilen Spots eine entscheidende Rolle für die Transfektionsrate. Ausgehend von der entwickelten Screening Methode kann ein tiefgreifendes Verständnis der Struktur-Funktion Relation erfolgen, das ein rationales Design von Transfektionsreagenzien ermöglicht, die auf den Zelltyp und der Art der Nukleinsäuren zugeschnitten ist.

Als Voraussetzung für ein Screening nach Wirkstoffen oder Chemikalien auf einer strukturierten Oberfläche, ist es wichtig, dass die Mikro-Spots einzeln vorliegen, um eine Kreuzkontamination durch schnell diffundierende Chemikalien zu verhindern. Die entwickelten superhydrophil–superhydrophob mikrostrukturierten Oberflächen konnten daher ebenfalls genutzt werden, um Arrays von Zellen in isolierten Tropfen oder Hydrogelen herzustellen. Über Verringerung der Lebensfähigkeit von HeLa Zellen in Hydrogel- Mikro-Spots mit vor-gedrucktem Doxorubicin, konnte gezeigt werden, dass Wirkstoffe nach dem Spotten auf die mikrostrukturierte Oberfläche und einer anschließendem Trocknungsschritt ihre Wirksamkeit erhalten und keine Kreuzkontamination auftreten.

Die Möglichkeit die Adhäsion und Migration der Zellen durch die superhydrophoben Barrieren zu verhindern, verringert sich mit der Zeit, da Proteine auf der Oberfläche adsorbieren und die Zellen konfluent werden. Um eine längere Kultivierung der Zellen zu ermöglichen, wurde daher in der vorliegenden Arbeit eine neue Methode entwickelt um Mikrostrukturen aus superhydrophobe Flüssigkeiten herzustellen, die über 40 Tage stabil blieben und die Zelladhäsion effektiv unterdrückten.

Acknowledgements

I am grateful to Prof. Dr. Martin Bastmeyer for his guidance as my Doktorvater and for being the Referent for my PhD thesis.

I would like to thank Prof. Dr. Frank Breitling for taking his time to be my Korreferent.

I am very thankful to Dr. Pavel Levkin for giving me the opportunity to work on many interesting projects, for always showing interest in my work, and for providing critical feedback through our discussions. I am also very appreciative of his encouragement to grow both academically and personally.

I would like to thank all of my group members, past and present, for their helpful suggestions, discussions about life, and providing a friendly place to work. I hope that we will keep in contact in the future.

I am grateful to Incella GmbH for providing me with ScreenFect[®]A transfection reagent, and especially to Karina Schwarz for our discussions about cell microarrays.

I would like to thank the screening center at the Institute of Toxicology and Genetics and especially Ravi Peravali for allowing me to use the screening microscopes.

I would like to thank Sebastian Schillo for providing his engineering expertise to the collaboration projects we started together and his continued efforts on the projects. I am also very grateful for his help with the German translation of my abstract.

I am grateful to the Helmholtz Association's Initiative and Networking Fund (Helmholtz University Young Investigator Group, Grant VH-NG-621) for the financial support.

I would like to thank the BioInterfaces International Graduate School for providing helpful academic resources and fostering an interdisciplinary work environment.

I am especially grateful to Steven Boles, my husband, best friend, and personal chef, for his constant words of encouragement and support and for bringing us to Karlsruhe in the first place. I am happy that we experienced this adventure together.

I am lucky to have a family that gives me continuous love and support and is always there to encourage me when I need it the most.

Table of Contents

Abstract.....	iii
Zusammenfassung	v
Acknowledgements.....	vii
Table of Contents.....	ix
List of Figures	xi
List of Tables.....	xiii
List of Abbreviations.....	xiv
1 Introduction.....	15
1.1 Fabrication and applications of superhydrophilic–superhydrophobic patterned substrates	18
1.1.1 Article.....	19
1.2 High-throughput cell screening.....	34
1.2.1 Reverse cell transfection microarrays	34
1.2.2 Screening cells in 3D hydrogels.....	39
1.3 Liposome-mediated transfection	41
1.4 Screening of lipid libraries	46
1.5 Objectives of this PhD work	55
2 Superhydrophobic–superhydrophilic micropatterning: towards genome-on-a-chip cell microarrays	57
2.1 Article.....	59
2.2 Supporting information	66
3 Superhydrophilic–superhydrophobic patterned surfaces as high-density cell microarrays: optimization of reverse transfection.....	75
3.1 Article.....	77
3.2 Supporting information	93
4 Surface patterning via thiol-yne click chemistry: an extremely fast and versatile approach to superhydrophilic–superhydrophobic micropatterns	99
4.1 Article.....	102
4.2 Supporting information	110
5 DropletMicroarray: facile formation of arrays of microdroplets and hydrogel micropads for cell screening applications	123
5.1 Article.....	125

5.2	Supporting information.....	139
6	Micropatterning hydrophobic liquid on a porous polymer surface for long-term selective cell-repellency.....	147
6.1	Article	149
6.2	Supporting information.....	159
7	Facile and multiple replication of superhydrophilic–superhydrophobic patterns using adhesive tape.....	169
7.1	Article	171
7.2	Supporting information.....	181
8	Discussion	187
8.1	Improving the method of fabrication for superhydrophilic–superhydrophobic patterned surfaces	187
8.2	Using hydrophobicity to pattern liquids and cells	190
8.3	Technical aspects of using the superhydrophilic–superhydrophobic patterned surfaces for high-density cell microarrays.....	194
8.3.1	Precise and accurate control of the volume printed.....	194
8.3.2	Controlling the relative humidity during printing.....	194
8.3.3	High density of spots without cross-contamination of liquids or cells..	196
8.3.4	Transparency of the polymer film	197
8.4	The influence of various parameters on reverse cell transfection	198
8.4.1	Drying time of the printed arrays.....	198
8.4.2	Cell incubation time.....	198
8.4.3	Cell seeding density	199
8.4.4	Surface chemistry of the superhydrophilic spot	199
8.4.5	Inclusion of gelatin and fibronectin in the mixture.....	200
8.4.6	Ratio of pDNA to transfection reagent	201
8.4.7	Dilution buffer used during lipoplex formation.....	202
8.4.8	Transfection efficiency	202
8.5	Culturing cells in arrays of microdroplets and hydrogels.....	205
8.6	Methods to easily and cheaply produce multiple patterned substrates.....	208
8.7	Outlook	209
	References	211
	Curriculum vitae.....	233

List of Figures

Figure 1.1 Examples of superhydrophilicity and superhydrophobicity found in nature	21
Figure 1.2 Advantages of superhydrophilic–superhydrophobic patterns	22
Figure 1.3. Using hydrophilic–hydrophobic patterns to shape liquids into more complex geometries	25
Figure 1.4 Cell adhesion on a micropatterned surface	27
Figure 1.5 Cells on superhydrophilic regions of silicon nanowire (SiNW) array patterns	29
Figure 1.6 Patterning and co-culturing of multiple cell types	30
Figure 1.7 Hydrogels on hydrophilic–superhydrophobic surfaces	32
Figure 1.8 Transfected cell microarray procedure	35
Figure 1.9 Cells on a transfected cell microarray	37
Figure 1.10 Modified cell seeding procedure on transfected cell microarrays	38
Figure 1.11 Platform for performing a toxicity screen in 3D	40
Figure 1.12 Liposome structures predicted by the packing parameter, P	42
Figure 1.13 Nanocarrier–cell interaction: entry pathways and cellular barriers	44
Figure 1.14 Cellular barriers to nucleocytoplasmic traffic of pDNA	45
Figure 1.15 Synthesis of lipidoids consisting of alkyl-acrylate, alkyl-acrylamide, and amino molecules	47
Figure 1.16 Combinatorial synthesis of lipidoids for DNA delivery	49
Figure 1.17 Combinatorial synthesis of lipidoids with unsaturated or saturated hydrophobic tails	50
Figure 1.18 Combinatorial synthesis of cationic thioether lipids via thiol-yne chemistry	53
Figure 1.19 Combinatorial synthesis of lipidoids via alkylation of amines	54
Figure 2.1 Schematic of cell microarrays	60
Figure 2.2 Schematic of superhydrophilic–superhydrophobic pattern fabrication	62
Figure 2.3 Images of microarrays	63
Figure 2.4 Cells cultured on microarrays	64
Figure 2.S1 SEM images of HEMA-EDMA surfaces	68
Figure 2.S2 XPS measurements of HEMA-EDMA surfaces	69
Figure 2.S3 Transparency of the array	70
Figure 2.S4 UV-Vis-NIR spectra	70
Figure 2.S5 Time-lapse images of cells cultured on a microarray	72
Figure 2.S6 Cells cultured on microarrays in a Cassie–Baxter vs. Wenzel state	73
Figure 3.1 Schematic of the reverse transfection procedure using patterned surfaces	78
Figure 3.2 Confinement of droplets printed on a patterned vs. glass surface	80
Figure 3.3 Minimal cross-contamination of transfection mixtures between neighboring microspots	83

Figure 3.4 Transfection efficiency and cell number on COOH-modified microspots.	85
Figure 3.S1 Droplets of increasing volume printed on a patterned surface	93
Figure 3.S2 Transfection efficiency and cell number on NH ₂ -modified microspots...	94
Figure 3.S3 Reverse transfection with Lipofectamine [®] 2000 on COOH-modified microspots	98
Figure 4.1 Alkyne surface modification via UV-induced thiol-yne click chemistry.	104
Figure 4.2 Fabrication of superhydrophilic–superhydrophobic patterns via thiol-yne photo-click reactions	107
Figure 4.3 ToF-SIMS results and chemical/cell patterning	109
Figure 4.S1 Schematic of alkyne surface fabrication.....	110
Figure 4.S2 SEM images and water contact angle measurements.....	111
Figure 4.S3 Kinetics of the esterification reaction.....	112
Figure 4.S4 Raman spectra of HEMA-EDMA and alkyne surfaces.....	113
Figure 4.S5 UV-Vis-NIR transmittance spectra of HEMA-EDMA surfaces	113
Figure 4.S6 Raman spectra of modified alkyne surfaces	114
Figure 4.S7 Raman spectra of cysteamine-modified surfaces	115
Figure 4.S8 Stability of the superhydrophobic surface	116
Figure 4.S9 Ethanol–water solution on a superhydrophobic patterned surface.....	117
Figure 4.S10 Inverse superhydrophobic–superhydrophilic patterns.....	117
Figure 4.S11 HeLa-GFP cells cultured for 48 h on a patterned surface.....	118
Figure 5.1 Formation of a DropletMicroarray using the rolling droplet method.....	127
Figure 5.2 Images of DropletMicroarrays with different geometries	128
Figure 5.3 Droplet volume quantification and reproducibility	130
Figure 5.4 Encapsulation of cells in arrays of microdroplets and hydrogel micropads	132
Figure 5.5 Doxorubicin cytotoxicity screen using hydrogel micropads	135
Figure 5.S1 Application of the DropletMicroarray for deposition of substances	141
Figure 5.S2 Dependence of the water droplet volume on the liquid surface tension.	143
Figure 5.S3 HT1080-eGFP cells encapsulated in hydrogel micropads	144
Figure 5.S4 Cells encapsulated in hydrogel micropads for 6 days	144
Figure 6.1 Formation of hydrophobic liquid patterns	151
Figure 6.2 Stability of hydrophobic liquid micropatterns	152
Figure 6.3 Cell-repellency of hydrophobic liquid micropatterns and surfaces	154
Figure 6.4 HEK 293 cells reversely transfected on hydrophobic liquid arrays	157
Figure 6.S1 Water contact angle measurements	160
Figure 6.S2 Different hydrophobic liquid pattern geometries cultured with cells.....	161
Figure 6.S3 Cells cultured on hydrophobic liquid surfaces or PEG SAM surfaces...	163
Figure 6.S4 Cell migration across hydrophobic liquid barriers and superhydrophobic Cassie–Baxter air barriers	165
Figure 6.S5 Cell viability on hydrophobic liquid barriers and superhydrophobic Cassie–Baxter air barriers.....	166

Figure 7.1 Schematic representation of the transfer of a hydrophilic–hydrophobic pattern in a polymer film onto adhesive tape.....	175
Figure 7.2 Photos of 12 consecutive copies of a patterned polymer film.....	176
Figure 7.3 SEM images and water contact angle measurements of copies of a polymer film.....	177
Figure 7.4 Using the copies of a patterned BMA-AMPS polymer film as substrates for reverse cell transfection	179
Figure 7.S1 SEM image of the cross section of a copied polymer film	181
Figure 7.S2 Photos of droplets on curved copies of a patterned surface	182
Figure 7.S3 Images of 12 copies of a patterned surface colored with dye	183
Figure 7.S4 Graph of the fluorescence intensity of 12 copies colored with dye	183
Figure 7.S5 Reverse cell transfection on a copy of a pattern	185
Figure 8.1 Wenzel and Cassie–Baxter states	188
Figure 8.2 Effect of irradiation time on photografting	188
Figure 8.3 Coffee-ring effect	195

List of Tables

Table 3.S1 Transfection efficiency and cell number on NH ₂ -modified microspots.....	95
Table 3.S2 Transfection efficiency and cell number on COOH-modified microspots	96
Table 5.S3 Dependence of the water droplet volume on the geometry and area of the superhydrophilic spot.....	142
Table 5.S4 Dependence of the water droplet volume on the size of the superhydrophilic spot for a given geometry	143
Table 7.S1 Average water contact angle values of 12 copies of a polymer film.....	184

List of Abbreviations

BMA	butyl methacrylate
DMPAP	2,2-dimethoxy-2-phenylacetophenone
ECM	extracellular matrix
EDMA	ethylene dimethacrylate
GFP	green fluorescent protein
H2B	histone H2B
HEMA	2-hydroxyethyl methacrylate
NaOAc	sodium acetate
pDNA	plasmid DNA
PEG	poly(ethylene glycol)
PFPMA	2,2,3,3,3-pentafluoropropyl methacrylate
WCA	water contact angle
YFP	yellow fluorescent protein

1 Introduction

Performing gene overexpression or silencing studies *in vitro* can help to elucidate the role of genes and their involvement in various biological pathways. High-throughput screening using microtiter plates has become a powerful platform for scaling up the number of genes or chemicals that can be tested in one experiment, but it is still relatively expensive to implement. Cell microarrays have become a valuable tool for high-throughput screening due to their miniaturized format and savings of precious cells, reagents, and consumables.

One application of cell microarrays is their use for reverse cell transfection studies where libraries of genes are printed and dried on a glass slide, and then cells are seeded and allowed to adhere on the whole slide. Clusters of transfected cells form within a background of untransfected cells. The live cell clusters can be visualized using high-content, real-time imaging to follow cellular events or fixed cells can be assayed by techniques such as fluorescence microscopy, immunofluorescence, *in situ* hybridization, chemiluminescence, or autoradiography. The miniaturized format of cell microarrays also allows for the saving of expensive assaying reagents in comparison with microtiter plates. An added advantage is that batches of arrays can be printed at once and then used to test different experimental conditions such as cell type, culture time, addition of chemicals to the culture medium, and downstream assays.

To minimize mixing of the different chemicals and cell clusters between each spot of interest, the spacing between the spots need to be large enough. However, depending on the composition of the printed mixture and diffusion rate of the chemical, neighboring spots can still exert an effect on each other by diffusion of chemicals through the shared culture medium. In addition, the spot size of the printed mixtures can vary depending on the properties of the liquid and the surface, making it difficult to control the concentration of each printed mixture and to compare the results. The cell microarray technique is usually limited to screening adherent cells in 2D, but cell screening platforms suitable for screening nonadherent cells as well as cells in 3D microenvironments would open up new possibilities for conducting cell studies and allow for the combined screening of chemical as well as physical stimuli.

As part of this PhD work, we aimed to develop a cell-screening chip that could address the above-mentioned issues such as confinement of liquids and cells in individual microspots and the ability to screen cells in a 2D as well as 3D format. We explored whether the unique properties of superhydrophilicity and superhydrophobicity patterned on a porous polymer surface could offer advantages over the conventional glass slides that are usually used for cell microarrays. Furthermore, we needed to

establish the reverse transfection protocol on the new surfaces to achieve good transfection efficiency while minimizing cell toxicity.

Most screening of cells in 3D microenvironments are performed by manually pipetting individual hydrogel drops or using a printing robot, but we worked towards developing a method that uses the large difference in wettability between the superhydrophilic and superhydrophobic regions to passively dispense high-density arrays of isolated droplets in one simple step. Culturing cell encapsulated in the separated droplets or hydrogels addresses the problem of cross-contamination of chemicals between the spots. One of the objectives was to develop a relatively simple method so that it could be easily implemented, unlike other methods for culturing cells in isolated droplets such as microfluidic devices which can be fairly sophisticated in terms of controlling the delivery of reagents or changing the culture medium but complicated due to the pumps, valves, and programming required to operate the devices.

Although viral vectors are known to be efficient for gene delivery, they can have problems of safety and toxicity due to immunogenicity and unspecific targeting. Other non-viral methods of gene delivery have been actively studied and developed, including cationic liposomal transfection reagents. For gene expression studies *in vitro*, liposome-mediated transfection is frequently used to deliver nucleic acids into cells. Although liposomes are generally considered safer than viral vectors, they are usually less efficient and the exact mechanism of liposome-mediated transfection is still not fully understood. While the ability of certain liposomes to deliver nucleic acids into cells before being degraded in cellular compartments is being carefully studied, concurrently combinatorial chemistry is being used to create libraries of lipids with systematic variations in the chemistry and structure of the lipid with the hope of identifying efficient transfection reagents and to discover any structure–function relationships. The results from these studies could help to logically design the future generation of transfection reagents.

Our group is also involved in the synthesis and screening of lipid libraries. For this part of the PhD work, the superhydrophilic–superhydrophobic patterned surfaces were used as cell microarrays for reverse transfection experiments with a model liposome from one of our novel lipid libraries. Although the structure and chemistry of the lipids themselves greatly affect the ability for gene delivery, the interaction of the lipoplexes and the cells with the underlying substrate also seems to be important, especially for substrate-mediated transfection. We aimed to identify factors that influence reverse transfection apart from the composition of the lipid itself, such as the surface chemistry of the substrate and supplementary components of the printed transfection mixture, which could have implications for future cell microarrays and gene

delivery techniques and be applied to continuing cell screening experiments to identify efficient and non-toxic transfection reagents.

Although there are many different methods to create protein- and cell-repellent surfaces, their effectiveness and stability depend on the contents of the surrounding medium and the interactions at the liquid–solid interface. As the functional groups on the surface degrade or when proteins accumulate on the surface, the surface loses its anti-fouling properties. Since controlling the adsorption of chemicals or cells on surfaces is important for applications such as cell microarrays, cell patterning, tissue engineering, and diagnostic devices, it is important to create anti-fouling surfaces that show long-term repellency and stability in various conditions. To achieve this, we developed and tested the cell-repellent properties of three different surfaces based on the concept of superhydrophobicity in the Cassie–Baxter state or slippery hydrophobic liquid-infused porous surfaces. The objective was to develop a reliable and versatile method to create substrates that demonstrated good stability for use as cell or droplet microarrays.

Although there are many different methods available for creating superhydrophilic–superhydrophobic patterned surfaces, the complete procedure must be repeated to fabricate the multiple substrates needed for each experiment and can consume a lot of materials and time. To our knowledge, there are no methods available for making multiple “copies” from one original substrate, so we aimed to develop a simple and cheap method to achieve this while retaining the morphological and chemical surface properties of the original substrate. We tested the method of applying and removing adhesive tape from the original patterned polymer film to transfer one thin layer of polymer at a time to the tape.

The remainder of this chapter provides a brief background on concepts related to the field of superhydrophilic–superhydrophobic patterned surfaces and cell screening methods, and includes current examples in this field of research. Lastly, the specific objectives of this PhD work are presented.

1.1 Fabrication and applications of superhydrophilic–superhydrophobic patterned substrates

In recent years, functionalized surfaces have shown promise as tools in biological studies. In this PhD work, superhydrophilic–superhydrophobic patterned surfaces were developed and applied for cell screening applications. Here, the basic concepts of hydrophilicity and hydrophobicity are introduced and examples of their diverse applications are given. This section was excerpted from a Progress Report that we originally published in *Advanced Materials* in January 2013 and is reproduced with permission from John Wiley and Sons (Ueda & Levkin, 2013a).

Emerging applications of superhydrophilic–superhydrophobic micropatterns

Erica Ueda¹ and Pavel A. Levkin^{1,2,*}

¹ Institute of Toxicology and Genetics, Karlsruhe Institute of Technology, Postfach 3640, 76021 Karlsruhe, Germany

² Department of Applied Physical Chemistry, Heidelberg University, Im Neuenheimer Feld 253, 69120 Heidelberg, Germany

Adv. Mater. **2013**, *25*, 1234–1247. DOI: 10.1002/adma.201204120

Author contributions:

Erica Ueda performed the literature search and wrote the manuscript.



Pavel A. Levkin contributed to the outline of the content and edited the manuscript.



1.1.1 Article

Abstract

Water on superhydrophilic surfaces spreads or is absorbed very quickly, and exhibits water contact angles close to zero. We encounter superhydrophilic materials in our daily life (e.g. paper, sponges, textiles) and they are also ubiquitous in nature (e.g. plant and tree leaves, *Nepenthes* pitcher plant). On the other hand, water on completely non-wettable, superhydrophobic surfaces forms spherical droplets and rolls off the surface easily. One of the most well known examples of a superhydrophobic surface is the lotus leaf. Creating novel superhydrophobic surfaces has led to exciting new properties such as complete water repellency, self-cleaning, separation of oil and water, and antibiofouling. However, combining these two extreme states of superhydrophilicity and superhydrophobicity on the same surface in precise two-dimensional micropatterns opens exciting new functionalities and possibilities in a wide variety of applications from cell, droplet, and hydrogel microarrays for screening to surface tension confined microchannels for separation and diagnostic devices. We briefly describe the methods for fabricating superhydrophilic–superhydrophobic patterns and highlight some of the newer and emerging applications of these patterned substrates that are currently being explored. We also give an outlook on current and future applications that would benefit from using such superhydrophilic–superhydrophobic micropatterns.

Introduction

Superhydrophilic surfaces are characterized as having high surface energies and both advancing and receding water contact angles (WCAs) close to 0° . Superhydrophobic surfaces are characterized as having low surface energies and WCAs greater than 150° . In addition, superhydrophobic surfaces possess low WCA hysteresis, meaning the difference between the advancing and receding WCAs is less than 10° , which is also reflected in a low tilt angle, i.e. a water droplet rolls off the surface when the surface is tilted no more than 10° . Surface roughness is defined as the ratio of the actual surface area to the projected surface area and is greater than 1 for rough surfaces. For hydrophilic surfaces, increasing the roughness of the surface will usually increase the apparent hydrophilicity of the surface, whereas increasing the roughness of a hydrophobic surface will usually increase the apparent hydrophobicity of the surface. Liquids on a rough hydrophobic surface can be in either a Wenzel or Cassie–Baxter state. In the Wenzel state, the liquid is in complete contact with the surface such that no air is trapped between the liquid and the rough surface (Wenzel, 1936). A droplet in the Wenzel state is pinned to the surface. In the Cassie–Baxter state, air is trapped between the liquid and the asperities of the rough surface such that the percent of solid that is in contact with liquid approaches zero (Cassie & Baxter, 1944). A droplet in the Cassie–Baxter state will bounce or roll off the surface.

Superhydrophilic and superhydrophobic surfaces are prevalent in nature and inspire biomimetic designs for controlling surface wettability. Several excellent reviews were dedicated to both superhydrophilic and superhydrophobic biomimetic surfaces (Hancock *et al.*, 2012b; Koch & Barthlott, 2009; Song *et al.*, 2009; Yan *et al.*, 2011; Yao *et al.*, 2011). Superhydrophilic surfaces found in nature are often porous, such as those in mosses (Fig. 1.1A). Many superhydrophobic plant surfaces possess roughness at multiple length scales due to the presence of hairs, epidermal cells, or 3D waxes. One of the most-well known examples of a natural superhydrophobic surface is the lotus leaf (Barthlott & Neinhuis, 1997). The superhydrophobicity of the lotus leaf is attributed to the hierarchical roughness of the randomly oriented, small, hydrophobic wax tubules on top of convex cell papillae (Fig. 1.1B). The Cassie–Baxter state is also useful for the underwater respiration of insects and leaves of wetland plants (Pedersen & Colmer, 2012).

There are many advantages that arise from the combination of the extreme difference in wettability between superhydrophilic and superhydrophobic patterned regions, as exemplified in Fig. 1.2: A) the geometry and positioning of liquid droplets can be easily controlled; B) micropatterns can be prefilled with aqueous solutions without the need for surfactants; C) superhydrophilic patterns can be used as surface tension confined microchannels; D) droplets can be positioned extremely close to each other on a surface; E) superhydrophobic regions in a Cassie–Baxter state can be used to create “air-grid” patterns to control bioadhesion; and F) the discontinuous dewetting effect arising from the extreme difference in WCAs between the superhydrophilic and superhydrophobic regions can be used to passively dispense aqueous solution into the superhydrophilic spots without wetting the superhydrophobic background.

An example of hydrophilic–hydrophobic patterns found in nature is the cups of lichens (Hamlett *et al.*, 2011). The cup-like bodies on a stalk, or podetium, of lichens possess three levels of structural hierarchy and are superhydrophobic, which limits the uptake of water. Water drops do not adhere to the podetia except for at a few hydrophilic spots found on the rim of the cups. Water droplets from mist or drizzle become pinned at these hydrophilic spots and are absorbed through the pores in the rim (Fig. 1.1C), or the droplets become too large and roll down the superhydrophobic sides. This allows lichens to uptake water, but also prevents the formation of water layers on the surface that could interfere with the discharge of lichen spores into the air, which is necessary for their reproduction.

Desert beetles are often used as an example of hydrophilic–hydrophobic patterns found in nature. They are able to collect water from fog due to the non-waxy hydrophilic peaks and waxy hydrophobic sides and troughs of the bumps on their backs (Fig. 1.1D–F) (Parker & Lawrence, 2001). Water nucleates on the hydrophilic peaks and the droplet grows to a critical size after which it rolls down the hydrophobic bumps.

Many groups have reported the patterning of superhydrophobic surfaces to mimic the beetle's ability to capture water from humid air (Dorrer & Ruhe, 2008b; Garrod *et al.*, 2007; Ishii *et al.*, 2009; Thickett *et al.*, 2011; Zhai *et al.*, 2006). These examples show that designs from nature can inspire new surface structures for real-world applications such as water collection, underwater gas transport, and drag reduction.

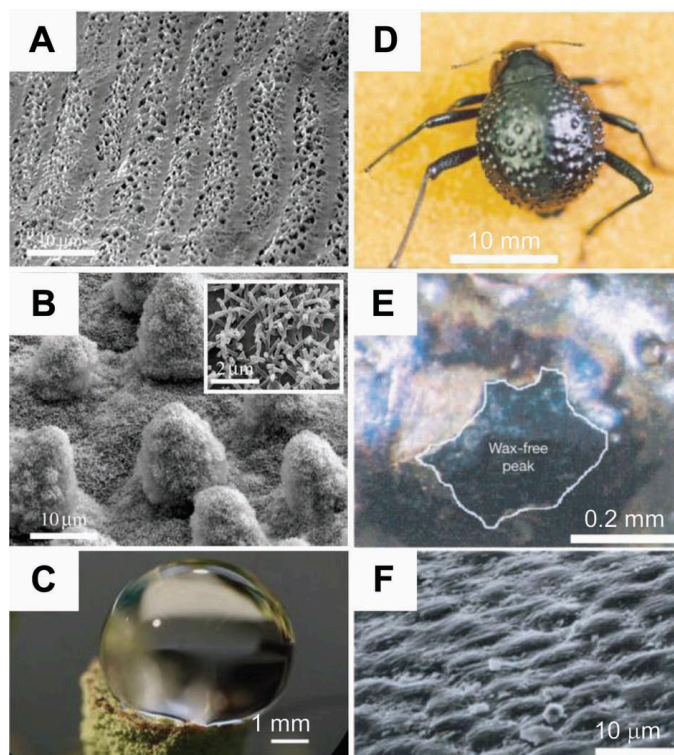


Figure 1.1 Examples of superhydrophilicity and superhydrophobicity found in nature

(A) The superhydrophilic porous cell structure of the epidermis of moss *Rhacocarpus purpurescens*. (B) The superhydrophobic hierarchical structures of the lotus leaf composed of convex (papillose) cells with superimposed nanostructure-forming wax crystals. Reproduced with permission (Koch & Barthlott, 2009). Copyright © 2009 The Royal Society. (C) A water droplet fastened by superhydrophilic microspots on the rim of the superhydrophobic cup-like structure of the *Cladonia chlorophaea* lichen. Reproduced with permission (Hamlett *et al.*, 2011). Copyright © 2011 Springer. (D) Superhydrophilic peaks and superhydrophobic troughs on the surface of an adult female beetle. (E) Depressed areas of the black beetle are stained waxy, whereas the peaks of the bumps are wax-free. (F) Scanning electron micrograph of the textured surface of the depressed areas. Reproduced with permission (Parker & Lawrence, 2001). Copyright © 2001 Nature Publishing Group.

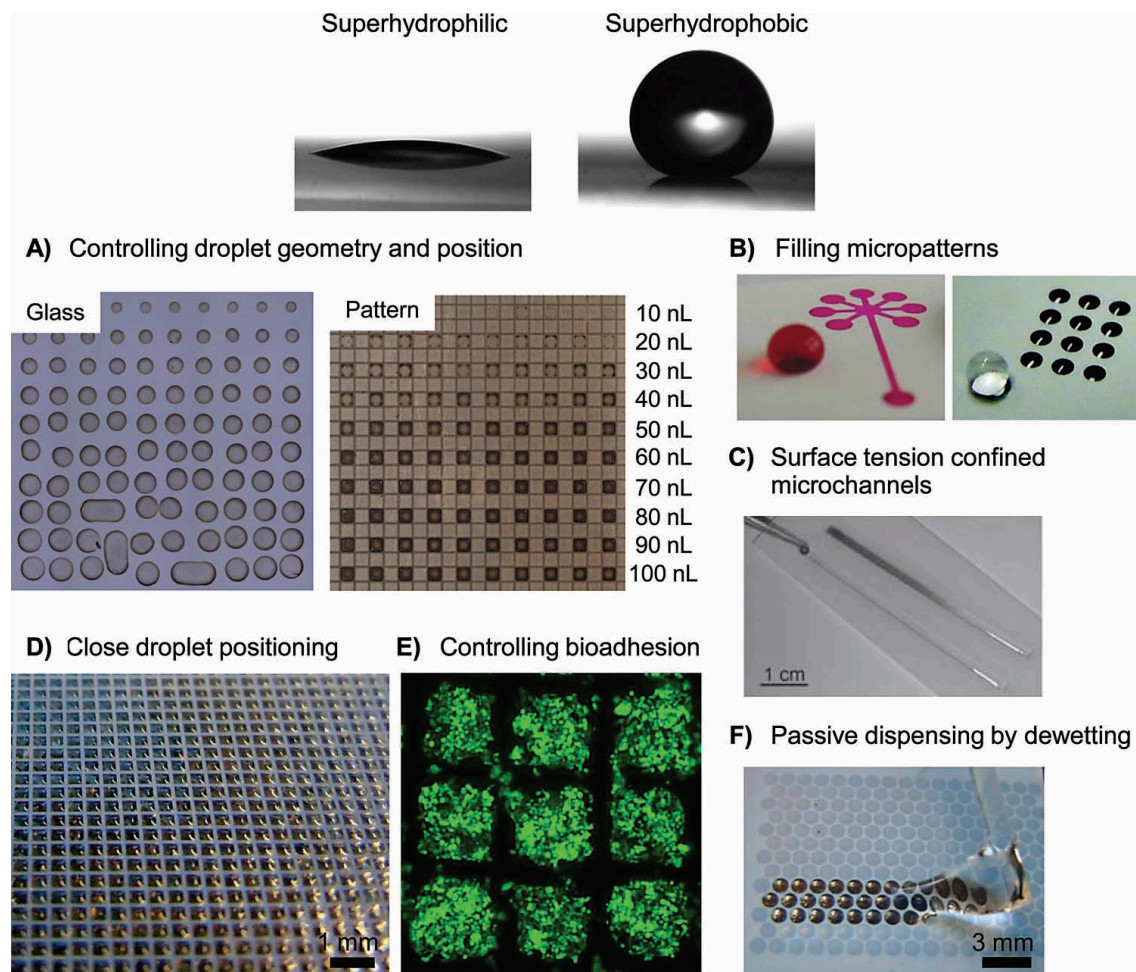


Figure 1.2 Advantages of superhydrophilic–superhydrophobic patterns.

Top: A water droplet being absorbed on a superhydrophilic surface, and a water droplet on a superhydrophobic polymer surface. Reproduced with permission (Geyer *et al.*, 2011). Copyright © 2011 John Wiley and Sons. (A) Pictures showing the inability to control the size and geometry of a dye solution when printed on glass, whereas the same solution printed on an array of 500 μm superhydrophilic squares separated by 62.5 μm superhydrophobic barriers is confined within the squares independent of the printed volume (unpublished results). (B) Left: Superhydrophilic pattern filled with aqueous dye solution. Reproduced with permission (Zahner *et al.*, 2011). Copyright © 2011 John Wiley and Sons. Right: Array of superhydrophilic spots filled with water and a water droplet on the superhydrophobic background. Reproduced with permission (Li *et al.*, 2012a). Copyright © 2012 American Chemical Society. (C) Fluid stripes on a hydrophobic coated slide, one with a dye gradient. Reproduced with permission (Hancock *et al.*, 2011a). Copyright © 2011 Wiley John Wiley and Sons. (D) DropletMicroarray formed by dipping the patterned substrate (335 μm superhydrophilic

squares, 60 μm superhydrophobic barriers) into water. Reproduced with permission (Ueda *et al.*, 2012). Copyright © 2012 Royal Society of Chemistry. (E) Fluorescent cells cultured on a patterned substrate (335 μm superhydrophilic squares, 60 μm superhydrophobic barriers) for 48 h. Reproduced with permission (Geyer *et al.*, 2011). Copyright © 2011 John Wiley and Sons. (F) Snapshot of water being moved along a patterned surface (1 mm diameter superhydrophilic circles, 100 μm superhydrophobic barriers) to form droplets only in the superhydrophilic spots by discontinuous dewetting. Reproduced with permission (Ueda *et al.*, 2012). Copyright © 2012 Royal Society of Chemistry.

We will focus on the advances in the formation and applications of superhydrophilic–superhydrophobic patterns within the last few years. Although there are many methods published for creating superhydrophilic (Dorrer & R  he, 2008a; Jokinen *et al.*, 2008; Lee *et al.*, 2012a), superhydrophobic (Cao *et al.*, 2009; Crick & Parkin, 2010; Dorrer & R  he, 2008a; Du *et al.*, 2013; Guo *et al.*, 2011; Jokinen *et al.*, 2008; Kato & Sato, 2012; Krumpfer & McCarthy, 2011; Lee *et al.*, 2012a; Papadopoulou *et al.*, 2011; Shahsavan *et al.*, 2012; Shirtcliffe *et al.*, 2011; Zhang & Seeger, 2011a), or superoleophobic (Kota *et al.*, 2012; Xue *et al.*, 2012; Zhang & Seeger, 2011b) surfaces for interesting applications such as anti-fogging, anti-fouling (Epstein *et al.*, 2012), self-cleaning (Ganesh *et al.*, 2011; Liu & Jiang, 2012) and water/oil separation (Zhang & Seeger, 2011a), here, we aim to discuss how the properties and functionalities of both superhydrophilicity and superhydrophobicity on the same substrate can be utilized. We also highlight emerging applications for such patterned substrates in the areas of patterning of liquids, biomolecules, and cells, miniaturized separation and diagnostics, cell and chemical microarrays, 3D microenvironment screening, digital microfluidics, and chemical synthesis in droplets. As one can see, superhydrophilic–superhydrophobic surfaces have a wide variety of applications.

Applications of superhydrophilic–superhydrophobic patterns

We present some of the emerging applications that take advantage of the combination of both wetting properties of superhydrophilic and superhydrophobic surfaces. In general, superhydrophilic–superhydrophobic patterned surfaces are used to control wetting and non-wetting regions or bioadhesive and non-bioadhesive regions. Some of the examples we present use hydrophilic or hydrophobic patterns, but we comment on how they may benefit from the extreme wetting or non-wetting properties of superhydrophilicity or superhydrophobicity, respectively.

Patterning complex geometries with liquids

Superhydrophilic–superhydrophobic patterns (or hydrophilic–hydrophobic patterns) provide a unique opportunity to precisely control the geometry and shape of liquids. For example, Hancock *et al.* used a simple method to passively generate gradients of molecules or particles (Hancock *et al.*, 2011a). Hydrophobic boundaries created simply by applying a tape mask and a hydrophobic spray on a glass slide and then dried for two days allowed fabrication of open hydrophilic regions bounded by a hydrophobic background. When a solution was pipetted in the hydrophilic stripe, the difference in curvature pressure drove the flow and created a concentration gradient by convection as the hydrophobic boundaries contained the flow in the hydrophilic stripe. In addition, Hancock *et al.* used the same hydrophilic–hydrophobic patterns to create gradients of soluble factors, cells, and microspheres in 3D hydrogels by photocrosslinking prepolymeric solutions in the hydrophilic stripes (Hancock *et al.*, 2011b). Layers of multi-gradient hydrogels were also formed (Piraino *et al.*, 2012). Liu *et al.* also used complex, geometric hydrophilic-hydrophobic patterns to create 3D hydrogels, which were subsequently used as molds to form PDMS channels (Liu *et al.*, 2009).

Hancock *et al.* further used these hydrophilic–hydrophobic patterns to shape liquids into more complex geometries, at both the macro- and microscale, to control the deposition of microparticles and cells or to create shaped hydrogels (Fig. 1.3) (Hancock *et al.*, 2012a). By using finite element simulations to predict the liquid shapes, they could pre-design the hydrophilic–hydrophobic patterns based on the desired particle deposition or gradient formation. Addition of surfactant was needed to lower the surface tension of the liquid in order for it to completely fill the complex pattern geometries at the microscale. This could be improved by using a superhydrophilic surface that rapidly and uniformly spreads the solution, eliminating the need for surfactant. Also, increasing the hydrophobicity and using a surface with low WCA hysteresis as the background could eliminate the leftover droplets after liquid patterning.

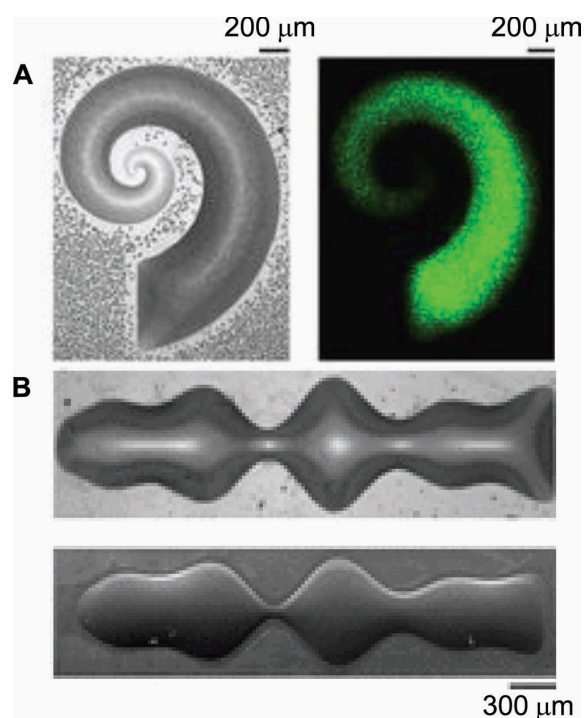


Figure 1.3. Using hydrophilic–hydrophobic patterns to shape liquids into more complex geometries

(A) Patterning of 1 μm microspheres on substrates under spiral microdroplets. (B) Double sine wave microdroplet before crosslinking (top) and microgel after crosslinking (bottom). Reproduced with permission (Hancock *et al.*, 2012a). Copyright © 2012 Wiley John Wiley and Sons.

Using pre-patterned superhydrophilic microchannels for separation of peptides

Han *et al.* used a superhydrophilic channel photopatterned in a superhydrophobic porous polymer layer to separate peptides of different hydrophobicity and isoelectric point by two-dimensional thin layer chromatography (2D TLC) (Han *et al.*, 2010). Photografting using a mixture of 2-acrylamido-2-methyl-1-propanesulfonic acid and 2-hydroxyethyl methacrylate through a photomask created a 600 μm -wide superhydrophilic channel in the 50 μm -thin superhydrophobic poly(butyl methacrylate-*co*-ethylene dimethacrylate) layer. The first separation was performed inside the virtual microchannel in ion exchange mode using an aqueous mobile phase, which moved only within the hydrophilic channel due to the large difference in surface tension and confinement by the superhydrophobic background. The second separation was performed according to the hydrophobicity of the peptides through the superhydrophobic region in the orthogonal second dimension using a mobile phase based on acetonitrile, which could move orthogonally to the hydrophilic channel

through the superhydrophobic porous layer due to the much lower surface tension of the organic mobile phase. The detection was performed by desorption electrospray ionization (DESI) mass spectroscopy directly from the polymer surface, which was possible because of the open nature of the system. This example shows the potential of open surface microfluidic systems based on superhydrophilic–superhydrophobic patterns to be paired with a variety of detector systems in the field of miniaturized separation and diagnostic applications.

Controlling adhesion of proteins, cells, or bacteria

Surface modifications to control bioadhesion have been well studied (Hook *et al.*, 2009a; Yuan *et al.*, 2011) and one of the most established methods is to passivate the surface using polyethylene glycol (PEG) or other derivatives (Hook *et al.*, 2009b; Na *et al.*, 2006; Yamaguchi *et al.*, 2012). Other hydrophilic polymer brushes were also shown to be very effective against fouling from biological fluids (Rodriguez-Emmenegger *et al.*, 2012). Ishizaki *et al.* demonstrated that the design of superhydrophilic–superhydrophobic patterns can influence cell adhesion and morphology, and ECM production (Ishizaki *et al.*, 2010). Superhydrophobic films were deposited on glass plates or Si wafers by microwave plasma enhanced chemical vapor deposition of a trimethylmethoxysilane and Ar gas mixture. Then, deep UV light with a wavelength of 172 nm was irradiated on the substrate for 30 min through a photomask to create superhydrophilic regions. The process resulted in an irregular surface topography composed of granular particles and nanoscale pores on the order of a few hundred nanometers in diameter, which contributed to the superhydrophobicity. The static, advancing, and receding WCAs of the superhydrophobic surface were 155°, 157°, and 153°, respectively. The static WCA of the superhydrophilic surface was 0°.

Furthermore, Ishizaki *et al.* showed that the cells could immediately adhere to the superhydrophilic surfaces in a highly selective manner after seeding, whereas the cells needed 24–72 h after seeding to adhere to the superhydrophobic surfaces (Fig. 1.4A,B). This difference in cell attachment was attributed to the difference in protein absorption between the superhydrophilic and superhydrophobic surfaces. More time was needed for the cells to produce their own extracellular matrix (ECM) and form a protein layer suitable for cell attachment on superhydrophobic surfaces. It was also demonstrated that cells were able to spontaneously migrate and recognize the superhydrophilic regions after being seeded, and coalesced there and grew to confluence after 24 h. Maintenance of the cell pattern depended on the distance between the superhydrophilic spots. At short inter-spot distances of 150 μm , cells in the superhydrophilic spots became confluent and began to make contact with cells in neighboring spots. However, with larger inter-spot distances of 400 μm , no physical cell-cell communication occurred between cells in neighboring spots (Fig. 1.4C–E).

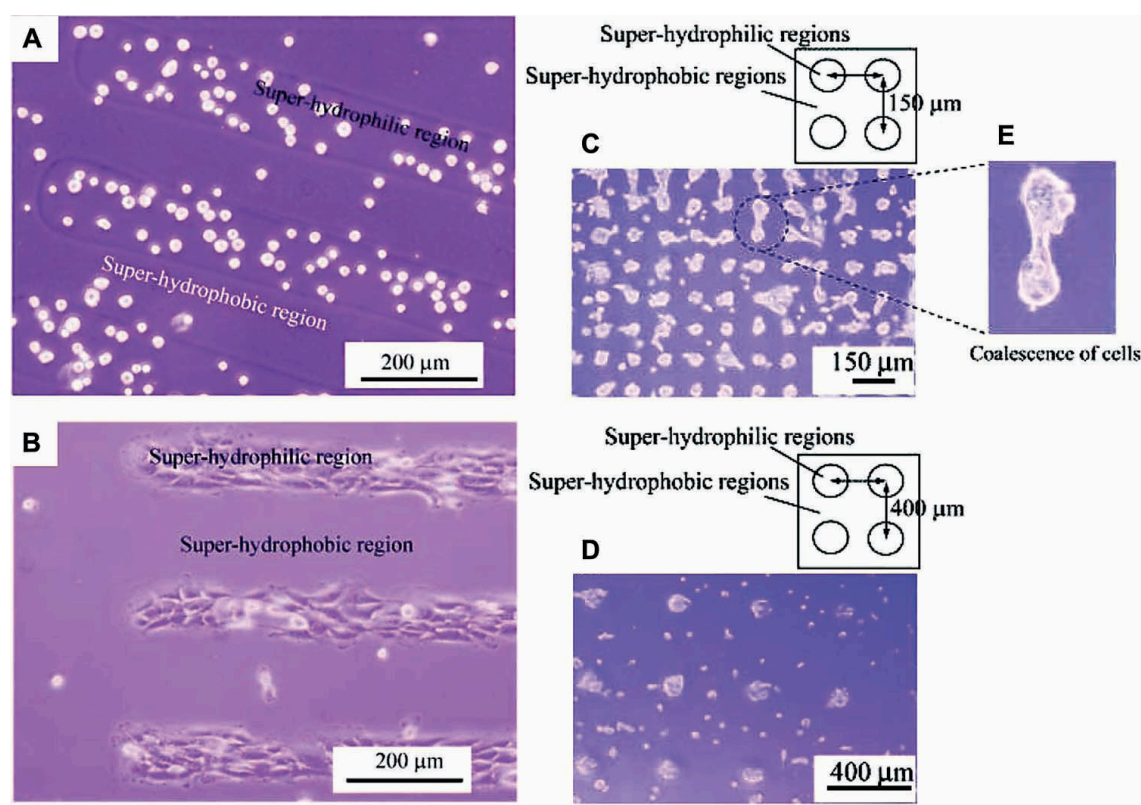


Figure 1.4 Cell adhesion on a micropatterned surface

Phase-contrast images of cell adhesion behavior on a micropatterned surface after culturing for (A) 1 h and (B) 24 h. Phase-contrast images of cells adhering on surfaces micropatterned with superhydrophilic circles spaced (C) 150 μm or (D) 400 μm apart. (E) Enlarged phase-contrast image of cells adhering on the superhydrophilic regions. Reproduced with permission (Ishizaki *et al.*, 2010). Copyright © 2010 American Chemical Society.

Oliveira *et al.* studied differential cell adhesion and proliferation on superhydrophobic and superhydrophilic polystyrene (PS) surfaces created by phase separation and UV/Ozone (UVO) irradiation, respectively (Oliveira *et al.*, 2011). Ethanol was added to a PS/tetrahydrofuran (THF) solution and a few drops of this mixture were applied to smooth PS surfaces of 0.25 mm thickness for 5 s, after which the excess mixture was removed and the substrate immersed in ethanol. The substrates were dried at room temperature, and the resulting random nano- and microstructures created an average surface roughness of 13 μm and transformed the surface to superhydrophobic (static WCA of 151°). To create superhydrophilic–superhydrophobic patterned surfaces, the rough superhydrophobic PS surfaces were modified by UVO irradiation through a hollowed mask for 18 min to create superhydrophilic regions with a static WCA of 0°. In comparison to tissue culture PS (TCPS), SaOs-2 (human primary

osteosarcoma) and ATDC5 (mouse chondrocyte teratocarcinoma-derived) cells did not significantly attach or proliferate on either smooth hydrophobic or rough superhydrophobic PS surfaces, whereas L929 (mouse lung fibroblast) cells reached confluence on both surfaces after 6 days. This was explained by the fact that L929 cells and fibroblasts in general have higher proliferation rates and L929 cells can proliferate even in unfavorable culture conditions compared to other cell types. SaOs-2 cells adhered more to hydrophilic and superhydrophilic surfaces versus hydrophobic or superhydrophobic surfaces after 24 h and even after 6 days. Although, in general, highly wettable surfaces are known to inhibit protein adsorption, surfaces with chemical groups rich in oxygen, such as carboxyl groups, can bind cells directly and support high cell adhesion as was reported in the paper. Higher initial cell adhesion on the rough superhydrophilic versus smooth hydrophilic surface was attributed to the increase in surface area due to the roughness, thus allowing more cell–surface contact.

Oliveira *et al.* also made superhydrophilic–superhydrophobic patterns by UVO irradiation of superhydrophobic surfaces through a hollowed mask to create $1 \times 1 \text{ mm}^2$ superhydrophilic regions (Oliveira *et al.*, 2011). When the patterned substrates were immersed and cultured in a suspension of SaOs-2 cells for 6 days, the superhydrophilic regions were densely populated with cells while only a few cells occupied the superhydrophobic regions. In another experiment where drops of cell suspension were deposited and cultured only in the superhydrophilic regions, the cells remained adhered only in the superhydrophilic regions for at least 2 days.

Piret *et al.* showed selective cell adhesion to superhydrophilic rather than superhydrophobic patterned areas of silicon nanowire (SiNW) arrays (Piret *et al.*, 2011). Vertically aligned SiNW arrays were prepared by chemically etching silicon wafers in a silver nitrate/hydrofluoric acid aqueous solution, followed by removal of deposited silver to produce superhydrophilic surfaces with static WCAs $< 5^\circ$. Chemical modification with an octadecyltrichlorosilane (OTS) hexane solution for 16 h created a superhydrophobic SiNW surface with a static WCA of 160° and low hysteresis ($0\text{--}2^\circ$). Micropatterned superhydrophilic–superhydrophobic SiNW surfaces were then fabricated using standard optical lithography techniques to form $50 \times 50 \text{ }\mu\text{m}^2$ superhydrophilic squares separated by $20 \text{ }\mu\text{m}$ superhydrophobic barriers. Chinese Hamster Ovary K1 (CHO-K1) cells expressing eGFP were cultured on superhydrophilic–superhydrophobic patterned SiNW arrays for 24 and 48 h (Fig. 1.5A). The cells seemed to selectively adhere to the superhydrophilic regions and remain within the squares, while a very low density of cells was observed on the superhydrophobic regions. Cell projections were clearly shown to intimately contact and coat the superhydrophilic SiNW regions and suggested strong cell adhesion, whereas the superhydrophobic SiNW regions seemed to exhibit a Cassie–Baxter state and the presence of air pockets trapped within the asperities of the SiNW substrate prevented cell–surface interaction.

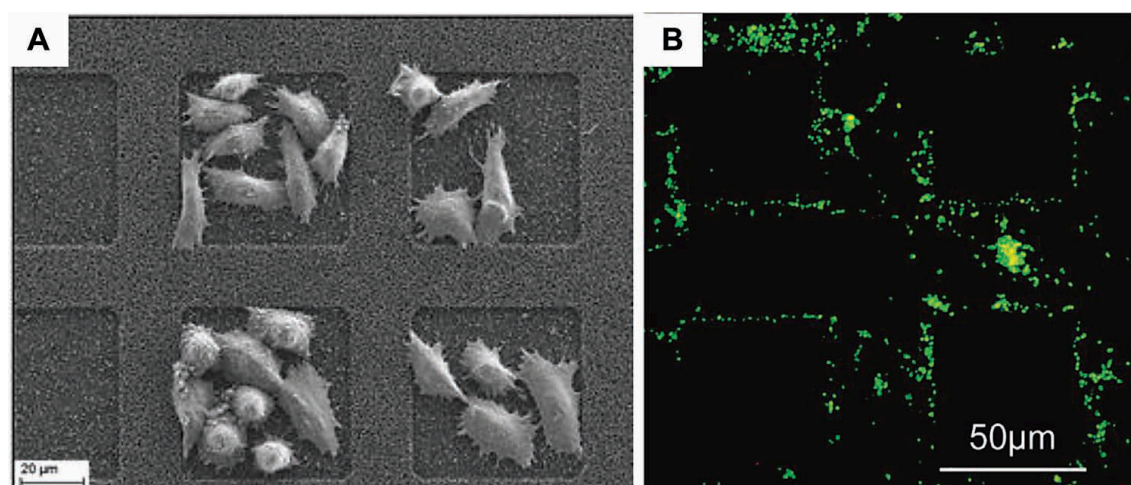


Figure 1.5 Cells on superhydrophilic regions of silicon nanowire (SiNW) array patterns

(A) SEM images of CHO-K1 cells trapped within the superhydrophilic regions of silicon nanowire (SiNW) array patterns. Reproduced with permission (Piret *et al.*, 2011). Copyright © 2011 Royal Society of Chemistry. (B) Fluorescent images of superhydrophobic patterned SiNW arrays after incubation in a *B. cereus* spore solution. Reproduced with permission (Galopin *et al.*, 2010). Copyright 2010 © American Chemical Society.

Similarly, Galopin *et al.* showed selective adhesion of *Bacillus cereus* (*B. cereus*) spores on patterned SiNW surfaces consisting of $50 \times 50 \mu\text{m}^2$ superhydrophilic squares separated by $25 \mu\text{m}$ superhydrophobic barriers (Galopin *et al.*, 2010). Substrates were immersed in an aqueous *B. cereus* spore solution for 30 min at room temperature, and then rinsed several times by vertical dipping in Milli-Q water. However, in this case, repulsive forces between the superhydrophilic SiNWs and the hydrophobic spores and the shear forces from the subsequent vertical rinsing steps were enough to almost completely remove spores from the superhydrophilic regions and drag them to the superhydrophobic regions where they immediately adhered (Fig. 1.5B). Spore adhesion was attributed to the significant attraction between the apolar chains of the spores and the alkyl groups of the OTS-terminated (super)hydrophobic regions. Even high shear stresses caused by vortexing in Milli-Q water for 1 min were not strong enough to remove adherent spores, suggesting that they were strongly attached to the (super)hydrophobic surfaces.

Efremov *et al.* introduced a convenient method for creating patterns of multiple cell types on a hydrophilic–superhydrophobic porous polymer substrate (Efremov *et al.*, 2012). Cell positioning on the substrate was realized by parallel formation of multiple

cell-containing microreservoirs confined to the geometry of highly hydrophilic regions surrounded by superhydrophobic borders formed in a nanoporous polymer film (Fig. 1.6). As a case study, the patterns were used to monitor and analyze the cross-talk between two cell populations via Wnt signaling molecules. This work exemplifies how superhydrophilic–superhydrophobic patterns can facilitate cell patterning or tissue engineering as well as studies of cell–cell signaling processes *in vitro*.

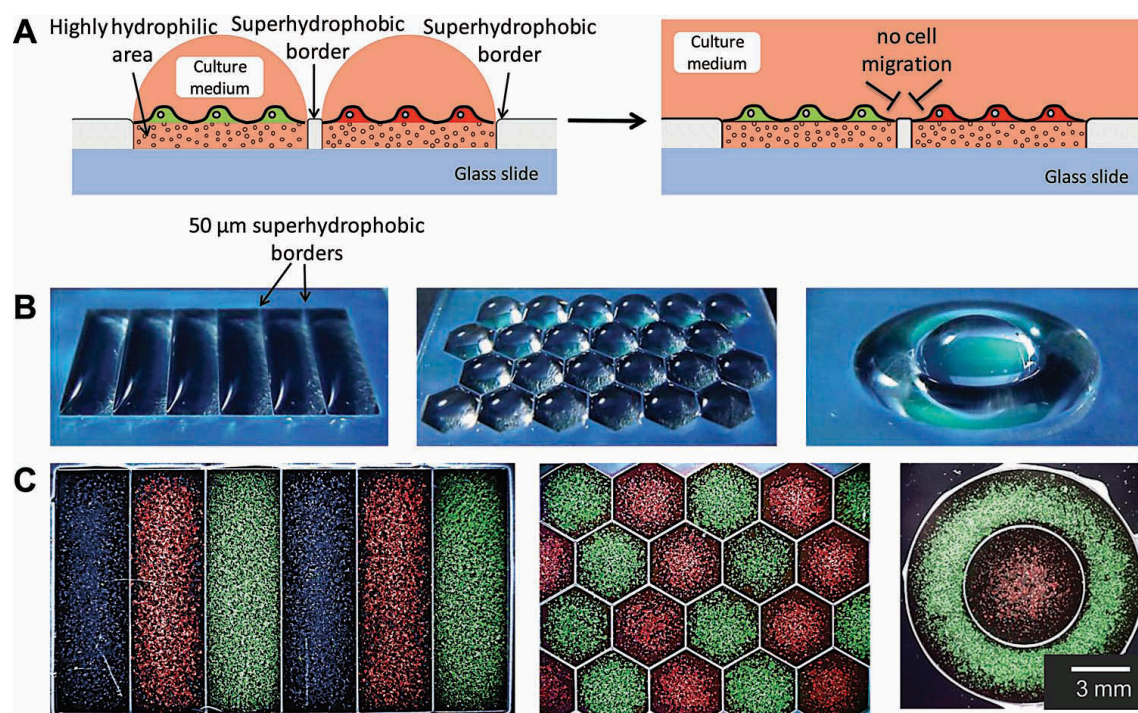


Figure 1.6 Patterning and co-culturing of multiple cell types

(A) Schematic of co-cultures of multiple cell types formed on superhydrophilic–superhydrophobic patterned polymer substrates. (B) Hydrophilic–superhydrophobic patterns filled with water to form droplets of different geometries. (C) Combined brightfield and fluorescent micrographs of different cells patterned in different geometries and in close proximity. Reproduced with permission (Efremov *et al.*, 2012). Copyright © 2012 Elsevier.

Cell encapsulation in droplet and hydrogel arrays

Although reverse cell transfection microarrays, which were first developed by the group of Sabatini (Ziauddin & Sabatini, 2001), allow a highly parallelized and miniaturized method of screening thousands of substances rapidly, it is limited to culturing one cell type in shared medium conditions and is not compatible with nonadherent cell types or screening in 3D microenvironments. To address these limitations, progress in this field

has led to creating arrays of droplets or hydrogel micropads using superhydrophilic–superhydrophobic patterns, which allow different substances or cell types to be isolated in each individual spot on the same substrate. Unlike microfluidic platforms where samples can be wasted in channels and regions of dead volumes, these new methods allow for the direct dispensing of substances and cells, which may be scarce, onto each spot followed by the appropriate bioassays (Lee *et al.*, 2012b).

Neto *et al.* deposited droplets of cell suspension on a hydrophilic–superhydrophobic patterned substrate and cultured cells in the isolated droplets (Neto *et al.*, 2011). Superhydrophobic polystyrene (PS) surfaces with nano- and microscale roughness were created using a phase-separation method and a static WCA of 156° was measured. The wettability of the rough surfaces was controlled from superhydrophobic to superhydrophilic using UVO irradiation. Liquids were well confined within the $1 \times 1 \text{ mm}^2$ (super)hydrophilic spots due to the large difference in surface tension in comparison with the superhydrophobic background, and the liquids spread more easily in the spots with increasing UVO irradiation time (Fig. 1.7A). Protein solutions containing different concentrations of human serum albumin (HSA) and human plasma fibronectin (HFN) were individually hand-dispensed in hydrophilic (static WCA of 40°) spots and incubated on the surface for different amounts of time, washed, and then used for cell experiments. A $10 \mu\text{l}$ droplet of cell suspension was individually dispensed in each hydrophilic spot and cultured for 4 h. In general, more cells were detected in spots with higher amounts of HFN, which is in agreement with the fact that albumin is a passivating protein and fibronectin is cell adhesive due to the presence of integrin binding domains. The reported method to deposit isolated drops of cell suspension on a hydrophilic–superhydrophobic pattern allows different media or different cell types or numbers to be cultured in each spot, and could be used for combinatorial screens. The cells in this experiment were cultured in the droplets for only 4 h, but since many experiments will require longer incubation times, the possibility for this will need to be proven.

Salgado *et al.* performed a combinatorial screen of the chemical composition and cytocompatibility of 3D hydrogels in an array format on hydrophilic–superhydrophobic patterned substrates (Salgado *et al.*, 2012). UVO irradiation through a hollowed photomask was used to create 4 mm^2 hydrophilic (static WCA of 72°) squares separated by 0.5 mm on a superhydrophobic polystyrene (PS) surface (static WCA of 152°). Chitosan, collagen, and hyaluronic acid were combined with alginate at different ratios to create 24 combinations of alginate-based polymers. The polymer solutions were mixed with cells and then dispensed on the hydrophilic squares using a micropipette, followed by the addition of CaCl_2 to ionically crosslink the polymers, and then immersed in culture medium. The hydrogels were contained within the hydrophilic spots by the superhydrophobic background (Fig. 1.7B,C). Fibroblast (L929) or pre-

osteoblast (MC3T3-E1) cells were encapsulated in the hydrogels for 24 h and both non-destructive (live/dead cell staining and image analysis) and destructive (proliferation assay and dsDNA quantification) methods were used to analyze the cytocompatibility of the hydrogels. This platform shows the potential of using (super)hydrophilic–superhydrophobic patterned surfaces to create hydrogel arrays to study the effect of cell–material or cell–molecule interactions in 3D microenvironments.

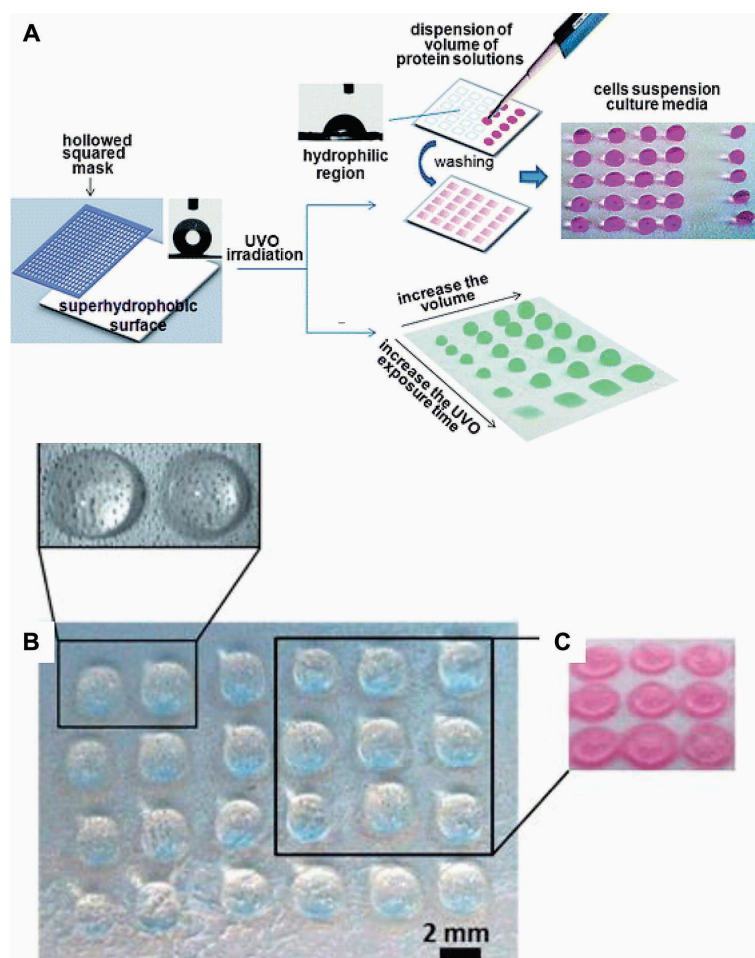


Figure 1.7 Hydrogels on hydrophilic–superhydrophobic surfaces

(A) Schematic of the procedure used to produce hydrophilic–superhydrophobic surfaces to test cell–protein interactions. Droplets of different volumes from 2–8 μl confined in wettable regions produced by different UVO irradiation times from 1–12 min.

Reproduced with permission (Neto *et al.*, 2011). Copyright © 2011 Royal Society of Chemistry. (B) Hydrogels dispensed in hydrophilic spots. (C) Alginate-based hydrogels after 24 h of immersion in culture medium. Reproduced with permission (Salgado *et al.*, 2012). Copyright © 2012 Royal Society of Chemistry.

Droplet microarrays for chemical synthesis and screening

Surface tension-confined arrays are also useful for applications outside of cell screening. Mugheri et al. combined surface tension microarrays and piezoelectric dispensing to synthesize and profile new enzyme inhibitors of the NS3/4A serine protease of the hepatitis C virus (HCV) (Mugheri *et al.*, 2009). The protease plays an essential role in the maturation and immune evasion of HCV. The microarray pattern they formed had 800 hydrophilic spots of 500 μm diameter on a hydrophobic surface to maintain the position of the arrayed nanodroplets. A set of 200 hydrazides was generated and 20,100 distinct dihydrazones were synthesized inside the nanodroplets. Potent inhibitors of the NS3/4A protease were identified. This work demonstrates that arrays of droplets formed on hydrophilic–hydrophobic patterned surfaces can be used for the synthesis of small molecules and the high-throughput quantitative analysis of enzyme kinetics, and is thus an extremely useful tool for creating combinatorial libraries and miniaturizing drug discovery efforts.

From the same group, Burchak et al. used the hydrophilic–hydrophobic patterned surfaces to form droplets for the synthesis and screening of autofluorescent drug-like molecules that could act as bioimaging probes (Burchak *et al.*, 2011). 1600 unique combinations were created and screened in the droplets, and the fluorescence was analyzed with a microarray scanner. The crucial role of the amidine structure in the appearance of fluorescence was discovered. This shows the feasibility and great potential of combinatorial synthesis and screening of chemical libraries in droplet microarrays.

1.2 High-throughput cell screening

With an increasing number of bioactive molecules available for testing, cheaper and more efficient methods are needed for cell screening. Although methods for cell screening using microwell plates is relatively well established, it requires a lot of expensive consumables and reagents and each experiment is labor intensive. In this PhD thesis, we discuss a new method for performing 2D and 3D cell screens using superhydrophilic–superhydrophobic patterned surfaces. Therefore, we will introduce the current methods in this field that are related to our work, specifically cell microarrays for reverse transfection and 3D hydrogel–cell arrays.

1.2.1 Reverse cell transfection microarrays

Over the last decade, reverse cell transfection microarrays have been developed for genetic screening (Baghdoyan *et al.*, 2004; Cheng *et al.*, 2010; Erfle *et al.*, 2007; Hu *et al.*, 2006; Neumann *et al.*, 2006; Stürzl *et al.*, 2008; Wood *et al.*, 2012). The method was first introduced by the group of Sabatini as an alternative to protein microarrays to identify drug targets and as a gene expression system to discover the role of genes in cellular processes (Ziauddin & Sabatini, 2001). They mixed cDNAs cloned in expression vectors in an aqueous solution of gelatin and printed ~1 nl at a 400 μm spot pitch on a (gamma-aminopropyl)silane-coated glass slide using a robotic arrayer. The printed slides were dried before being covered with a lipid transfection reagent (Effectene) for 10–20 min and then seeded with adherent cells (Figure 1.8). HEK 293 cells grew on the whole slide, but 30–80 cells transfected with GFP cDNA were clustered in the area of the printed cDNA–gelatin spots that were 120–150 μm in diameter. This method was termed “reverse transfection”. They demonstrated the potential of these “transfected cell microarrays” by screening a library of 192 cDNAs in HEK 293T cells to identify proteins involved in tyrosine kinase signaling, apoptosis, and cell adhesion.

The method of reverse transfection is also compatible with gene suppression studies through RNA interference. Silva *et al.* used short hairpin RNA (shRNA)-expression constructs to target genes involved in proteasome-mediated proteolysis and those involved in cytokinesis (Silva *et al.*, 2004). They screened 30 shRNAs targeting different proteasome subunits and 8 shRNAs targeting the mitotic motor protein Eg5. The transfection mixtures consisted of the nucleic acids mixed with sucrose, Effectene transfection reagent, and gelatin, and were printed onto (gamma-aminopropyl)silane-coated glass slides using a robotic arrayer to form spots of 400–500 μm in diameter. After drying the slides overnight at RT, HEK 293T cells were seeded on the whole surface and incubated for 60 h before analysis. shRNAs targeting the subunits of the 26S proteasome resulted in accumulation of the reporter protein due to defects in proteolysis. shRNAs targeting Eg5 resulted in the expected aberrant spindle

morphology. They also compared the screening results with those performed in 96-well plates, and found comparable results in terms of sensitivity and specificity. In addition, no loss in silencing efficiency was noticed when the shRNA arrays were stored up to 2 months at 4°C. They also estimated that 100–500 spots on the transfected cell microarrays could be analyzed with the same material required to perform a single transfection in one well of a 96-well plate. This demonstrates the cost-saving potential of using transfected cell microarrays.

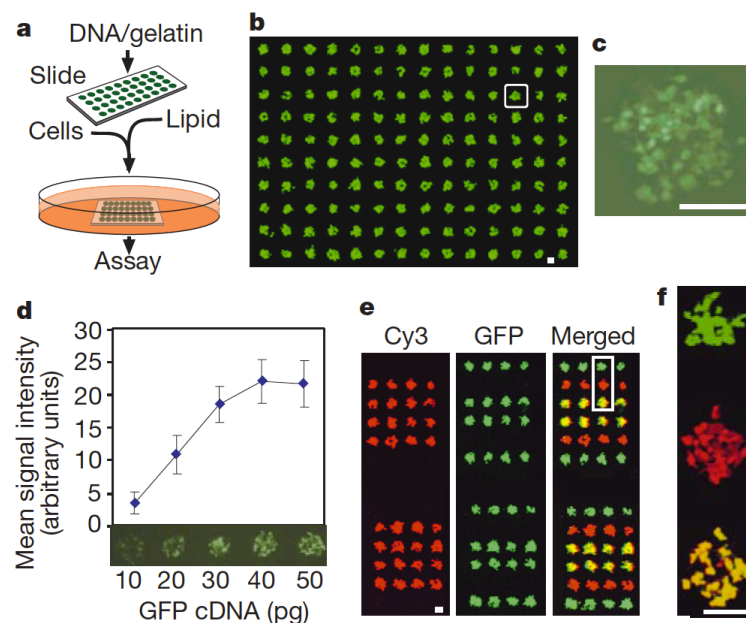


Figure 1.8 Transfected cell microarray procedure

(a) Protocol for making microarrays of transfected cells. (b) Laser scan image of a GFP-expressing microarray made from a slide printed in a 14×10 pattern with a GFP expression construct. (c) Higher magnification image obtained with fluorescence microscopy of the cell cluster boxed in (b). Scale bar, $100 \mu\text{m}$ (d) Expression levels of cell clusters in a microarray are proportional, over a four-fold range, to the amount of plasmid DNA printed on the slide. Indicated amounts of the GFP construct assume a 1 nl printing volume. The graph shows the mean \pm s.d. of the fluorescence intensities of the cell clusters ($n = 6$). The fluorescent image is from a representative experiment. (e) Co-transfection is possible with transfected cell microarrays. Arrays with elements containing expression constructs for HA–GST, GFP or both were transfected and processed for immunofluorescence and imaged with a laser scanner. Cy3, cell clusters expressing HA–GST; GFP, cell clusters expressing GFP; merged, superimposition of Cy3 and GFP signals. Yellow color indicates co-expression. Scale bar, $100 \mu\text{m}$. (f) Enlarged view of boxed area of scan image from (e). Reproduced with permission (Ziauddin & Sabatini, 2001). Copyright © 2001 Nature Publishing Group.

In most of the procedures for cell microarrays, the cells are allowed to adhere and grow over the whole surface without separation between the cells on the transfected spots and those on the background (Figure 1.9). Rantala et al. introduced a method to promote cell adhesion only to the printed spots and tested the method with 92 different adherent cell types (Rantala *et al.*, 2011). In addition, they used the reverse transfection cell microarrays to screen 492 G-protein couple receptor (GPCR) coding genes for their impact on the growth and survival of human prostate cancer cells. The transfection mixtures consisted of siRNA mixed with siLentFect transfection reagent, Matrigel, and sucrose, and were printed onto untreated polystyrene microplates using a microarray printer. Cells were dissociated with HyQtase and resuspended in the same conditioned culture medium for cell seeding on the microarrays. The cells were only allowed 10–15 min to adhere and the remaining unadhered cells were washed away, resulting in cells that grew mainly on the printed spots (Figure 1.10). Androgen responsive VCaP, LAPC-4 prostate cancer cells, and RWPE-1 non-malignant prostate epithelial cells were cultured on the siRNA microarrays for 48 h, followed by immunostaining for Ki-67 as a proliferation marker and cleaved poly(ADP-ribose) polymerase (PARP) as an apoptosis marker. They were able to identify two GPCRs that had the strongest impact on prostate cancer cell growth and showed that their results correlated well with data from clinical samples. It was also noted that the consumption of siRNAs and reagents for the microarray method was up to 200-fold less than for 384-well plates, and antibody consumption was up to 400-fold less.

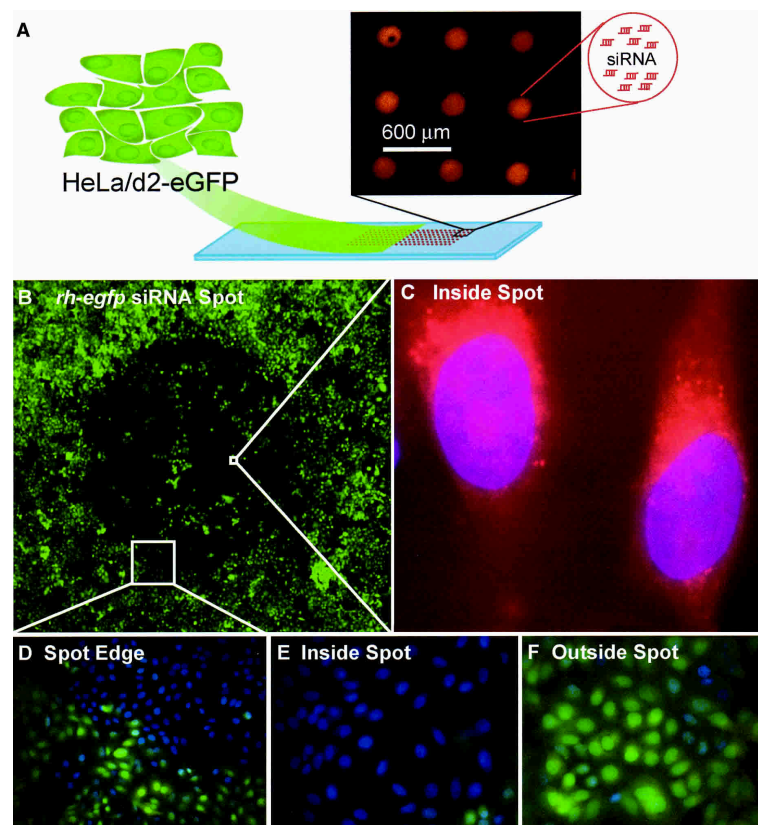


Figure 1.9 Cells on a transfected cell microarray

The RNAi microarray platform. (A) HeLa cells expressing a destabilized version of eGFP (HeLa/d2eGFP) cells were plated on slides arrayed with an *egfp* siRNA (2.5 ng) tagged with fluorescent rhodamine (*rh-egfp*). HeLa/d2eGFP cells grown on an *rh-egfp* siRNA microarray slide for 72 h were fixed with 2% paraformaldehyde and counterstained with DAPI. (B) An *rh-egfp* spot (2.5 ng siRNA) showing the localized inhibition of green fluorescence (25 \times , green channel only). (C) The uptake of *rh-egfp* siRNA-lipoplexes showing cellular accumulation of the siRNA in silenced cells (1000 \times). (D) A clear edge to the arrayed *rh-egfp* siRNA spot was present only in the green channel (200 \times , overlaid green and blue images), with (E) inhibition of eGFP fluorescence occurring within the spot (400 \times , overlaid green and blue images). (F) No inhibition of eGFP fluorescence in cells was observed around the *rh-egfp* siRNA spot (400 \times , overlaid green and blue images). Reproduced with permission (Mousses *et al.*, 2003). Copyright © 2003 Cold Spring Harbor Laboratory Press.

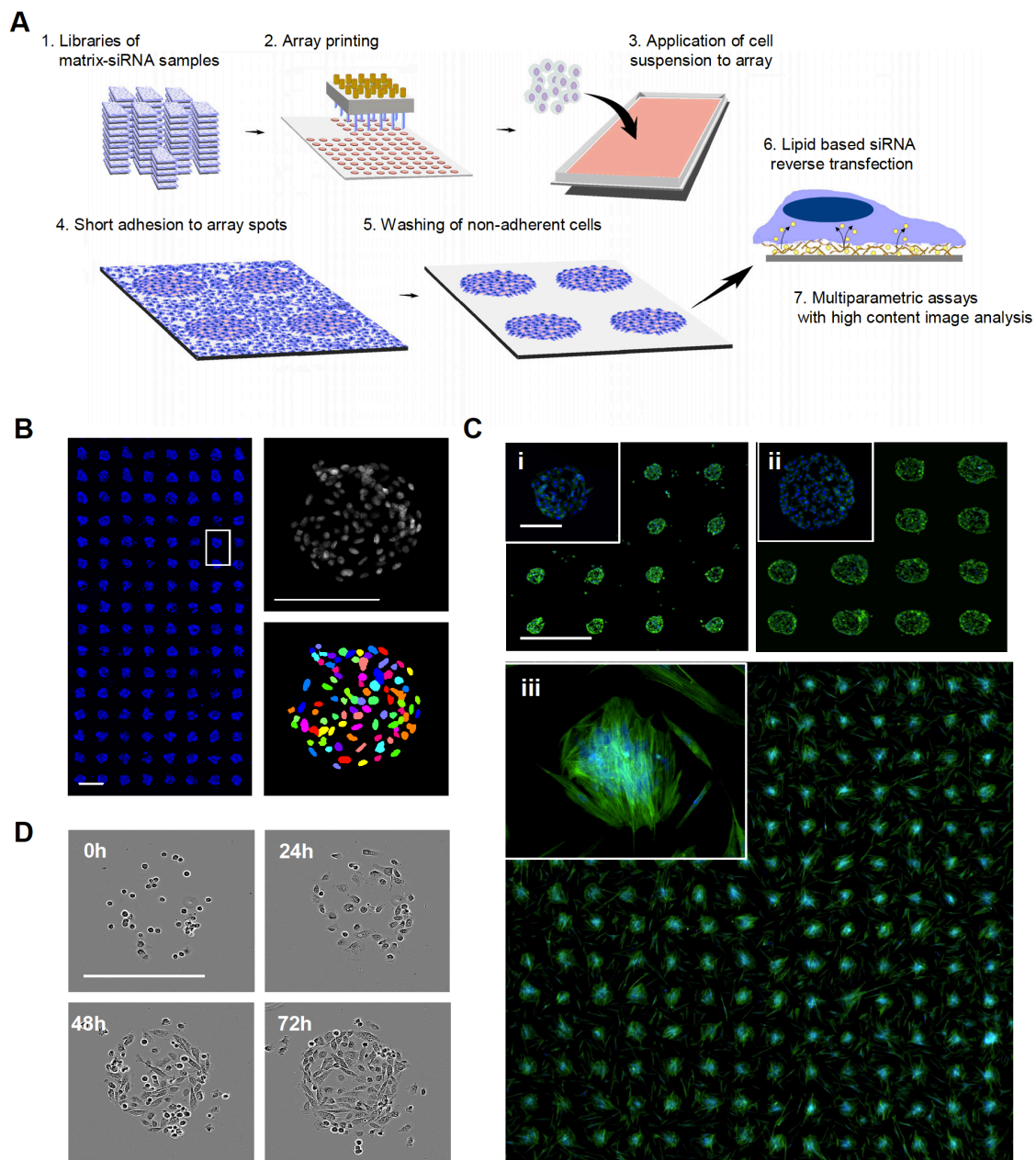


Figure 1.10 Modified cell seeding procedure on transfected cell microarrays

(A) CSMA work flow: siRNA samples in a printing solution containing transfection lipid and extra-cellular matrix proteins are robotically printed on a hydrophobic polystyrene surface. A suspension of adherent cells is allowed to adhere onto the array spots, followed by washing un-adhered cells off, leaving adhered cells only to printed array positions. After reverse transfection for a selected time, the arrays are stained using e.g. traditional multi-label immunostaining protocols for high content image analysis of multiple parameters. (B) CSMA method allows production of high density patterned cell arrays. Left panel displays a microarray scanned view of 200 μm cell spots with 500 μm spot spacing. Scale bar 0.5 mm. Right panel: Due to the spatially

confined layout of the spots, automated imaging and segmentation of cells on CSMA spots can be performed using automated image analysis software. Scale bar 200 μm . (C) Microscopic image and microarray scanned view of 200 μm CSMA spots (Top left panel;i) and 400 μm spots (Top right;ii) of PC-3 cells stained for DNA (blue) and F-Actin (green) after 48 h culture. Microscopic image and microarray scanned view of 200 μm CSMA spots (Bottom;iii) of primary prostate stromal cells cultured for 48 h and stained for DNA (blue) and F-Actin (green). Scale bar 900 μm . (D) Phase contrast microscopic images from a timelapse series of PC-3 cells cultured on 200 μm array spots for 72 h. Reproduced with permission (Rantala *et al.*, 2011). Copyright © 2011 BioMed Central Ltd.

1.2.2 Screening cells in 3D hydrogels

Lee *et al.* developed a 3D cell culture array to perform a toxicity screen of drugs and their cytochrome P450-generated metabolites (Lee *et al.*, 2008). Glass slides were first treated with 3-aminopropyltrimethoxysilane followed by poly(styrene-*co*-maleic anhydride). 20×54 arrays of 10 nl drops containing poly-L-lysine and BaCl_2 were printed on the surface using a microarray spotter and allowed to dry, then 20 nl drops of an alginate solution containing HepB3 cells were spotted on top and gelation instantly occurred (DataChip). To expose the cells to P450-generated metabolites, a complementary array of alginate gels containing P450 isoforms (MetaChip) was stamped on top of the cell–alginate gel array for 6 h (Figure 1.11). The cell–alginate gel array was then rinsed and cultured for another 3 days before assessing cell viability. IC_{50} values for 27 compounds and their P450-generated metabolites were determined, and 13 compounds were found to be reactive toward one or more P450 isoforms, resulting in either the activation or deactivation of the toxic response in Hep3B cells.

Fernandes *et al.* also used a 3D cell culture array platform consisting of cells encapsulated in alginate gels, but to track the stem cell fate of mouse embryonic stem cells (mES) (Fernandes *et al.*, 2010). A poly-L-lysine– Ba^{2+} solution was spotted onto poly(styrene-*co*-maleic anhydride) coated glass slides using a non-contact microarrayer, followed by the spotting of a cell suspension containing alginate on top in high humidity conditions. The alginate gelled immediately to form 60 nl drops with a diameter of $<800 \mu\text{m}$ at a pitch of $<1200 \mu\text{m}$ in a 14×20 array. At an initial seeding density of 100 cells per gel, mES cells could be cultured for at least 5 days without a significant decrease in cell viability, although increased seeding densities resulted in lower growth rates. mES cells encapsulated in the alginate gels were able to expand without differentiating when cultured for 5 days in a serum-free medium supplemented with leukemia inhibitory factor (LIF), as shown by positive Oct-4 staining. However, without LIF supplementation, the mES cells spontaneously differentiated towards a

neural fate as indicated by high levels of Sox1 expression and negligible levels of Oct-4 and Nanog in Sox1-GFP-knock-in mES cells after 6 days of culture in the alginate gels. The sandwiching method was also used to study the effects of tretinoin and fibroblast growth factor-4 (FGF-4) on the pluripotency of mouse ES cells. 60 nl drops of tretinoin and FGF-4 were printed on methyltrimethoxysilane-coated glass slides and then stamped on top of the cell–alginate gel array and incubated overnight. The cell–alginate gel array was then rinsed and cultured for an additional 3 days, and then stained for Oct-4 and Nanog. Cells exposed to a combination of tretinoin and FGF-4 showed decreased levels of Oct-4 and Nanog, suggesting that cell differentiation was induced.

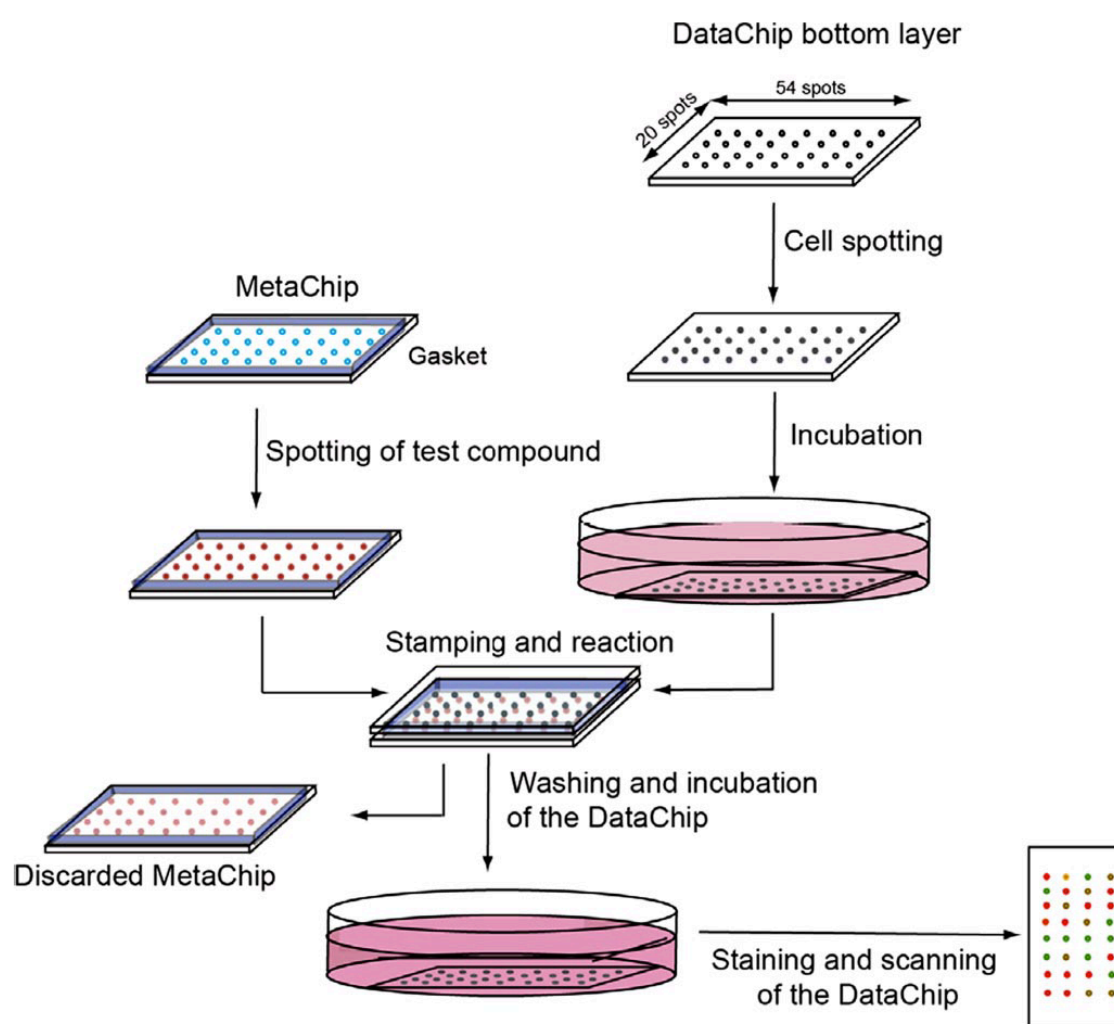


Figure 1.11 Platform for performing a toxicity screen in 3D

Schematic of the DataChip platform for direct testing of compound toxicity or coupling with the MetaChip for evaluating toxicity of P450-generated metabolites. Reproduced with permission (Lee *et al.*, 2008). Copyright © 2008 National Academy of Sciences.

1.3 Liposome-mediated transfection

Transfection using DNA alone is a very inefficient process since DNA is not usually able to spontaneously enter cells due to its size and charge and due to the multitude of enzymatic and membrane barriers present in cells. For this reason, a wide variety of methods have been developed to facilitate this process, but liposome-mediated transfection has proven to be a good alternative to viral vectors for gene delivery as they are relatively easy to produce and chemically modify, and they have demonstrated acceptable transfection efficiencies and low toxicity (Balazs & Godbey, 2011; Wasungu & Hoekstra, 2006). Many cationic lipids that have been synthesized are now commercially available transfection reagents that are commonly used in biological laboratories (*e.g.*, Lipofectamine). Successful cell transfection depends on the ability of liposomes to condense and pack DNA to form lipoplexes, the interaction of the lipoplexes with the cell surface, the efficiency of lipoplex internalization, the release of the nucleic acids from the lipoplexes and intracellular compartments such as endosomes before being degraded, the translocation of the nucleic acids from the cytosol into the nucleus, and finally the transcription efficiency.

Liposomes are often formed from cationic lipids, which are amphiphilic molecules consisting of a hydrophilic, cationic headgroup (*e.g.*, amine) attached via a linker (*e.g.*, glycerol) to a usually double hydrocarbon chain or a cholesterol derivative. The positively charged amines in the polar head group can facilitate the binding of liposomes to negatively charged DNA as well as interaction of the lipoplexes with negatively charged components of the cell membrane before being taken up by the cell. The structure of the formed liposome can be predicted by a factor known as the packing parameter, defined as $P = v/(al_c)$, where v is the volume of the hydrocarbon region, a is the effective area of the head group, and l_c is the critical length of the lipid tail (Figure 1.12). The packing parameter emphasizes the relevance of the ratio of the area occupied by the hydrophobic region versus that of the hydrophilic region. When the area occupied by the hydrocarbon chains is much larger than that of the head group such that $P > 1$, the lipids tend to adopt the inverted hexagonal phase, which has demonstrated to be an important step for releasing DNA from the uptaken lipoplexes into the cytosol by destabilization of the lipid bilayer structure. Neutral “helper” lipids with $P > 1$, such as dioleoylphosphatidylethanolamine (DOPE), are often mixed with cationic lipids to aid in the fusion of lipoplexes with cellular membranes and to promote the conversion from a lamellar to a non-lamellar liposome structure to enhance endosomal escape of DNA into the cytosol, a mechanism that was consistently found to be associated with superior transfection efficiencies (Koynova, 2010).

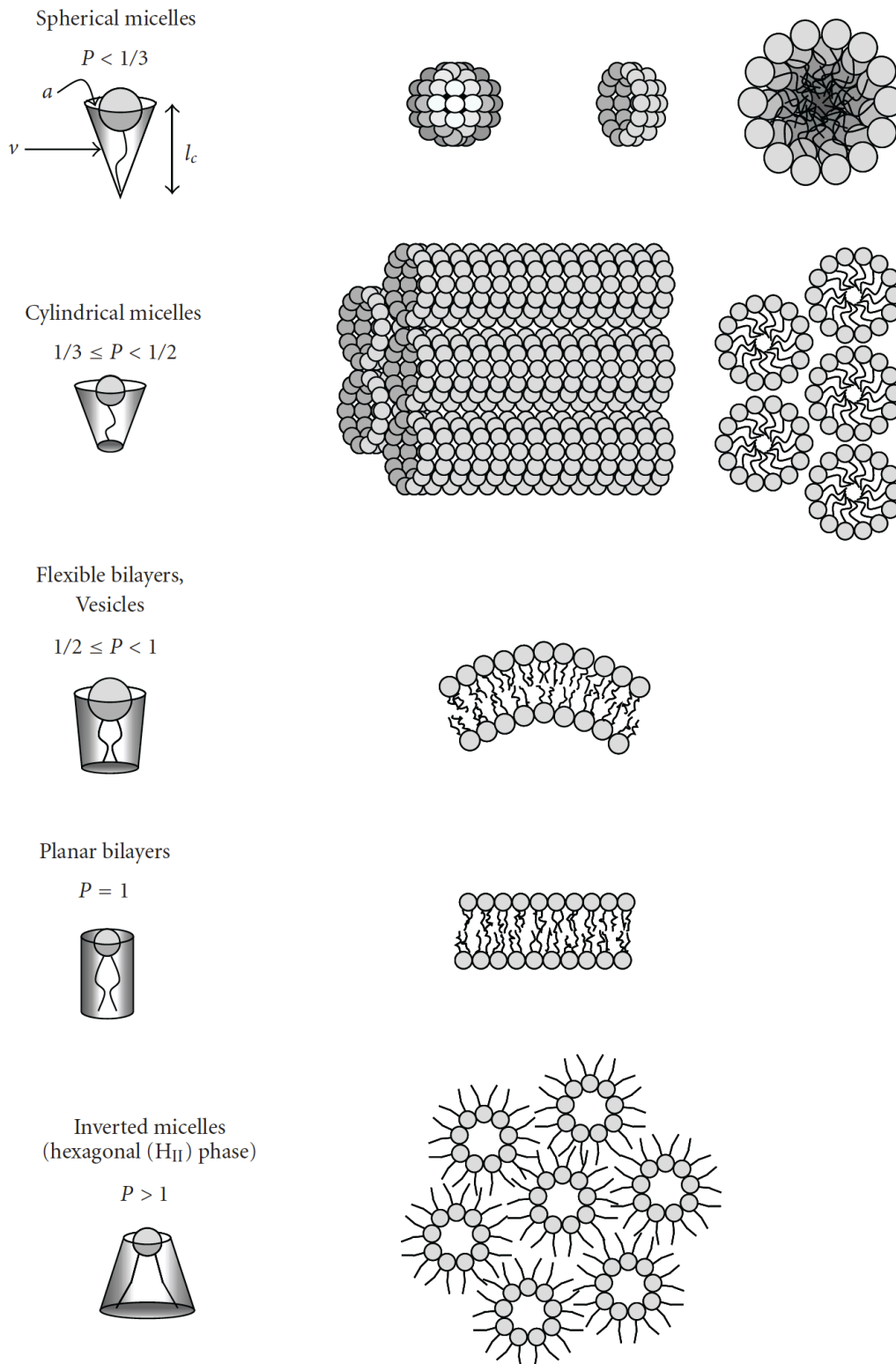


Figure 1.12 Liposome structures predicted by the packing parameter, P .

Reproduced with permission (Balazs & Godbey, 2011). Copyright © 2011 Daniel A. Balazs and WT. Godbey.

The general description of lipoplexes as DNA packed neatly within liposomes is more likely oversimplified as indicated by studies showing that plasmids enwrap themselves within the amphiphilic lipids in a multilamellar fashion with DNA rods sandwiched between lipid bilayers (Koynova, 2010; Rehman *et al.*, 2013). In addition, fusion between the lipoplexes can occur to form large lipoplex assemblies. This highlights the importance of the chemistry and structure of the cationic lipids in dictating the final lipoplex assemblies and consequent transfection efficiency (Pedroso de Lima *et al.*, 2003).

Although the exact mechanisms of lipoplex internalization by cells are still being investigated, the first step is thought to be driven by the electrostatic interactions between the cationic lipoplexes and the negatively charged cell surface components such as proteoglycans containing various glycosaminoglycan chains including heparan, dermatan, and chondroitin sulfates (Parker *et al.*, 2004). Clathrin- and caveolae-mediated endocytosis and macropinocytosis most probably play a significant role in the actual uptake of lipoplexes into the cell (Figure 1.13) (Hoekstra *et al.*, 2007; Rehman *et al.*, 2013). Due to a size limit of approximately 200 nm for the internalization of particles by non-phagocytic eukaryotic cells, it is thought that efficient transfection occurs for lipoplexes in this size range (Rejman *et al.*, 2004). A major aim in the internalization of lipoplexes is to avoid their trafficking to lysosomal compartments where both the liposomes and nucleic acids could be degraded, thus preventing successful transfection. Even if internalization of the lipoplexes occurs and degradation of the lipoplexes is avoided, the DNA still needs to be released from the cellular compartments as well as from the lipoplex itself into the cytosol. The required membrane perturbation could involve either fusion between lipoplexes and organelle membranes, or a local and transient membrane perturbation initiated by the interaction of cationic and membrane lipids that leads to pore-like structures that allow the passage of nucleic acids.

Another possible barrier to successful transfection is the translocation of the DNA across the intact nuclear membrane into the nucleus for transcription (Figure 1.14). This process was shown to be much more efficient in proliferating cells rather than postmitotic cells due to disassembly of the nuclear membrane during the G2–M stage of the cell cycle (Lechardeur & Lukacs, 2006; Parker *et al.*, 2004). For noncycling or postmitotic cells, entry of DNA into the nucleus is limited to passage through nuclear pore complexes.

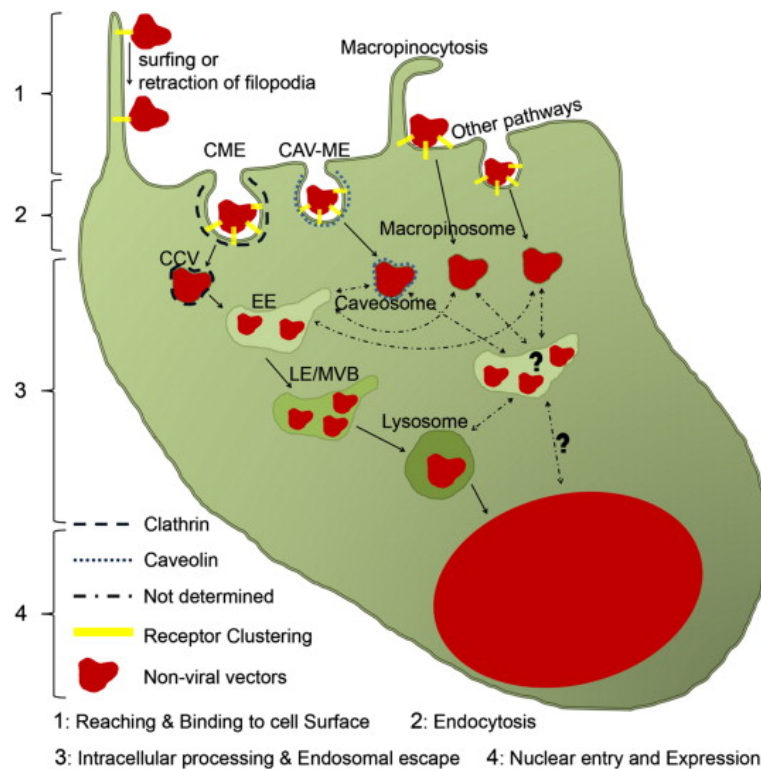


Figure 1.13 Nanocarrier–cell interaction: entry pathways and cellular barriers

For nucleic acid delivery, the nanocarriers have to overcome several extracellular and intracellular barriers. Binding to the cell surface may occur following processing along filopodia (1) or by direct interaction with the cell surface, after which the particles may enter the cell via various endocytic pathways (2). Following subsequent intracellular processing, the release of contents may occur from distinct endocytic compartments, as induced by various mechanisms, including lipid mixing and nonbilayer-induced membrane perturbation (lipoplexes) or endosomal escape, based on a mechanism known as the proton sponge effect (polyplexes) (3). In a final step, plasmids and antisense oligonucleotides are delivered to the nucleus (4). The nanocarriers can be endocytosed via various endocytic pathways including clathrin dependent (CME) and clathrin independent endocytosis. The latter involves caveolae mediated endocytosis (CAV-ME), macropinocytosis, and various other endocytic mechanisms which may include e.g. caveolin-1 independent raft dependent endocytosis, flotilin mediated endocytosis, ARF6-mediated endocytosis, F/CLIC (fluid phase/clathrin independent carrier) endocytosis. Reproduced with permission (Rehman *et al.*, 2013). Copyright © 2013 Elsevier.

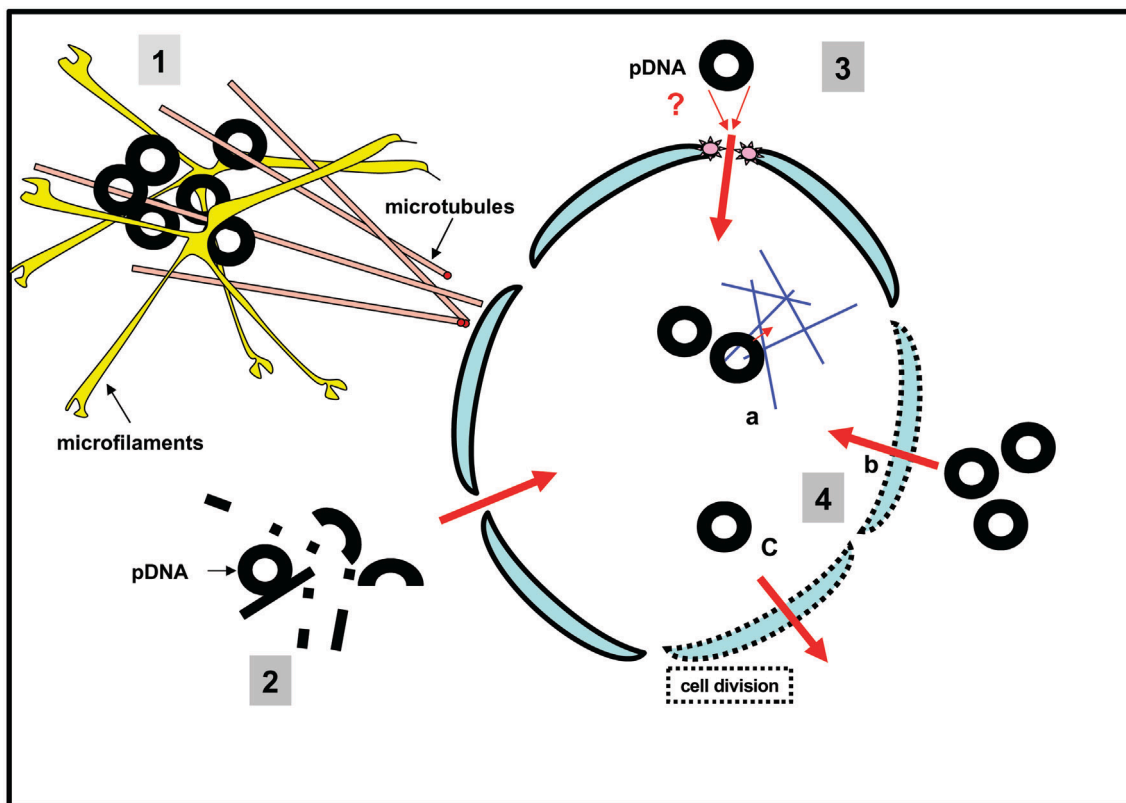


Figure 1.14 Cellular barriers to nucleocytoplasmic traffic of pDNA

Cellular barriers that are implicated in the low efficiency of pDNA uptake: 1) the cytoskeleton and molecular crowding restrict the diffusional mobility of pDNA in the cytoplasm, 2) degradation of pDNA by constitutively active cytosolic nuclease(s), 3) restricted translocation efficiency of pDNA in the nucleus, and 4) limited transcriptional activity of pDNA in the nucleus. Transcription of pDNA is conceivably influenced by interactions with nuclear matrix components (a). Upon the disassembly of the nuclear envelope both nuclear entry (b) and escape (c) of pDNA may occur. Reproduced with permission (Lechardeur & Lukacs, 2006). Copyright © 2006 Mary Ann Liebert, Inc.

1.4 Screening of lipid libraries

Since the method of liposome-mediated transfection is still not fully understood, several groups including ours have used the approach of synthesizing libraries of lipid-like molecules followed by high-throughput screening in microtiter plates to identify efficient and non-toxic transfection reagents. By using combinatorial chemistry techniques, the lipid libraries can be synthesized in a relatively simple and efficient manner with control over variations in the lipid chemistry and structure. This allows for the systematic testing of different lipids to understand the structure–function relationship and ultimately for the rational design of liposomal transfection reagents with high efficiency and low toxicity.

Work from the groups of Anderson and Langer led to a method for the rapid synthesis of over 1,200 structurally diverse lipidoids based on the conjugate addition of alkyl-acrylates or alkyl-acrylamides to primary or secondary amines (Figure 1.15) (Akinc *et al.*, 2008). First, a pilot library of ~700 lipidoid members were synthesized with variations in the alkyl chain length from C10 to C18, the linker as either a degradable ester or more stable amide, the primary R group on the amine, and the introduction of a constitutive positive charge to certain lipidoids by quaternization of the amine with the alkylating agent methyl iodide. The lipidoids were tested for their ability to deliver siRNA targeting firefly luciferase (siLuc) to a HeLa cell line stably expressing both firefly (*Photinus pyralis*) and *Renilla* (*Renilla reniformis*) luciferase, then the ratio of firefly to *Renilla* luciferase expression was measured. Transfection was enhanced when using lipidoids containing more than two amines per head unit (e.g., monomers 61-64, 95-103) and either two long amide tails (e.g., N₁₆) or several smaller amide tails (e.g., 98N₁₂). Based on the pilot screening, they synthesized a second library of 500 lipidoids to include lipidoids with even shorter amide tails (e.g., N₁₁, N₉) and more head units (e.g., monomers 109–117) with the possibility to link a diverse number of tails. 56 lipidoids were found to induce gene silencing at levels similar to Lipofectamine[®] 2000. The most efficient lipidoids had several structural similarities such as amide linkages, more than two alkyl tails, 8–12 carbon tail lengths, and one secondary amine. Although gene silencing was more efficient with commercial transfection reagents at lower lipoplex concentrations in HeLa and HepG2 cells, the lipidoids showed more efficient silencing in primary bone marrow–derived macrophages.

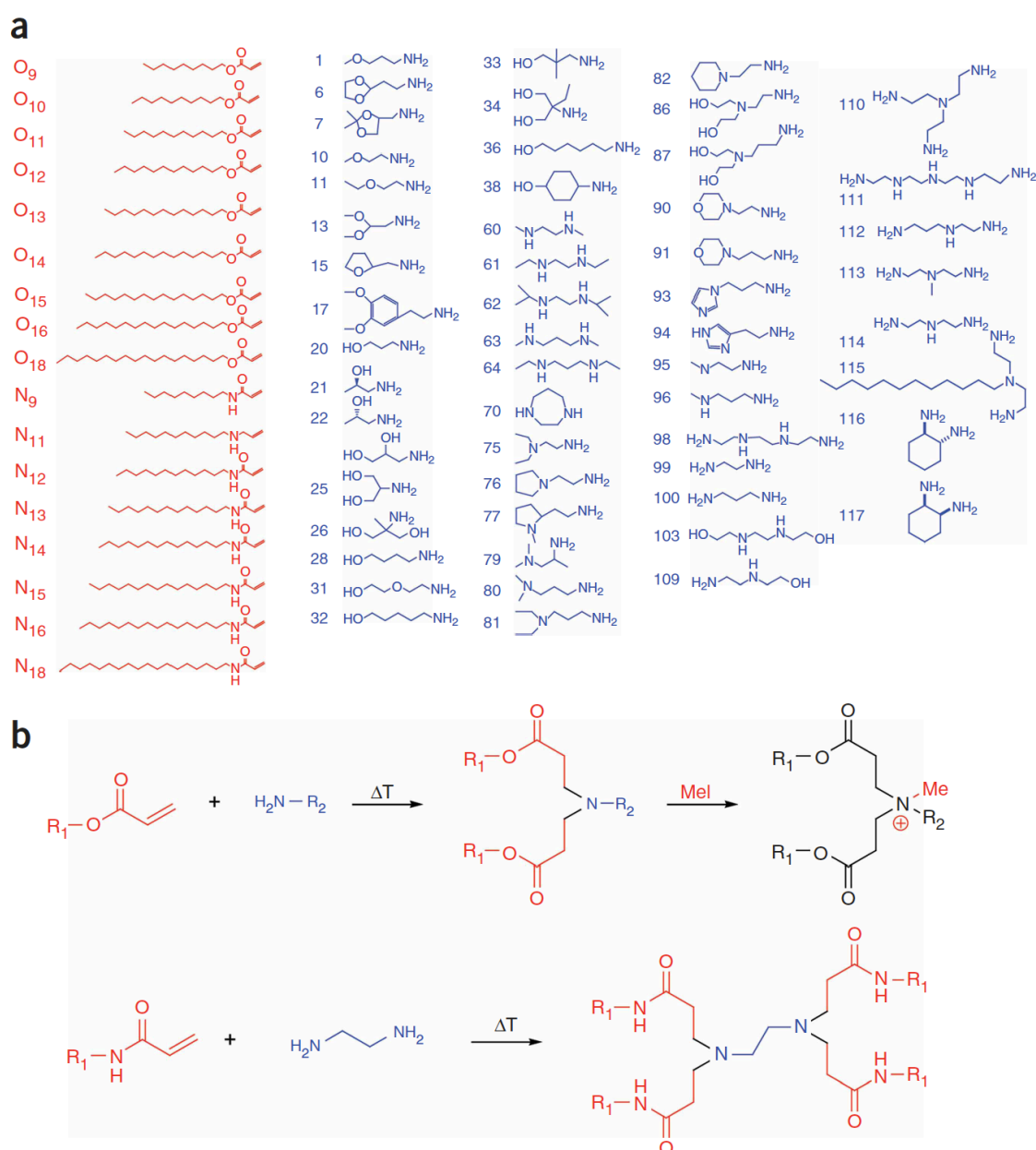


Figure 1.15 Synthesis of lipidoids consisting of alkyl-acrylate, alkyl-acrylamide, and amino molecules

(a) Alkyl-acrylate, alkyl-acrylamide, and amino molecules were used to synthesize a combinatorial library of lipidoids. (b) Synthesis occurs through the conjugate addition of amines to an acrylate or acrylamide. Depending on the number of addition sites in the amino monomer, lipidoids can be formed with anywhere from 1 to 7 tails. Amino groups in the lipidoid can be quaternized by treatment with methyl iodide. For ease of nomenclature, lipidoids are named as follows: (amine number)(acrylate or acrylamide)-(number of tails)(“+” if quaternized). Reproduced with permission (Akinc *et al.*, 2008). Copyright © 2008 Nature Publishing Group.

In continued work from the groups of Anderson and Langer, Sun et al. also used the method of reacting amines with lipophilic acrylates, acrylamides, or epoxides to build a library of lipidoids composed of different amines and tail types and lengths, this time to test transfection with DNA. (Figure 1.16) (Sun *et al.*, 2012). HeLa cells were transfected with plasmid DNA encoding β -galactosidase (β -gal) in 96-well plates and enzymatic assays were used to quantify the level of β -gal expression. Lipidoids composed of amine 86 (*N,N*-bis(2-hydroxyethyl)ethylene diamine) or amine 87 (*N*-(3-aminopropyl)diethaneamine) with two medium-length tails (C14 or C15 for acrylamide and acrylate, respectively, and C14 or C16 for epoxide) displayed high transfection efficiencies. Lipidoids with amide linkers had much higher transfection efficiencies than those with ester and hydroxyl groups. It was found that lipidoids with an ester linker were not stable and degraded within an hour via hydrolysis, resulting in low transfection efficiencies. The acrylamide and epoxide conjugated with amine 87 (14N-87 and 16C-87) delivered DNA more efficiently than those conjugated with amine 86 (14N-86 and 16C-86), while for the lipidoids synthesized from acrylate, the reverse results were observed. Lipidoid 14N-87 was able to efficiently self-assemble with DNA through electrostatic interactions and form individual, condensed, and multilamellar structure lipoplexes (~100 nm) with DNA intercalated between the lipid bilayers, whereas 14O-87 and 16C-87 tended to form loose “spaghetti and meatball-like structures”, resulting in a higher transfection efficiency with lipidoid 14N-87 compared to 14O-87 and 16C-87. At a low positive/negative (P/N) charge ratio (<5), the DNA encapsulation percentage was low for all three lipidoids, leading to low transfection efficiencies. Increasing the P/N ratio resulted in increased DNA encapsulation of 80–90% for lipidoids 14N-87 and 16C-87 and 60% for 14O-87, correlating with the more efficient delivery of DNA by 14N-87 and 16C-87 than by 14O-87.

suspected to inhibit efficient release of the nucleic acid in the cell and thus result in low transfection efficiency. Additionally, the amine groups in the lipidoids played a critical role in determining the transfection efficiency, and it was shown that a secondary amine and a hydrophilic group incorporated in a lipidoid facilitated gene delivery.

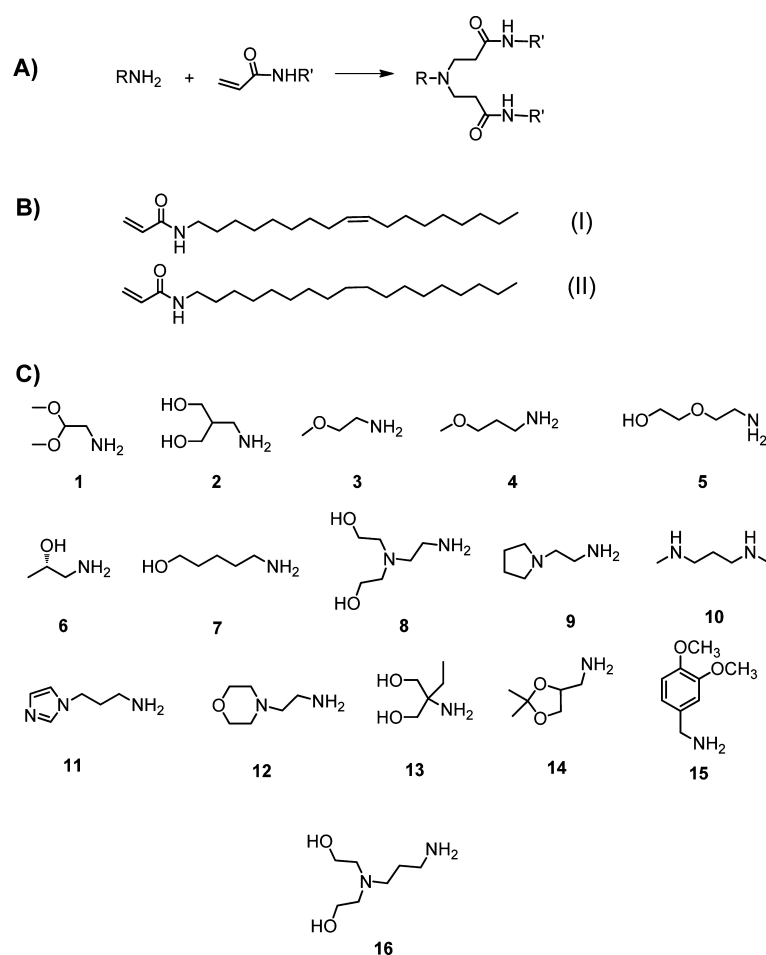


Figure 1.17 Combinatorial synthesis of lipidoids with unsaturated or saturated hydrophobic tails

(A) Synthesis route of lipidoids. (B) Chemical structures of acrylamides used. (C) Amines used for lipidoids synthesis. Reproduced with permission (Wang *et al.*, 2012). Copyright © 2012 American Chemical Society.

In work from our group, Li et al. presented a facile two-step method based on thiol-yne click chemistry for the synthesis of biomimetic cationic thioether lipids possessing two hydrophobic tails of variable lengths and a linker group structurally mimicking the glycerol core of phospholipids (Figure 1.18) (Li *et al.*, 2012b). 8 different alkyl thiols (alkyl chain length from C6 to C16), 2 alkynyl carboxylic acid linkers bearing a terminal triple bond, and 7 different cationic amines were used to synthesize the library. All 112 cationic lipids were mixed with the neutral co-lipid 1,2-di-(9Z-octadecenoyl)-*sn*-glycero-3-phosphoethanolamine (DOPE) at a lipid/DOPE molar ratio of 1.3:1 to form liposomes, and more than 10% of the lipids showed highly efficient transfection when delivering plasmid DNA to HEK 293T cells. Lipids containing undecyl (C11) and dodecyl (C12) hydrophobic tails showed enhanced transfection efficiency compared to lipids with shorter or longer tails, and all cationic head groups tested other than the morpholine head group (amine 2) showed high activity when combined with C11 or C12 hydrophobic tails. This indicated that the length of the hydrophobic alkyl groups was more important than the nature of the cationic head group for efficient cell transfection. The effects of the particle size, surface charge, and stability of the liposomes and lipoplexes on cell transfection were also studied. To achieve high transfection efficiencies, a particle size of 100–200 nm before mixing with plasmid DNA and a stable positive charge (above +50 mV) of the lipoplexes after complexation with DNA were found to be optimal. One of the successful hits, lipid A1C11, was also demonstrated to efficiently transfect mouse embryonic stem cells (mESC) with pDNA and mouse embryonic fibroblast (MEF) with siRNA.

In another work from our group, Li et al. developed a single-step method based on the alkylation of 20 different amines with 10 alkyl halides of different lengths to synthesize a library of cationic lipidoids (Figure 1.19) (Li *et al.*, 2013b). Each lipidoid mixture contained both single, double, and in some cases multi-alkylated amines. The lipidoids were mixed with DOPE at molar ratio of 1:1 and diluted in NaOAc/HOAc pH 5 buffer to protonate the amino head groups of the lipidoids. 4 of the 12 lipidoid mixtures that showed the ability to transfect HEK 293T cells with pDNA had an efficiency equal to or greater than that of Lipofectamine[®] 2000, and increasing the length of hydrophobic tails from C14 up to C18 resulted in an increase in transfection efficiency. Lipidoids containing either 1-(2-aminoethyl)pyrrolidine (1) or 3-(dimethylamino)-1-propylamine (4) showed the highest activity. For this lipid library, it seemed that both the length of hydrophobic tails and the nature of the cationic head groups were important factors for efficient transfection.

The ratio of mono- and disubstituted lipidoids in the mixture was also found to affect the transfection efficiency. Two lipidoid mixtures from the hits (1C12, 1C16) were purified, and 1C12 was found to consist mainly of double-chain lipidoids (1C12-D) whereas 1C16 consisted of both single (1C16-S) and double (1C16-D) alkyl chains.

The double-tailed lipidoids 1C12-D and 1C16-D showed significant transfection efficiencies, which increased as the amount of DNA added to liposomes was decreased to the optimal amount of 75 ng of pDNA per 0.4 μ L of liposome solution per 96-well. This effect was attributed to the increased size of the lipoplexes from 200–600 nm to more than 2 μ m and the change in surface charge from +60 mV to –60 mV as the amount of pDNA was increased relative to the liposome. Lipidoid 1C16-S, consisting of only one hydrophobic tail, showed very low transfection efficiency. This was attributed to the continuous increase in the size of 1C16-S lipoplexes above 1 μ m with time, whereas the size of 1C16-D lipoplexes stabilized at 450 nm within 30 min after mixing the liposomes with DNA. Overall, these results indicate that small particle size and high positive surface charge are two important parameters to achieve high transfection efficiency. It was also found that the amount of DOPE mixed with the liposomes did not significantly affect the size and surface charge of the lipoplexes or the transfection efficiency. Lastly, Li et al. also demonstrated that combining single- and double-tailed 1C16 lipidoids enhanced cell transfection due to the different roles that they play in lipoplex formation. It was found that addition of the single-tailed lipid 1C16-S increased the surface charge of the liposomes and lipoplexes, while addition of the double-tailed lipid 1C16-D led to the formation of smaller and more stable lipoplexes.

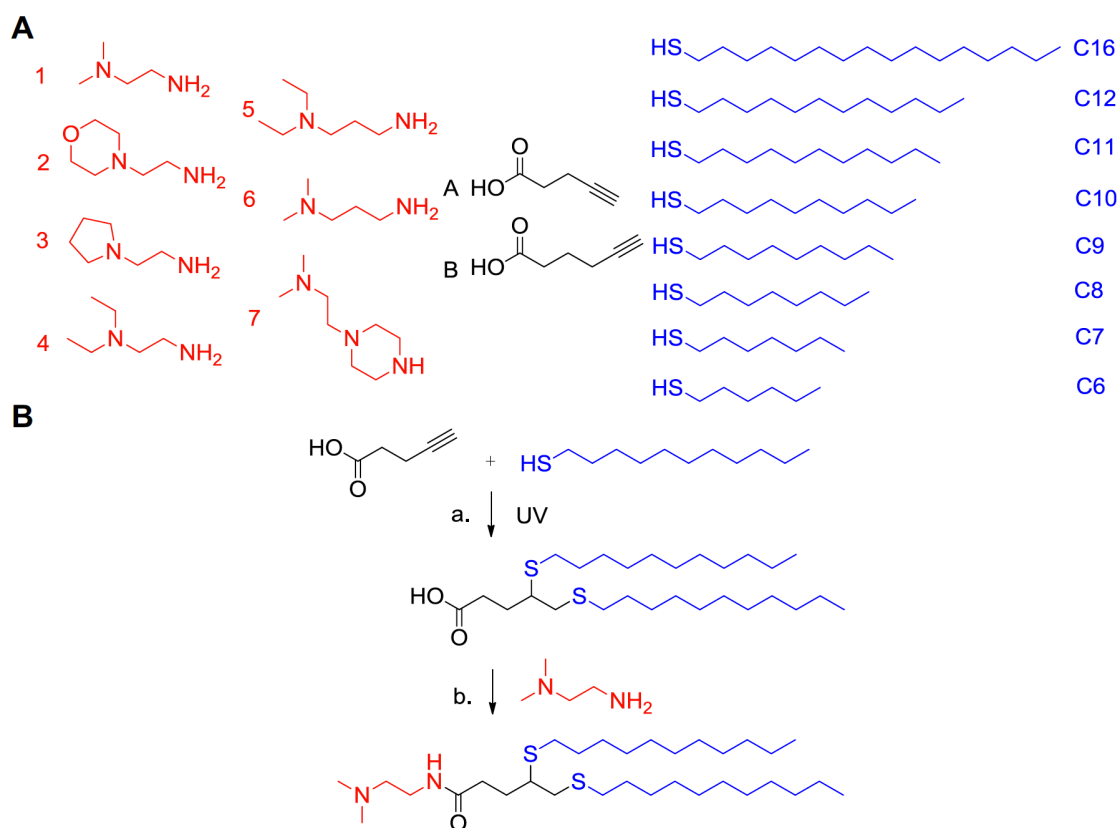


Figure 1.18 Combinatorial synthesis of cationic thioether lipids via thiol-yne chemistry

(A) Seven amines, two alkynes, and eight alkyl thiols (C6–C12, C16) were used in the synthesis. (B) Synthesis scheme of a typical lipid from the library. Reproduced with permission (Li *et al.*, 2012b). Copyright © 2012 Elsevier.

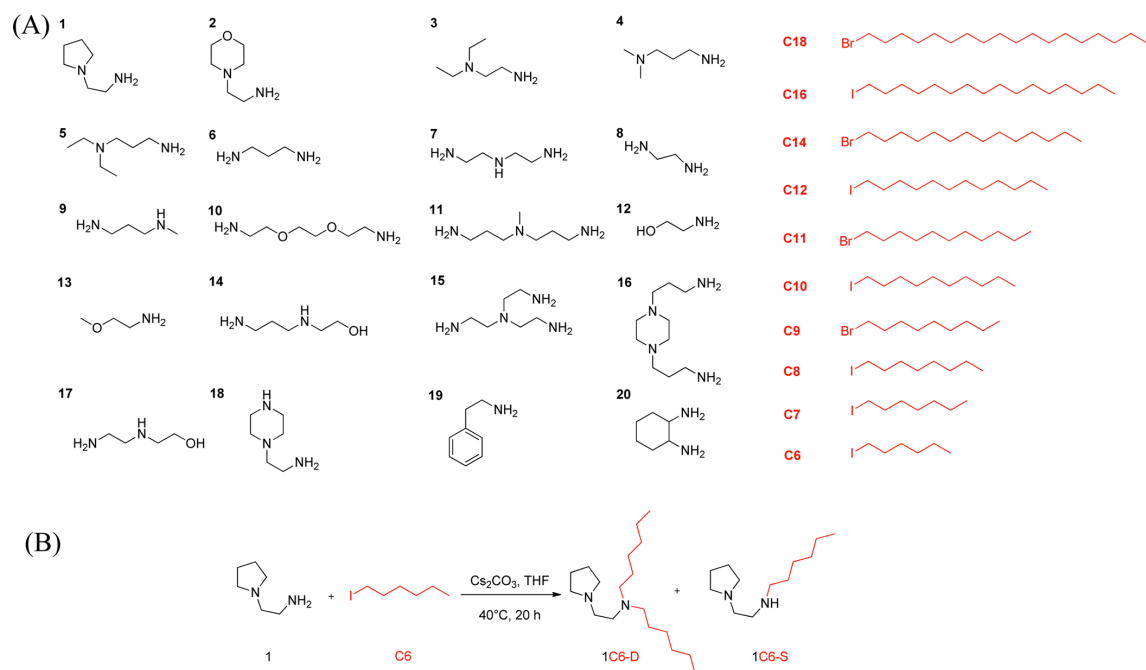


Figure 1.19 Combinatorial synthesis of lipidoids via alkylation of amines

(A) Twenty amines and 10 alkylhalides (C6–C12, C14, C16, and C18) were used in the synthesis. (B) Scheme of the synthesis of one typical lipidoid from the library.

Reproduced with permission (Li *et al.*, 2013b). Copyright © 2013 American Chemical Society.

1.5 Objectives of this PhD work

A variety of chemical and genetic libraries are becoming more widely available for scientific research, however, most research groups do not have the tools necessary to carry out such large-scale screens. Usually, expensive automated equipment such as pipetting robots and high-throughput screening microscopes are needed in addition to the costly libraries. The work in this PhD contributes to our overall goals of providing a cell-screening chip that is simple and cost effective to use and developing highly efficient transfection reagents, which are used in almost every biology lab.

Superhydrophilic–superhydrophobic patterned surfaces have a wide range of applications, but an interesting biological application is the ability to pattern cells as well as aqueous solutions. Therefore, one of the main focuses of this PhD work was to combine our superhydrophilic–superhydrophobic patterned surfaces and our novel transfection reagents to create high-density transfected cell microarrays. These microarrays could then be used, for example, for high-throughput screening of different DNA or RNA libraries to determine the function of genes, or for screening lipid libraries to identify efficient transfection reagents.

Transfection experiments are commonly performed in the liquid state in microtiter plates, so the first objective was to determine if transfection would still work after the lipoplexes had been printed and dried on our nanoporous, polymer surfaces. We tested a commonly used transfection reagent, Lipofectamine[®] 2000, as well as a novel transfection reagent, ScreenFect[®]A, in HEK 293 cells, a commonly used cell line. Once we established that the method of reverse cell transfection worked on our surfaces, the next objective was to determine what factors in our system affect transfection and how to improve the transfection efficiency while minimizing cytotoxicity. Therefore, we tested many factors such as the printing and drying conditions, the cell seeding density, the cell incubation time, the concentration of plasmid DNA in the mixture, the ratio of plasmid DNA to transfection reagent, the concentration of gelatin and fibronectin in the mixture, and the hydrophilic surface chemistry. Since ScreenFect[®]A had never been used for reverse cell transfection, it was important to find the optimal conditions for transfection since it would serve as a model liposome for the other synthesized lipids.

Although the transfection mixtures showed little cross-contamination between the hydrophilic microspots, this may not be true when screening a library of chemicals that have high diffusion rates. Therefore, it would be advantageous to culture cells in arrays of isolated droplets or hydrogels such that each microspot containing a different chemical is separated rather than immersed in a shared culture medium. One of our future goals is to identify chemicals that can enhance the process of cell transfection. As a first step towards achieving this, the objectives for this part of the PhD work were to develop a simple method to create arrays of droplets or hydrogels encapsulating cells

while ensuring cell viability in the small droplet volumes, and to determine if chemicals that were pre-printed in the hydrophilic spots were able to diffuse into the droplet or hydrogel and exert a biological effect. We used the method of discontinuous dewetting to create arrays of individual hydrogels encapsulating cells on hydrophilic microspots that were pre-printed with doxorubicin, a cytotoxic anti-cancer drug, to test our system.

Even though the superhydrophobic barriers were able to inhibit cell adhesion and confine cells within each superhydrophilic spot, the cell-repellent properties diminished over time. Therefore, we aimed to find an alternative method for creating stable and non-toxic surfaces with long-term, anti-biofouling properties. We tested the concept of creating a slippery, liquid layer on a surface to study the stability and cell-repellent properties and compared it with existing anti-fouling surfaces.

In an effort to reduce the materials and time needed to fabricate the superhydrophilic–superhydrophobic patterned surfaces for each experiment, we aimed to develop a method to create multiple copies from a single patterned surface. We tested the ability to transfer the patterned polymer to adhesive tape one thin layer at a time while retaining the properties of the original substrate.

2 Superhydrophobic–superhydrophilic micropatterning: towards genome-on-a-chip cell microarrays

In this chapter, the initial method we used for creating superhydrophilic–superhydrophobic patterned surfaces is presented and their application as high-density cell microarrays is demonstrated. The superhydrophilic microspots absorb aqueous solutions while the superhydrophobic barriers confine the solutions, thus prevent cross-contamination between the microspots and allowing the microspots to be used as reservoirs for transfection mixtures. In addition, the superhydrophobic barriers prevented cell proliferation and cell migration between the microspots. This chapter was originally published as an article in *Angewandte Chemie International Edition* in July 2011 and is reproduced with permission from John Wiley and Sons (Geyer *et al.*, 2011).

Superhydrophobic–superhydrophilic micropatterning: towards genome-on-a-chip cell microarrays

Florian L. Geyer, Erica Ueda, Dr. Urban Liebel, Dr. Nicole Grau and Dr. Pavel A. Levkin

F. L. Geyer, E. Ueda, Dr. U. Liebel, Dr. P. A. Levkin

Institute of Toxicology and Genetics

Karlsruhe Institute of Technology (Germany)

Dr. N. Grau

Medical Faculty Mannheim University of Heidelberg (Germany)

F. L. Geyer, Dr. P. A. Levkin

Department of Applied Physical Chemistry University of Heidelberg (Germany)

Author contributions:

Florian L. Geyer designed and performed the experiments and analysis, and wrote the manuscript.



Erica Ueda contributed to the live cell imaging and reverse cell transfection experiments, and edited the manuscript.



Dr. Urban Liebel contributed helpful discussions about the design of the array and assisted in the method for image analysis.

Dr. Nicole Grau produced the stably transfected cell lines MTly-CMV-eGFP-neo and MTly-CMV-mCherry-neo.

Dr. Pavel A. Levkin contributed to the original idea of the project, the experimental design, and editing of the manuscript.



2.1 Article

Living cells are extremely complex biological systems, and a variety of cell assays have been developed to study these systems *in vitro*. Cell microarrays have emerged as a promising technique that enable cell assays in a highly parallel and miniaturized manner (Hoheisel, 2006; Hook *et al.*, 2006; Perrimon & Mathey-Prevot, 2007; Wheeler *et al.*, 2005; Yarmush & King, 2009). However, owing to cross-contamination and cell migration problems, the density of most current cell microarrays is still limited (Erflé *et al.*, 2007, 2008). Herein, we describe a facile method for the fabrication of arrays of superhydrophilic microspots separated by superhydrophobic barriers. We show that such arrays provide a great opportunity to solve both the cross-contamination and cell-migration problems of living cell microarrays and to enable fabrication of ultra high-density cell microarrays that can be used for genome-wide cell screens using a single array.

The method for the preparation of arrays presented herein is based on creating a grid-like superhydrophobic pattern by UV-initiated photografting on a glass plate coated with a thin layer of superhydrophilic, biocompatible, and transparent nanoporous poly(2-hydroxyethyl methacrylate-co-ethylene dimethacrylate) (HEMA-EDMA). The geometry and size of the produced superhydrophilic spots and superhydrophobic barriers can be precisely controlled by a photomask. The extreme wettability of the microspots guarantees an easy and homogeneous adsorption of the spotting solutions, while narrow superhydrophobic barriers effectively prevent cross-contamination of the spotting solutions between adjacent microspots. Cell experiments carried out with several commonly used cell lines confirmed preferential adhesion and proliferation of cells on the superhydrophilic spots and virtually no cell growth on the superhydrophobic barriers. Finally, the narrow 60 μm superhydrophobic gaps between the spots proved to be highly efficient barriers against cell migration.

The aims of main applications of cell microarrays are to screen chemical (Bailey *et al.*, 2004; Yarmush & King, 2009) or genomic (Hook *et al.*, 2006; Wheeler *et al.*, 2005; Yarmush & King, 2009; Ziauddin & Sabatini, 2001) libraries or to systematically investigate the local cellular microenvironment (Flaim *et al.*, 2005; Hook *et al.*, 2006; Soen *et al.*, 2006; Yarmush & King, 2009). Application of this technique for functional characterization of the genome using the method of reverse cell transfection to perform genome-wide gain- or loss-of-function experiments has attracted exceptional attention (Erflé *et al.*, 2007, 2008; Hook *et al.*, 2006; Neumann *et al.*, 2010; Perrimon & Mathey-Prevot, 2007; Stürzl *et al.*, 2008; Wheeler *et al.*, 2005; Ziauddin & Sabatini, 2001). To produce a microarray for reverse cell transfection, solutions of transfection reagents containing gelatin are printed on a solid substrate in an array pattern and dried. Then, cells are seeded on the array and the uptake of nucleic acids by the cells growing on

each spot results in an array of locally transfected cells within a lawn of non-transfected cells (Figure 2.1A) (Hook *et al.*, 2006). When compared to microwell plates, the cell-microarray approach offers reduced assay volume, increased assay density and throughput, the possibility for long-term storage (Erfle *et al.*, 2007), and eliminates the need for high-throughput fluid transfer equipment once the spotted array is created (Yarmush & King, 2009). The absence of physical barriers separating the probes facilitates microscopy-based analysis of the results (Erfle *et al.*, 2007; Reymann *et al.*, 2009).

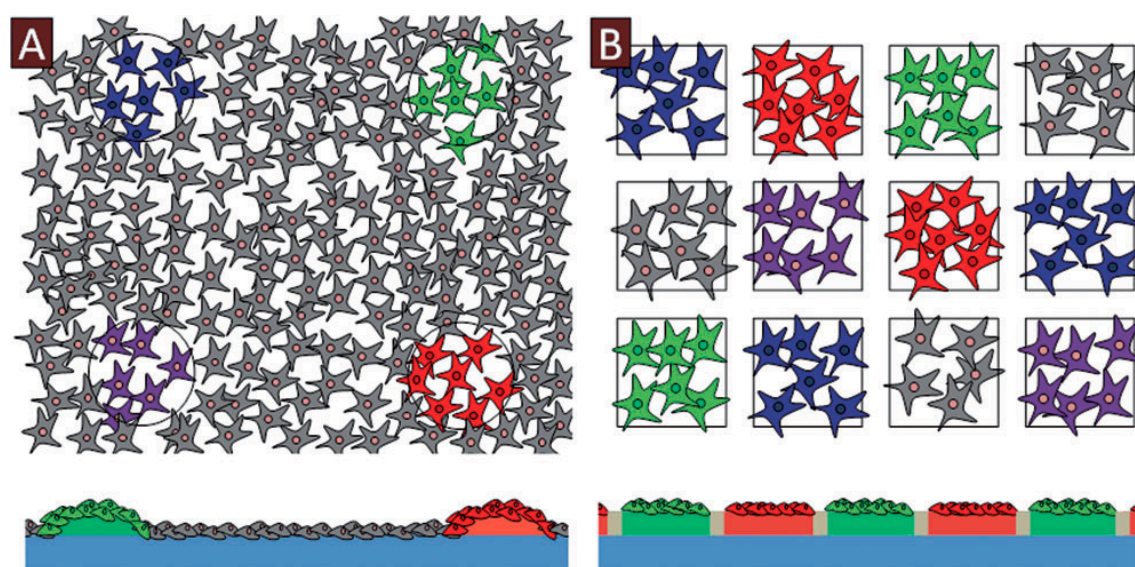


Figure 2.1 Schematic of cell microarrays

(A) Representation of the current state-of-the-art cell microarray. Left: transfected cell clusters are localized in a lawn of non-transfected cells. Cell migration is not controlled; cross-contamination and spot geometry prevent dense spot packing. Bottom: cross-section of the array. The transfection reagents are located in gel pads; cells settle on top of them. (B) View of a desired cell microarray. Precise control of spot geometry, size, and density is possible; cells can only settle on microspots containing the transfection reagents; isolated transfected cell clusters are formed; migration and cross-contamination are prevented.

However, today's cell microarrays have several important limitations. First, the area between spots containing transfection reagents is usually occupied by non-transfected cells, which can easily intrude the spots with transfected cells. In the same way, transfected cells can migrate between adjacent spots. Another problem is that the lack of physical barriers between microspots leads to cross-contamination (Erfle *et al.*,

2008; Hook *et al.*, 2006; Reymann *et al.*, 2009) of the transfection solutions between adjacent spots. Finally, the composition and droplet size of a transfection solution printed on a substrate influence the size and circular shape of the produced microspots, thus limiting the spot-to-spot homogeneity and density of the produced array. These problems have been forcing researchers to keep the distance between microspots relatively large (usually 1 mm or more), thereby limiting the array density and depreciating the potential of the technology (Erflé *et al.*, 2008; Reymann *et al.*, 2009). Figure 2.1A shows the current state-of-the-art cell microarray with the above-mentioned limitations, and Figure 2.1B shows a desired cell microarray with all the limitations solved.

To create a substrate with a superhydrophilic–superhydrophobic pattern, we first prepared a circa 12.5 μm -thin superhydrophilic nanoporous HEMA-EDMA film (Figure 2.2A). This film is synthesized by photopolymerization of a prepolymer mixture between two glass plates (Levkin *et al.*, 2009). The thickness of the polymer film is controlled by two strips of Teflon foil that keep the glass plates apart. The prepolymer mixture consists of the monomer 2-hydroxyethyl methacrylate (24 wt%), the cross-linker ethylene dimethacrylate (16 wt%), a porogen (60 wt%), and the initiator 2,2-dimethoxy-2-phenylacetophenone (1 wt% with respect to monomers). A mixture of cyclohexanol and n-decanol (4:1 w/w) is a suitable porogenic solvent, which leads to the nanoporous structure of the polymer with a pore size in the range of 100–500 nm according to the scanning electron microscope (SEM) images (Figure 2.2D; Supporting Information, Figure 2.S1). The small size of the pores is important for achieving transparency of the wetted polymer film due to reduced light scattering (Supporting Information, Figure 2.S4). The combination of the high porosity (60%) of the polymer coated on a glass plate with the hydrophilic hydroxyethyl surface functionality makes the plate extremely wettable with static, advancing, and receding water contact angles (WCAs) close to 0° in the case of a dry surface and a static WCA of 15° in the case of the wetted surface (Supporting Information, Figure 2.S2).

The next step in the creation of the array is the preparation of a grid-like superhydrophobic pattern on the superhydrophilic HEMA-EDMA film (Figure 2.2B). To create the superhydrophobic pattern, the HEMA-EDMA surface is modified with brushes of poly(2,2,3,3,3-pentafluoropropyl methacrylate-co-ethylene dimethacrylate) (PFPPMA-EDMA) by photografting (Rånby, 1992). The method of photografting consists of UV irradiation of the porous polymer wetted with a mixture composed of 2,2,3,3,3-pentafluoropropyl methacrylate, ethylene dimethacrylate, initiator benzophenone, and a water/tert-butyl alcohol mixture as solvent. According to SEM, photografting does not alter morphology of the porous structure, while the X-ray photoelectron spectroscopy (XPS) measurements clearly show modification of the HEMA-EDMA surface with pentafluoropropyl functionalities (Supporting Information,

Figure 2.S2). The surface modification results in the transformation of the superhydrophilic surface into a superhydrophobic material with static, advancing, and receding WCAs as large as 165° , 167° , and 157° , respectively (Figure 2.2D; Supporting Information, Figure 2.S2). As photografting is a photochemical method, we use a standard photomask for creating precise patterns of superhydrophobicity on the superhydrophilic substrate. The patterning process is accurate on a micrometer scale, can be applied to large areas, and takes place throughout the whole thickness of the porous polymer film (Figure 2.3).

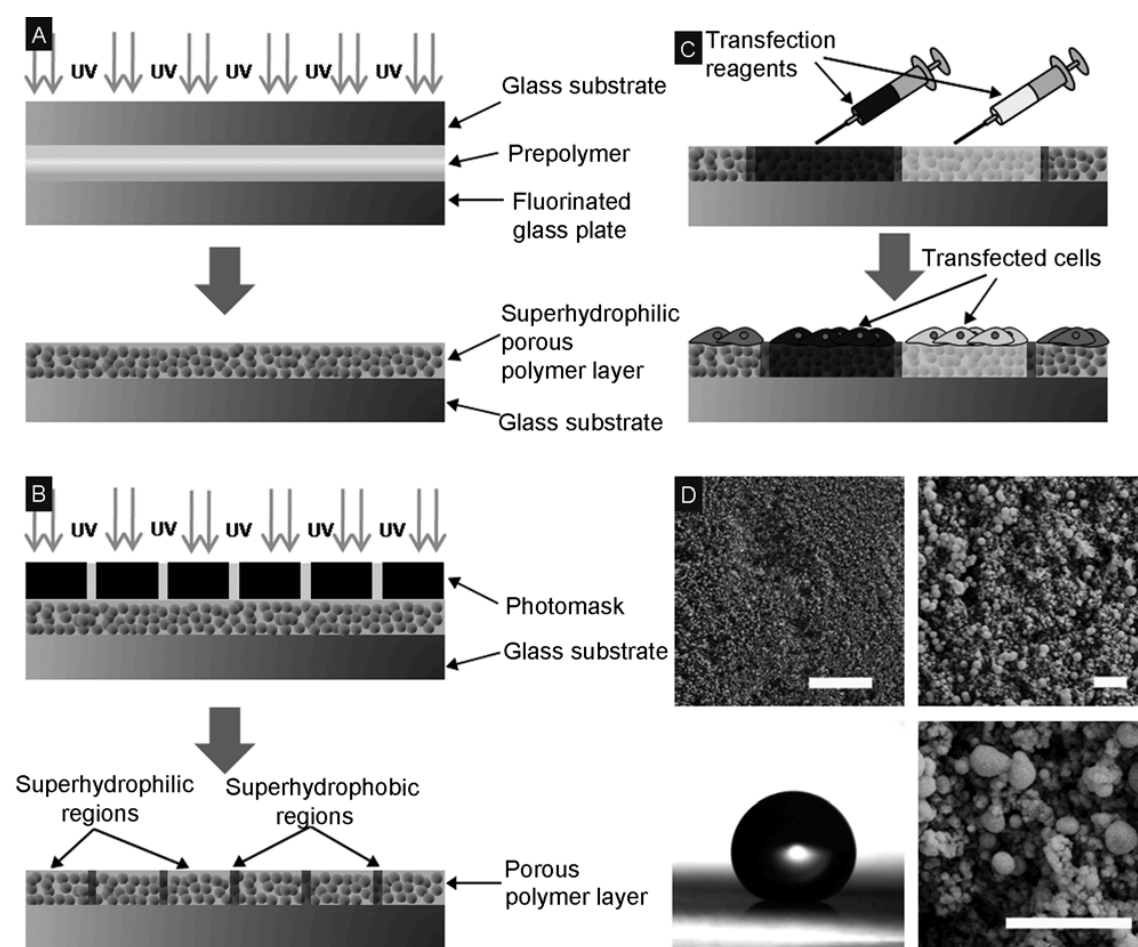


Figure 2.2 Schematic of superhydrophilic–superhydrophobic pattern fabrication

(A) The preparation of a superhydrophilic porous polymer film on a glass substrate by UV-initiated free-radical polymerization. (B) Fabrication of the superhydrophobic grid-like pattern on the superhydrophilic surface by UV-initiated photografting. (C) Representation of an application of the array in a cell-screening experiment (for example, reverse cell transfection): the array is printed with transfection mixtures and dried. Seeded cells are transfected by the reagents incorporated into the

superhydrophilic spots. (D) Water droplet on the superhydrophobic nanoporous HEMA-EDMA photografted with PFPMA, and SEM images of the same polymer. Scale bars: top left: 10 μm , top right and bottom: 1 μm .

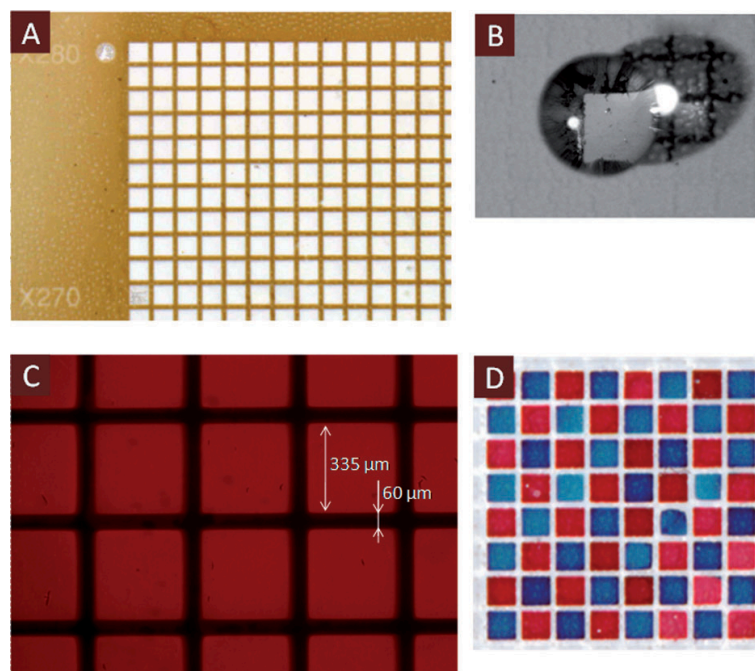


Figure 2.3 Images of microarrays

(A) Part of the array with 50400 superhydrophilic microspots on an $11 \times 7 \text{ cm}^2$ glass slide. (B) A water droplet in a single superhydrophilic microspot. The droplet does not spread because of the superhydrophobic barriers. (C) Fluorescent microscope image showing the array with spots filled with Rhodamine 6G. (D) The array with microspots filled with alternating water solutions of Neutral Red and Methylene Blue dyes.

Based on criteria for performing an efficient single-chip genome-wide RNAi cell-screening experiment, we designed a photomask (see the Supporting Information) that was used to create an ultra high-density array of 50400 superhydrophilic square spots separated by narrow 60 μm -wide superhydrophobic barriers (Figure 2.3).

The surface of an ideal high-density array for reverse cell transfection should fulfill the following biological requirements: 1) it should be biocompatible and nontoxic; 2) cells should adhere to the microspots; 3) cells should not occupy the area between the microspots; and 4) cell migration between neighboring microspots should be minimized. We tested the behavior of several commonly used cell lines on the superhydrophilic–superhydrophobic array that was produced. Fluorescent rat mammary

carcinoma cells (MTly-CMV-eGFP-neo and MTly-CMV-mCherry-neo), Hepa, and HEK 293 cells were seeded on the array and incubated for 2 days, which is the time usually required for a reverse cell transfection experiment (Erfle *et al.*, 2008; Neumann *et al.*, 2010). Cell seeding procedures were optimized to obtain a monolayer of cells on the non-grafted areas after 48 h of incubation. Figure 2.4 shows the results of these experiments. The superhydrophilic microspots were populated by all tested cell types. At the same time, superhydrophobic gaps separating the microspots were significantly less occupied. Moreover, cells sitting on the superhydrophobic gaps were apparently apoptotic, as was testified by round cell morphologies and the absence of their motility. Thus, this cell behavior leads to the formation of arrays of isolated cell colonies in each superhydrophilic microspot separated by superhydrophobic barriers.

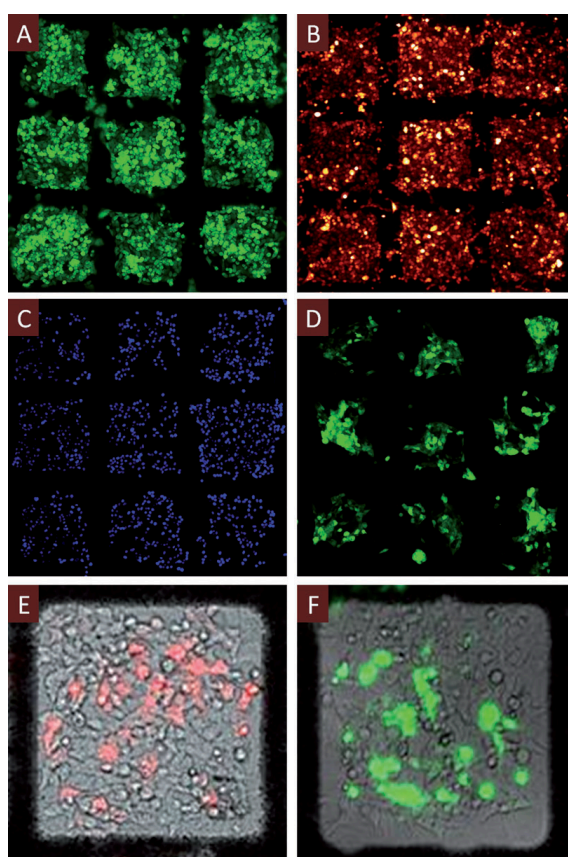


Figure 2.4 Cells cultured on microarrays

Fluorescent microscope images of four different cell lines after growing for 48 h on the array. (A) MTly-eGFP cells. (B) MTly-mCherry cells. (C) HEK cells, DAPI-stained. (D) Hepa cells, eGFP expressing. HEK cells transfected with different plasmids sitting on two superhydrophilic spots. (E) mCherry plasmid. (F) eGFP plasmid.

For HEK 293 cells, we quantified the difference between cell occupation of the superhydrophilic spots and the superhydrophobic areas. After two days of culturing, 79 cells on average occupy one superhydrophilic spot, and less than 2 cells can be found on a superhydrophobic barrier between two spots. Similar experiments with MTly-mCherry cells at three different time points showed that there was almost no difference immediately after the initial precipitation of cells, and the produced difference in cell occupation constantly increased during the cell growth and proliferation (Supporting Information, Figure 2.S5). This process is clearly seen from the time-lapse videos recorded for MTly-eGFP and HEK 293 cells (Supporting Information, Videos S1–3). These videos also confirm that there is virtually no cell migration between neighboring microspots, despite the distance of only 60 μm .

Superhydrophobicity is a result of combination of micro- and nanoscale roughness and the intrinsic hydrophobicity of a material. A rough, superhydrophobic surface usually consists of small asperities. Water can either penetrate these and wet the whole surface (Wenzel state), or remain on top of them owing to its surface tension (Cassie–Baxter state) (Li *et al.*, 2007; Quéré, 2005). We hypothesized that the surprising cell-resistant properties of the superhydrophobic barriers was the result of air trapped inside the porous polymer surface, that is, the Cassie–Baxter state. To investigate this hypothesis, we analyzed cell behavior on arrays transformed into the Wenzel state. The difference in cell occupation between microspots and the wetted barriers was significantly decreased for the MTly cells (Supporting Information, Figure 2.S6B). In the case of HEK 293 cells, no pattern at all was formed on the array in the Wenzel state and the cells could freely migrate and proliferate (Supporting Information, Figure 2.S6C).

To show the applicability of the array for reverse cell transfection experiments, we filled several microspots with two different plasmid-based mixtures for reverse cell transfection (Stürzl *et al.*, 2008). The array was dried, seeded with HEK 293 cells, and incubated for 48 h. The resulting expression of mCherry and green fluorescent proteins in HEK 293 cells is shown in Figure 2.4 E,F.

In conclusion, we have developed a facile method for creating ultra high-density cell microarrays based on the photochemical preparation of superhydrophilic spots separated by thin superhydrophobic barriers. We envision that this technology will enable fabrication of “genome-on-a-chip” cell microarrays and will transform genome-wide cell-screening experiments into a significantly more affordable and convenient biological method. Finally, the new technique can be used for patterning cell clusters in a predetermined spatial order and for creating high-density cell microarrays for testing other classes of biologically active compounds. Experiments for creating cell microarrays for screening proteins and drug candidates are now underway in our laboratory.

2.2 Supporting information

Array preparation

Glass surface modification

To achieve covalent attachment of the polymer layer, the glass surfaces are first activated and then functionalized with an anchor-group for methacrylates. Cleaned glass-plates are immersed in 1 M NaOH for 1 h and afterwards washed with deionized water followed by immersing them in 1 M HCl for 30 min, washing with deionized water and drying with a nitrogen gun.

Modification of glass-plates: Several drops of a solution containing 20 vol% 3-(trimethoxysilyl)propyl methacrylate in ethanol adjusted to pH = 5 with acetic acid are dropped on an activated glass-plate. The plate is covered with another activated glass-plate. No bubbles should be trapped between the two plates. The solution is reapplied after 30 min. After another 30 min the plates are washed with acetone and dried with a nitrogen gun.

Fluorination of glass-plates: An activated glass-plate is placed in a vacuumed desiccator together with a vial containing several drops of tridecafluoro-(1,1,2,2)-tetrahydrooctyltrichlorosilane overnight.

Polymerization procedure and photografting

Two strips of Teflon film (American Durafilm Co.), defining the thickness of the polymer layer, are placed at the edges of a glass-plate and another glass-plate is clamped on top of it. The polymerization mixture is injected in the mold between them and irradiated for 15 min with 12.0 mW cm^{-2} 260 nm UV-light. The mold is then carefully opened using a scalpel.

Microporous polymers: Two plates modified with the methacrylate-anchor are used for polymerization. For microporous polymers (mixtures 2,3), the glass-plates can be easily separated using a scalpel after the polymerization has finished. The polymer usually breaks easily and a homogeneous rough surface is formed. A layer with approximately the spacer's thickness adheres to the top plate while a very thin layer adheres to the bottom plate. The plates are extensively washed with methanol or ethanol and kept in methanol for some minutes.

Nanoporous polymers: By decreasing the average pore size in order to obtain a transparent polymer, the polymer gains mechanical strength and the separation of the plates becomes non-trivial. Plates held together by a nanoporous polymethacrylate are not only hard to separate with a scalpel, but the polymer also breaks inhomogeneously and the resulting topographical inhomogeneity is unsuited for a microarray surface.

With an inert, fluorinated bottom-plate, breaking of the layers can be avoided. The impossibility of covalent attachment to this plate for the growing polymer allows for the whole polymer to stick to the top plate during the separation process. The fluorinated plate can be reused several times. The resulting nonporous superficial layer can be easily removed by applying and rapidly removing adhesive film (“Scotch tape”) immediately after separating the plates while the layer is still wetted with porogen. A homogeneous, porous surface is formed. The plate is washed extensively with methanol or ethanol and kept in methanol for some minutes.

Photografting: The method of photografting consists of UV-irradiation of the porous polymer wetted with a photografting mixture composed of a mixture of 2,2,3,3,3-pentafluoropropyl methacrylate (PFPMA), EDMA, initiator benzophenone, and a water/tert-butanol mixture as a solvent. The polymer layer is wetted with the respective photografting mixture and covered with a fluorinated plate. The photomask is placed on top and it is irradiated for 30 min with 12.0 mW cm^{-2} 260 nm UV-light. The obtained pattern is washed extensively with methanol or ethanol and kept in methanol for some hours.

Polymerization mixtures:

Nanoporous HEMA-EDMA (mixture 1): poly(2-hydroxyethyl methacrylate-co-ethylene dimethacrylate) (HEMA-EDMA): HEMA (24 %wt.), EDMA (16 %wt.), 1-decanol (12 %wt.), cyclohexanol (48 %wt.) and 2,2-dimethoxy-2-phenylacetophenone (DMPAP) (1 %wt. with respect to monomers).

Microporous HEMA-EDMA (mixture 2): poly(2-hydroxyethyl methacrylate-co-ethylene dimethacrylate): HEMA (24 %wt.), EDMA (16 %wt.), 1-decanol (40 %wt.), cyclohexanol (20 %wt.) and 2,2-dimethoxy-2-phenylacetophenone (1 %wt. with respect to monomers).

Microporous BMA-EDMA (mixture 3): poly(butyl methacrylate-co-ethylene dimethacrylate): BMA (24 %wt.), EDMA (16 %wt.), 1-decanol (40 %wt.), cyclohexanol (20 %wt.) and 2,2-dimethoxy-2-phenylacetophenone (1 %wt. with respect to monomers).

Photografting mixture:

Crosslinked 2,2,3,3,3-pentafluoropropyl methacrylate grafting-mixture (Photomixture 1): 15 %wt. 2,2,3,3,3-pentafluoropropyl methacrylate, 1 %wt. ethylene dimethacrylate in 1/3 (v./v.) mixture of water-tert-butanol containing 0.25 %wt. benzophenone

Designing a cell microarray for genome-wide cell screening experiments

The design of a photomask is based on the following considerations. To perform an efficient single-chip genome-wide RNAi cell screen, at least 50000 separate cell transfection experiments have to be carried out to cover a full genome RNA library (~23000 genes) in duplicate and including all necessary control experiments. Another important criterion is the area of a superhydrophilic spot, which should be large enough to accommodate at least ~100–200 cells per spot to achieve statistical significance (Neumann *et al.*, 2010) and thus equals an area of about $105 \mu\text{m}^2$. In order to accommodate 50000 such spots on the area of a standard microtiter plate, spots should have square geometry for realizing dense packing and the gap between adjacent spots should be about $60 \mu\text{m}$ or less. Based on criteria for performing a genome-wide RNAi cell screen, we designed a photomask containing 50400 dark squares ($335 \times 335 \mu\text{m}$) separated by $60 \mu\text{m}$ UV-transparent gaps on the area of about $11 \times 7 \text{ cm}$, i.e. the usable area of a standard microwell plate. Using this photomask, an ultrahigh-density array of 50400 superhydrophilic square spots separated by narrow superhydrophobic barriers has been created (Figure 2.3).

Array properties

To visualize the changing morphology from microporous to nanoporous HEMA-EDMA (mixtures 1,2), scanning electron micrographs were taken from both polymer surfaces (Figure 2.S1). It can clearly be seen that the feature-sizes (pore-size, globule-size) significantly decrease for a polymer created from mixture 1 in comparison to a polymer created from mixture 2. This is a sole effect of the changing porogen composition, as the same monomers are being used in the same ratios.

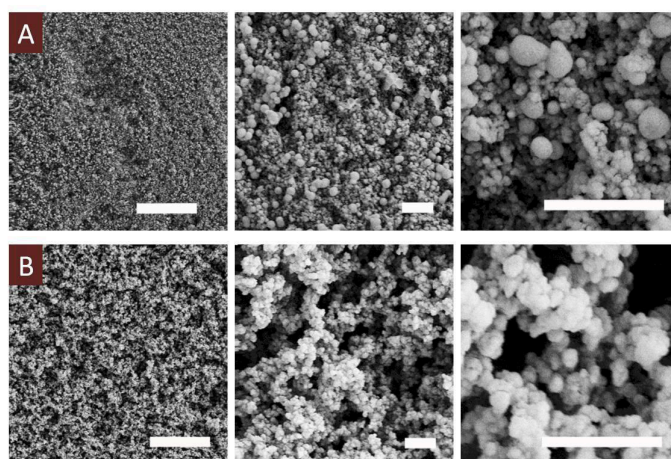


Figure 2.S1 SEM images of HEMA-EDMA surfaces

(A) Surface of the nanoporous HEMA-EDMA (mixture 1). Scale bars from left to right: $10 \mu\text{m}$, $1 \mu\text{m}$, $1 \mu\text{m}$. (B) Surface of the microporous HEMA-EDMA (mixture 2). Scale bars from left to right: $10 \mu\text{m}$, $1 \mu\text{m}$, $1 \mu\text{m}$.

X-ray photoelectron spectroscopy (XPS) measurements confirmed the surface modification by photografting (Figure 2.S2D).

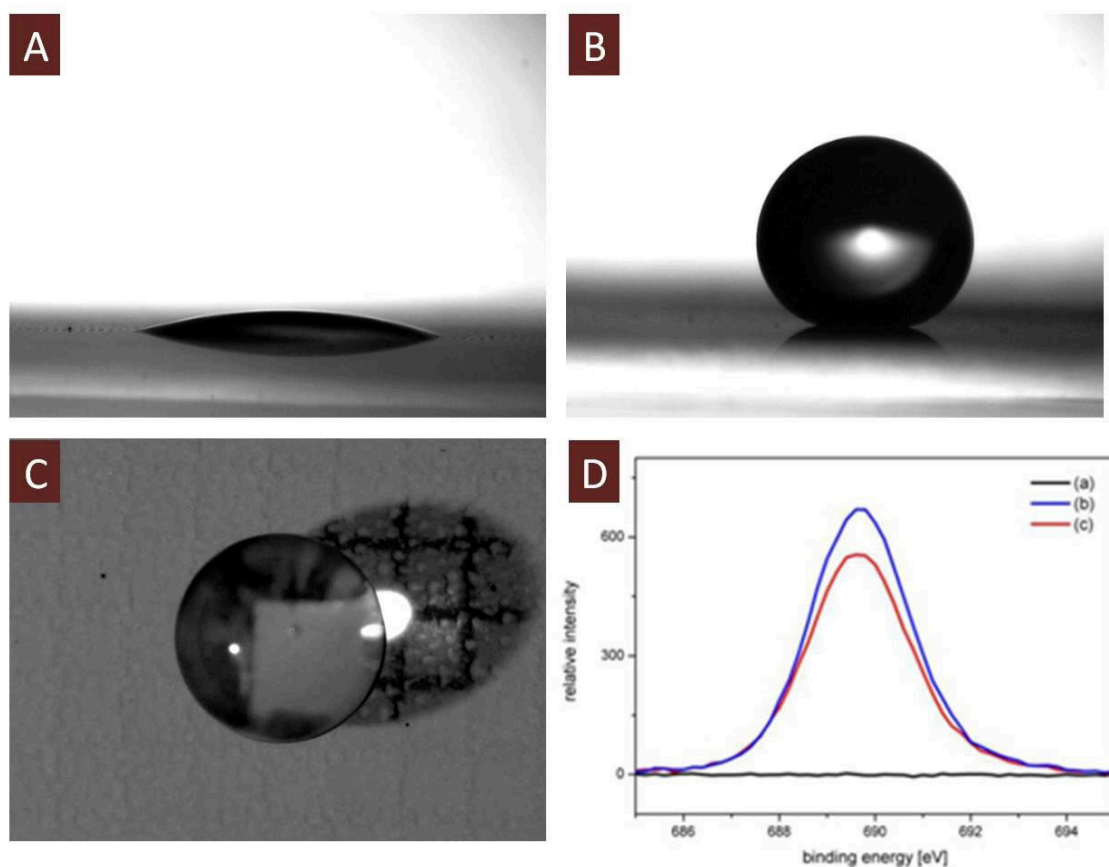


Figure 2.S2 XPS measurements of HEMA-EDMA surfaces

(A) Photograph of a water droplet on HEMA-EDMA nanoporous surface; (B) a water droplet on the HEMA-EDMA nanoporous surface photografted with PFPMA; (C) a single superhydrophilic microspot of the array filled with a water droplet; (D) XPS fluorine peaks obtained from an $8 \times 4 \text{ mm}^2$ area on the unmodified HEMA-EDMA (black line), HEMA-EDMA photografted by PFPMA without a photomask (blue line) and a HEMA-EDMA surface photografted with PFPMA through a grid-like photomask to create the array (red line).

A nanoporous HEMA-EDMA photografted with PFPMA-EDMA on a large area possesses static, advancing, and receding WCAs of 165° , 167° , and 157° , respectively (Figure 2.S2B). A microporous poly(butyl methacrylate-*co*-ethylene dimethacrylate) (BMA-EDMA) (mixture 3), which is known for its superhydrophobic properties, shows static θ_{stat} , advancing θ_{adv} , and receding θ_{rec} water contact angles of only 153° , 161° , and

151°. Despite the decreased pore sizes, the contact angles of the PFPMA-photografted HEMA-EDMA are even higher than for microporous BMA-EDMA. This is clearly an effect of the extremely hydrophobic fluorinated side chain.

When wetted with water, square shaped droplets are kept in each spot of an array. The spots turn transparent (transition to Wenzel state) (Figure 2.S4), while the barriers remain in a dry and water repelling Cassie–Baxter state (Figure 2.S3A). The Cassie–Baxter state can be visualized by imaging an array wetted with water and irradiating it with light from a low angle. The reflection of light from the superhydrophobic areas is clearly seen under a microscope (Figure 2.S3C). Due to their low surface energy, ethanol and other organic solvents easily wet both spots and barriers, thereby making the whole array transparent (Figure 2.S3B).



Figure 2.S3 Transparency of the array

Pictures of an array placed on a printed paper sheet: (A) wetted with water; (B) wetted with ethanol. (C) Brightfield image of the barriers in a Cassie–Baxter state.

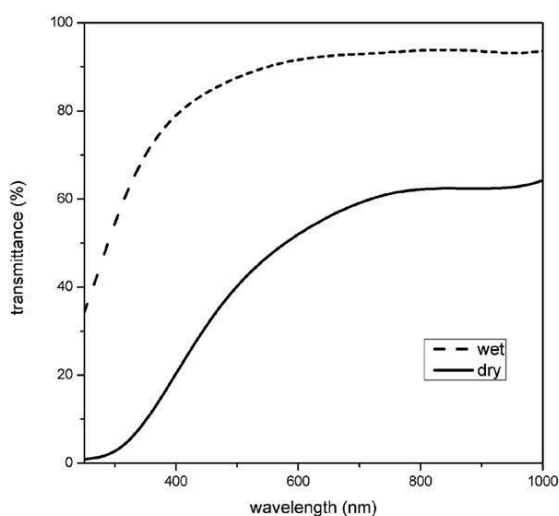


Figure 2.S4 UV-Vis-NIR spectra

UV-Vis-NIR transmittance spectra of wetted and dry nanoporous HEMA-EDMA.

Cell studies

Cell culturing and observation

All cell-culturing takes place under the clean bench. Cell suspension is obtained by trypsinizing a confluent (80% monolayer) culture grown in a Petri dish in an incubator (37°C, 5% CO₂) for 2–3 days. Trypsinization is stopped by adding 10 ml Dulbecco's Modified Eagle's Medium (DMEM) containing serum.

HEK 293, GFP-expressing Hepa 1.6 cells, eGFP-expressing mouse mammary carcinoma cells, and mCherry-expressing rat mammary carcinoma cells are cultured in DMEM containing 10% of fetal bovine serum (FBS). For sterilization the polymer-coated glass-slides are kept in ethanol for some minutes, dried in air, and placed in Petri dishes. Medium is added so that the plates are fully covered. Then, cell suspension is added and it is homogenized with a pipette. The seeded arrays are incubated at 37°C, 5% CO₂.

The array occupation is imaged in brightfield- and fluorescence-mode of a fluorescence microscope 48 h after seeding. For observing the non-fluorescent HEK 293 cells, they are first stained with 4',6-diamidino-2-phenylindole (DAPI) (1/10000 v/v in phosphate buffered saline (PBS)). First, the array occupied by HEK 293 cells is aspirated. PBS is added carefully from the side and it is aspirated again. A solution of 4% formaldehyde in PBS is added and the cells are fixed for 40 min without waving the dishes. It is aspirated again and DAPI is added, then the cells are stained for 40 min without waving. The dish is aspirated again and PBS is added. It is imaged 20 min later without changing the PBS again.

For investigating the cell migration on the arrays, time lapse microscopy is used to observe the growth of HEK 293 and eGFP-expressing mouse mammary carcinoma cells for 48 h (Videos S1,2). A fluorescent time-lapse microscope equipped with a full environmental chamber is used to observe the cell microarray for 48 h.

In Video S1, two air bubbles trapped on the surface during the seeding process can be seen. This sometimes happens when the dry array is initially wetted; the formed bubbles can be easily removed by homogenizing the suspension with a pipette. Bubbles prevent cells from precipitating from the suspension onto the spot surface. After the bubble has dissolved in water, a cell-free spot can be observed. It can be seen that no cells intrude the unoccupied spots until the adjacent spots become too confluent and the cell layer is forced to grow outside its confinement. Videos S2 (merged brightfield and GFP channels) and S3 (GFP channel) show eGFP-expressing mouse mammary carcinoma cells growing on the array. In the beginning, cells precipitate everywhere. As they start growing, it can be seen that movement of the cells that initially precipitated on the grafted barriers is drastically decreased. Cells growing on the barriers virtually do

not migrate. Moreover, cells growing in the hydrophilic squares do not enter the grafted areas.

These experiments show that not only do cells prefer adhering to the hydrophilic surface, but that cell migration across the barriers into adjacent spots is minimized, thus enabling the formation of narrow spatially separated cell clusters.

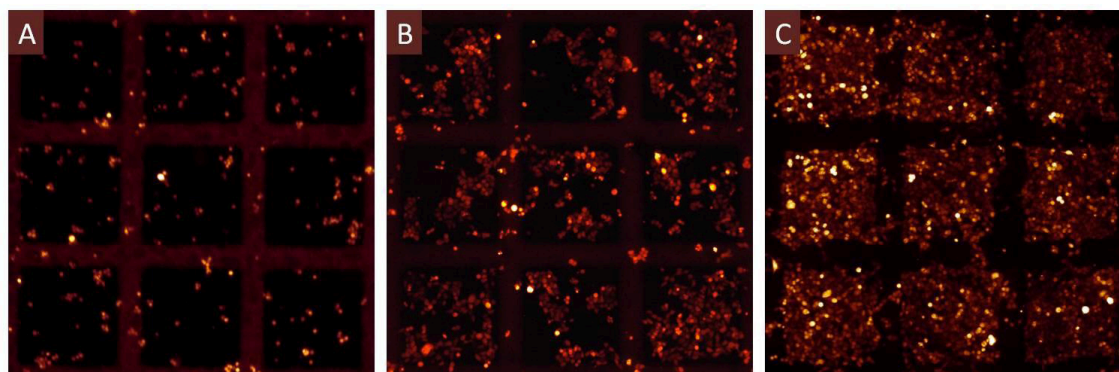


Figure 2.S5 Time-lapse images of cells cultured on a microarray

(A) mCherry-expressing rat mammary carcinoma cells on the seeding day, (B) after one day, (C) and after two days of culturing.

Quantification of cell occupation

For HEK 293 cells we quantified the difference between cell occupation of the superhydrophilic spots and the superhydrophobic areas. We use the ratio of cell density (cells per unit of surface area) on the microspots to that on the superhydrophobic areas. The cell densities are determined from the fluorescence microscope images using the LabView software. After two days of culturing, the ratio for HEK 293 cells was 7.5. In average, 79 cells occupy one spot and less than 2 cells can be found on the grafted material between two spots. It should be mentioned, that cells sitting on the barriers are usually adherent to a confluent cell layer from a hydrophilic square, which spreads outside its confinement for spatial reasons. These cells do not contribute to cross-migration as long as the layer does not spread to an adjacent spot, but decrease the determined ratio.

Origin of cell resistant properties: superhydrophobic surface in Cassie–Baxter or Wenzel state

For sterilization the polymer-coated glass slides are kept in ethanol for some minutes; this also transitions the superhydrophobic areas to the Wenzel state. To keep the Wenzel

state, the array is not dried, but immediately placed in PBS for some minutes. The PBS is exchanged two times to remove all ethanol. For seeding the array, the PBS is aspirated and cell suspension is added.

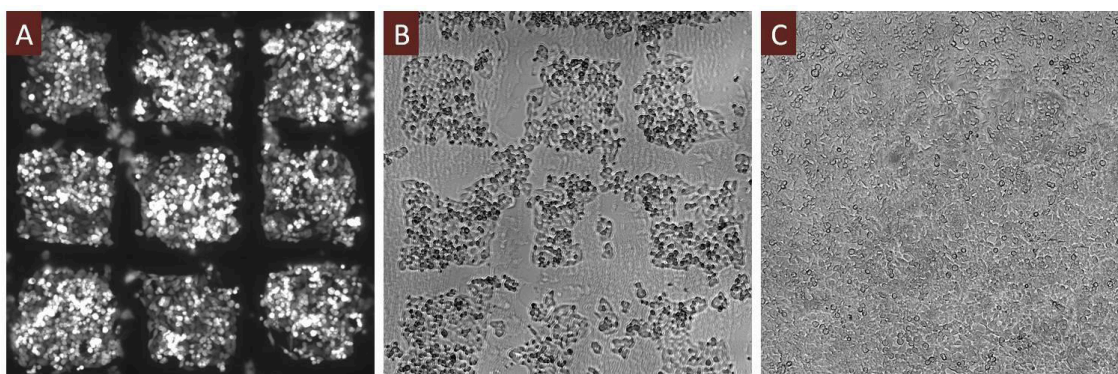


Figure 2.S6 Cells cultured on microarrays in a Cassie–Baxter vs. Wenzel state

Cells cultured on the array for 48 h. Mouse mammary carcinoma cells seeded on the array in (A) Cassie–Baxter state, GFP channel and in (B) Wenzel state. (C) HEK 293 cells seeded on the array in Wenzel state.

The influence of the superhydrophobic state on the cell behavior is investigated with HEK 293 and eGFP-expressing mouse mammary carcinoma cells. While for the mouse cells, a contrast between cell proliferation on grafted and non-grafted areas can be seen even in Wenzel state, no pattern is visible in the case of the HEK 293 cells. It can be concluded that the fluorination of the surface increases cell resistance. However, the highly water repellent Cassie-Baxter state is essential for making surfaces that can efficiently prevent cell-migration and cell proliferation of different cell types.

Cell transfection

Cell transfection is carried out according to a standardized protocol (Stürzl *et al.*, 2008). A 0.4 M solution of sucrose in DMEM was prepared and filtered through a 0.22 μm sterile filter. 1.5 μg DNA in 5 μl water are added to 3 μl of the sucrose solution. 3.5 μl Lipofectamine[®] 2000 (Invitrogen) are added to the mixture and it is incubated for 20 min at room temperature, afterwards 7.25 μl of 0.2% (w/v) gelatin (Sigma) solution are added. The sterilized patterned substrates are manually spotted with a pipette or a sterile needle under the clean bench. The spotted samples are dried overnight and stored sterile at room temperature before HEK 293 cells are seeded.

Experimental details

Materials and instrumentation: All polymerization and photografting were carried out on an OAI Model 30 deep UV collimated light source (San Jose, CA, USA) fitted with an USHIO 500 W Hg-xenon lamp (Japan). Irradiation power was calibrated to 12.0 mW cm^{-2} (5.10 mW cm^{-2} after cover plate, 4.77 mW cm^{-2} after cover plate and photomask) using an OAI 360 UV Power Meter with a 260 nm probe head. Scanning electron microscopy images were obtained using the LEO 1530 SEM (Institute of Nanotechnology at the KIT). The samples were gold sputtered with 15 nm gold using the Balzers Union MED 10. For UV-VIS-NIR spectra, a Micropack DH-2000-BAL UV-Vis-NIR light source was used. XPS measurements were carried out on a Leybold-Heraeus MAX200 with an EA200 hemispheric energy-analysator as the energy dispersive element and a 300 W magnesium anode as the X-ray source. ImageJ software with a DropSnake plugin was used to measure static and dynamic water contact angles. LabView was used for the quantification of the cell-occupation of HEK 293 cells as seen in Figure 2.4. Schott (Germany) Nexterion Glass B UV transparent glass-plates were used as substrates for polymer layers. For the time-lapse experiments, an Axiovert 200M automated microscope suited with a CO₂ and temperature control chamber was used. For the pictures seen in Figures 2.4B–D and 2.S5 a Leica DM 5500 fluorescence microscope was used.

Butyl methacrylate was purchased from Fluka, all other monomers from Sigma-Aldrich. Monomers were purified before usage by passing them through a short column packed with basic aluminum oxide to remove the inhibitors. Biochemicals were purchased from Invitrogen. Cell lines were provided by the Institute of Toxicology and Genetics (Karlsruhe Institute of Technology). The colored pattern in Figure 2.3D was obtained via manually addressing alternating spots with a 0.3 mm i.d. needle. Blue spots were colored with methylene blue (8 g L^{-1}), red spots with neutral red (8 g L^{-1}).

For the occupational experiments seen in Figure 2.4, eGFP-expressing mouse mammary carcinoma cells were seeded on the array with an initial density of $90000 \text{ cells cm}^{-2}$ (Figure 2.4A), mCherry- expressing rat mammary carcinoma cells were seeded in an initial density of $17500 \text{ cells cm}^{-2}$ (Figures 2.4B, 2.S5), HEK 293 cells were seeded with an initial density of $15300 \text{ cells cm}^{-2}$ (Figure 2.4C) and eGFP-expressing Hepa 1.6 cells were seeded with an initial density of $33100 \text{ cells cm}^{-2}$ (Figure 2.4D). For the time lapse experiments, HEK 293 cells were seeded with an initial density of $36000 \text{ cells cm}^{-2}$, mouse mammary carcinoma cells were seeded with an initial density of $90000 \text{ cells cm}^{-2}$. For the reverse transfection, HEK 293 cells were seeded with an initial density of $60000 \text{ cells cm}^{-2}$.

3 Superhydrophilic–superhydrophobic patterned surfaces as high-density cell microarrays: optimization of reverse transfection

Previously, we introduced the concept of using superhydrophilic–superhydrophobic patterned surfaces as cell microarrays. In this chapter, more recent work is presented with two major improvements. First, the method of pattern fabrication was improved by implementing a faster and more robust procedure developed in our group using UV-induced thiol-yne click chemistry (presented in the next chapter). Second, we acquired a non-contact piezoelectric dispenser that enabled us to accurately address and dispense transfection mixtures into each hydrophilic microspot, thus allowing us to identify and test several factors that influence transfection efficiency and toxicity for a new transfection reagent. This chapter will be submitted as an article for publication.

Superhydrophilic–superhydrophobic patterned surfaces as high-density cell microarrays: optimization of reverse transfection

Erica Ueda,^a Wenqian Feng^{ab} and Pavel A. Levkin^{*ac}

^a Institute of Toxicology and Genetics, Karlsruhe Institute of Technology, 76021 Karlsruhe, Germany

^b Department of Organic Chemistry, Heidelberg University, 69120 Heidelberg, Germany

^c Department of Applied Physical Chemistry, Heidelberg University, Germany

Author contributions:

Erica Ueda designed and performed the experiments and analysis, and wrote the manuscript.



Wenqian Feng developed the fabrication method for the superhydrophilic–superhydrophobic patterned surfaces, which will be submitted as an article for publication separately.



Pavel A. Levkin contributed to the original idea of the project, the experimental design, and editing of the manuscript.



3.1 Article

Abstract

Liposomal reagents are frequently used to transfect cells with nucleic acids for gene expression analysis, but their efficiency and toxicity can vary widely depending on factors such as the cell type and the nucleic acid to be delivered into the cell. Recently, a library of biomimetic lipids was synthesized in an effort to identify efficient and non-toxic transfection reagents, and to ultimately understand the structure–function relationship for the rational design of new lipids. To be able to screen the lipids in an efficient and economical way, we developed high-density superhydrophilic–superhydrophobic micropatterned polymer substrates such that the superhydrophobic barriers confined both the printed transfection mixtures and the seeded cells within each superhydrophilic spot. One of the novel lipids from the lipid library, ScreenFect[®]A, was chosen as a model for the other lipids and was used to test the method of reverse transfection on the patterned surfaces. HEK 293 cells were cultured on the printed microarrays for two days, and several factors that influenced transfection efficiency and cell number were identified. Higher levels of transfection were achieved on 3-mercaptopropionic acid versus cysteamine-functionalized hydrophilic spots, as well as when gelatin and fibronectin were added to the transfection mixture, while minimizing the amount of transfection reagent improved cell viability. We demonstrate that reversely transfected cell microarrays can be used to test the efficiency and toxicity of novel transfection reagents, and can subsequently be used to optimize the transfection conditions before performing further genetic screens.

Introduction

Gene expression analysis through overexpression and knockdown studies is a powerful tool to help identify the unknown functions of genes and proteins and their role in biological pathways (Boutros & Ahringer, 2008; Echeverri & Perrimon, 2006; Krausz, 2007; Moffat & Sabatini, 2006; Mohr *et al.*, 2010; Mukherji *et al.*, 2006). This information could be used to elucidate genetic determinants of diseases and potential therapies (Kassner, 2008; MacKeigan *et al.*, 2005; Xia & Wong, 2012). Screening of gene libraries can be performed using microtiter plates, but that can require large amounts of costly reagents and materials. High-density cell microarrays offer a cost-effective alternative by being able to screen thousands of probes at once in a miniaturized and parallelized manner (Erfle *et al.*, 2007; Fujita *et al.*, 2012; Geyer *et al.*, 2011; Mannherz *et al.*, 2006; Neumann *et al.*, 2006; Rajan *et al.*, 2011; Rantala *et al.*, 2011; Silva *et al.*, 2004; Starkuviene *et al.*, 2007; Stürzl *et al.*, 2008; Wheeler *et al.*, 2005).

Liposomal reagents are often used to transfect cells when performing genetic screens; however, their efficiency can be highly dependent on factors such as the cell type and the nucleic acid to be delivered into the cell and they can also cause high cytotoxicity. Recently, several groups including ours used combinatorial chemistry to create libraries of cationic lipid-like molecules, with the aim of synthesizing efficient and non-toxic transfection reagents and to ultimately understand the structure–function relationship (Akinc *et al.*, 2008; Li *et al.*, 2012b, 2013b; Mahon *et al.*, 2010; Sun *et al.*, 2012; Wang *et al.*, 2012). This could lead to a better understanding of the mechanisms of transfection, which are still not fully understood, and subsequently to the rational design of transfection reagents tailored to specific cell types or to the nucleic acids to be delivered.

To be able to screen the lipid libraries in an efficient and economical way, we aim to use the method of high-density reversely transfected cell microarrays (Ziauddin & Sabatini, 2001) to screen thousands of lipids at once while using fewer reagents and consumables. As opposed to using uncoated glass slides that are conventionally used for cell microarrays, in this work we used superhydrophilic–superhydrophobic micropatterned polymer substrates (Feng *et al.*, 2014) due to the ability of the superhydrophobic barriers to confine both the printed transfection mixtures and the seeded cells within each superhydrophilic spot (Fig. 3.1).

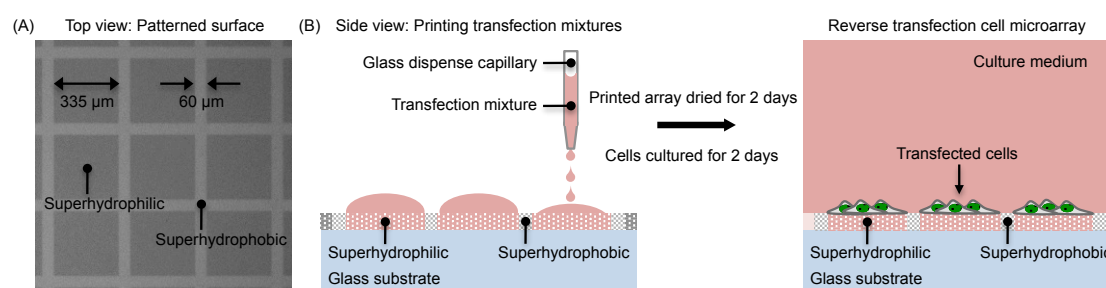


Figure 3.1 Schematic of the reverse transfection procedure using patterned surfaces

(A) Brightfield image of a 12.5 μm -thick nanoporous polymer patterned surface indicating the $335 \times 335 \mu\text{m}^2$ superhydrophilic square regions separated by 60 μm -wide superhydrophobic barriers. The superhydrophilic squares were functionalized with either cysteamine or 3-mercaptopropionic acid, and the superhydrophobic barriers were functionalized with 1*H*,1*H*,2*H*,2*H*-perfluorodecanethiol. (B) Schematic showing the reverse transfection procedure using the patterned surfaces. Transfection mixtures were printed into individual superhydrophilic spots, which were contained by the superhydrophobic barriers, using a non-contact piezoelectric dispenser. The printed microarrays were dried for at least 2 days before cells were seeded on the whole

microarray. Cells adhered and grew within the superhydrophilic spots and were confined by the superhydrophobic barriers. Cell transfection was analyzed after culturing the cells for 2 days.

We used a Scienion sciFLEXARRAYER S11 non-contact piezoelectric dispenser with drop volume detection to be able to accurately and precisely print solutions into individual superhydrophilic spots without touching the surface. Unlike other instruments typically used to print solutions on surfaces, such as microarrayers, the S11 dispenser does not contact or damage the surface and the volume printed can be easily controlled, whereas the volume delivered by microarray pins can vary depending on the pin type, solution properties, and surface properties (Barbulovic-Nad *et al.*, 2006).

We chose one of the novel liposomal transfection reagents, ScreenFect[®] A, from the library mentioned above as a model for the other lipid-based reagents and tested whether the method of reverse transfection would work with the newly synthesized lipids on the patterned polymer substrates. Then, we identified several variables in our system that affected transfection and determined how to improve the transfection efficiency while minimizing cytotoxicity. Variables such as the printing and drying conditions, the cell seeding density, the cell incubation time, the surface chemistry of the superhydrophilic spot, the concentration of plasmid DNA in the mixture, the ratio of plasmid DNA to transfection reagent, the dilution buffer used, and the inclusion of gelatin and fibronectin in the mixture were all important factors for successful transfection.

We demonstrate that the superhydrophilic–superhydrophobic micropatterned surfaces can be used as high-density transfected cell microarrays to identify efficient transfection reagents and to optimize the transfection conditions for a particular experimental setup before performing further genetic screens.

Results and discussion

Comparison of the drop volume and spot area of mixtures printed on the patterned surfaces versus uncoated glass

To maximize the number of samples that can be tested on a single patterned substrate, we wanted to achieve a high-density array of printed spots. In this work, a pattern size of $335 \times 335 \mu\text{m}^2$ hydrophilic squares separated by $60 \mu\text{m}$ hydrophobic borders (hereafter referred to as 335-60 μm) was used, which results in approximately 6000 useable spots and each spot is within the field of view of a $20\times$ microscope objective (Fig. 3.1A). To compare the spot density that can be achieved on the patterned surfaces versus a standard glass slide, increasing volumes of a transfection mixture containing fluorescent Rhodamine 6G dye for visualization were printed onto a 335-60 μm

polyfluorodecanethiol–cysteamine pattern and onto an uncoated glass slide at a spot pitch of 395 μm . At least 20 nl of the mixture could be dispensed into a single $335 \times 335 \mu\text{m}^2$ hydrophilic spot before the drop mixed with the adjacent drops in the neighboring spots (Fig. 3.2A), whereas the 5 nl drops already began to touch when printed onto the uncoated glass slide and completely merged at volumes above 5 nl (Fig. 3.2B). At least 100 nl of mixture could be contained within a single $335 \times 335 \mu\text{m}^2$ hydrophilic spot when dispensing into every other hydrophilic spot (Supporting Information, Fig. 3.S1). These results demonstrate that when printing more than 5 nl/spot, the patterned surfaces allow for a much higher spot density than an uncoated glass slide.

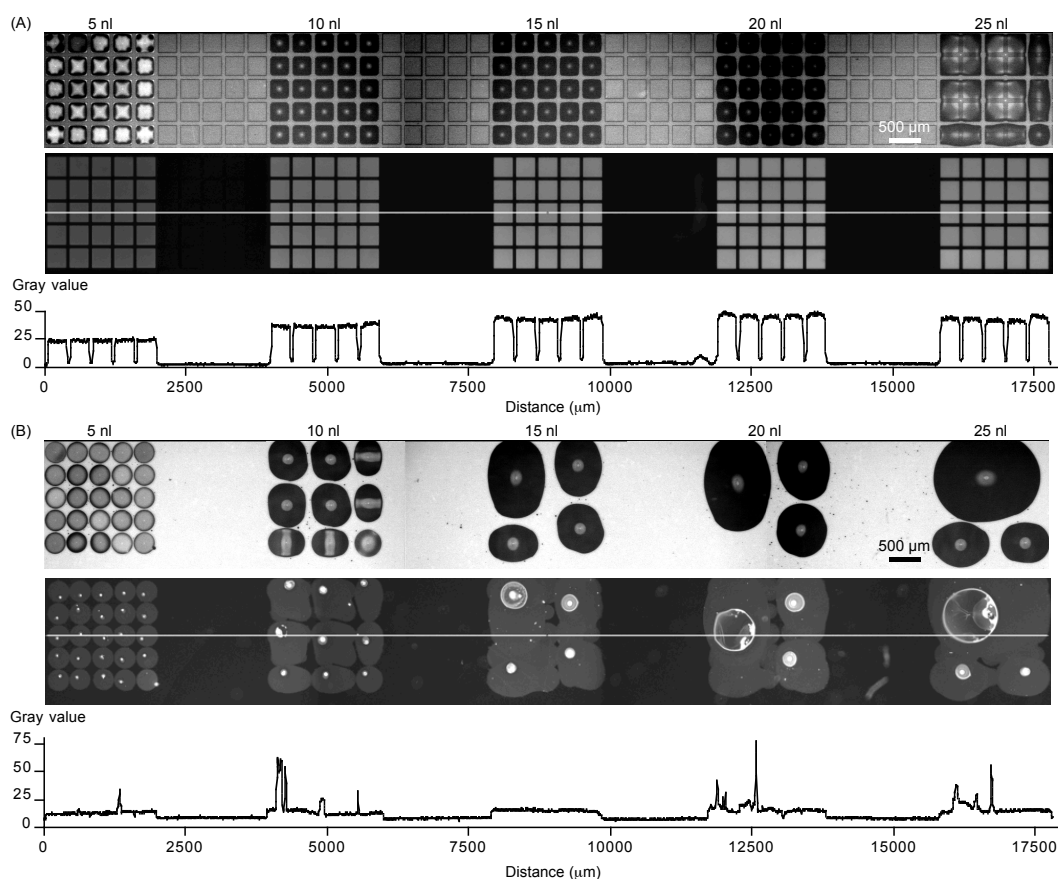


Figure 3.2 Confinement of droplets printed on a patterned vs. glass surface

Each hydrophilic spot can be individually addressed with the dispensing device, and the hydrophobic barriers can confine large volumes within a single hydrophilic spot. 5×5 arrays of 5, 10, 15, 20, and 25 nl of transfection mixture containing Rhodamine 6G dye (0.1 mg ml^{-1} final concentration) were printed at a pitch of 395 μm onto a $335\text{-}60 \mu\text{m}$ polyfluorodecanethiol–cysteamine pattern (A) and a glass slide (B). The images show the droplets on the surfaces after printing, grayscale fluorescence image after drying,

and fluorescence intensity profile plot along the white line. The exposure time was 0.01 s and 1 s for the fluorescence image of the patterned surface (A) and of the glass surface (B), respectively. The brightness and contrast of the images were enhanced for visualization.

To facilitate experimental reproducibility for reverse cell transfection, it is important to control the spot size of the printed mixture so that the amount of transfection mixture per unit area is comparable from one printed spot to another. The area of each 5 nl spot printed in a 5×5 array onto a 335-60 μm polyfluorodecanethiol–cysteamine pattern and onto an uncoated glass slide was measured after drying based on the fluorescence of the Rhodamine 6G dye contained in the transfection mixture (Fig. 3.2). The mean spot area of the 5 nl drops was $0.109 \pm 0.003 \text{ mm}^2$ (SD) on the patterned surface and $0.116 \pm 0.004 \text{ mm}^2$ (SD) on the glass surface, and the coefficient of variation was calculated to be 2.90% and 3.55%, respectively.

Although the low coefficients of variation demonstrate the low variability of the spot areas on both surfaces, one advantage was that the patterned surfaces showed a homogeneous fluorescence signal in each printed hydrophilic spot whereas the fluorescence signal on the uncoated glass slide was mostly concentrated at a single location as indicated by the high intensity fluorescence signal in each spot (Fig. 3.2, note the difference in exposure times). This suggests that solutions printed on the patterned surfaces could be distributed more homogeneously within the spot due to pinning of the drops at the edges of the hydrophilic–hydrophobic pattern and slow drying from the whole surface of the drop in high humidity conditions. For example, a 20 nl drop took approximately 10 min to evaporate at 95% RH. On an uncoated glass surface, a drop is not pinned at the edges and as the drop dries from the edges inward the diameter shrinks and can result in a higher concentration in the center. However, we noticed that Rhodamine 6G dye mixed with the transfection mixture resulted in more homogeneously dried spots versus just the dye mixed with water, probably due to the presence of gelatin and sucrose in the transfection mixture.

Another advantage of using the patterned surfaces as arrays is the control of the printed spot size even with varying drop volumes, whereas on an uncoated glass slide the printed spot size depends on the drop volume as well as on the properties of the printed solution such as viscosity and surface tension due to uncontrolled spreading of the drop on the surface. The mean spot area did not change significantly (p value = 0.0779) when printing a larger volume of 10 nl ($0.108 \pm 0.002 \text{ mm}^2$) compared with 5 nl ($0.109 \pm 0.003 \text{ mm}^2$) on the same patterned surface, demonstrating that even with increasing drop volumes the spot area remains constant.

Confinement of adherent cells within the superhydrophilic spots by the superhydrophobic barriers

We have demonstrated that solutions can be printed and confined within each individual hydrophilic spot. Next, we show that the superhydrophobic barriers can confine adherent cells within each hydrophilic spot, thus allowing us to use the patterned surfaces as high-density cell microarrays. HEK 293 cells and HeLa cells were seeded and cultured on 335-60 μm polyfluorodecanethiol–cysteamine patterned surfaces for 2 days without any additional medium exchange or washing steps. Optimal seeding densities of 35,000 cells cm^{-2} for HEK 293 cells and 30,000 cells cm^{-2} for HeLa cells were consistently used to ensure a high cell density after 2 days of culture. Fig. 3.3A,B shows that cells preferentially adhered and grew in the hydrophilic spots as opposed to the superhydrophobic barriers. The number of cells occupying the superhydrophilic and superhydrophobic regions was counted and normalized to the surface area. No HEK 293 cells and only 1.6% of HeLa cells occupied the superhydrophobic barriers. This was an improvement compared to our previously published results using a different superhydrophilic–superhydrophobic patterned surface (briefly described below) where we quantified 13% of HEK 293 cells on the superhydrophobic barriers (Geyer *et al.*, 2011).

We previously demonstrated the ability of superhydrophobic surfaces in the Cassie–Baxter state to minimize cell adhesion and migration due to air trapped within the porous, superhydrophobic polymer layer and at the interface between the polymer layer and aqueous medium (Geyer *et al.*, 2011). For those experiments, we used the method of UV-initiated photografting to fabricate the superhydrophilic–superhydrophobic patterned surfaces. In this work, we used a method recently developed in our group based on a thiol-yne photoclick reaction to fabricate the superhydrophilic–superhydrophobic patterned surfaces (Feng *et al.*, 2014). The thiol-yne click photopatterning method is much faster, more versatile and reliable, and has a higher patterning resolution than our previously used photografting method. Therefore, we used this method to fabricate the patterned surfaces in this work and in addition the superhydrophobic barriers showed improved efficiency at inhibiting cell adhesion and cell migration between the superhydrophilic spots.

Minimal cross-contamination of transfection mixtures between the neighboring hydrophilic spots

In order for the patterned surfaces to be a useful tool for cell screening and an improvement upon conventional transfected cell arrays on glass slides, we wanted to be sure that the separation of the hydrophilic spots by only 60 μm would not result in high levels of cross-contamination of the printed transfection mixtures between the neighboring spots. To test this, we printed two different transfection mixtures in a checkerboard pattern with either 1.5 ng of pCS2+-GFP or pCS2+-mCherry plasmid

with Lipofectamine[®] 2000, and 20 ng of gelatin and 5 ng of fibronectin per spot (Fig. 3.3C). We defined the percentage of cross-contamination as the ratio of foreign cells (i.e. expressing the reporter gene that was not printed in that spot) to the total number of cells per spot, and it was calculated to be only 0.26% on average when HEK 293 cells were cultured on the array for 2 days. This indicates that diffusion of the lipoplexes across the 60 μm superhydrophobic barriers to the neighboring spots is minimal and close-packing of the spots on the patterned substrates does not compromise the transfection results.

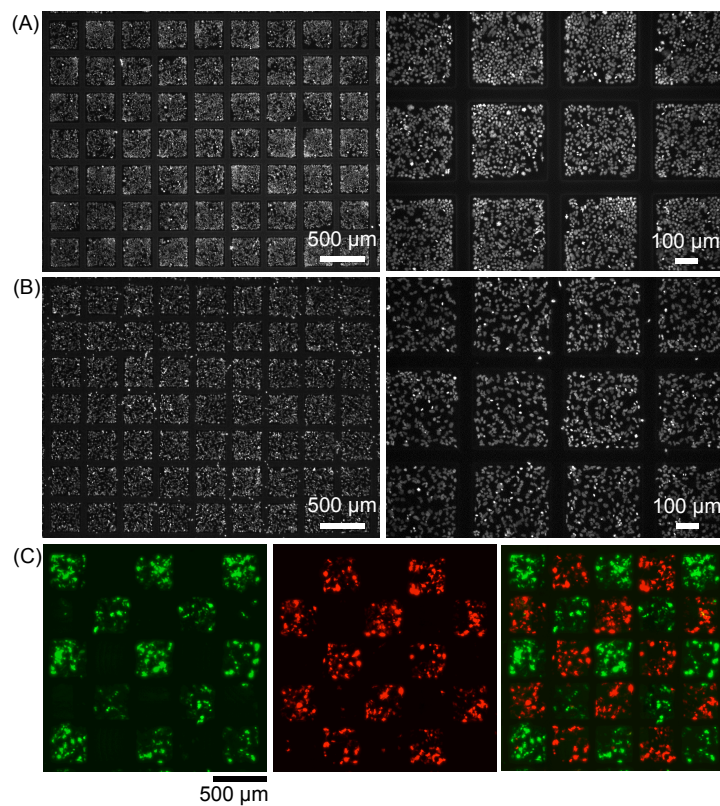


Figure 3.3 Minimal cross-contamination of transfection mixtures between neighboring microspots

The superhydrophobic barriers can confine adherent cells and transfection mixtures within a single hydrophilic spot. (A) HEK 293 cells seeded at $35,000 \text{ cells cm}^{-2}$ and (B) HeLa cells seeded at $30,000 \text{ cells cm}^{-2}$ were cultured on 335-60 μm polyfluorodecanethiol–cysteamine patterned surfaces for 2 days, and then fixed and stained with the nuclear marker DAPI. The brightness and contrast of the images were enhanced for visualization. (C) Fluorescence and overlay of fluorescence images showing that cells transfected in a checkerboard pattern with either pCS2+-GFP or

pCS2+-mCherry plasmid exhibited minimal cross-contamination between the neighboring spots.

Influence of the surface chemistry of the hydrophilic spot on reverse transfection

It has been shown in the literature that surface charge and hydrophilicity influence the immobilization of lipoplexes on the surface and consequently cell transfection (Pannier *et al.*, 2005). It has also been demonstrated that the immobilization and slow release of DNA complexes from a surface resulted in improved and sustained transfection compared to delivery of the DNA complexes to the media (Segura & Shea, 2002). Therefore, we hypothesized that there would be an interaction between the charged lipoplexes and the surface chemistry of our patterned polymer surfaces, which in turn could influence transfection efficiency.

Initially, cysteamine-modified (NH₂) patterned surfaces were used and low levels of reverse transfection for all of the mixtures tested was observed, attaining a maximum transfection efficiency of 15% with HEK 293 cells but a 28% decrease in cell number in comparison to blank spots (Supporting Information, Fig. 3.S2, Table 3.S1). Therefore, microspots modified with 3-mercaptopropionic acid (COOH) were also tested, which resulted in an increase in transfection efficiency for 25 of the 26 mixtures tested while the average number of cells growing in each spot was comparable for both surfaces (Fig. 3.4, Supporting Information Table 3.S2). Thus, COOH-modified surfaces were found to enhance reverse transfection compared to NH₂-modified surfaces.

Influence of the inclusion of gelatin and fibronectin on reverse transfection

Molecules or protein mixtures that promote cell adhesion, such as gelatin, fibronectin, and Matrigel, are often included in transfection mixtures when using glass substrates for cell microarrays (Erflé *et al.*, 2007; Rantala *et al.*, 2011; Stürzl *et al.*, 2008). These molecules are added to promote cell adhesion and growth only in the area of the printed spots since there is nothing to prevent the cells from migrating between the spots on a standard glass substrate. The inclusion of a matrix such as gelatin was also demonstrated to help maintain the spot integrity of a printed transfection mixture after drying and to increase the transfection efficiency (Mannherz *et al.*, 2006). Even though the superhydrophobic barriers on the patterned surfaces are sufficient for confining cells within each microspot, we tested whether the inclusion of gelatin and fibronectin was still necessary for reverse transfection.

Superhydrophilic–superhydrophobic patterned surfaces as high-density cell microarrays: optimization of reverse transfection

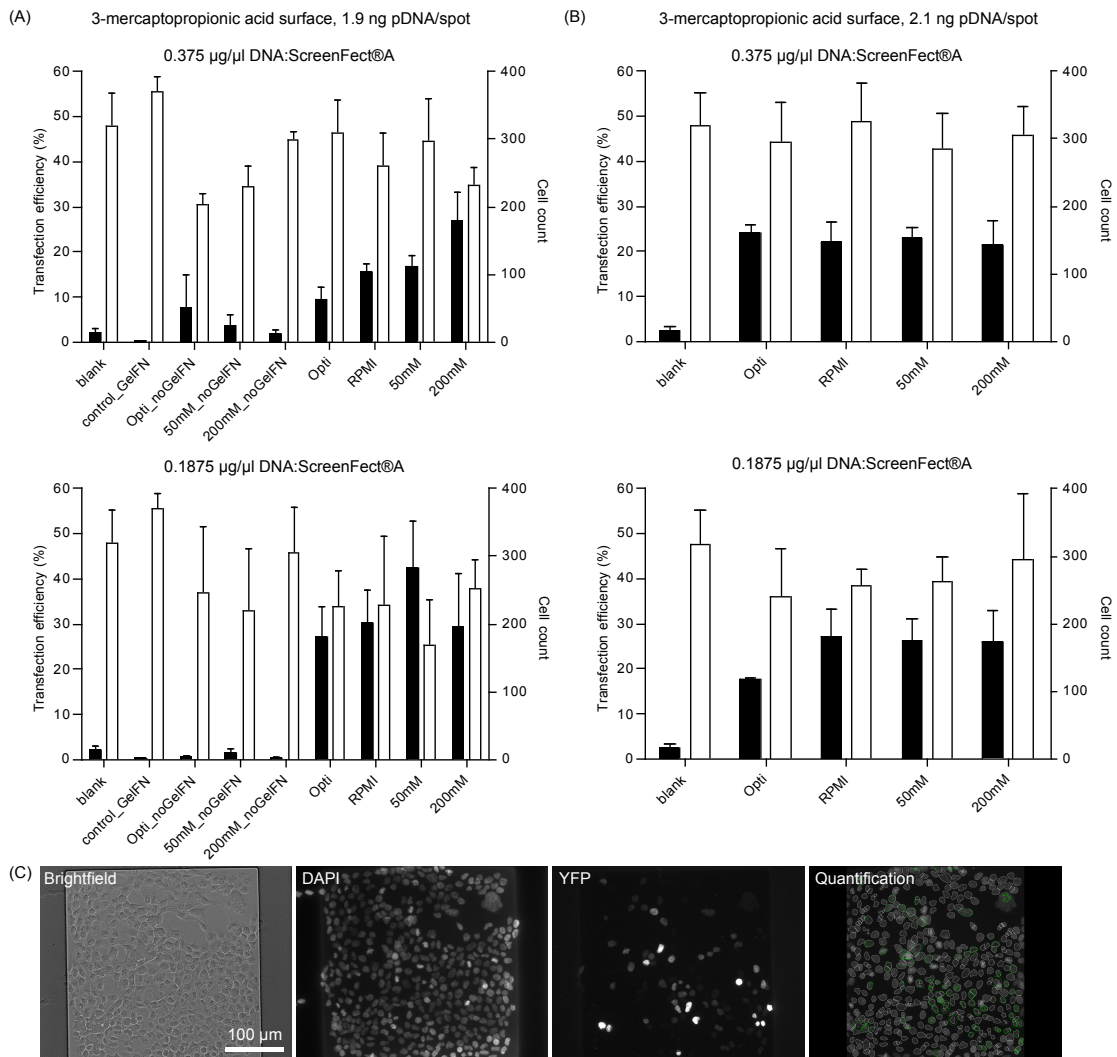


Figure 3.4 Transfection efficiency and cell number on COOH-modified microspots

Dependence of the transfection efficiency and the number of cells per spot on the ScreenFect[®]A ratio, the dilution buffer, the gelatin/fibronectin concentration, and the amount of pDNA on 3-mercaptopropionic acid-functionalized hydrophilic spots. The mean (SD) transfection efficiency (black bars) and the mean (SD) number of cells (white bars) per hydrophilic spot are shown for HEK 293 cells reversely transfected with either 1.9 ng (A) or 2.1 ng (B) of pCS2+-H2B-YFP DNA per spot. Each spot was printed with pDNA mixed with ScreenFect[®]A at ratios of 0.375 µg µl⁻¹ (top) or 0.1875 µg µl⁻¹ (bottom), 20 ng of gelatin (Gel) and 5 ng of fibronectin (FN), and either Opti-MEM[®], RPMI, 50 mM NaOAc, or 200 mM NaOAc as the dilution buffer. Blank indicates spots without anything printed, control_GelFN indicates spots printed with only 20 ng of gelatin and 5 ng of fibronectin (no lipoplexes), and noGelFN indicates transfection mixtures without gelatin or fibronectin (only lipoplexes in the buffer indicated). (C) Brightfield and fluorescence images of reversely transfected HEK 293 cells within a 3-mercaptopropionic acid hydrophilic spot printed with 2.1 ng of pCS2+-

H2B-YFP DNA mixed with ScreenFect[®]A at a ratio of 0.375 $\mu\text{g } \mu\text{l}^{-1}$ using RPMI as the buffer and 20 ng of gelatin and 5 ng of fibronectin. To quantify transfection efficiency, the YFP-positive cells (green outline) is calculated as a percentage of the total cell count by identifying the DAPI-positive cells (white outline).

Using COOH-patterned surfaces, 1.9 ng of pCS2+-H2B-YFP pDNA mixed at a ratio of either 0.375 or 0.1875 $\mu\text{g pDNA}:\mu\text{l ScreenFect}^{\text{®}}\text{A}$ using different dilution buffers (Opti-MEM[®], 50 mM NaOAc ScreenFect[®] dilution buffer, or 200 mM NaOAc) was printed per hydrophilic spot. The transfection mixtures were printed with either no gelatin/fibronectin or with 20 ng/spot of gelatin and 5 ng/spot of fibronectin. Very low levels of transfection (0.36–7.64%) occurred when no gelatin/fibronectin was added to the mixtures, whereas the inclusion of gelatin as well as fibronectin enhanced the transfection efficiency for all conditions with HEK 293 cells (Fig. 3.4A). For example, at a condition of 1.9 ng/spot of pCS2+-H2B-YFP pDNA mixed at a ratio of 0.375 $\mu\text{g pDNA}:\mu\text{l ScreenFect}^{\text{®}}\text{A}$ using 200 mM NaOAc as the dilution buffer, the mean transfection efficiency increased 16-fold from 1.69% to 26.80% just by adding 20 ng/spot of gelatin and 5 ng/spot of fibronectin. The inclusion of gelatin and fibronectin also increased the transfection efficiency when Lipofectamine[®] 2000 was used as the transfection reagent (Supporting Information, Fig. 3.S3). HEK 293 cells were cultured for 2 days on COOH-modified superhydrophilic spots printed with 1.5 ng of pCS2+-H2B-YFP plasmid mixed with Lipofectamine[®] 2000 diluted in Opti-MEM[®], 20 ng of gelatin, and 5 ng of fibronectin. The mean transfection efficiency and number of cells per spot was $27 \pm 9.5\%$ and 328 ± 49 , respectively.

The increase in transfection efficiency when gelatin and fibronectin were added to the mixtures could have been due to encapsulation and maintenance of the integrity of the lipoplexes on the surface after drying by the viscous nature of gelatin. In addition, the need to include cell adhesion molecules such as gelatin/fibronectin could be to promote cell–surface interactions for more efficient uptake of the lipoplexes into the cell. The role that cell adhesion molecules play in cell–surface interactions is known to promote adhesion to the substrate by increasing anchoring to the surface and delaying rear-retraction, which can slow down migration or immobilize cells (Schmidt & Friedl, 2010). This can lead to cells that are more spread on the surface, which has also been shown to increase transfection (Blacklock *et al.*, 2010).

Influence of the pDNA concentration, the ratio of pDNA to transfection reagent, and the dilution buffer on reverse transfection

The ratio of nucleic acid to liposomal transfection reagent can influence the surface charge and size of the formed lipoplexes, which in turn affects cellular uptake, and could thus be an important factor that determines transfection efficiency and toxicity

(Bengali *et al.*, 2005; Li *et al.*, 2013b; Rehman *et al.*, 2013). In addition, protonation of the amine head group of the lipid is thought to be an important factor for compacting the pDNA during lipoplex formation and promoting interaction with the cell surface, and it was previously demonstrated that lipoplexes with a positive zeta potential resulted in more efficient liquid phase transfection (Li *et al.*, 2012b). Therefore, we tested different buffers for diluting ScreenFect[®]A before complex formation with pDNA. Two ratios of pDNA:ScreenFect[®]A (0.375 and 0.1875 $\mu\text{g } \mu\text{l}^{-1}$) were tested at two concentrations of pCS2+-H2B-YFP pDNA per spot (1.9 and 2.1 ng) with the use of different dilution buffers in the mixture (Opti-MEM[®], RPMI, 50 mM NaOAc SFDB, and 200 mM NaOAc) on COOH-patterned surfaces.

At 1.9 ng of pDNA per hydrophilic spot, reducing the ratio of plasmid DNA to ScreenFect[®]A from 0.375 to 0.1875 $\mu\text{g } \mu\text{l}^{-1}$ resulted in an increase in transfection efficiency but a decrease in the mean number of cells per spot for all of the dilution buffers except 200 mM NaOAc, ranging from a 29–47% decrease in the mean cell count per spot relative to a blank spot without anything printed (Fig. 3.4A). When the amount of pDNA per spot was increased to 2.1 ng, the transfection efficiency slightly increased but did not significantly change between both pDNA:ScreenFect[®]A ratios for all of the dilution buffers except Opti-MEM[®] ($p = 0.006$), and the mean number of cells per spot for the lower ratio of 0.1875 $\mu\text{g } \mu\text{l}^{-1}$ decreased by only 5–25% compared to the blank spots (Fig. 3.4B). Almost no transfection was observed when 1.5 ng/spot of pDNA or less was printed (data not shown). Decreasing the ratio of pDNA to transfection reagent for a given amount of pDNA means that the relative amount of transfection reagent is increased, and this could have caused some cytotoxicity as indicated by the more drastic reduction in cell number for the lower pDNA:transfection reagent ratio and the presence of some cells with apoptotic bodies and condensed nuclei.

At 2.1 ng of pDNA per hydrophilic spot mixed at a ratio of 0.375 $\mu\text{g } \mu\text{l}^{-1}$ with ScreenFect[®]A, there was no significant difference in the mean transfection efficiency (21–24%) or the mean number of cells per spot (294–325) for all of the dilution buffers tested (Fig. 3.4B). Since amines are weak bases and their conjugate acids have pKa values around 10–11, they can be protonated with all of the buffers used: the pH 5 NaOAc buffers as well as Opti-MEM[®] pH 7.1–7.4 and RPMI pH 7.0–7.4. These results suggest that all of the buffers tested in the transfection mixture for lipoplex formation were suitable for reverse transfection.

Experimental

Fabricating the superhydrophilic–superhydrophobic patterned surfaces

UV-initiated polymerization was used to create a 12.5 μm -thin, nanoporous poly(2-hydroxyethyl methacrylate-co-ethylene dimethacrylate) (HEMA-EDMA) film on a Nexterion[®] glass B uncleaned slide (Cat. #1017698, Schott Technical Glass Solutions

GmbH, Jena, Germany) based on a method that we previously published (Feng *et al.*, 2014; Geyer *et al.*, 2011). The only difference here was that we did not use tape to remove the top layer of the polymer film after polymerization.

Next, the superhydrophilic–superhydrophobic micropattern was fabricated using a method recently developed in our group termed UV-initiated thiol-yne click photopatterning. This is a relatively simple and quick method for patterning any thiol-bearing molecule on a reactive alkyne surface using thiol-yne click chemistry. A comprehensive discussion about the method and characterization are provided in another paper (Feng *et al.*, 2014). To briefly describe the procedure, the HEMA-EDMA surface was first functionalized with alkyne groups by immersing the substrates in 50 ml of a dichloromethane solution containing 56 mg of 4-(dimethylamino)pyridine (Cat. #851055, Novabiochem[®]) and 111.6 mg of 4-pentynoic acid (Cat. # L09282, Alfa Aesar). 180 μ l of N,N'-diisopropylcarbodiimide (#A19292, Alfa Aesar) was then added and the solution was stirred for 4 h. After the esterification procedure, the substrate was rinsed with ethanol.

Lastly, the alkyne surface was functionalized with hydrophobic or hydrophilic thiols to create the micropatterned surface. In a dark room, 200 μ l of a 1*H*,1*H*,2*H*,2*H*-perfluorodecanethiol (5% v/v in acetone, Cat. #660493, Sigma-Aldrich) solution was pipetted onto the alkyne substrate, covered with a photomask, and then irradiated with 260 nm UV light at 6 mW cm⁻² for 1 min. The substrate was rinsed with acetone and dried before pipetting 200 μ l of cysteamine hydrochloride (15 wt%, Cat. #A1546, AppliChem) or 3-mercaptopropionic acid (15% v/v, Cat. #M5801, Aldrich Chemistry) in a 1:1 water:ethanol solution on the surface. The substrate was covered with a fluorinated quartz slide, irradiated with 260 nm UV light at 6 mW cm⁻² for 1 min, and rinsed with ethanol.

General protocol for making the transfection mixtures

pCS2+ expression vectors encoding for histone H2B fused with yellow fluorescent protein (H2B-YFP), green fluorescent protein (GFP), or mCherry fluorescent protein under the control of the simian cytomegalovirus IE94 promoter were provided by the Institute of Toxicology and Genetics at Karlsruhe Institute of Technology. The plasmids were transformed in electrocompetent *E. coli* cells and purified according to the QIAGEN Plasmid Maxi Kit (Cat. #12162, QIAGEN GmbH, Hilden, Germany). Plasmid DNA concentrations were measured using a NanoDrop ND-1000 Spectrophotometer (Peqlab Biotechnologie GmbH, Erlangen, Germany).

All transfection mixtures were based on the following general protocol, with adjustments in the concentration or volume of the mixture components to obtain the various mixtures. Different dilution buffers were tested in the transfection mixtures: Opti-MEM[®] (Cat. #31985, Life Technologies GmbH), Roswell Park Memorial Institute

(RPMI) 1640 medium (Cat. #21875, Life Technologies GmbH), 50 mM NaOAc ScreenFect[®] dilution buffer (SFDB, Incella GmbH), and 200 mM NaOAc. The sodium acetate (NaOAc) dilution buffers were pH 5.

Dilution buffer containing 0.8 M sucrose (Cat. #4621.1, Carl Roth GmbH, Karlsruhe, Germany) was freshly prepared by dissolving the sucrose in a water bath at 37°C and vortexing to mix well, and then filtered with a 0.45 µm sterile syringe filter. 2.1 µl of the buffer–sucrose solution was mixed into 1.75 µl of plasmid DNA (1.2 µg µl⁻¹ of pCS2+-H2B-YFP, pCS2+-empty vector, pCS2+-GFP, or pCS2+-mCherry) in a PCR tube (Cat. #3741, Corning Life Sciences). In a separate PCR tube, 4.12 µl of additional buffer was mixed into 5.6 µl of ScreenFect[®] A (Cat. #S-3001, Incella GmbH, Eggenstein-Leopoldshafen, Germany) and incubated for 5 min at RT. The ScreenFect[®] A solution was mixed into the plasmid DNA solution and incubated for 20 min at RT.

When adding gelatin or fibronectin to the transfection mixture, a 1.4% (w/v) gelatin (Cat. #9391, Sigma-Aldrich Chemie GmbH, Munich, Germany) in water solution was freshly prepared by dissolving the gelatin in a water bath at 37°C and vortexing to mix well. The solution was filtered with a 0.45 µm sterile syringe filter. 1.43 µl of the gelatin solution and 5 µl of a 0.1% (w/v) human fibronectin (Cat. #354008, BD Biosciences) in water solution were mixed into the lipoplex solution. The mixtures were pipetted into a 384-well microarray/high sample recovery plate (Cat. #X7022, Molecular Devices GmbH, Biberach an der Riss, Germany). When printed at 20 nl per spot, this transfection mixture resulted in 2.1 ng pDNA at a ratio of 0.375 µg µl⁻¹ pDNA:ScreenFect[®] A, 20 ng gelatin, and 5 ng fibronectin per spot.

For mixtures containing Lipofectamine[®] 2000 (Cat. #52758, Life Technologies GmbH) instead of ScreenFect[®] A as the transfection reagent, the ratio of DNA to Lipofectamine[®] 2000 was 0.429 µg µl⁻¹.

Printing transfection mixtures onto the substrates

Mixtures were printed onto substrates using a sciFLEXARRAYER S11 non-contact piezoelectric dispenser and uncoated glass piezo dispense capillaries (PDC 80) from Scienion AG (Berlin, Germany). Freshly de-gassed and filtered MilliQ water was used as the system fluid. The printing chamber was maintained at 95% RH and the source plate was cooled to 12°C to minimize evaporation of the mixtures. 20 nl of transfection mixture per hydrophilic spot was printed unless stated otherwise. After allowing the printed mixtures to dry in the humidified printing chamber, they were transferred to a sterile petri dish and stored for at least 2 days in a sealed box containing silica gel desiccant.

Quantification of the fluorescence intensity and spot size of printed transfection mixtures

5×5 arrays of 5, 10, 15, 20, and 25 nl of transfection mixture containing Rhodamine 6G dye (0.1 mg ml⁻¹ final concentration) were printed at a pitch of 395 μm onto a 335-60 μm polyfluorodecanethiol–cysteamine pattern and a glass slide (Fig. 3.2). Fluorescence images were obtained using a Keyence BZ-9000E fluorescence microscope (Keyence Deutschland GmbH, Neu-Isenburg, Germany). The exposure time was 0.01 s and 1 s for the fluorescence image of the 335-60 μm polyfluorodecanethiol–cysteamine patterned surface (Fig. 2A) and of the glass surface (Fig. 3.2B), respectively. The fluorescence intensity in Fig. 2 was quantified using the Plot Profile function in ImageJ (National Institutes of Health, USA). All graphs were plotted using Prism 4 software (GraphPad Software, La Jolla, CA).

The area of each 5 nl dried spot in Fig. 3.2 was measured by adjusting the brightness/contrast and threshold of the 8-bit images, and then using the Analyze Particles function in ImageJ. An unpaired t test was performed to calculate the two-tailed P value to compare the mean area of the 5 nl and 10 nl spots printed onto the patterned surface. We note that some error in the calculation of the spot area is probably due to uneven illumination in the image from the microscope.

Seeding and culturing cells on the substrates

Human embryonic kidney (HEK 293) cells were provided by the Institute of Toxicology and Genetics at Karlsruhe Institute of Technology. Human cervical carcinoma (HeLa CCL2) cells were obtained from DSMZ GmbH (Braunschweig, Germany). Cells were cultured in Dulbecco's Modified Eagle Medium (DMEM, Cat. #41965, Life Technologies GmbH, Darmstadt, Germany) supplemented with 10% fetal bovine serum (Cat. #A15-151, PAA Laboratories) and 1% penicillin-streptomycin (Cat. #15140, Life Technologies GmbH) in a humid incubator at 37°C with 5% CO₂, and were passaged every 2–3 days. Cells were detached with HyClone™ HyQTase™ (Cat. #SV30030.01, Thermo Fisher Scientific, Schwerte, Germany) and counted using a Neubauer hemacytometer before seeding on slides. Slides were placed in one corner of a Nunc™ 4-well rectangular dish (Cat. #267061, Thermo Fisher Scientific). We recommend first pipetting 200 μl of medium in the well, and then placing the slide in the well and firmly pressing down with sterile tweezers to spread the medium under the slide. This will prevent the cell suspension from going under the slide and reduce variations in cell density on the slide surface. 10 ml of cell suspension was slowly pipetted from one corner of the well and left undisturbed for 10 min before the dish was carefully moved into the incubator. HEK 293 and HeLa CCL2 cells were seeded at 35,000 cells cm⁻² and 30,000 cells cm⁻², respectively, on the patterned substrates. For reverse cell transfection experiments, cells were cultured for two days on the microarrays.

Fixing, staining, and coverslipping cells on the microarrays

2 ml of medium was slowly aspirated from a corner of the rectangular well. 2 ml of a solution containing 18.5% formaldehyde (1:1 dilution of 37% stock solution, Cat. #104003, Merck Millipore, Darmstadt, Germany), 0.5% Triton X-100, and 2.5 $\mu\text{g ml}^{-1}$ of 4',6-diamidino-2-phenylindole dihydrochloride (DAPI, 1:2000 dilution of 5 mg ml^{-1} stock, Cat. #D1306, Life Technologies GmbH) in Dulbecco's phosphate-buffered saline with calcium and magnesium (DPBS, Cat. #14040, Life Technologies GmbH) was slowly pipetted into the well for a final concentration of 3.7%, 0.1%, and 0.5 $\mu\text{g ml}^{-1}$, respectively. After 15 min of incubation at RT, the slide was transferred to a 10 cm petri dish containing 20 ml of DPBS with calcium and magnesium and incubated for 5 min. The slide was mounted with Shandon Immu-Mount (Cat. #9990402, Thermo Fisher Scientific) and a #1 coverslip (Cat. #BB024060A1, Gerhard Menzel GmbH, Braunschweig, Germany).

Quantification of the cell count and transfection efficiency

High-throughput imaging was performed using cell[^]R MT20E imaging hardware, an Olympus IX81 microscope, and scan[^]R software (Olympus Soft Imaging Solutions GmbH, Münster, Germany). Images were taken using a 20 \times objective such that the whole hydrophilic square was centered in the field of view. The total number of YFP-positive cells and the total number of DAPI-stained cells was counted using CellProfiler image analysis software (Broad Institute Imaging Platform, Cambridge, MA). The transfection efficiency was quantified as the ratio of transfected cells to DAPI-stained cells. Errors are given as standard deviation (SD). At least 6 replicates per slide and at least 2 slides were tested for each transfection mixture.

Conclusions

We demonstrated that superhydrophilic–superhydrophobic micropatterned surfaces are suitable for use as high-density cell microarrays due to the benefits of being able to confine both the printed transfection mixtures and the seeded cells within a single spot with almost no cross-contamination of either between the spots, even at a small spot pitch. We showed how variation of the transfection mixture components as well as the surface chemistry affected the transfection efficiency and the number of cells per spot, and we used this information to optimize transfection with a novel liposomal transfection reagent. Liposomal transfection reagents are widely used, but they are expensive and could be improved in terms of transfection efficiency and toxicity. These high-density cell microarrays could be further used to screen lipid libraries to identify the best transfection reagents for different cell types and nucleic acids, and ultimately help to elucidate the structure–function relationship of cell transfection. The superhydrophilic–superhydrophobic patterned surfaces could also be adapted for screening of other chemical libraries such as siRNAs (Erfle *et al.*, 2008; Neumann *et*

al., 2006; Rantala *et al.*, 2011) or extracellular matrix molecules (Reticker-Flynn *et al.*, 2012). In addition, the ability to easily functionalize the surface with a variety of terminal thiol-containing molecules could also allow arrays of bioactive substances such as peptides to be created (Feng *et al.*, 2014).

3.2 Supporting information

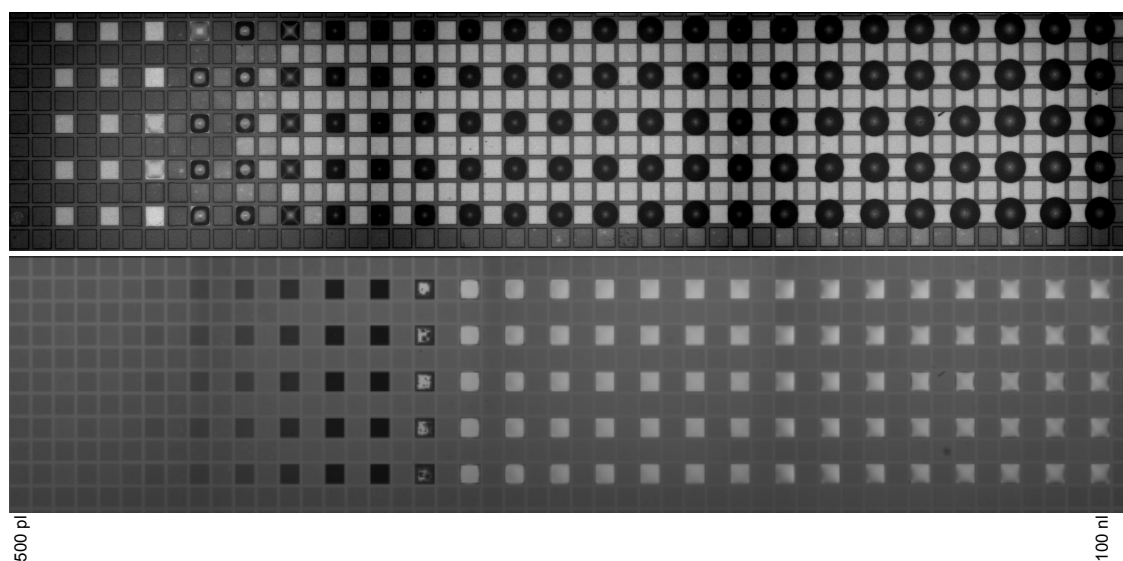


Figure 3.S1 Droplets of increasing volume printed on a patterned surface

500 pl–100 nl of transfection mixture printed onto a 335-60 μm polyfluorodecanethiol–cysteamine pattern at 790 μm pitch. Images taken in brightfield after printing (top) and after drying (bottom).

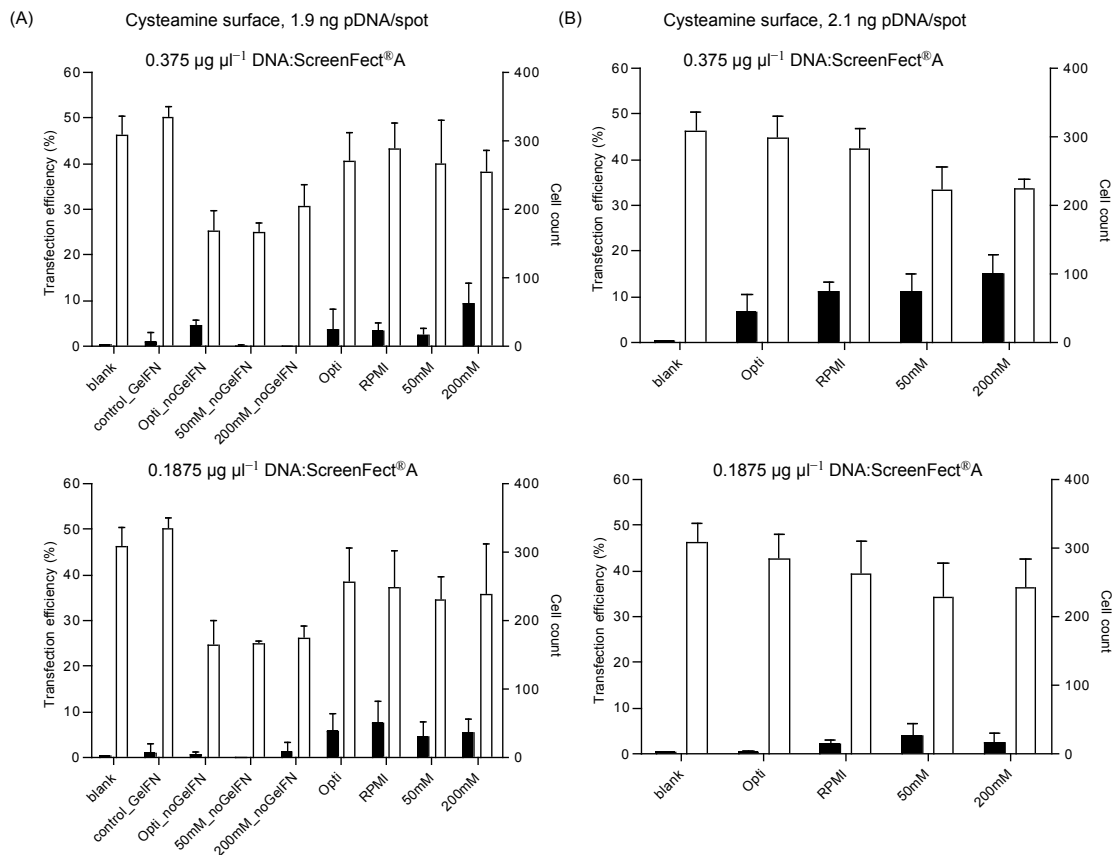


Figure 3.S2 Transfection efficiency and cell number on NH₂-modified microspots

Dependence of the transfection efficiency and the number of cells per spot on the ScreenFect[®]A ratio, the dilution buffer, the gelatin/fibronectin concentration, and the amount of pDNA on cysteamine-functionalized hydrophilic spots. The mean (SD) transfection efficiency (black bars) and the mean (SD) number of cells (white bars) per hydrophilic spot are shown for HEK 293 cells reversely transfected with either (A) 1.9 ng or (B) 2.1 ng of pCS2+-H2B-YFP DNA per spot. Each spot was printed with pDNA mixed with ScreenFect[®]A at ratios of 0.375 µg µl⁻¹ (top) or 0.1875 µg µl⁻¹ (bottom), 20 ng of gelatin (Gel) and 5 ng of fibronectin (FN), and either Opti-MEM[®], RPMI, 50 mM NaOAc, or 200 mM NaOAc as the dilution buffer. Blank indicates spots without anything printed, control_GelFN indicates spots printed with only 20 ng of gelatin and 5 ng of fibronectin (no lipoplexes), and noGelFN indicates transfection mixtures without gelatin or fibronectin (only lipoplexes in the buffer indicated).

Table 3.S1 Transfection efficiency and cell number on NH₂-modified microspots

The transfection efficiency and the number of cells per spot for transfection mixtures printed onto NH₂-modified hydrophilic spots. The data is graphed in Fig. 3.S2.

1.9 ng pDNA/spot, 0.375 µg µl ⁻¹ DNA:ScreenFect® A				
Mixture	Transfection efficiency (%)	SD	Cell count/spot	SD
blank	0.29	0.14	309	28
control_GelFN	1.00	1.92	335	17
Opti_noGelFN	4.49	1.32	168	29
50mM_noGelFN	0.13	0.19	166	15
200mM_noGelFN	0.00	0.00	205	32
Opti	3.51	4.65	270	43
RPMI	3.24	1.96	288	38
50mM	2.40	1.69	267	63
200mM	9.32	4.63	255	32

1.9 ng pDNA/spot, 0.1875 µg µl ⁻¹ DNA:ScreenFect® A				
Mixture	Transfection efficiency (%)	SD	Cell count/spot	SD
blank	0.29	0.14	309	28
control_GelFN	1.00	1.92	335	17
Opti_noGelFN	0.53	0.75	164	37
50mM_noGelFN	0.00	0.00	167	4
200mM_noGelFN	1.36	1.93	174	18
Opti	5.81	3.71	256	50
RPMI	7.44	4.78	247	56
50mM	4.65	3.33	231	35
200mM	5.38	3.20	239	73

2.1 ng pDNA/spot, 0.375 $\mu\text{g } \mu\text{l}^{-1}$ DNA:ScreenFect [®] A				
Mixture	Transfection efficiency (%)	SD	Cell count/spot	SD
blank	0.29	0.14	309	28
Opti	6.78	3.80	298	43
RPMI	11.05	2.30	281	38
50mM	11.01	4.07	223	63
200mM	15.13	3.98	224	32

2.1 ng pDNA/spot, 0.1875 $\mu\text{g } \mu\text{l}^{-1}$ DNA:ScreenFect [®] A				
Mixture	Transfection efficiency (%)	SD	Cell count/spot	SD
blank	0.29	0.14	309	28
Opti	0.26	0.24	285	35
RPMI	2.06	1.13	263	47
50mM	3.83	2.90	227	51
200mM	2.51	2.15	242	43

Table 3.S2 Transfection efficiency and cell number on COOH-modified microspots

The data is graphed in Fig. 3.4.

1.9 ng pDNA/spot, 0.375 $\mu\text{g } \mu\text{l}^{-1}$ DNA:ScreenFect [®] A				
Mixture	Transfection efficiency (%)	SD	Cell count/spot	SD
blank	2.00	0.95	318	50
control_GelFN	0.32	0.12	370	23
Opti_noGelFN	7.64	7.30	204	15
50mM_noGelFN	3.56	2.40	229	32
200mM_noGelFN	1.69	1.16	299	13
Opti	9.41	2.64	309	49
RPMI	15.42	1.83	261	48
50mM	16.72	2.36	296	64
200mM	26.80	6.38	232	26

Superhydrophilic–superhydrophobic patterned surfaces as high-density cell microarrays:
 optimization of reverse transfection

1.9 ng pDNA/spot, 0.1875 $\mu\text{g } \mu\text{l}^{-1}$ DNA:ScreenFect [®] A				
Mixture	Transfection efficiency (%)	SD	Cell count/spot	SD
blank	2.00	0.95	318	50
control_GelFN	0.32	0.12	370	23
Opti_noGelFN	0.70	0.32	246	96
50mM_noGelFN	1.54	0.85	220	90
200mM_noGelFN	0.36	0.17	305	66
Opti	27.13	6.62	226	52
RPMI	30.09	7.39	227	101
50mM	42.27	10.44	168	68
200mM	29.22	11.98	252	42

2.1 ng pDNA/spot, 0.375 $\mu\text{g } \mu\text{l}^{-1}$ DNA:ScreenFect [®] A				
Mixture	Transfection efficiency (%)	SD	Cell count/spot	SD
blank	2.38	0.95	318	50
Opti	23.94	2.04	294	59
RPMI	21.93	4.53	325	57
50mM	22.76	2.62	284	53
200mM	21.39	5.30	304	44

2.1 ng pDNA/spot, 0.1875 $\mu\text{g } \mu\text{l}^{-1}$ DNA:ScreenFect [®] A				
Mixture	Transfection efficiency (%)	SD	Cell count/spot	SD
blank	2.38	0.95	318	50
Opti	17.58	0.46	239	71
RPMI	27.01	6.11	257	24
50mM	26.16	4.86	263	36
200mM	25.76	7.07	296	98

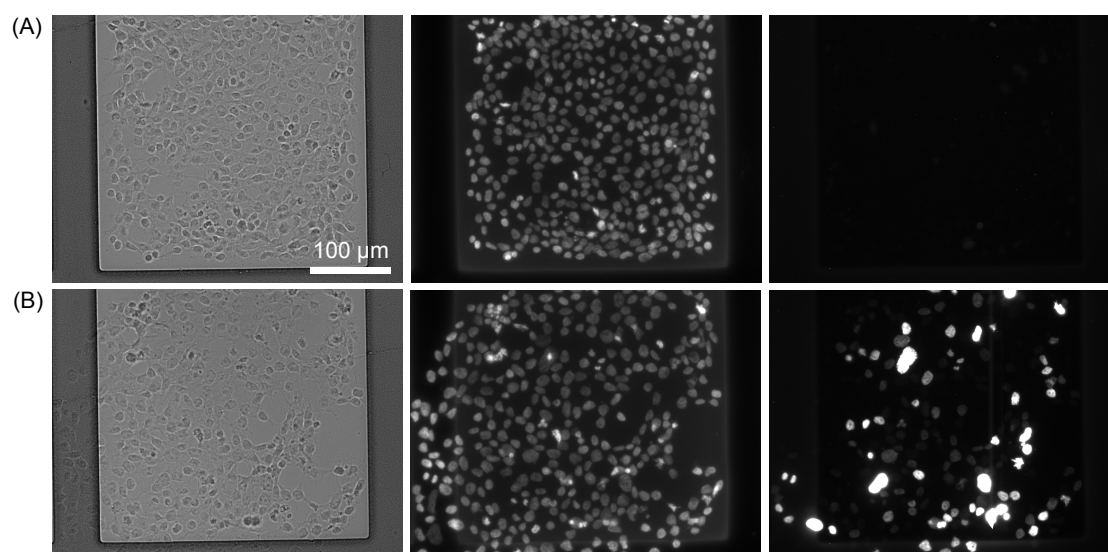


Figure 3.S3 Reverse transfection with Lipofectamine[®] 2000 on COOH-modified microspots

Brightfield and fluorescence images of reversely transfected HEK 293 cells within a 3-mercaptopropionic acid hydrophilic spot printed with 1.5 ng/spot of pCS2+-H2B-YFP DNA mixed with Lipofectamine[®] 2000 at a ratio of $0.439 \mu\text{g} \mu\text{l}^{-1}$ using Opti-MEM as the dilution buffer, and either (A) no gelatin/fibronectin or (B) 20 ng of gelatin and 5 ng of fibronectin per spot.

4 Surface patterning via thiol-yne click chemistry: an extremely fast and versatile approach to superhydrophilic–superhydrophobic micropatterns

An extremely fast and initiator-free approach to create superhydrophilic–superhydrophobic micropatterns via UV-induced sequential thiol-yne click chemistry is described. The photopatterning can be performed at room temperature in variety of solvents, including water, and can be also used for making high-density peptide or cell microarrays. This chapter was originally published as an article in *Advanced Materials Interfaces* in July 2014 and is reproduced with permission from John Wiley and Sons (Feng *et al.*, 2014).

Surface patterning via thiol-yne click chemistry: an extremely fast and versatile approach to superhydrophilic–superhydrophobic micropatterns

Wenqian Feng, Linxian Li, Erica Ueda, Junsheng Li, Stefan Heißler, Alexander Welle, Oliver Trapp and Pavel A. Levkin*

W. Feng, L. Li, E. Ueda, J. Li, Dr. P. A. Levkin

Institute of Toxicology and Genetics

Karlsruhe Institute of Technology

76021 Karlsruhe, Germany

E-mail: levkin@kit.edu

W. Feng, L. Li, Prof. Dr. O. Trapp

Department of Organic Chemistry

Heidelberg University

69120 Heidelberg, Germany

J. Li, Dr. P. A. Levkin

Department of Applied Physical Chemistry

Heidelberg University

69120 Heidelberg, Germany

S. Heißler, Dr. A. Welle

Institute of Functional Interfaces

Karlsruhe Institute of Technology

76021 Karlsruhe, Germany

Author contributions:

Wenqian Feng designed and performed the experiments and analysis, and wrote the manuscript.

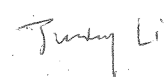


Linxian Li contributed to the original idea of the project and edited the manuscript.

Erica Ueda adapted the surface patterning method for her own experiments and edited the manuscript.



Junsheng Li contributed to the original idea of the project and edited the manuscript.



Stefan Heißler provided the Raman spectrometer.

Alexander Welle performed the time-of-flight secondary ion mass spectrometry (ToF-SIMS) measurements.

Oliver Trapp advised Wenqian Feng during his PhD.

Pavel A. Levkin contributed to the experimental design and edited the manuscript.



4.1 Article

Superhydrophobic surfaces are characterized by extreme water repellency with water contact angles (WCA) greater than 150° , and a WCA hysteresis of less than 10° (Deng *et al.*, 2011; Gao & Jiang, 2004; Lafuma & Quéré, 2003; Li *et al.*, 2007; Nakajima *et al.*, 1999; Wang & Jiang, 2007). On the contrary, water spreads immediately on superhydrophilic surfaces leading to WCAs less than 10° (Feng *et al.*, 2005; Wang *et al.*, 1997). Both superhydrophobicity and superhydrophilicity are the result of a combination of high surface roughness with either hydrophobic or hydrophilic material, respectively (Deng *et al.*, 2011; Gao & Jiang, 2004; Lafuma & Quéré, 2003; Nakajima *et al.*, 1999). Combining these two extreme properties on the same surface in precise two-dimensional micropatterns opens exciting new functionalities and possibilities in a wide variety of applications from cell (Geyer *et al.*, 2011; Ueda & Levkin, 2013b; Ueda *et al.*, 2012; Ziauddin & Sabatini, 2001), droplet (Jokinen *et al.*, 2012; Kobaku *et al.*, 2012; Mertaniemi *et al.*, 2011; Ueda *et al.*, 2012), and hydrogel microarrays (Song *et al.*, 2010; Ueda *et al.*, 2012) for screening to surface tension-confined microfluidic channels for separation and diagnostic devices (Han *et al.*, 2010; Ueda & Levkin, 2013a; Xing *et al.*, 2011). A number of methods for making superhydrophobic–superhydrophilic micropatterns have been introduced over the past decade. For example, methods based on UV-induced decomposition of hydrophobic coatings on different substrates (alumina, TiO_2 film or SiO_2) were reported (Ishizaki *et al.*, 2010; Kwak *et al.*, 2010; Lai *et al.*, 2008, 2009; Nakata *et al.*, 2010; Nishimoto *et al.*, 2009a, b; Tadanaga *et al.*, 2000; Zhang *et al.*, 2007a, b). Photoinduced modification of carbon nanotubes with hydrophilic azides (Pastine *et al.*, 2008), plasma treatment (Garrod *et al.*, 2007; Jokinen *et al.*, 2008; Sainiemi *et al.*, 2011), microprinting (Lai *et al.*, 2013; Li *et al.*, 2012a; Zhai *et al.*, 2006), or mussel-mimetic deposition of dopamine in combination with soft-lithography (Kang *et al.*, 2010) have been described. In our previous work, we introduced a method based on UV-initiated photografting for making superhydrophobic–superhydrophilic micropatterns on porous polymer films (Geyer *et al.*, 2011; Zahner *et al.*, 2011). Recently, Manna *et al.* reported an amine reactive superhydrophobic surface that permits post-fabrication by amine-functionalized molecules (Manna *et al.*, 2012). Most of the described methods, however, proceed slowly (e.g., 15 min irradiation time in the case of photografting) (Geyer *et al.*, 2011; Zahner *et al.*, 2011), lack the ability to easily tailor or modify the properties by different target functional groups, or require harsh conditions (e.g., plasma treatment or UV-induced decomposition), organic solvents (i.e., incompatible with aqueous conditions) and, therefore, cannot be directly applied to make patterns of biomolecules. These limitations restrict the range of possible practical applications of produced superhydrophobic–superhydrophilic micropatterns. Developing a universal method that

is facile, versatile, as well as provides good optical and chemical surface properties remains a big challenge.

To meet this challenge, here we present an extremely fast (<15 s), initiator-free surface modification method compatible with aqueous conditions for creating superhydrophobic–superhydrophilic micropatterns using thiol-yne “click” chemistry (Bhairamadgi *et al.*, 2013; Fairbanks *et al.*, 2009; Hoogenboom, 2010) (Figure 4.1A). Phototriggered thiol-yne reactions have been explored as a viable approach to surface modifications, such as using different thiols to modify “yne”-containing polymer brushes (Hensarling *et al.*, 2009), immobilizing gold nanoparticles on a polymer surface site-specifically (Guerrouache *et al.*, 2012), and creating micropatterns on a monolayer by microcontact printing (Wendeln *et al.*, 2010). To our knowledge, however, this type of functionalization strategy has never been applied to create superhydrophobic–superhydrophilic micropatterns. Here we show that an alkyne functionalized porous polymethacrylate surface could be easily transformed into either a superhydrophobic or superhydrophilic surface under UV irradiation. We show that the reaction is extremely fast and requires as little as 0.5 s of UV irradiation in the presence of an initiator and only 5 s without any initiator. The functionalization can be performed in various solvents including water (Figure 4.1) allowing to pattern biomolecules. In this way, superhydrophobic–superhydrophilic micropatterns incorporating different orthogonal reactive functional groups (*e.g.*, OH, NH₂, or COOH) could be created using this method. An application of the produced superhydrophobic–superhydrophilic structures to pattern cells as well as the use of the thiol-yne photo-click method to pattern cysteine-containing peptides are presented.

To fabricate a nanoporous polymer layer modified with alkyne groups (Figure 4.S1), we used a 12.5 μm-thin porous polymer layer of poly(2-hydroxyethyl methacrylate-*co*-ethylene dimethacrylate) (HEMA-EDMA) prepared on a glass substrate according to previously published procedure (Geyer *et al.*, 2011). The resulting HEMA-EDMA polymer layer has high surface roughness (50% porosity and 80–250 nm pores based on SEM, Figure 4.S2) and is highly wettable with static (θ_{st}), advancing (θ_{adv}), and receding (θ_{rec}) WCAs close to ~4.2°, 7.1°, and 0°, respectively (Figure 4.S2). The HEMA-EDMA surface was modified with 4-pentynoic acid by a standard esterification procedure (Supporting Information). The analysis of the WCA variation over time and within the depth of the polymer film verified that the modification proceeded completely throughout the thickness of the polymer layer after 4 h of the reaction time (Figure 4.S3). The θ_{st} of the polymer surface increased from 4.2° to 124° after the esterification. The intense peak at 2120 cm⁻¹ in the Raman spectrum (Figure 4.S4) also confirmed the presence of terminal alkyne groups (Guerrouache *et al.*, 2012). After surface modification, the polymer layer maintained its porous structure and did not show significant changes of the morphology (SEM in Figure 4.S2). Due to the small size of the pores (Levkin *et al.*, 2009), the light scattering

on the wetted polymer layer is reduced leading to more than 90% transmittance of visible light (Figure 4.S5). The resulting alkyne porous polymer can be functionalized via the thiol-yne click reaction to transform the surface either into a superhydrophobic or superhydrophilic surface depending on whether a hydrophobic or hydrophilic thiol being used (Figures 4.1B,C). As a general procedure, the porous alkyne surface is wetted with a thiol solution, covered with a quartz slide, and irradiated with 260 nm UV light (12 mW cm^{-2}) at room temperature.

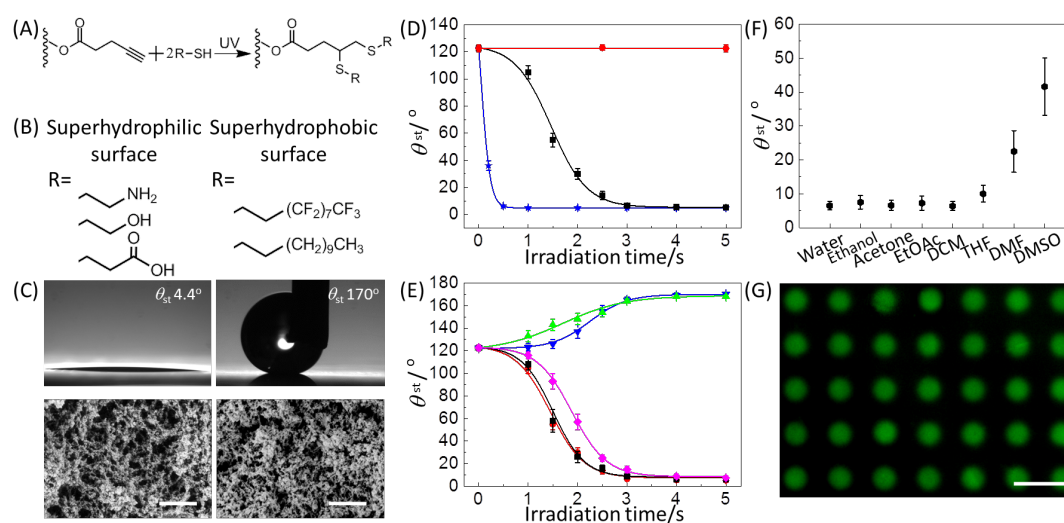


Figure 4.1 Alkyne surface modification via UV-induced thiol-yne click chemistry

(A) Schematic representation of the alkyne surface modification via UV-induced thiol-yne click chemistry; (B) Examples of thiols used for the formation of either superhydrophilic or superhydrophobic surfaces; (C) Water droplet on a cysteamine-modified superhydrophilic surface (left) and on a *1H,1H,2H,2H*-perfluorodecanethiol modified superhydrophobic surface (right), and SEM images of the corresponding porous polymers. (D,E) Kinetics of the alkyne surface modification using the thiol-yne click chemistry. The θ_{st} of the polymer layer modified using: (D) cysteamine with (blue) or without (black) photoinitiator 2,2-dimethoxy-2-phenylacetophenone (DMPAP) and with DMPAP but without UV irradiation (red); (E) cysteamine (black squares), 3-mercaptopropionic acid (red circles), 2-mercaptoethanol (purple diamonds), *1H,1H,2H,2H*-perfluorodecanethiol (blue triangles), and 1-dodecanethiol (green triangles) without DMPAP upon UV irradiation. (F) θ_{st} of the alkyne surfaces functionalized using 3-mercaptopropionic acid dissolved in different solvents; no photoinitiator; 5 s UV irradiation. Results from 3 different samples and two measurements per sample. (G) Fluorescence microscope image of a fluorescein- β -Ala-GGGGC peptide pattern prepared by the thiol-yne reaction on the alkyne porous surface carried out in aqueous solution. Scale bars: 1 μm (C) and 500 μm (G).

In general, long UV irradiation times can lead to oxidation and degradation of the substrate as well as to the damage of biomolecules used for functionalization. Most of the existing UV-based techniques for the formation of superhydrophobic–superhydrophilic patterns require irradiation times ranging from several minutes to several hours, which limits possible applications of such methods (Ishizaki *et al.*, 2010; Kwak *et al.*, 2010; Lai *et al.*, 2008, 2009; Nakata *et al.*, 2010; Nishimoto *et al.*, 2009a, b; Tadanaga *et al.*, 2000; Zahner *et al.*, 2011; Zhang *et al.*, 2007b, a). On the other hand, functionalization of the alkyne-surface with cysteamine using the thiol-yne reaction required as little as 0.5 s of UV irradiation in the presence of 2,2-dimethoxy-2-phenylacetophenone (DMPAP) as a photoinitiator to transform the hydrophobic alkyne polymer ($\theta_{st} = 124^\circ$) into a superhydrophilic surface ($\theta_{st} = 4.4^\circ$) (Figure 4.1D). The same reaction without the photoinitiator required only 5 s for the functionalization and no reaction happened without UV light. The thiol-ene reaction without a photoinitiator was reported previously by Cramer *et al.* (Cramer *et al.*, 2004). Without UV irradiation, however, the WCAs of the surface did not change at all even in the presence of the photoinitiator, indicating that there was no physisorption of the thiols on the surface.

Figure 4.1E shows the fast kinetics of the initiator-free surface modification as well as the ability to use different thiols to create either superhydrophobic or superhydrophilic surfaces. Modification of the surface with hydrophobic 1-dodecanethiol or 1*H*,1*H*,2*H*,2*H*-perfluorodecanethiol endows the porous surface with superhydrophobicity (θ_{adv} , θ_{st} , and θ_{rec} being as high as 171° , 169° , and 162° or 173° , 170° , and 164° , respectively). In the Raman spectra, sharp decline of the alkyne bands ($\sim 2120\text{ cm}^{-1}$) was observed (Figure 4.S6). No sign of the vinyl sulfide species ($\sim 1657\text{ cm}^{-1}$) was detected (Figure 4.S7), indicating full conversion of the alkyne groups to the 1,2-dithioether adduct (Levkin *et al.*, 2009). Figure 4.S8 shows the stability test of superhydrophobic surfaces. The static WCAs of the surfaces in air, PBS buffer, and acetic and basic water solutions (pH = 5 and 10) remained above 160° after 120 h incubation. Due to the protein adsorption, the WCA of the surface decreased in DMEM solution containing 10 vol% FBS. The porous structure of the HEMA-EDMA polymer layer plays an important role in fabricating superhydrophobic or superhydrophilic surfaces. Using the thiol-yne reaction under the same conditions, the functionalization of an alkyne-modified non-porous HEMA-EDMA surface with cysteamine leads to a decrease of θ_{st} from 63° to 44° and the functionalization with 1*H*,1*H*,2*H*,2*H*-perfluorodecanethiol leads to an increase of θ_{st} from 63° to 110° after 5 s UV irradiation.

The ability to perform the thiol-yne surface functionalization in different both apolar and polar solvents including water can increase the number of possible thiols applicable for the functionalization. Water is especially interesting in terms of its environmental impact, low cost, and the compatibility with thiol-containing biomolecules, such as proteins or peptides. To test the ability to use the thiol-yne-based

surface functionalization in different solvents, we modified the alkyne HEMA-EDMA surface with 3-mercaptopropionic acid dissolved in several common solvents (Figure 4.1F). Based on the water contact angle measurements, the reaction proceeded extremely fast in ethanol, acetone, ethyl acetate, DCM, THF, and water. The hydrophobic alkyne-modified polymer could be transformed into the superhydrophilic surface after only 5 s of irradiation. The reaction in DMF and DMSO required 15 s of the irradiation to make the surface superhydrophilic. The fact that the reaction proceeds well in water and without an initiator can be important for the rapid functionalization of such surfaces with biomolecules. This has been shown by patterning a fluorescein- β -Ala-GGGGC peptide containing a terminal cysteine residue on the alkyne functionalized HEMA-EDMA surface (Figure 4.1G). The pattern was prepared by irradiating the alkyne surface wetted with an aqueous solution of the peptide (0.25 mg/L) during 15 s.

The advantage of using a reactive surface for patterning is that the non-irradiated areas remain reactive after the first step of patterning and can be subsequently modified to create patterns of a secondary functionality. Importantly, the second step of modification does not require a photomask as a reactive alkyne pattern is generated during the first step of irradiation through a photomask. Figure 4.2 shows schematically the process for creating superhydrophobic–superhydrophilic micropatterns. First, the alkyne porous layer is wetted with an acetone solution containing 5 vol% 1*H*,1*H*,2*H*,2*H*-perfluorodecanethiol and irradiated with UV light through a photomask yielding a pattern of superhydrophobic as well as reactive alkyne areas (Figure 4.S9). After removing the photomask and washing with acetone, the whole surface is subjected to a second thiol-yne reaction with cysteamine hydrochloride (15 wt% ethanol solution), leading to the modification of unreacted alkyne groups and the formation of a superhydrophobic–superhydrophilic pattern. It is worth nothing that θ_{rec} on the superhydrophobic areas decreased by only 2° after the second modification step.

Figure 4.2B shows examples of well-defined superhydrophobic–superhydrophilic patterns of different sizes and geometries prepared by this method. Multicomponent patterns with feature sizes as small as 10 μm (Figure 4.2C) could be produced. Using the method from Ueda et al. (Ueda *et al.*, 2012), it is possible to create high-density arrays of completely separated microdroplets (DropletMicroarray approach) on the produced superhydrophobic–superhydrophilic patterns (Figure 4.2D). Due to the reduced light scattering, the superhydrophilic nanoporous polymer layer becomes transparent when wetted with water (Figure 4.S3), allowing easier discrimination of spots and facilitating the use of inverted microscopes.

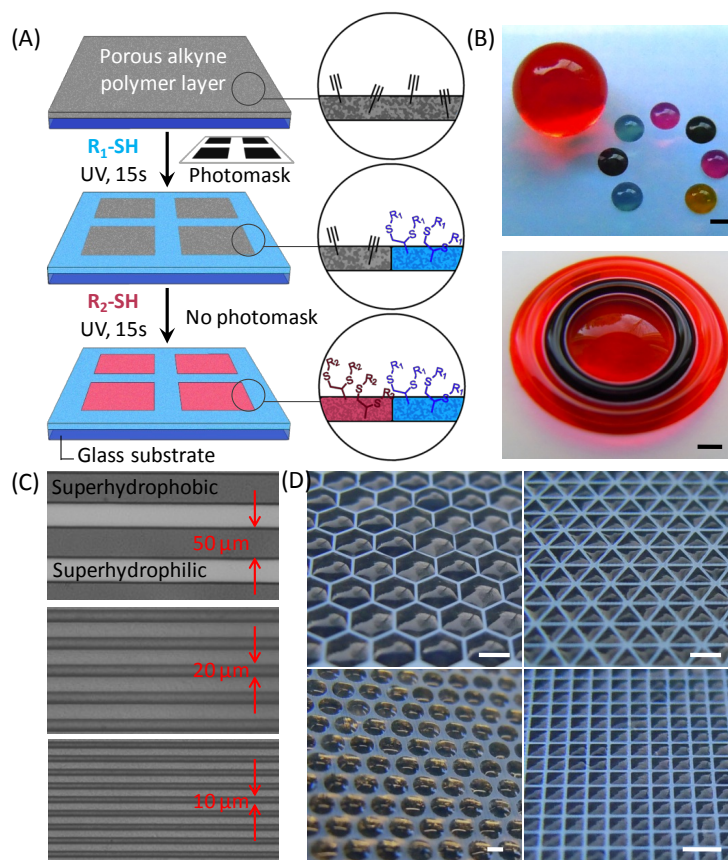


Figure 4.2 Fabrication of superhydrophilic–superhydrophobic patterns via thiol-yne photo-click reactions

(A) Schematic representation of the thiol-yne photo-click reaction for creating superhydrophobic–superhydrophilic micropatterns using the alkyne-modified porous polymer layer as a substrate. Optical images of (B) superhydrophilic–superhydrophobic patterns filled with dye water solutions; superhydrophobic gap between the two rings is 100 μm ; (C) Superhydrophilic regions (light areas) separated by superhydrophobic gaps (dark areas) of different widths; (D) DropletMicroarrays formed by dipping the superhydrophobic–superhydrophilic arrays with different geometries into water. Wetted parts become transparent (dark). Scale bars are 1 mm.

To further improve this method and to avoid possible modification of the residual alkyne groups remaining after the first irradiation step, we used an ethanol-water (1:1) solution instead of pure ethanol to dissolve cysteamine. In this case, the contact angle (θ_{st}) of the ethanol-water solution on the alkyne-functionalized and the fluorinated surfaces was 0° and $135 \pm 3^\circ$, respectively. Thus, the cysteamine solution could only wet the alkyne-functionalized areas ($\theta_{\text{st}} = 0^\circ$), while the fluorinated areas remained dry

(Figure 4.S9). This simple method completely prevents immobilization of the thiol on the superhydrophobic areas during the second functionalization step. This was confirmed by time-of-flight secondary ion mass spectrometry (ToF-SIMS) (Figure 4.3A).

Another advantage of this sequential surface modification method is that inverse patterns can be obtained simply by switching the order of the two chemicals in the patterning procedure (Figure 4.3B,C and 4.S10A). The grids of water microchannels on the inverse patterns shown in Figure 4.3C (right) can be used, for example, as barriers for confining water immiscible organic solvents in the hydrophobic spots (Figure 4.S10B).

Finally, we show that the produced superhydrophobic micropatterns show excellent cell repellent properties superior to those produced by a previously described photografting technique (Efremov *et al.*, 2012; Geyer *et al.*, 2011). To visualize this, HeLa-GFP cells were seeded on an array of superhydrophilic spots and superhydrophobic barriers and incubated for 2 days. Figure 4.3D and Figure 4.S11 show that cells adhered well to the superhydrophilic microspots, demonstrating the biocompatibility and nontoxicity of the surface, however, less than 1% of cells occupied the superhydrophobic regions separating the microspot areas after 2 days of culture.

In conclusion, we have developed an extremely fast initiator-free method based on the thiol-yne click chemistry for the rapid fabrication of superhydrophobic–superhydrophilic micropatterns. The method can be applied to a variety of different functional molecules, containing, for example, unprotected OH, NH₂, or COOH groups, as long as a terminal thiol group is present. Thus, functional and/or reactive superhydrophobic and superhydrophilic micropatterns can be created. We also showed that the patterning could be performed in aqueous conditions, making this method useful for biological applications, where rapid transformation and benign aqueous conditions are crucial. Given the swiftness, versatility, mild reaction conditions, as well as compatibility with various chemistries and solvents, we believe that this method will find numerous applications for creating multifunctional superhydrophobic–superhydrophilic micropatterns.

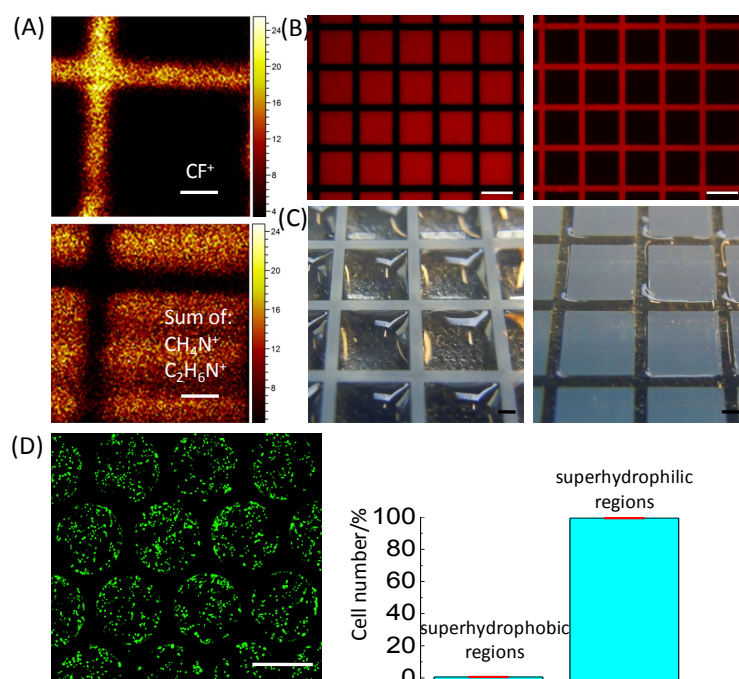


Figure 4.3 ToF-SIMS results and chemical/cell patterning

(A) ToF-SIMS 2D graphs of positive CF^+ -ion and the sum of CH_4N^+ and $C_2H_6N^+$ -ions, showing the patterning of *1H,1H,2H,2H*-perfluorodecanethiol and cysteamine, respectively. (B) Fluorescence microscope images showing the inverse superhydrophobic-superhydrophilic patterns filled with aqueous solution of Rhodamine B; (C) The superhydrophilic regions of inverse superhydrophobic–superhydrophilic patterns filled with water. Inverse patterns produced using the same photomask by switching the order in which the hydrophobic and hydrophilic regions were created; (D) Fluorescence microscope images of Hela-GFP cells after growing for 48 h on a superhydrophobic–superhydrophilic array, showing the preferential adherence of cells on superhydrophilic spots and less than 1% occupation on the superhydrophobic barriers. Scale bars are 100 μm (A), 300 μm (B) and 1 mm (C and D).

4.2 Supporting information

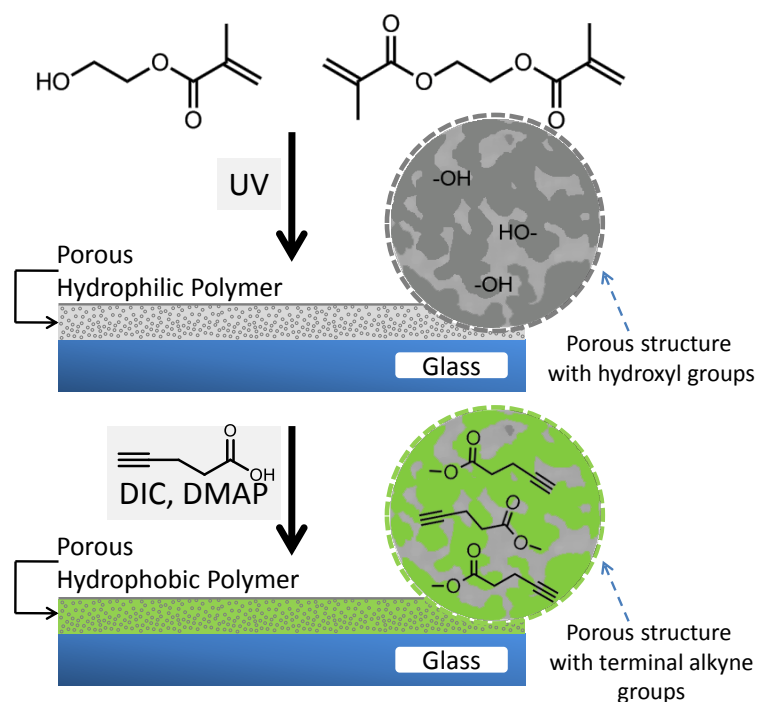


Figure 4.S1 Schematic of alkyne surface fabrication

Firstly, a 12.5 μm thin, hydrophilic porous polymer film was prepared on a glass substrate using photoinitiated copolymerization of 2-hydroxyethyl methacrylate and ethylene dimethacrylate (HEMA-EDMA) in the presence of porogens. After immersing in a dichloromethane solution containing 4-pentynoic acid, coupling reagent *N,N'*-diisopropylcarbodiimide (DIC), and catalyst 4-(dimethylamino)pyridine (DMAP) and stirring at RT for 4 h, the polymer film underwent esterification to form a porous surface functionalized with alkyne groups.

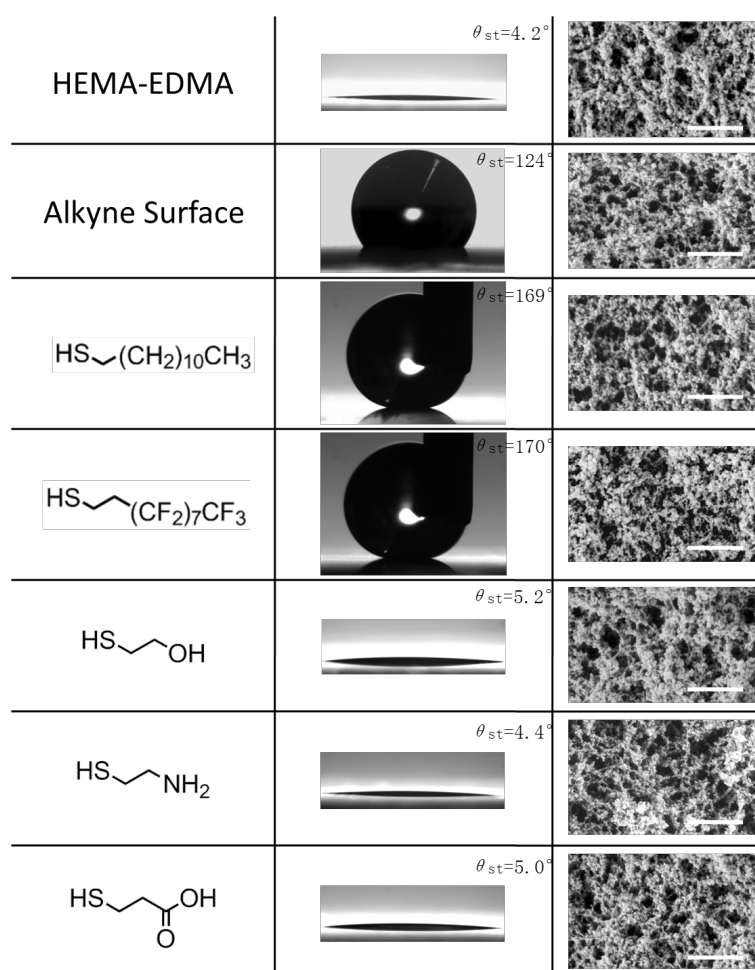


Figure 4.S2 SEM images and water contact angle measurements

Water droplets on various polymer layers and the corresponding SEM images: HEMA-EDMA, alkyne-functionalized HEMA-EDMA, as well as alkyne surfaces modified with 1-dodecanethiol, 1*H*,1*H*,2*H*,2*H*-perfluorodecanethiol, 2-mercaptoethanol, cysteamine, and 3-mercaptopropionic acid. The static WCAs are 4.2°, 124°, 169°, 170°, 5.2°, 4.4°, and 5.0° respectively. Scale bars are 1 μm.

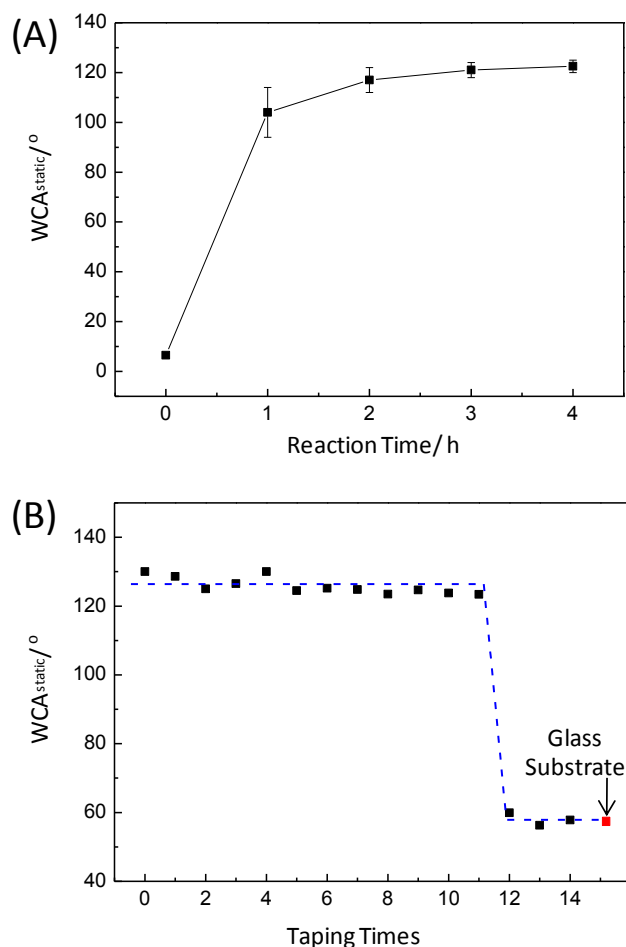


Figure 4.S3 Kinetics of the esterification reaction

(A) The esterification progress was characterized by measuring the static WCA on the polymer layer during the esterification. The graph shows the increase of the static WCA on the porous polymer layer as a function of the reaction time. The static WCA on the surface is still about 124° after 24 h of the reaction time. (B) To characterize the esterification within the porous polymer, the superficial surface layer was removed by attaching conventional pressure-sensitive tape (Scotch tape) to the polymer layer and then peeling it off layer by layer. After each layer was removed with the tape, the static WCA was measured at the same spot on the polymer film (esterification for 4 h). The red spot shows the static WCA of a bare glass substrate. After taping 11 times, the polymer layer shows the same static WCAs as a bare glass substrate, indicating that the esterification reaction takes place throughout the whole thickness of the polymer layer. We measured five different spots and all showed the same trend.

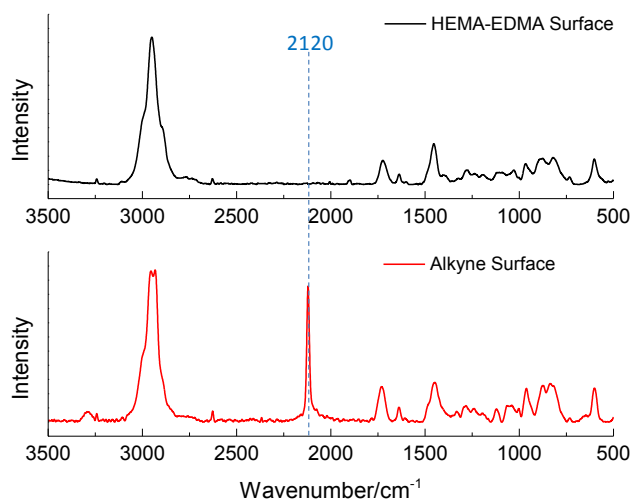


Figure 4.S4 Raman spectra of HEMA-EDMA and alkyne surfaces

Raman spectra of the HEMA-EDMA polymer surface (top, black) and a 4-pentynoic acid-functionalized alkyne polymer surface (bottom, red). The intense band at ~ 2120 cm⁻¹ supports the presence of $-C\equiv C-H$ units on the alkyne surface.

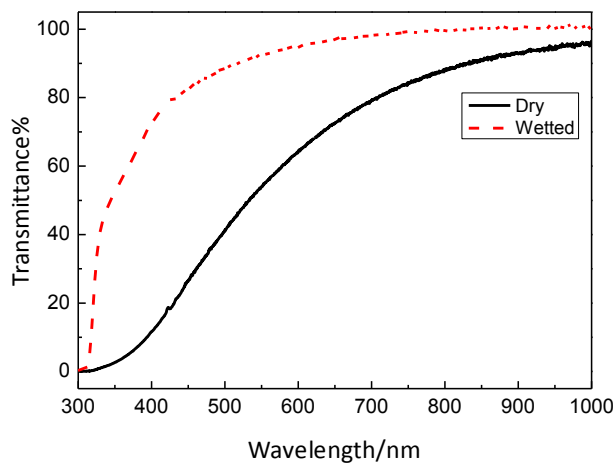


Figure 4.S5 UV-Vis-NIR transmittance spectra of HEMA-EDMA surfaces

UV-Vis-NIR transmittance spectra of wetted and dry porous HEMA-EDMA surfaces.

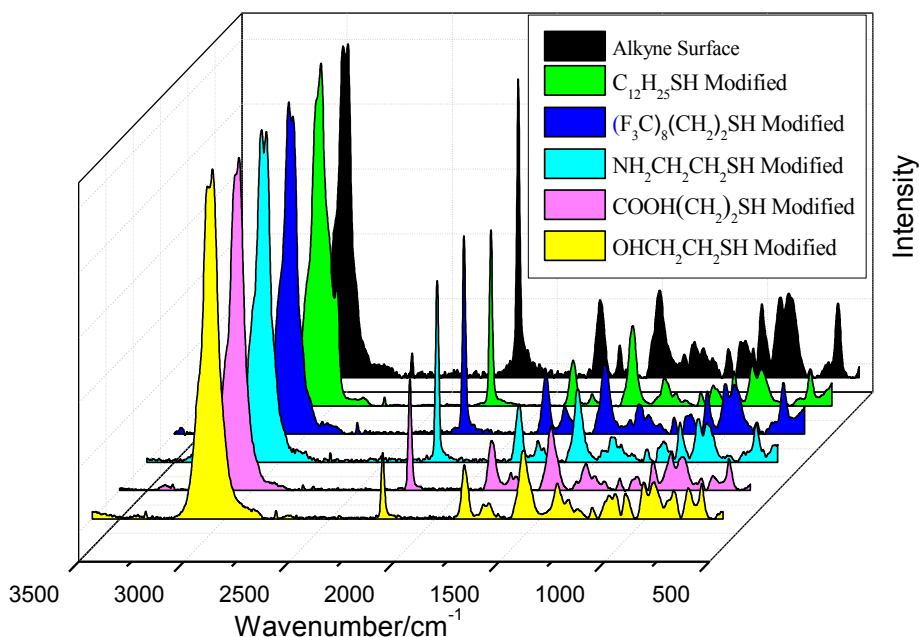


Figure 4.S6 Raman spectra of modified alkyne surfaces

The Raman spectra of a non-modified alkyne surface (black), as well as alkyne surfaces modified with 1-dodecanethiol (green), *1H,1H,2H,2H*-perfluorodecanethiol (dark blue), cysteamine (light blue), 3-mercaptopropionic acid (pink), and 2-mercaptoethanol (yellow). The decline of the band ratios of $\sim 2940\text{ cm}^{-1}$ (C-H alkyl free vibrations) to $\sim 2120\text{ cm}^{-1}$ ($\text{C}\equiv\text{C}$ triple bond stretch) illustrates that the alkyne groups react with several kinds of thiols. Some alkyne groups are buried inside the polymer and not accessible, thus the alkyne signal ($\sim 2120\text{ cm}^{-1}$) would not disappear even after long UV irradiation.

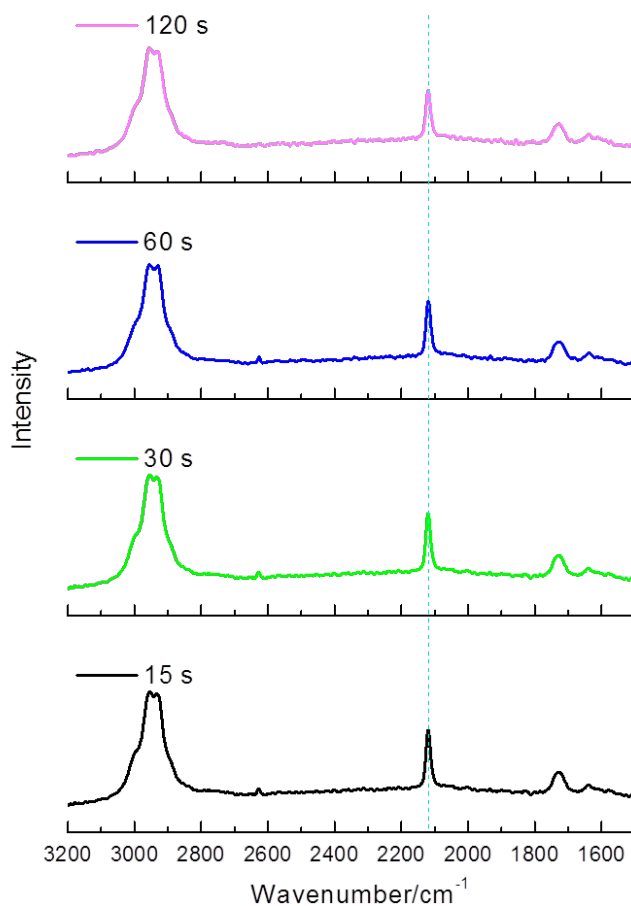


Figure 4.S7 Raman spectra of cysteamine-modified surfaces

The Raman spectra of cysteamine-modified alkyne surfaces at different UV irradiation times. The band ratio of $\sim 2940\text{ cm}^{-2}$ (C-H alkyl free vibrations) to $\sim 2120\text{ cm}^{-2}$ (C≡C triple bond stretch) remains the same, illustrating that 15 s is enough for the complete functionalization of the alkyne groups with thiols.

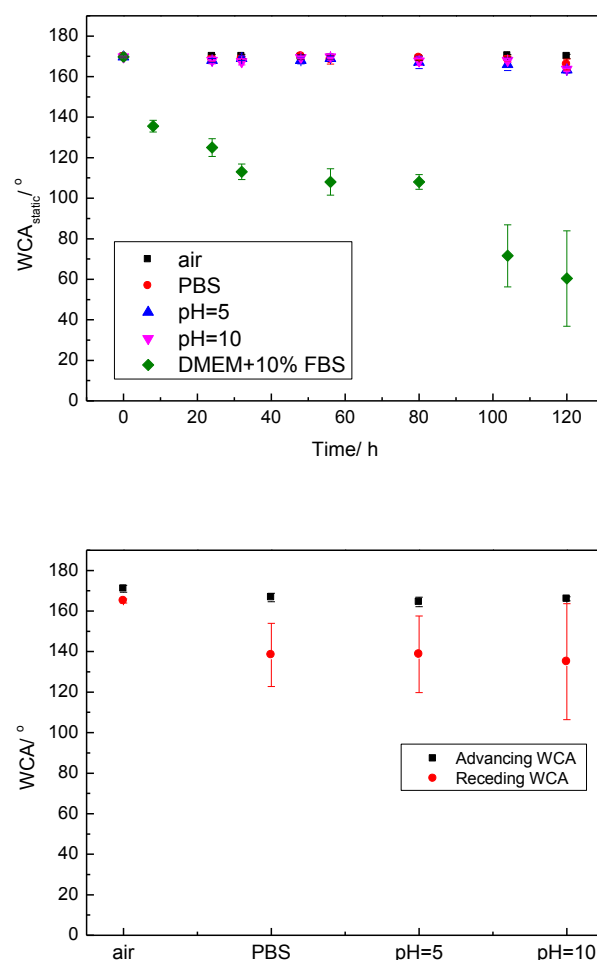


Figure 4.S8 Stability of the superhydrophobic surface

The stability test of superhydrophobic surfaces in air, PBS buffer, DMEM solution with 10% FBS (often used in cell culture), and both acetic and basic water solutions (pH = 5 and 10) for 120 h. A) Static WCAs of superhydrophobic surfaces as a function of the incubation time in different environments. The static WCAs of the surfaces in air, PBS buffer, and acetic and basic water solutions (pH = 5 and 10) remained above 160° after 120 h of incubation. Due to protein adsorption, the WCA of the surface in DMEM+FBS solution decreased. B) The advancing and receding WCAs of the surfaces after incubation for 120 h in different environments. The advancing WCAs almost remained the same after incubation. The receding WCAs of the surface in PBS buffer and acetic and basic water solutions decreased slightly.

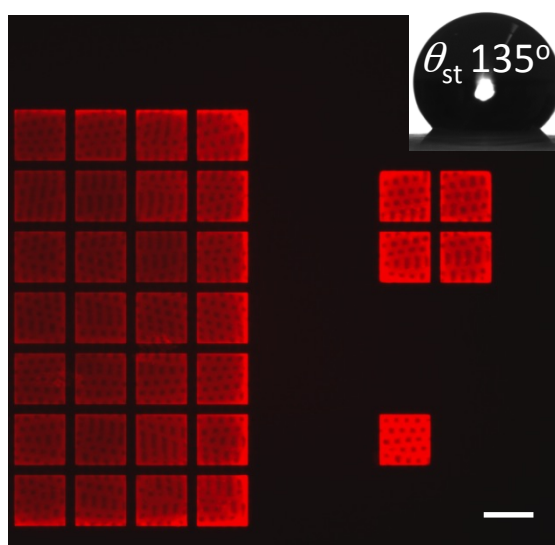


Figure 4.S9 Ethanol–water solution on a superhydrophobic patterned surface

Superhydrophobic micropattern with alkyne-functionalized squares and superhydrophobic *1H,1H,2H,2H*-perfluorodecanethiol-modified barriers. The alkyne spots are wetted with an ethanol-water solution containing Rhodamine B. The dye solution can only wet the alkyne spots and is repelled by the superhydrophobic barrier. No leaking occurs outside of the single spot containing the dye solution. Insert: a droplet of 1:1 ethanol:water solution on a *1H,1H,2H,2H*-perfluorodecanethiol modified superhydrophobic surface. The static water contact angle is 135° . Scale bar is 1 mm.

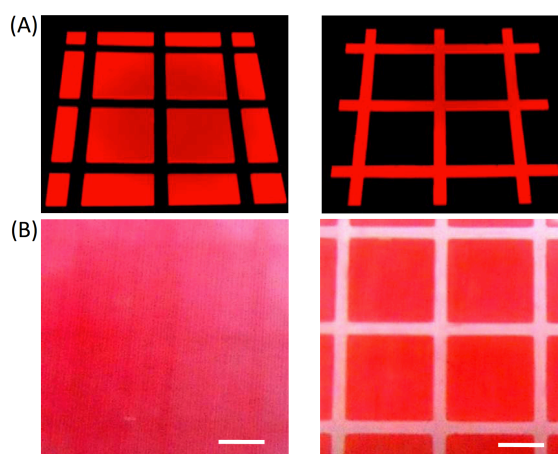


Figure 4.S10 Inverse superhydrophobic–superhydrophilic patterns

(A) Laser confocal fluorescence microscope images showing the inverse superhydrophobic–superhydrophilic patterns filled with a water solution of Rhodamine B dye. The sides of the squares are $300\ \mu\text{m}$. (B) A hexadecane solution of hydrophobic Oil Red O dye wetting both superhydrophilic and superhydrophobic areas (left); the

same surface covered with the hexadecane solution of Oil Red O dye after wetting the superhydrophilic barriers with water. The water layer protects the superhydrophilic regions from being impregnated with the hexadecane solution (right). Scale bars are 1 mm.

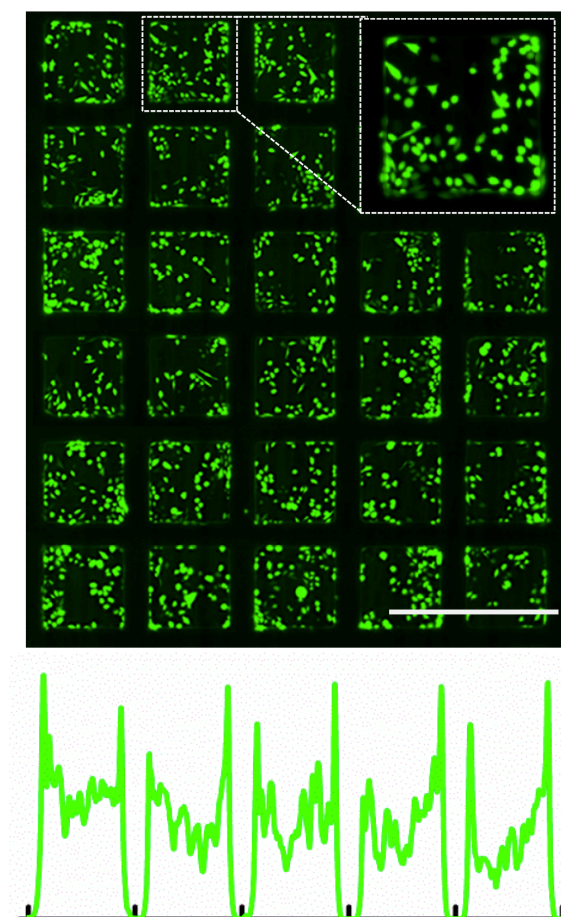


Figure 4.S11 HeLa-GFP cells cultured for 48 h on a patterned surface

Fluorescence microscope images of HeLa-GFP cells after growing for 48 h on a superhydrophobic–superhydrophilic patterned array. Less than 1% of the total number of cells occupied the superhydrophobic barriers. Green graph shows the intensity profile of the green fluorescence vs. distance. Scale bar is 1 mm.

Materials and methods

2-hydroxyethyl methacrylate (HEMA) and ethylene dimethacrylate (EDMA) were purchased from Sigma-Aldrich (Germany) and purified using a short column filled with basic aluminum oxide to get rid of the inhibitors. The food dyes used in Figure 4.2 were obtained from August Thomsen Corp. (USA). All the other chemicals were purchased from Sigma-Aldrich (Germany) and used without further purification. HeLa-GFP cells

were purchased from Biocat (Germany). The GFP-peptide containing thiol group (fluorescein- β -Ala-GGGGC) was obtained from Dr. Cornelia Lee-Thedieck at the Institute of Functional Interfaces at Karlsruhe Institute of Technology. Schott (Germany) Nexterion Glass B UV transparent glass plates were used as substrates for polymer layers. The polymerizations and photografting were carried out on an OAI Model 30 deep-UV collimated light source (San Jose, CA) fitted with an USHIO 500 W Hg-xenon lamp (Japan).

Characterization

SEM images were obtained using the LEO 1530 Gemini scanning electron microscope (Zeiss, Germany) at the Institute of Nanotechnology (INT), KIT. Before SEM measurement, the samples were sputtered with a 30 nm gold layer using a Cressington 108 auto sputter coater (INT, KIT). The Raman spectra were obtained by a Bruker Senterra confocal Raman microscope (Bruker Optics, Ettlingen, Germany) at the Institute of Functional Interfaces (IFG), KIT which provides a frequency doubled NdYAG Laser $\lambda = 532$ nm, $P = 20$ mW as excitation source. The distributions of cysteamine fragments and perfluorinated fragments on the surface were confirmed by time of flight secondary ion mass spectrometry (ToF-SIMS) (ION TOF Inc., Münster, Germany), IFG, KIT. The inverse patterns filled with Rhodamine dye solution were imaged using a Leica Confocal Microscope SPE. The fluorescein-peptide pattern and HeLa-GFP cells were imaged on a Keyence BZ-9000 fluorescence microscope (Japan). A UK 1115 digital camera from EHD imaging (Germany) was used to take images of the water droplet on the surface under ambient conditions. ImageJ software with a Dropsnake plugin was used to measure the water contact angle. ImageJ software with a 3D Viewer plugin was used to create 3D images from Confocal Microscope SPE data.

Preparation of 12.5 μm -thin porous HEMA-EDMA films

Here, we employed a recently published procedure developed in our group to make nanoporous HEMA-EDMA polymer layers (Geyer *et al.*, 2011). Briefly, two 12.5 μm -thin strips of Teflon film (American Durafilm Co.) were placed at the edges of one 3-(trimethoxysilyl)propyl methacrylate modified glass-plate ($25 \times 75 \times 1$ mm, width \times length \times thickness) and one fluorinated glass slide was clamped on top of it. 70 μL of polymerization mixture of HEMA (24 wt%), ethylene dimethacrylate (EDMA) (16 wt%), 1-decanol (12 wt%), cyclohexanol (48 wt%) and 2,2-dimethoxy-2-phenylacetophenone (DMPAP) (photoinitiator, 1 wt% with respect to monomers) was injected in the mold between the glass slides and irradiated for 15 min with 12.0 mW cm^{-2} 260 nm UV-light. The mold was then carefully opened using a scalpel.

The resulting non-porous superficial surface was removed by applying and rapidly removing adhesive film (“Scotch tape”) after separating the plates while the layer was

still wetted. A homogeneous porous surface was formed. The plate was washed extensively with ethanol and kept in ethanol for some minutes.

Preparation of 12.5 μm -thin non-porous HEMA-EDMA films

Two 12.5 μm -thin strips of Teflon film (American Durafilm Co.) were placed at the edges of one 3-(trimethoxysilyl)propyl methacrylate modified glass-plate ($25 \times 75 \times 1$ mm, width \times length \times thickness) and one fluorinated glass slide was clamped on top of it. 70 μL of polymerization mixture of HEMA (60 wt%), EDMA (40 wt%) and 2,2-dimethoxy-2-phenylacetophenone (DMPAP) (photoinitiator, 1 wt% with respect to monomers) was injected in the mold between the glass slides and irradiated for 15 min with 12.0 mW cm^{-2} 260 nm UV-light. The mold was then carefully opened using a scalpel. The resulting non-porous surface was washed extensively with ethanol and kept in ethanol for some minutes.

Preparation of alkyne modified HEMA-EDMA

Two glass plates coated with a HEMA-EDMA layer were immersed into 50 mL of dichloromethane solution containing 4-pentynoic acid (111.6 mg, 1.14 mmol) and catalyst 4-(dimethylamino)pyridine (DMAP) (56 mg, 0.46 mmol). Then, the coupling reagent *N,N'*-diisopropylcarbodiimide (DIC) (176.5 μL , 1.14 mmol) was added to the solution cooled to about 0°C , followed by stirring the solution at RT for 4 h. The plates were then washed extensively with acetone and kept in ethanol for several minutes, followed by drying.

Thiol-yne “click” reactions on the porous polymer layer

According to the solubility of a thiol, 1-dodecanethiol (5 vol%) and 1*H*,1*H*,2*H*,2*H*-perfluorodecanethiol (5 vol%) were dissolved in acetone, while 2-mercaptoethanol (15 vol%), cysteamine hydrochloride (15 wt%), and 3-mercaptopropionic acid (15 vol%) were dissolved in ethanol. These thiol solutions were not degassed prior to use.

The alkyne polymer layer was wetted with the respective thiol solution and covered with a fluorinated quartz slide ($25 \times 75 \times 1$ mm, width \times length \times thickness). All of the fabrications of superhydrophobic or superhydrophilic layers using thiol-yne reactions were performed by UV irradiation (12.0 mW cm^{-2} , 260 nm) without photoinitiator under ambient laboratory conditions. After the reactions, the samples were washed extensively with acetone and dried with a nitrogen gun.

To study the kinetics of the thiol-yne reactions on the alkyne polymer layer, polymer layers were wetted with a respective thiol solution, covered with a fluorinated quartz slide and irradiated with UV light for different times. Time exposures of UV light were controlled by a time-controller (OAI 150 Exposure Timer). The minimum exposure time is 0.1 s. After the reaction, the samples were washed extensively with

acetone and dried with a nitrogen gun. Then static WCAs of the polymer surfaces were measured.

Preparation of superhydrophobic–superhydrophilic micropatterns via click photopatterning

A typical example for the preparation of superhydrophobic–superhydrophilic micropatterns using subsequent thiol-yne reactions is presented. First, the alkyne porous layer was wetted with acetone solution containing 5 vol% 1*H*,1*H*,2*H*,2*H*-perfluorodecanethiol, covered by a fluorinated quartz slide, and irradiated by UV light through a photomask for 15 s. After removing the photomask, washing with acetone and drying, the polymer layer was wetted with an ethanol solution containing 15 wt% cysteamine hydrochloride and irradiated by UV light for another 15 s. Finally, the plate was washed extensively with acetone and dried with a nitrogen gun.

After the first reaction, the exposed fluoro-surface showed superhydrophobicity with θ_{st} , θ_{adv} , and θ_{rec} as high as 170°, 173°, and 164°, respectively, while the θ_{st} of unexposed alkyne functionalized areas were maintained at 124°. After the second reaction with cysteamine, the θ_{st} on the alkyne areas reduced to 4.4°. As for the fluorinated areas, the receding WCA decreased by only 2°, while the advancing WCA did not change at all and the surface maintained superhydrophobicity, confirming almost completeness of the reaction of the first step.

Preparation of inverse patterns

Patterns with superhydrophobic spots and superhydrophilic barriers can be created by switching the order of the thiols used for functionalization and using the same method and the same photomask.

Using the thiol-yne patterning method for creating peptide patterns

The alkyne HEMA-EDMA porous layer was first wetted with a 9/1 water/ethanol solution. Then, the plate was washed extensively with pure water to replace the ethanol-water solution with water. Excess of water was removed from the surface and 10 μ L of the aqueous peptide solution (fluorescein- β -Ala-GGGGC, 0.25 mg/mL) was dropped on the surface. The substrate was covered with a fluorinated quartz slide and a photomask. The polymer layer was then irradiated with UV light through a photomask for 15 s (6 mW cm⁻², 260 nm). Then, the plate was washed extensively with ethanol and dried with a nitrogen gun.

Cell microarray

Hela-GFP cells were cultured in DMEM containing 10% of fetal bovine serum (FBS). A cell suspension was obtained by trypsinizing a confluent (80% monolayer) culture

grown in a Petri dish in an incubator (37°C, 5% CO₂) for 2–3 days. For sterilization, the glass substrate with a superhydrophobic–superhydrophilic pattern was kept in ethanol for 20 min, dried in air, and placed in a 10 mL Petri dish. Then, 5 mL of cell-suspension was added so that the plate was fully covered (seeding density: 12100 cells cm⁻²). The seeded array was cultured in the incubator for 2 d.

5 DropletMicroarray: facile formation of arrays of microdroplets and hydrogel micropads for cell screening applications

Although we have demonstrated that cell microarrays can be useful cell screening tools in 2D and that there was minimal cross-contamination of the transfection mixtures between the hydrophilic microspots, this may not be true when screening a library of chemicals that have high rates of diffusion. Therefore, it would be advantageous to be able to isolate each microspot containing a different chemical as a self-contained microreactor rather than immerse the whole array of chemicals in a shared culture medium. In this chapter, we present a facile and novel method to create high-density arrays of thousands of separated microdroplets that can be used for high-throughput cell screening applications. We found that arrays of droplets of defined geometry and volume (DropletMicroarrays) spontaneously formed on the superhydrophilic–superhydrophobic patterned surfaces simply by moving an aqueous solution across the pattern. We demonstrate that the DropletMicroarray can be used to encapsulate chemicals and cells in the individually confined microdroplets as well as in arrays of hydrogel micropads. This chapter was originally published as an article in *Lab on a Chip* in October 2012 and is reproduced with permission from The Royal Society of Chemistry (Ueda *et al.*, 2012).

DropletMicroarray: facile formation of arrays of microdroplets and hydrogel micropads for cell screening applications

Erica Ueda,^a Florian L. Geyer,^{ab} Victoria Nedashkivska^{ab} and Pavel A. Levkin^{*ab}

^a Institute of Toxicology and Genetics, Karlsruhe Institute of Technology, Postfach 3640, Germany

^b Department of Applied Physical Chemistry, Heidelberg University, Germany

Lab Chip 2012, 12, 5218–5224. DOI: 10.1039/C2LC40921F

Author contributions:

Erica Ueda designed and performed the experiments and analysis, and wrote the manuscript.



Florian L. Geyer originally developed the fabrication method for the superhydrophilic-superhydrophobic patterned surfaces, which was first published in *Angew. Chem., Int. Ed.* 2011, 50, 8424–8427. DOI: 10.1002/anie.201102545.



Victoria Nedashkivska contributed Figure 2b and she performed the quantification of droplet volume experiments.

Pavel A. Levkin contributed to the original idea of the project, the experimental design, and editing of the manuscript.



5.1 Article

High-throughput (HT) screening of live cells is an immensely important and growing task in areas ranging from studies of gene functions using RNA interference (Lindquist *et al.*, 2011) and the search for new drug candidates (Wood *et al.*, 2012) to screenings of new gene delivery systems (Siegwart *et al.*, 2011) and the identification of factors controlling stem cell differentiation (Brafman *et al.*, 2012). During the last decade, cell microarrays—a miniaturized method for HT cell screening—have been developed (Baghdoyan *et al.*, 2004; Erfle *et al.*, 2007; Geyer *et al.*, 2011; Hook *et al.*, 2009b; Mousses *et al.*, 2003; Neto *et al.*, 2011; Rantala *et al.*, 2011; Stürzl *et al.*, 2008; Ziauddin & Sabatini, 2001). However, this method is limited to transfection of adherent cells and is unable to physically isolate one microspot from another. In addition, free diffusion of small molecules from neighboring microspots into the shared medium reduces the scope of possible applications of cell microarrays. Thus, most cell-based screenings are still performed using either 96- or 384-well microplates. The recent emphasis on screening of nonadherent or single cells (Lindström & Andersson-Svahn, 2010) and cells in 3D microenvironments (Pampaloni *et al.*, 2007; Skardal *et al.*, 2012) has also encouraged the development of new screening platforms.

Droplet microfluidics-based cell culture platforms are actively progressing and are able to address some of these issues. Cells encapsulated within picoliter- to microliter-sized droplets surrounded by an immiscible fluid, such as oil, are self-contained and can be rapidly produced (up to kHz). Positional organization of the droplets can aid in more efficient HT screening of these droplets, especially for visualization and time-lapse measurements. However, depending on the chip design, up to 90% of the droplets may not be trapped in a microfluidic static droplet array, so precious samples could be lost, and even if the droplets are immobilized they are shown to shrink over time due to the flow of oil (Huebner *et al.*, 2009). In addition, managing thousands of droplets in a microfluidic device can lead to complicated chip designs and many components, as well as long channels with high resistance to flow that can require higher pressures than the material can handle (Schmitz *et al.*, 2009). Another technology used to control small-scale droplet movement is digital microfluidics by electrowetting on dielectric (EWOD), which modulates the interfacial tension, using an electric field, between the droplet and the underlying electrode coated with a dielectric layer. Although this method can precisely control the movement of the droplet, it requires optimization of the actuation parameters for each droplet manipulation such as dispensing and splitting since the errors multiply with each step (Vergauwe *et al.*, 2011). While microfluidics-based platforms seem promising for screens requiring many complex droplet manipulations, a simpler platform that is still capable of screening bioactive molecules, adherent cells, nonadherent cells, and cells in 3D microenvironments is desirable.

In the present work, we describe a facile one-step method for creating thousands of isolated microdroplets with defined geometry and volume, herein referred to as a DropletMicroarray. We show that the extreme wettability contrast of superhydrophilic spots on a superhydrophobic background allows spontaneous separation of an aqueous solution, leading to the formation of high-density arrays of completely separated microdroplets. This rapid and facile droplet formation does not require manual pipetting or a liquid handling device. Bioactive molecules, nonadherent cells, or microorganisms can be trapped in the fully isolated microdroplets. In this work, we also show the application of the DropletMicroarray for the preparation of a high-density array of hydrogel micropads encapsulating live cells, which can be used for HT screening of cells in 3D microenvironments.

Results and discussion

Droplet formation

To make an array of superhydrophilic spots on a superhydrophobic surface, we employed a recently published procedure developed in our group (Geyer *et al.*, 2011). A 12.5 μm thin, superhydrophilic layer of nanoporous poly(hydroxyethyl methacrylate-*co*-ethylene dimethacrylate) (HEMA-EDMA) was photografted with 2,2,3,3,3-pentafluoropropyl methacrylate (PFPMMA) through a quartz chromium photomask to create superhydrophobic regions (details in Supporting Information). Using this method, arrays of superhydrophilic spots with specific geometry and size can be created. The superhydrophilic spots can be separated by superhydrophobic barriers with widths as narrow as 50 μm . Photografting occurs through the whole thickness of the porous polymer film, thus there is no mixing of solutions between the superhydrophilic spots (Geyer *et al.*, 2011). In this work, we used pattern geometries consisting of superhydrophilic circles (3 or 1 mm diameter, 100 μm barrier), triangles (3 or 1 mm side length, 100 μm barrier), hexagons (2 or 1 mm side length, 100 μm barrier), and squares (2 mm, 1 mm, 800 μm , 650 μm , 500 μm , 200 μm , or 100 μm side length, 100 μm barrier; 500 μm side length, 62.5 μm barrier; 335 μm side length, 60 μm barrier).

We show that it is possible to create arrays of thousands of microdroplets in a single step simply by dipping the substrate into an aqueous solution or rolling a droplet across the surface (Figs. 5.1 and 5.S1; Video S1). The rolling droplet method is useful for printing precious reagents because many spots can be filled without using a large amount of solution. Due to the extreme difference in wettability of the superhydrophilic spots compared to the superhydrophobic barriers, water is spontaneously removed from the barriers but fills the superhydrophilic regions. A similar process is described by Jackman *et al.* as discontinuous dewetting, where the differences in interfacial free energies of the surface and liquid cause an abrupt change in the receding water contact angle (WCA) as liquid moves from the superhydrophilic area to the superhydrophobic barrier (Jackman *et al.*, 1998). The liquid becomes pinned at the boundary between the

superhydrophilic and superhydrophobic areas, and as the liquid continues to move across the barrier the liquid film thins and eventually separates from the pinned droplet.

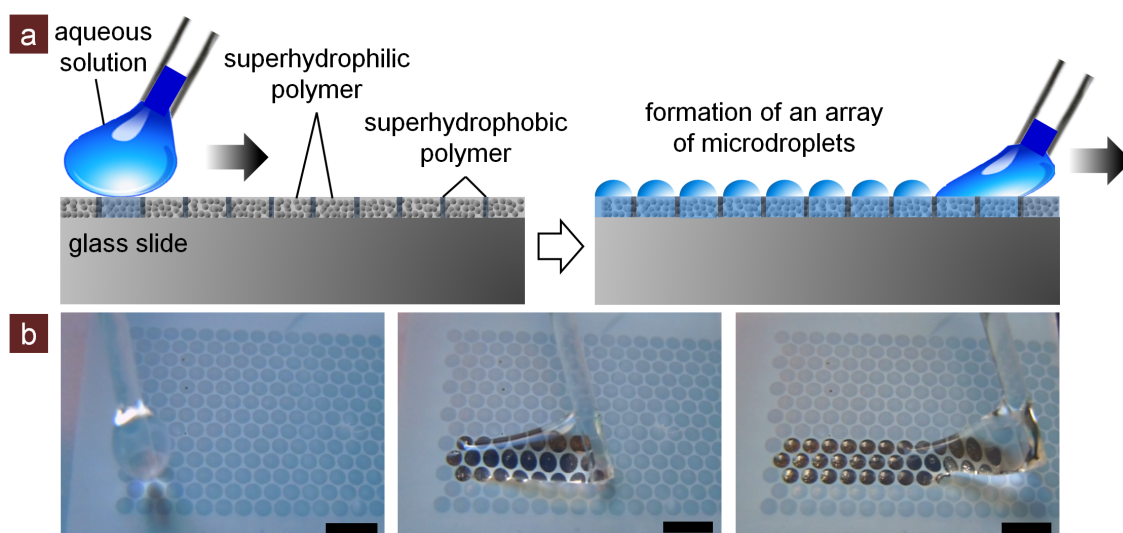


Figure 5.1 Formation of a DropletMicroarray using the rolling droplet method

(a) Schematic of a superhydrophilic, nanoporous polymer layer grafted with superhydrophobic moieties. When an aqueous solution is rolled along the surface, the extreme wettability contrast of superhydrophilic spots on a superhydrophobic background leads to the spontaneous formation of a high-density array of completely separated microdroplets. (b) Snapshots of water being rolled along a superhydrophilic–superhydrophobic patterned surface (1 mm diameter circles, 100 μm barrier) to form droplets only in the superhydrophilic spots. Scale bars are 3 mm.

The nanoporous HEMA-EDMA surface which is photografted with PFPMA on a large area possesses static, advancing, and receding WCAs of 165° , 167° , and 157° , respectively (Geyer *et al.*, 2011). No separated droplets could be formed on patterned substrates having a low receding WCA on 60 μm -wide hydrophobic barriers (data not published). This demonstrates that automatic formation of densely packed droplets will only occur when there is an extreme difference in the receding WCA between the hydrophilic and hydrophobic areas. In cases where there are insignificant differences between the receding WCAs, the formation of droplets is still possible if the width of the hydrophobic barriers are significantly increased, at the expense of droplet density and hence the throughput.

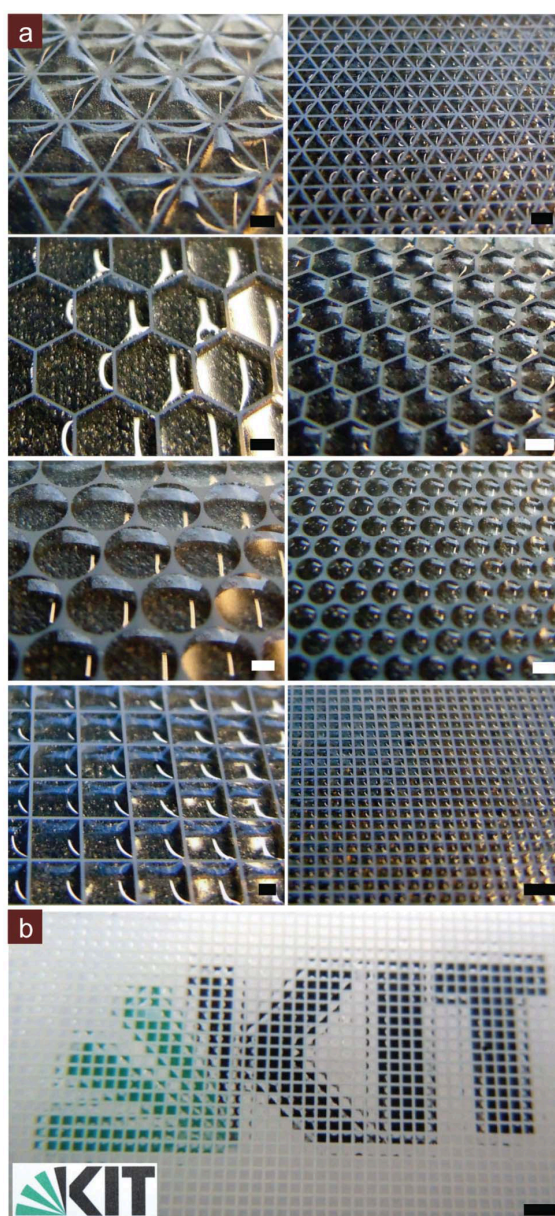


Figure 5.2 Images of Droplet Microarrays with different geometries

(a) Droplet Microarrays formed by dipping the superhydrophilic–superhydrophobic patterns of different geometries into water. (b) Wetted superhydrophilic–superhydrophobic micropattern becomes transparent and displays a lens effect, showing the underlying logo. Scale bars are 1 mm.

Examples of arrays of water microdroplets with different geometries and sizes are depicted in Fig. 5.2a. Formation of droplets in sharp-edged complex geometries, such as triangles, is also possible. As shown in the images, as soon as the nanoporous superhydrophilic areas are wetted, the polymer becomes transparent due to reduced light

scattering caused by matched refractive indexes, allowing easier discrimination of spots and facilitating the use of inverted microscopes. Each microdroplet functions as a small lens with the surface curvature determined by the geometry of the superhydrophilic spot (Fig. 5.2b).

The volumes of the individually formed droplets depend on the size and geometry of the superhydrophilic spots, as well as on the surface tension of the solution (Fig. 5.S2), and can be controlled between 700 pL and 3 μ L for the patterns we tested (Fig. 5.3a and Supporting Information). Thus, an array of 85,000 700 pL microdroplets can be easily formed in a matter of seconds on a microtiter plate-sized glass slide prepatterned with $200 \times 200 \mu\text{m}^2$ superhydrophilic squares separated by 100 μm wide superhydrophobic barriers. Approximately fifty-five 1536-well plates would be needed for the equivalent of 85,000 wells. It should be noted that although droplet microfluidics provides comparable or even higher throughput, the addressability of the droplets surrounded by oil and located inside microfluidic channels is significantly more difficult than that of droplets positioned in defined X,Y locations on the surface of the DropletMicroarray.

To determine if the volumes of the droplets are homogeneous and reproducible, square patterns (500 μm side length, 62.5 μm barriers) were dipped into Rhodamine 6G water solutions to create an array of 8 nL microdroplets, dried, and then imaged to measure the fluorescence intensities. Three different concentrations of Rhodamine 6G were tested (0.1, 0.05, and 0.025 mg ml^{-1}), and for each concentration three different substrates were measured. Multiple images were taken of each substrate. Fig. 5.3b shows an example of the selected regions of interest (ROI), and Fig. 5.3c compares the intensity profile from one sample at each of the three different Rhodamine 6G concentrations. The fluorescence intensities are relatively equal across each sample, and the intensity increases with Rhodamine 6G concentration. The slight variability of the Rhodamine 6G intensity within each square is probably due to the nature of the rough polymer surface. When the fluorescence intensity within each square was averaged over all three samples for each Rhodamine concentration, there was low variability in the measurements (Fig. 5.3d). The mean fluorescence intensities were $154 \pm 2.2\%$, $121 \pm 1.8\%$, $91.0 \pm 0.42\%$, and $6.09 \pm 0.35\%$ for Rhodamine 6G concentrations of 0.1, 0.05, 0.025, and 0 mg/ml, respectively. This indicates that the formation of isolated droplets on the superhydrophilic–superhydrophobic polymer surface is reproducible and results in low variability of the individual droplet volumes. This variability is comparable to what is achievable with optimized parameters in EWOD devices, which can have coefficient of variances as low as 2% (Vergauwe *et al.*, 2011).

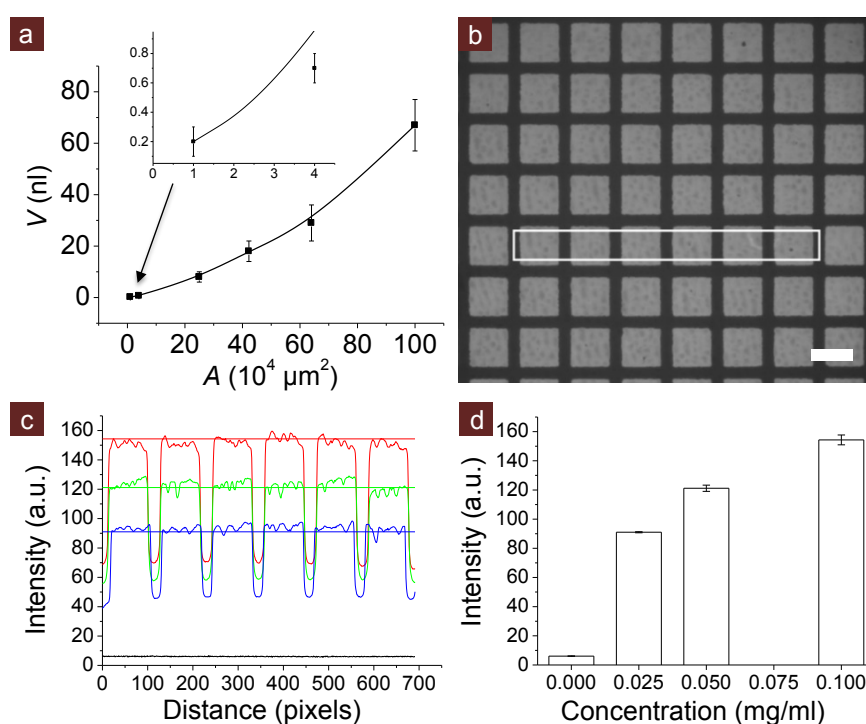


Figure 5.3 Droplet volume quantification and reproducibility

(a) Influence of the superhydrophilic spot area (A) on the average water droplet volume (V) confined in a single spot of square geometry ($100 \mu\text{m}$ superhydrophobic barriers for all patterns). Inset zooms in on the first two data points. Data in Table 5.S2. (b) An example of a ROI selected to quantify droplet reproducibility. Grayscale image shows 0.1 mg ml^{-1} Rhodamine 6G deposited on an array of superhydrophilic squares ($500 \mu\text{m}$ side length, $62.5 \mu\text{m}$ barrier) after drying in air. Scale bar is $500 \mu\text{m}$. (c) The fluorescence intensity profile of six squares ($500 \mu\text{m}$ side length, $62.5 \mu\text{m}$ barrier) from a representative sample for 3 different concentrations of Rhodamine 6G: 0.1 mg ml^{-1} (red), 0.05 mg ml^{-1} (green), 0.025 mg ml^{-1} (blue), and 0 mg ml^{-1} (black). Horizontal line is the mean fluorescence intensity across the triplicates analyzed for each Rhodamine 6G concentration (also shown in Fig. 5.3d). (d) The mean Rhodamine 6G fluorescence intensity in the superhydrophilic spots across the triplicates analyzed for each Rhodamine 6G concentration. Error bars are \pm SD.

With such small droplet volumes and large surface-to-volume ratios, methods to prevent evaporation of the droplets are critical. High humidity ($\sim 80\%$ RH) environments can slow evaporation, but we also found that Petri dishes, which were pre-humidified such that condensation formed on the lids, were able to inhibit evaporation of 8 nl water droplets formed on a pattern of squares ($500 \mu\text{m}$ side length, $62.5 \mu\text{m}$ barriers) for at least 8 h when kept in a room at ambient conditions (28°C , 40%

RH). Surrounding the substrate with drops of PBS instead of water also seemed to slow evaporation. In an incubator where it is much more humid, longer incubation times for cells, at least 24 h, is possible. Alternatively, the droplets can be covered with a layer of immiscible oil that is permeable to air.

Encapsulation of cells in arrays of microdroplets

The formation of DropletMicroarrays on the superhydrophilic–superhydrophobic nanoporous polymer substrate can be used as a rapid and convenient tool for the patterning of chemicals, particles, cells, or any other components present in an aqueous solution. Fig. 5.4a shows an array of microdroplets containing human cervical tumor cells stably expressing green fluorescent protein (HeLa-GFP) 18 h after droplet formation on a square pattern (500 μm side length, 62.5 μm barriers). The brightfield images show that the droplets have not evaporated, while the fluorescence images show that cells were present in each droplet on the array and no cells were present on the superhydrophobic barriers. This type of array combines the features of microplates, where cells present in individual wells are physically isolated from each other, with the advantages of miniaturization and parallelization of cell microarrays used for reverse cell transfection.

As opposed to droplet microfluidics, superhydrophilic spots on a DropletMicroarray can be directly pre-printed with libraries of small molecules or transfection reagents using a conventional contact or non-contact microprinter. The diffusion of small molecules will be confined to the individual microdroplets, which in turn can save a lot of precious materials and prevent inter-spot mixing. DropletMicroarrays allow the rapid formation of thousands of droplets of any tailored geometry or arrangement and the encapsulation of microorganisms. A disadvantage is that the small volume of the microdroplets limits the number of cells or time that cells can be cultured inside individual droplets to avoid nutrient starvation. For the 500 μm side length square pattern that forms droplets of approximately 8 nl, a single cell per droplet is equivalent to a cell concentration of 125,000 cells ml^{-1} . In a Petri dish with a confluent layer of cells, the cell concentration can be around 1 million cells ml^{-1} . This suggests that multiple cell divisions of a single cell or several cells cultured for a shorter time in the droplet would be acceptable. This limitation could also be overcome by optimizing the culture medium, or using inkjet printers, piezoelectric dispensers, or microfluidic devices to exchange medium in the droplets. Nevertheless, this one-step formation of thousands of microdroplets incorporating cells or other biological species can be useful for a variety of screening applications.

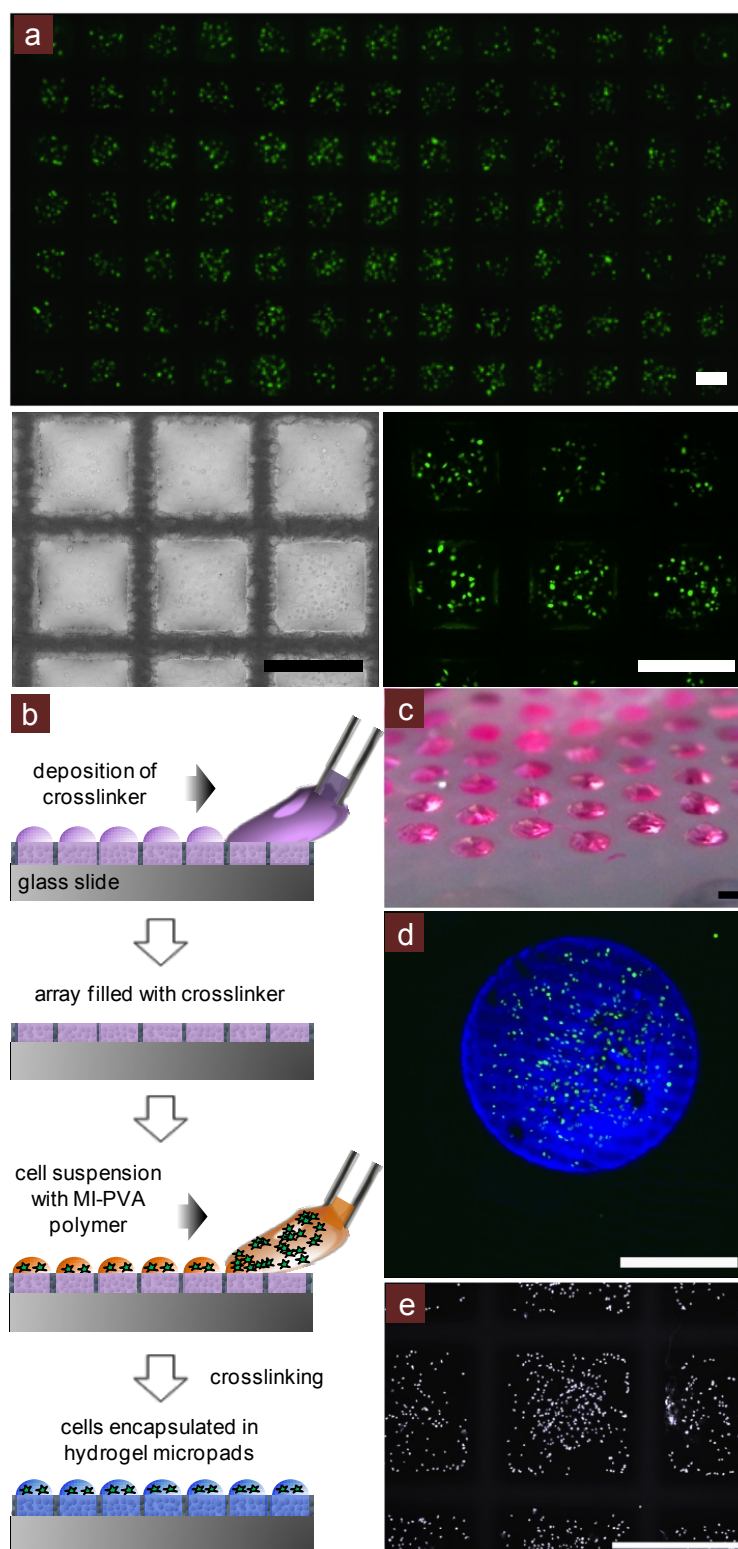


Figure 5.4 Encapsulation of cells in arrays of microdroplets and hydrogel micropads

(a) Fluorescent HeLa-GFP cells cultured in individual microdroplets for 18 h. (b) Schematic showing the formation of arrays of hydrogel micropads incorporating cells. First, PEG-crosslinker is deposited in the superhydrophilic spots using the rolling droplet method and then dried in air. Then, a cell suspension mixed with MI-PVA is deposited using the rolling droplet method and crosslinking occurs to form separated hydrogel micropads encapsulating cells. (c) Hydrogel micropads stained with Rhodamine 6G, in air. (d) Fluorescent HT1080-eGFP cells encapsulated in hydrogel micropads stained with 7-diethylamino-3-(4-maleimidophenyl)-4-methylcoumarin (blue) for gel visualization after hydrogel crosslinking and immersion in medium. Cells remain contained within the hydrogel. (e) Fixed and DAPI-stained (white) It-NES cells encapsulated in hydrogel micropads at day 6. Brightfield images in Fig. 5.S4. Scale bars are 500 μm .

Encapsulation of cells in arrays of hydrogel micropads

Culturing cells in 3D microenvironments, such as hydrogels, versus 2D cell culture has been shown to more closely mimic the *in vivo* situation (Skardal *et al.*, 2012). It was also shown that cell behavior in a 3D microenvironment can be different from the behavior of cells cultured on flat surfaces (Pampaloni *et al.*, 2007). Therefore, HT screening of cells in 3D systems is an important challenge which is yet to be fully realized.

We demonstrate the applicability of the DropletMicroarray for creating arrays of hydrogel micropads incorporating cells. Fig. 5.4b schematically shows the process of formation of an array of hydrogel micropads. In the first step, a poly(ethylene glycol) crosslinker bearing two thiol groups (PEG-crosslinker) is printed onto the superhydrophilic microspots by rolling a droplet across the surface, and then allowed to dry. In the next step, an array of microdroplets containing a solution of maleimide-functionalized polyvinyl alcohol (MI-PVA) and cells is created using the rolling droplet method. The thiol groups in the PEG-crosslinker form thioether bonds with the maleimide groups in the MI-PVA and crosslink the polymer to form a stable, biocompatible hydrogel within minutes in which living and nonadherent cells can be trapped. Thus, only *two steps* and several minutes are necessary to create an array of up to 85,000 hydrogel micropads for performing high-throughput cell screening.

After the hydrogel is formed, the array of hydrogel micropads incorporating cells can be immersed in cell culture medium or droplets of medium can be formed in the superhydrophilic spots to isolate each hydrogel micropad for further culturing. Fig. 5.4c shows an array of hydrogel micropads in air that have been incorporated with Rhodamine 6G dye for visibility. In addition, live cells (HT1080-eGFP human fibrosarcoma cells and long-term self-renewing neuroepithelial-like stem cells (It-NES

cells) derived from hESC lines H9) were encapsulated and distributed throughout the hydrogel micropads and imaged after hydrogel formation and six days, respectively (Figs. 5.4d,e, 5.S3, and 5.S4; Video S2) (Koch *et al.*, 2009). Incorporating the thiol-reactive probe, 7-diethylamino-3-(4-maleimidophenyl)-4-methylcoumarin, in the PEG-crosslinker mixture allows us to visualize successful crosslinking of the gel since it only fluoresces when it reacts with the thiol groups on maleimide. Figs. 5.4d and 5.S3 confirm that hydrogels were only formed within the superhydrophilic spots and no cells were observed outside the gel. Fig. 5.4e also demonstrates that no cells lie on the superhydrophobic barriers and are immobilized by the hydrogel in the superhydrophilic spots. The fluorescent HT1080-eGFP cells (Fig. 5.4d) can be visualized starting from the top to the bottom of the hydrogel in a 196 μm z-stack obtained using a confocal microscope (Video S2).

The two-step procedure introduced here to form hydrogels encapsulating cells in about 5 min is simple enough to be used for screening cells in 3D hydrogels. In principle, our superhydrophilic–superhydrophobic polymer substrate is compatible with other methods for forming hydrogels, provided the surface tension of the pre-hydrogel mixture is high enough. For example, UV-initiated curing of gelatin methacrylate (Nichol *et al.*, 2010; Qi *et al.*, 2010) or PEG diacrylate (Hancock *et al.*, 2012a; Qi *et al.*, 2010), or ionic crosslinking of alginate-based hydrogels (Fernandes *et al.*, 2010; Salgado *et al.*, 2012; Song *et al.*, 2010; Zawko & Schmidt, 2010) could be potentially formed on our substrate according to the referenced methods. For our method presented here, the MI–PVA hydrogel was especially appealing because it is a facile and quick method, gentle in terms of cell handling, and does not require exposing cells to UV light. In addition, the MI–PVA hydrogel can be easily incorporated with, for example, adhesive peptides such as RGD, other ECM motifs, signaling molecules, drugs, or other small molecules for 3D cell screenings.

Doxorubicin cytotoxicity screen using 3D hydrogel micropads

As a proof-of-concept of the application of arrays of hydrogel micropads for cell screening, we performed a cytotoxicity test by exposing human breast adenocarcinoma cells (MDA-MB-231) to doxorubicin, a chemotherapeutic drug known to induce apoptosis. Decreasing amounts of doxorubicin (25, 20, 15, 10, 5, and 2.5 ng) and a water control were pre-printed in superhydrophilic spots of a circular pattern (1 mm diameter, 500 μm superhydrophobic barriers). MI–PVA hydrogel micropads encapsulating MDA-MB-231 cells were formed in these spots and briefly immersed in medium to swell the hydrogel, and then removed from the medium to isolate each hydrogel micropad during incubation. After 18 h of incubation, the cells in the hydrogel micropads were stained with Calcein AM and propidium iodide (PI) to quantify live and dead cells, respectively.

The percentage of apoptotic cells exhibited a dose-dependency on the amount of pre-printed doxorubicin. The percentage of Calcein AM-positive cells decreased while the percentage of PI-positive cells increased with increasing amounts of pre-printed doxorubicin (Fig. 5.5). This demonstrates that doxorubicin was able to diffuse from the substrate into the hydrogel over the 18 h incubation time and induce apoptosis, and the hydrogel micropads were isolated such that no apparent mixing of doxorubicin and the water control was observed. This simple example shows the feasibility of screening cells in hydrogel micropads.

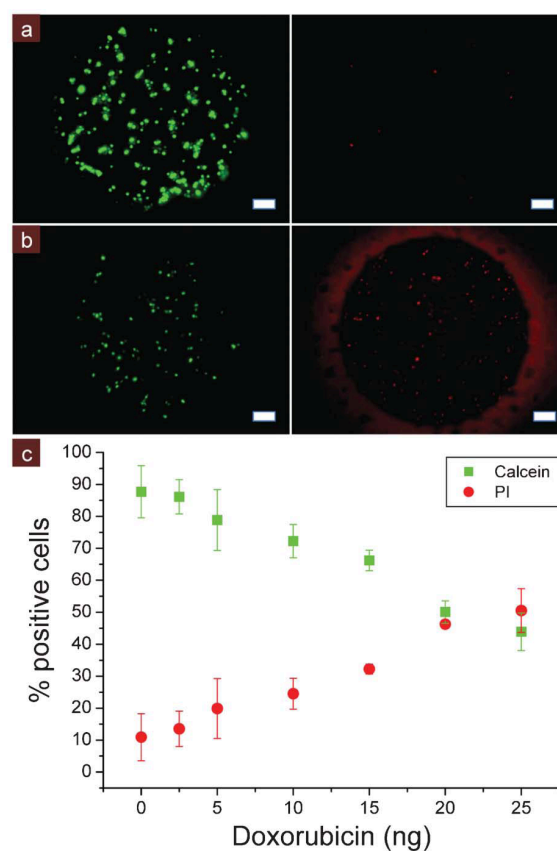


Figure 5.5 Doxorubicin cytotoxicity screen using hydrogel micropads

Doxorubicin cytotoxicity screen using hydrogel micropads encapsulating MDA-MB-231 cells. After 18 h of incubation, cells were stained with Calcein AM (green) and propidium iodide (PI) (red). (a) Stained cells in hydrogel micropad on spot pre-printed with water control. (b) Stained cells in hydrogel micropad on spot pre-printed with 25 ng of doxorubicin. Scale bars are 100 μm . Fluorescent intensity has been enhanced for visualization. (c) Mean percentage of Calcein AM and PI-positive cells per hydrogel micropad for each amount of pre-printed doxorubicin after 18 h of incubation. Error bars are \pm SD.

In terms of non-destructive bioassays, the hydrogel micropads are compatible with mainly live-cell imaging, monitoring fluorescent reporter genes, or immunofluorescence staining, and possibly enzymatic or colorimetric assays. The superhydrophobic barriers can contain different solutions in each superhydrophilic spot, thus different probes can be deposited and incubated on each spot. The main limitation against performing bioassays is washing of individual micropads without mixing. Destructive bioassays, such as Western blotting, may be possible since the hydrogel micropads containing cells can be physically addressed from outside, removed, and further degraded.

Materials and methods

All polymerizations and photografting were carried out on an OAI Model 30 deep-UV collimated light source (San Jose, CA) fitted with an USHIO 500 W Hg-xenon lamp (Japan). Irradiation intensity was calibrated to 12 mW cm^{-2} (5.10 mW cm^{-2} after cover glass slide, 4.77 mW cm^{-2} after cover glass slide and photomask) using an OAI 360 UV power meter with a 260 nm probe head. Schott (Germany) Nexterion Glass B UV transparent glass plates were used as substrates for polymer layers. Monomers were purchased from Sigma-Aldrich (Germany). Biochemicals were purchased from Life Technologies (Germany). HeLa-GFP cells were purchased from Biocat (Germany). HT1080-eGFP and MDA-MB-231 cells were provided by the Institute for Toxicology and Genetics at Karlsruhe Institute of Technology. Long-term self-renewing neuroepithelial-like stem cells (It-NES cells) derived from hESC lines H9 were generously provided by Dr. Philipp Koch at the University of Bonn.

Quantification of the reproducibility of individual droplet volumes

Substrates were dipped into a Rhodamine 6G water solution (0.1 mg ml^{-1} , 0.05 mg ml^{-1} , or 0.025 mg ml^{-1}) for 5 sec, removed to form a DropletMicroarray, and then dried in air. Patterns were imaged on a Leica MZ10 F widefield microscope ($2.5\times$ zoom, 2.47 ms exposure time) at three locations per sample and three samples per Rhodamine 6G concentration. Fluorescence intensity was quantified using ImageJ. ROI spanning six squares were selected on the images acquired for three different concentrations and the intensity profiles were plotted. To calculate the mean intensity and standard deviation over all three samples for each Rhodamine 6G concentration, many ROI within single squares were selected and the mean intensity of each histogram was measured to calculate the mean intensity and standard deviation across all three samples for each Rhodamine 6G concentration.

Hydrogel array formation

The 3-D Life PVA-PEG Hydrogel Kit from Cellendes GmbH (Germany) was used to form hydrogels. For hydrogel visualization, the crosslinker solution was prepared by

mixing 23 μl PEG-crosslinker + 2 μl of 1 mg/ml 7-diethylamino-3-(4-maleimidophenyl)-4-methylcoumarin in DMSO. Otherwise, just 25 μl of PEG-crosslinker was used. The patterned substrate was placed in a Petri dish. A pipette was used to roll the 25 μl of crosslinker solution across the patterned substrate. Only the hydrophilic spots were wetted with the crosslinker solution. The crosslinker solution was dried. The MI-PVA cell solution was prepared such that the final concentration of MI was 6 mM: 12.5 μl water + 2.5 μl 10X CB pH 5.5 buffer + 5 μl MI-PVA (30 mM MI stock) + 5 μl of 80×10^6 cells ml^{-1} cell suspension. A pipette was used to roll the 25 μl of MI-PVA-cell solution across the patterned substrate where the crosslinker solution was printed. This was done quickly and if available under humid conditions to prevent the gel from drying out. Droplets of medium or PBS were dispensed around the substrate and then put in a humidified incubator until the polymerization was finished (about 5 min). The hydrogel-cell array was then immersed in medium. See Video S2 to visualize the fluorescent HT1080-eGFP cells (Fig. 5.4d) starting from the top to the bottom of the hydrogel in a 196 μm z-stack obtained using a Leica TCS SP5 confocal microscope.

Doxorubicin cytotoxicity screen

Doxorubicin solutions (50, 40, 30, 20, 10, and 5 $\mu\text{g ml}^{-1}$ in water) and a water control were pipetted in a row at 0.5 μl each in the superhydrophilic spots of a circle patterned substrate (1 mm diameter, 500 μm barrier). Three replicate rows were printed on each of two different substrates. MI-PVA hydrogel micropads encapsulating MDA-MB-231 cells were formed as described above on the pre-printed spots, but instead using 5 μl of 20×10^6 cells ml^{-1} cell suspension. After the hydrogel was crosslinked in 5 min, the substrate was immersed in medium for 1 min to swell the hydrogel and then removed from the medium to isolate each hydrogel micropad during incubation. After 18 h of incubation, the cells in the hydrogel micropads were washed twice with PBS, stained with 0.5 μM Calcein AM, 500 nM PI, and 1 $\mu\text{g ml}^{-1}$ Hoechst 33342 for 20 min, rinsed once with PBS, and imaged as z-stacks on a Keyence BZ-9000 fluorescence microscope (Japan). The images were quantified in ImageJ using the Cell Counter plugin. All other procedures are explained in detail in the Supporting Information.

Conclusions

We developed a facile and rapid method to fabricate microarrays of separated, spatially organized droplets with controlled position, geometry, and volume on a superhydrophilic, nanoporous polymer surface patterned with superhydrophobic moieties. The droplets can encapsulate any substance dissolved or suspended in an aqueous solution, and drying the droplets results in the homogeneous deposition of the substance in the superhydrophilic microspots.

The droplet deposition method can also be used to form arrays of hydrogel micropads incorporating cells. Nonadherent cells or other microbiological species (amoeba, bacteria, yeast) can easily be immobilized in a high-density 3D array and used for biological screens. The small volumes of the droplets require fewer reagents compared to microplates and can enhance the detection of low abundance molecules or signals. The DropletMicroarray does not rely on physical barriers to separate the droplets, so the glass slides can be coverslipped if needed.

As opposed to droplet microfluidics where screenings of large libraries of molecules are difficult to perform in the droplets, DropletMicroarrays are compatible with both automated contact and noncontact printing techniques, thus combining the advantages of microarray technology and the HT compartmentalization abilities of droplet microfluidics. In combination with automated printing techniques, the droplets can be individually addressed or exactly a single cell cultured in each droplet (Yusof *et al.*, 2011). Our superhydrophilic–superhydrophobic surfaces could also be combined with technologies such as digital microfluidics to have full control of liquid movement across the surface and thus droplet formation (Barbulovic-Nad *et al.*, 2010; Witters *et al.*, 2011). It would also be possible to use our superhydrophilic–superhydrophobic surfaces to create crystal (Witters *et al.*, 2012) or protein arrays upon evaporation of droplets.

We envision DropletMicroarrays to be an important step towards the development of HT screening platforms that are practical and adaptable to screening nonadherent or single cells and 3D cell microenvironments with large libraries of molecules, such as drug candidates or nucleic acids. Currently, we are working towards several applications of this novel technology.

5.2 Supporting information

Superhydrophilic–superhydrophobic pattern preparation

Glass surface modification

To achieve covalent attachment of the polymer layer, the glass surfaces are first activated and then functionalized with an anchor group for methacrylates.

Activation of glass slides: Clean glass slides are immersed in 1 M NaOH for 1 h and afterwards washed with deionized water, and then immersed in 1 M HCl for 30 min, washed with deionized water, and dried with a nitrogen gun.

Modification of glass slides: Several drops of a solution containing 20% v/v 3-(trimethoxysilyl)propyl methacrylate in ethanol are dropped on an activated glass slide. The plate is covered with another activated glass slide. The solution is reapplied after 30 min. After another 30 min, the slides are washed with acetone and dried with a nitrogen gun.

Fluorination of glass slides: An activated glass slide is placed in a vacuumed desiccator together with a vial containing several drops of tridecafluoro-(1,1,2,2)-tetrahydrooctyltrichlorosilane over night.

Polymerization procedure and photografting

Polymerization: Two strips of Teflon film (American Durafilm Co.), defining the thickness of the polymer layer, are placed at the edges of a fluorinated glass slide and a modified glass slide is clamped on top of it. The polymerization mixture is injected in between the mold and irradiated for 15 min at 12 mW cm^{-2} with a 260 nm UV light. The mold is then carefully opened using a scalpel.

An inert, fluorinated glass slide is used as the bottom plate. The inability of covalent attachment of the growing polymer to the fluorinated glass slide allows for the whole polymer to stick to the top, modified glass slide during the separation process. The fluorinated glass slide can be reused several times. The resulting nonporous superficial layer can be easily removed by applying and rapidly removing adhesive film (Scotch tape) immediately after separating the plates while the layer is still wetted with porogen. The plate is washed extensively with methanol and kept in methanol for several hours to remove unreacted monomers and porogens.

Polymerization mixture: 2-hydroxyethyl methacrylate (24 wt%), ethylene dimethacrylate (16 wt%), 1-decanol (12 wt%), cyclohexanol (48 wt%), and 2,2-dimethoxy-2-phenylacetophenone (1 wt% with respect to monomers).

Photografting: The polymer layer is wetted with the photografting mixture and covered with a fluorinated glass slide. A quartz chromium photomask (Rose Fotomasken, Germany) is placed on top and it is irradiated for 30 min at 12 mW cm^{-2} with a 260 nm UV light. The obtained pattern is washed extensively with methanol and stored in methanol for several hours to remove excess monomer and porogen, and for sterilization before cell culture.

Photografting mixture: 2,2,3,3,3-pentafluoropropyl methacrylate (20 wt%), ethylene dimethacrylate (1.3 wt%), 1:3 (v/v) mixture of water:*tert*-butanol (78 wt%), benzophenone as the initiator (0.33 wt%).

Microdroplet formation with methyl green solution

Figure 5.S1 shows an array of squares and hexagons immersed in a methyl green water solution and slowly pulled out to form separated droplets in each superhydrophilic spot. After allowing the droplets to dry in air, methyl green is present only in the superhydrophilic spots and not on the superhydrophobic barriers. This demonstrates that the DropletMicroarray method can be used to deposit substances in one step into thousands of superhydrophilic spots of different geometries.

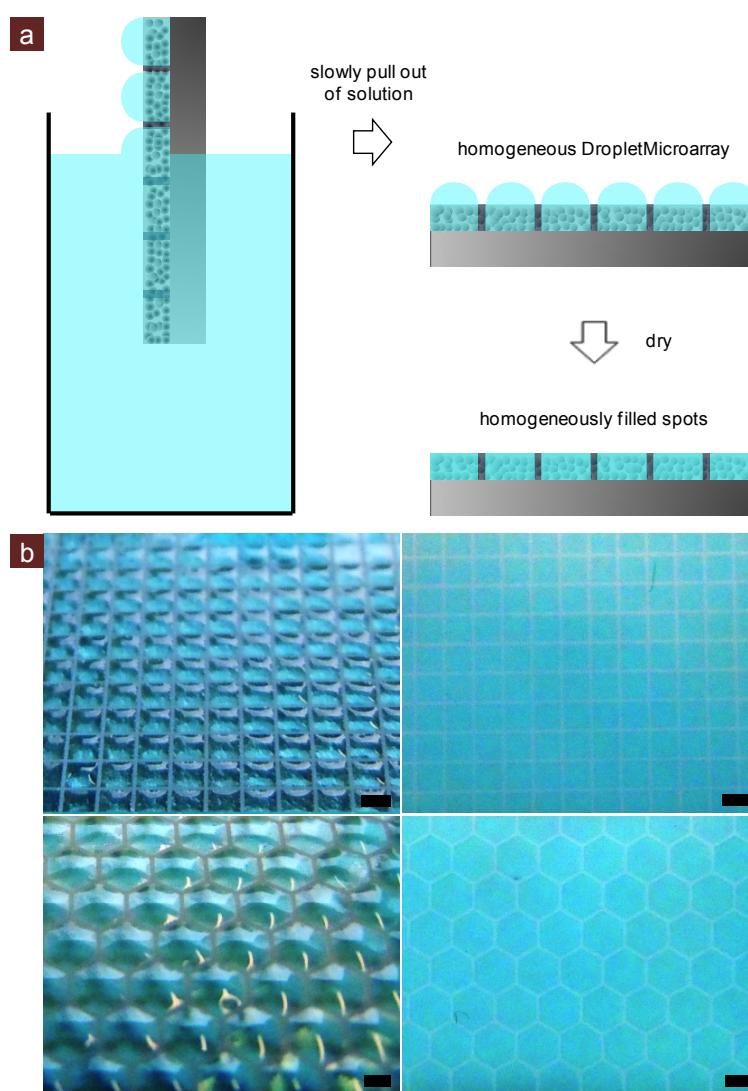


Figure 5.S1 Application of the DropletMicroarray for deposition of substances

(a) Schematic representation of the droplet deposition method. The superhydrophilic–superhydrophobic patterned substrate is immersed in an aqueous solution and pulled out of the solution to form homogeneous droplets in the superhydrophilic spots. (b) Microdroplets formed using a methyl green solution (left) and then dried (right). Scale bars are 1 mm.

Droplet volumes for different pattern geometries

With our superhydrophilic–superhydrophobic patterning technique, we had a smaller and larger droplet size limitation. The smallest microdroplets that could be produced had a volume of approximately 0.7 nl for a $200 \times 200 \mu\text{m}^2$ square pattern. This was mainly due to the limitations of the resolution using this patterning technique. The volume of large droplets is more difficult to control because of the increasingly important role of gravity. We observe this effect for $3 \times 3 \text{ mm}^2$ square patterns and larger.

Method for measuring volumes of water droplets:

1. Measure mass of water or other liquid that will be applied ($20 \mu\text{l}$, m_0).
2. Roll the droplet across the pattern of interest. Leftover solution is aspirated by pipette. Measure the mass of the leftover solution (m_1).
3. Determine the mass of the solution in a spot by subtracting the leftover mass from the initial mass and dividing it by the number of spots (N), $m=(m_0-m_1)/N$.
4. Calculate the volume of the droplet.

Table 5.S3 Dependence of the water droplet volume on the geometry and area of the superhydrophilic spot

All superhydrophobic barriers are $100 \mu\text{m}$.

Geometry	Area of the superhydrophilic spot, $10^6 \mu\text{m}^2$	Volume of droplet, nl
Triangle (1 mm side length)	0.433	14 ± 10
Circle (1 mm diameter)	0.785	72 ± 5
Square (1 mm side length)	1.000	67 ± 10
Hexagons (1 mm side length)	2.598	184 ± 50
Circle (3 mm diameter)	7.069	2815 ± 323

Table 5.S4 Dependence of the water droplet volume on the size of the superhydrophilic spot for a given geometry

The water droplet volume is greatly affected by the size of the superhydrophilic spot for a given geometry (here, square geometry). All superhydrophobic barriers are 100 μm . DropletMicroarrays were produced by the rolling drop method.

Side length of the superhydrophilic square, μm	Area of the superhydrophilic spot, $10^4 \mu\text{m}^2$	Volume of droplet, nl
100	1	0.2 ± 0.1
200	4	0.7 ± 0.1
500	25	8 ± 2
650	42.25	18 ± 4
800	64	29 ± 7
1000	100	67 ± 10

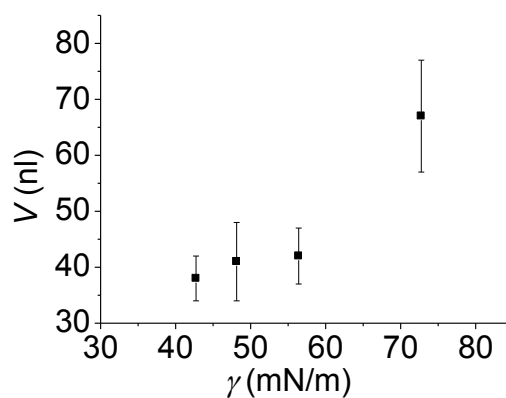


Figure 5.S2 Dependence of the water droplet volume on the liquid surface tension

Dependence of the water droplet volume (V) in a single spot of square geometry (1000 μm side length, 100 μm barrier) on the surface tension (γ) of the liquid (Vazquez *et al.*, 1995).

Hydrogel array images

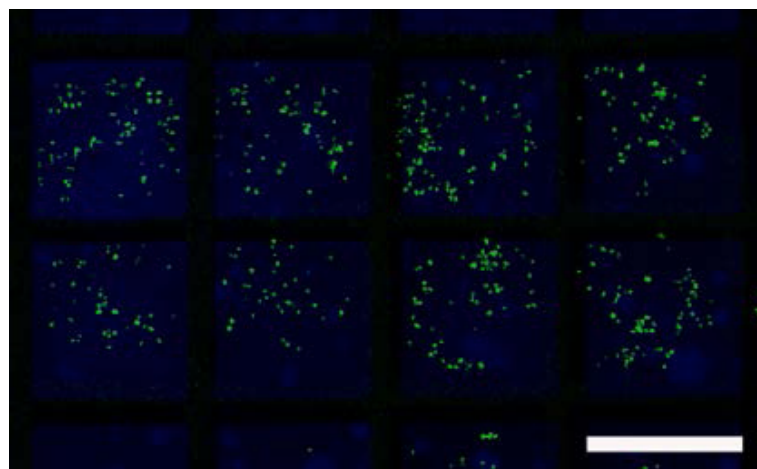


Figure 5.S3 HT1080-eGFP cells encapsulated in hydrogel micropads

Fluorescent HT1080-eGFP cells encapsulated in hydrogel micropads stained with 7-diethylamino-3-(4-maleimidophenyl)-4-methylcoumarin (blue) after hydrogel crosslinking and immersion in medium. Scale bar is 500 μm .

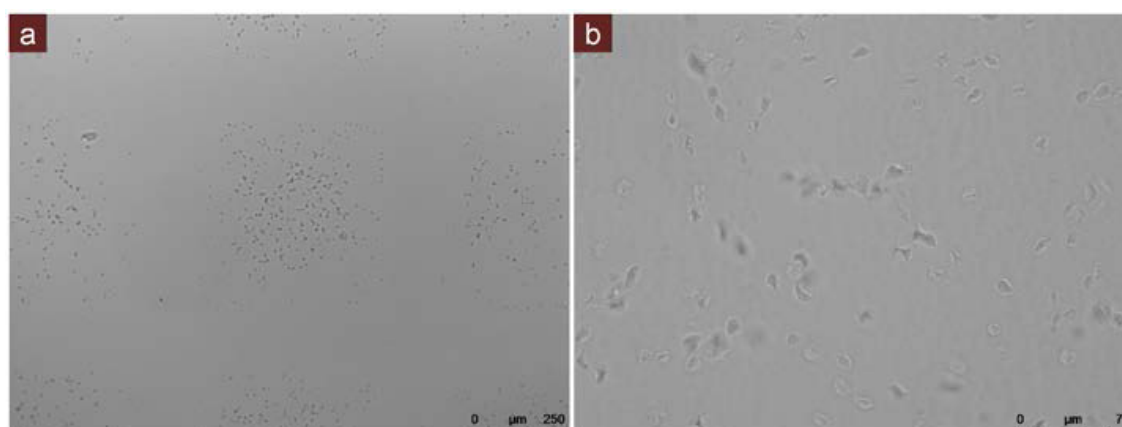


Figure 5.S4 Cells encapsulated in hydrogel micropads for 6 days

Fixed It-NES cells encapsulated in hydrogel micropads on day 6. Low (a) and high (b) magnification. DAPI channel image shown in Figure 5.4e.

Adhesion between the hydrogel micropads and the substrate was strong enough to handle standard cell fixation and permeabilization procedures, immunofluorescence staining procedures, and several washing steps without any indication of hydrogel detachment. Of course, physical detachment of the hydrogel micropad using stronger mechanical force is possible. In addition, when we used the thiol-reactive probe, 7-

diethylamino-3-(4-maleimidophenyl)-4-methylcoumarin, in the PEG-crosslinker mixture and visualized the hydrogel micropads with a confocal microscope, we saw blue fluorescence inside the thin polymer substrate, suggesting successful crosslinking of the gel within the supporting polymer film and physical attachment of the hydrogel micropads to the substrate.

Cell culture

Human cervical tumor cells stably expressing green fluorescent protein (HeLa-GFP) were cultured in DMEM (Gibco, Cat. #41966) supplemented with 10% FBS (PAA Laboratories, Cat. #A15-151) and 1% penicillin/streptomycin in a humid incubator at 37°C with 5% CO₂, and were split every two to three days. For selection of GFP-positive cells, 10 µg ml⁻¹ of Blasticidin was used. A cell suspension containing 2 × 10⁶ cells ml⁻¹ was used to form the DropletMicroarray in Fig. 5.3b and imaged on a Leica MZ10 F stereo microscope. A MI-PVA-cell solution containing 16,000 cells µl⁻¹ was used to form the cell-encapsulated hydrogel micropads in Fig. 5.3e and imaged on a Leica DM5500 B microscope.

Human fibrosarcoma cells stably expressing enhanced green fluorescent protein (HT1080-eGFP) were cultured in RPMI Medium 1640 (Gibco, Cat. #A10491) supplemented with 10% FBS (PAA Laboratories, Cat. #A15-151) in a humid incubator at 37°C with 5% CO₂, and were split every two to three days. For selection of eGFP-positive cells, 1 mg/ml of G418 was used. A MI-PVA-cell solution containing 16,000 cells µl⁻¹ was used to form the cell-encapsulated hydrogel micropads in Figs. 5.4d and 5.S3 and imaged on a Leica TCS SP5 confocal microscope and Leica DM5500 B microscope, respectively.

Long-term self-renewing neuroepithelial like stem cells (It-NES cells) derived from hESC lines H9 were cultured in DMEM/F12 containing N2 supplement (PAA Laboratories), 10 ng ml⁻¹ fibroblast growth factor 2 (FGF2), 10 ng ml⁻¹ epidermal growth factor (EGF) (both R&D Systems), 1:1000 B27 supplement (Invitrogen), and 1.6 mg L⁻¹ glucose in a humid incubator at 37°C with 5% CO₂. Cells were fixed in 4% paraformaldehyde in PBS for 20 min, permeabilized with 0.1% Triton X-100 in PBS, and stained with DAPI (Sigma-Aldrich). A MI-PVA-cell solution containing 40,000 cells µl⁻¹ was used to form the cell-encapsulated hydrogel micropads in Figs. 5.3e and 5.S4 and imaged on a Leica DM5500 B microscope.

Human breast adenocarcinoma cells (MDA-MB-231) were cultured in 1:1 F12:DMEM (Gibco, Cat. #21765 and #A10491) supplemented with 10% FBS (PAA Laboratories, Cat. #A15-151) in a humid incubator at 37°C with 5% CO₂, and were split every two to three days. A MI-PVA-cell solution containing 4,000 cells µl⁻¹ was used to form the cell-encapsulated hydrogel micropads in Figs. 5.5a,b and imaged on a Keyence BZ-9000 fluorescence microscope (Japan).

6 Micropatterning hydrophobic liquid on a porous polymer surface for long-term selective cell-repellency

Previously, we relied on the air layer trapped within and on the surface of the porous, superhydrophobic surfaces in the Cassie–Baxter state to prevent cell adhesion. However, the cell-repellent properties became less efficient after long culture times (more than 5 days at a high cell density) as the cells grew to confluence within the hydrophilic spots and proteins eventually covered the superhydrophobic surface. In this chapter, we introduce a new concept for patterning regions on surfaces that repel cell adhesion, which proved to be more efficient than conventional cell-repellent coatings such as polyethylene glycol-functionalized (PEGylated) surfaces. The method is very simple and is based on creating precise micropatterns of a hydrophobic liquid on a porous surface. This chapter was originally published as an article in *Advanced Healthcare Materials* in May 2013 and is reproduced with permission from John Wiley and Sons (Ueda & Levkin, 2013b).

Micropatterning hydrophobic liquid on a porous polymer surface for long-term selective cell-repellency

Erica Ueda¹ and Pavel A. Levkin^{1,2,*}

¹ Institute of Toxicology and Genetics, Karlsruhe Institute of Technology, Postfach 3640, 76021 Karlsruhe, Germany

² Department of Applied Physical Chemistry, Heidelberg University, Im Neuenheimer Feld 253, 69120 Heidelberg, Germany

Adv. Healthcare Mater. **2013**, *2*, 1425–1429. DOI: 10.1002/adhm.201300073

Author contributions:

Erica Ueda designed and performed the experiments and analysis, and wrote the manuscript.



Pavel A. Levkin contributed to the original idea of the project, the experimental design, and editing of the manuscript.



6.1 Article

Cell-repellent surfaces are essential for a range of applications including biosensors (Hasenbank *et al.*, 2008), microfluidic devices (Srigunapalan *et al.*, 2012), and anti-biofouling surfaces (Kuang & Messersmith, 2012). The majority of cell-repellent surfaces that exist so far are based on poly(ethylene glycol) (PEG) in the form of brushes (Ma *et al.*, 2004, 2006), self-assembled monolayers (SAMs) (Feldman *et al.*, 1999; Mrksich *et al.*, 1996; Ostuni *et al.*, 2001; Schilp *et al.*, 2009), or physisorbed PEG block copolymers (Otsuka, 2010). However, PEGylated surfaces can still adsorb serum proteins and they tend to oxidize under ambient conditions, thus restricting their long-term use (Nelson *et al.*, 2003; Schoenfish & Pemberton, 1998). The few other existing methods to create cell-repellent surfaces include coatings based on polyacrylamide (Nelson *et al.*, 2003) or hyaluronic acid (Fukuda *et al.*, 2006; Khademhosseini *et al.*, 2004), zwitterionic surfaces (Jiang & Cao, 2010; Kuang & Messersmith, 2012), and superhydrophobic surfaces (Geyer *et al.*, 2011; Ishizaki *et al.*, 2010; Oliveira *et al.*, 2011; Ueda & Levkin, 2013a). Despite a lot of research done in this field, surfaces possessing a combination of (a) efficient cell repellency, (b) long-term stability on the order of several days, and (c) patternability (i.e., the ability to create two-dimensional micropatterns of cell repellency) are still very rare.

Recently, the idea of forming a self-healing, slippery liquid-infused porous surface was introduced by the group of Aizenberg and demonstrated as an efficient ice- and stain-resistant as well as antibacterial coating (Epstein *et al.*, 2012; Kim *et al.*, 2012; Wong *et al.*, 2011). In this paper, we present a new hydrophobic liquid-infused porous polymer surface and demonstrate its highly efficient and long-term repellent properties against eukaryotic cells, which surpass that of a PEGylated surface. We also present a method to selectively and precisely pattern a hydrophobic liquid on a thin porous substrate to create cell-repellent micropatterns with defined geometries. We show that micropatterns of the hydrophobic liquid coating are able to effectively constrain mammalian cell migration for applications such as cell patterning and cell microarrays. We demonstrate the underwater stability of the hydrophobic liquid micropatterns for at least 40 days. In addition, the biocompatibility of the hydrophobic liquid micropatterns is shown in a proof-of-principle reverse cell transfection experiment.

For the experiments in this paper, we used a superhydrophilic nanoporous layer of poly(hydroxyethyl methacrylate-*co*-ethylene dimethacrylate) produced by UV-initiated free radical polymerization, followed by UV-initiated photografting of 2,2,3,3,3-pentafluoropropyl methacrylate through a quartz photomask to create superhydrophobic regions (Geyer *et al.*, 2011). The method to selectively pattern hydrophobic liquid on hydrophilic-hydrophobic substrates is schematically shown in Figure 6.1. First, a

nanoporous polymer surface with superhydrophilic regions on a superhydrophobic background was wetted with water to form droplets in the superhydrophilic regions (Figure 6.1a, step 1). Due to the extreme wettability contrast, the superhydrophobic pattern remains dry (Ueda *et al.*, 2012). Second, a thin layer of hydrophobic liquid was spread over the surface while the water droplets were still contained in the superhydrophilic regions. The hydrophobic liquid we used in all of our experiments was Krytox[®] GPL 103, a low molecular weight fluorine end-capped homopolymer of hexafluoropropylene epoxide. The hydrophobic liquid only penetrated the superhydrophobic pattern (Figure 6.1a, step 2). Third, the hydrophobic liquid layer was washed under a stream of water to remove the hydrophobic liquid layer from the superhydrophilic regions (Figure 6.1a, step 3). The hydrophobic liquid that fills the superhydrophobic nanoporous polymer does not wash away and forms a stable micropattern on the polymer surface. To use the hydrophobic liquid pattern in cell experiments, the substrate is then immersed in medium containing cells and the water droplets in the superhydrophilic regions are replaced with the medium (Figure 6.1a, step 4). Figure 6.1b–d shows water droplets separated by hydrophobic liquid barriers for various pattern geometries. The superhydrophobic nanoporous polymer becomes transparent when it is filled with the hydrophobic liquid. We will refer to these superhydrophilic–hydrophobic liquid patterned surfaces as *hydrophobic liquid micropatterns*.

Prolonged stability of the hydrophobic liquid micropatterns is important, especially for long-term cell experiments. To test stability, we immersed a hydrophobic liquid micropattern into an aqueous solution of Rhodamine 6G dye for 41 days to indicate the interface between the wetted superhydrophilic regions and the hydrophobic liquid barriers. We observed a decrease in the average width of the hydrophobic liquid barriers from 101 μm to 48.7 μm after 2 days, but no further decrease was observed during immersion of the substrate for an additional 39 days (Figure 6.2a,b). The measured width of the hydrophobic liquid barriers after equilibrium was reached was closer to the spacing on the photomask of 62.5 μm . We believe this initial decrease in the width of the hydrophobic liquid barriers is due to the unsharp interface at the edges of the superhydrophilic pattern that arise from scattering of UV light at the edges of the photomask pattern. This leads to hydrophobic barriers that are initially wider than the photomask pattern, with less efficient grafting occurring at the outer edges of the hydrophobic barriers where the surface is not directly irradiated with UV light. We believe this unsharp interface could be minimized by decreasing the distance of the photomask from the surface during photografting (currently, 1 mm) and by using a UV lamp with perfectly collimated light.

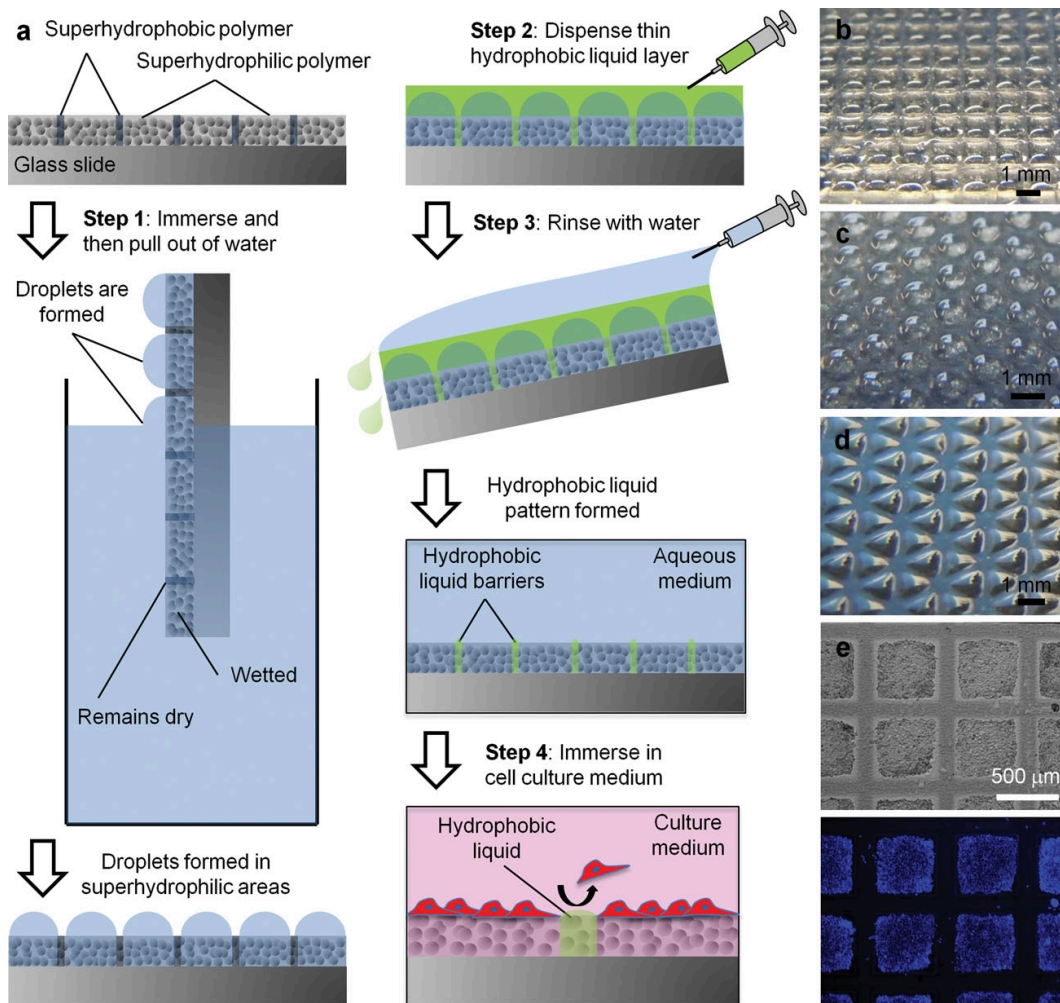


Figure 6.1 Formation of hydrophobic liquid patterns

(a) Schematic of a superhydrophilic nanoporous polymer surface with superhydrophobic moieties. Step 1: when the superhydrophilic–superhydrophobic patterned substrate is immersed in water, the superhydrophilic areas become easily wetted while the superhydrophobic areas remain dry. When the substrate is pulled out of water, only the superhydrophilic areas remain filled with water and distinct droplets are formed. Step 2: a thin layer of hydrophobic liquid is applied over the water droplets, but infuses only the non-wetted superhydrophobic areas. Step 3: the surface is rinsed with water to wash off the unstable hydrophobic liquid layer covering the water droplets. The hydrophobic liquid infused in the superhydrophobic areas remains stable, resulting in the formation of a hydrophobic liquid pattern. Step 4: cells cultured on hydrophobic liquid patterns adhere to the superhydrophilic areas, but are easily removed from the hydrophobic liquid barriers by weak shear forces. (b–d) Water droplets in superhydrophilic spots separated by 100 μm hydrophobic liquid barriers for different array pattern geometries: (b) 1 mm side length square, (c) 1 mm diameter circle, (d) 1 mm side length triangle. (e) HEK 293 cells cultured on a hydrophobic liquid

micropattern (500 μm side length square, 100 μm barrier). Brightfield and DAPI channel (blue) images are shown.

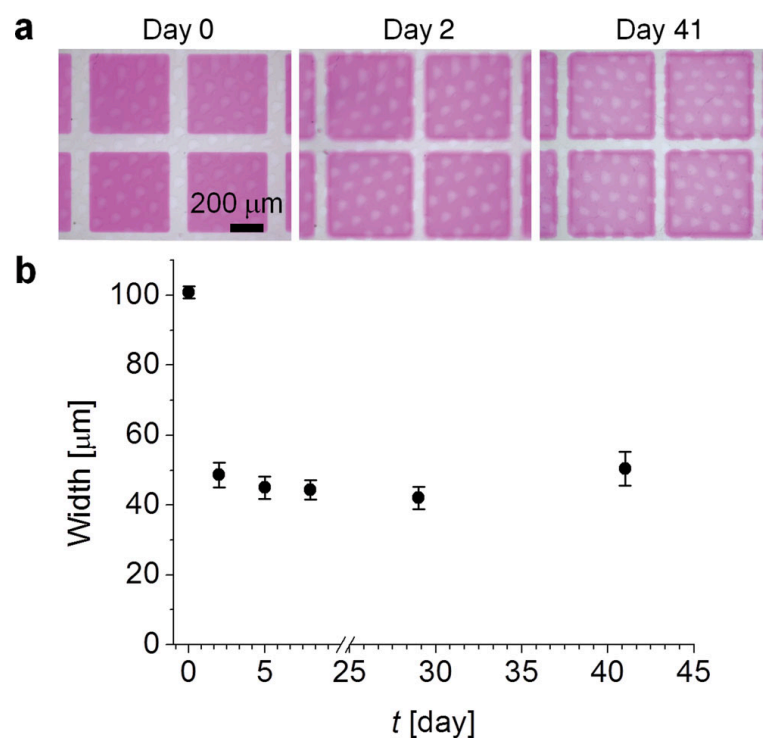


Figure 6.2 Stability of hydrophobic liquid micropatterns

(a) Time-lapse color images of superhydrophilic spots separated by hydrophobic liquid barriers (500 μm side length square, 62.5 μm barrier) while immersing the substrate in Rhodamine 6G solution for 41 days. (b) Average (SD) measured widths of the hydrophobic liquid barriers over time while immersing the substrate in Rhodamine 6G solution for 41 days.

To further demonstrate the stability of the hydrophobic liquid infused in our superhydrophobic porous polymer substrates, we covered non-patterned superhydrophobic substrates with hydrophobic liquid over a large surface area, immersed them in cell culture medium, and then measured the water contact angles (WCAs) on days 0 and 7 (Figure 6.S1). The mean static (θ_{st}), advancing (θ_{adv}), and receding (θ_{rec}) WCAs for the superhydrophobic surfaces infused with hydrophobic liquid on day 0 before immersion in cell culture medium were $117 \pm 1^\circ$, $121 \pm 1^\circ$, and $110 \pm 0.7^\circ$, respectively. There were no significant changes in the WCAs by day 7, with mean θ_{st} , θ_{adv} , and θ_{rec} of $119 \pm 2^\circ$, $119 \pm 2^\circ$, and $113 \pm 1^\circ$, respectively. Furthermore, the same hydrophobic liquid-infused substrates were stored at ambient conditions for an additional 34 days. Again, there were no significant changes in the WCAs of the

hydrophobic liquid surface, with mean θ_{st} , θ_{adv} , and θ_{rec} of $119^\circ \pm 1^\circ$, $116^\circ \pm 0.6^\circ$, and $112^\circ \pm 1^\circ$, respectively. For comparison, we performed the same experiment with superhydrophobic substrates that were not infused with hydrophobic liquid. The mean θ_{st} , θ_{adv} , and θ_{rec} for the superhydrophobic surfaces on day 0 before immersion in cell culture medium were $151 \pm 2^\circ$, $154 \pm 0.5^\circ$, and $144 \pm 6^\circ$, respectively. However, by day 7 the mean θ_{st} , θ_{adv} , and θ_{rec} for the superhydrophobic surfaces had decreased significantly to $60 \pm 16^\circ$, $83 \pm 14^\circ$, and $22 \pm 21^\circ$, respectively. These WCA measurements indicate that the superhydrophobic surface infused with hydrophobic liquid is much more stable than the superhydrophobic surface alone, whether immersed in solution or stored in air.

The liquid nature of the slippery layer formed on the hydrophobic liquid-infused porous surface resembles the liquid-like interface of a hydrated PEGylated surface, which is attributed to the cell resistance of PEG surfaces. Thus, we hypothesized that our method to create micropatterns of the hydrophobic liquid could be used to create highly efficient eukaryotic cell-repellent areas on surfaces. To test this, we cultured human cervical tumor cells stably expressing green fluorescent protein (Hela-GFP) on hydrophobic liquid micropatterns for 7 days (Figure 6.3a–c). The micropatterned hydrophobic liquid barriers are easily distinguished even after 7 days of culture (Figure 6.3b). The mean area fraction of cells on the hydrophobic liquid barriers versus the superhydrophilic regions after 7 days of culture was $3.6\% \pm 2.1\%$ and $43\% \pm 2.4\%$, respectively, indicating that most cells occupy the superhydrophilic regions as opposed to the hydrophobic liquid barriers (Figure 6.3c). The cells that initially settle on a superhydrophilic spot migrate and proliferate within the superhydrophilic spot, and the hydrophobic liquid barriers are able to contain the cells within this superhydrophilic spot even when the cells become very confluent. The few cells that do remain on the hydrophobic liquid barrier after 7 days in culture have a rounder morphology compared to cells on the superhydrophilic region and can be easily removed by shear forces when gently washing the substrate. This suggests that the cells do not readily adhere and grow on the hydrophobic liquid even after 7 days of culture. Other cell types (HT1080-eGFP, HEK 293, MTly-CMV-eGFP-neo) also showed preferential adhesion and growth in the superhydrophilic spots as opposed to on the hydrophobic liquid barriers (Figure 6.S2, Video S1).

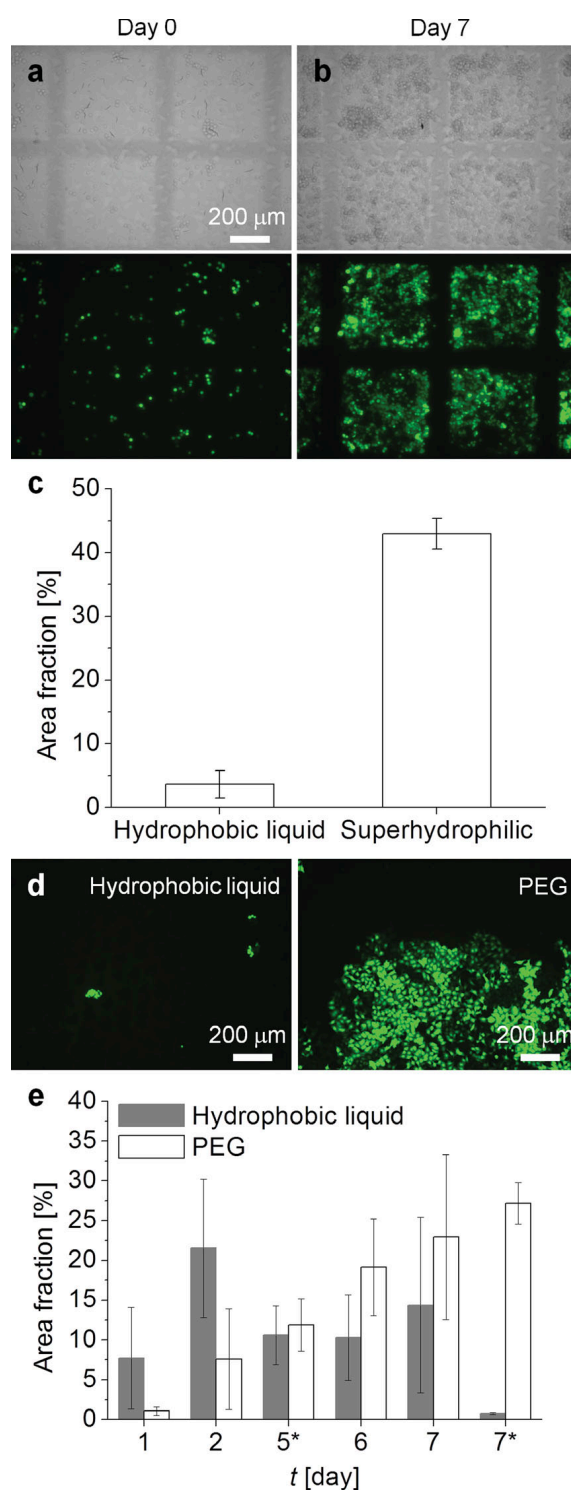


Figure 6.3 Cell-repellency of hydrophobic liquid micropatterns and surfaces

(a-c) HeLa-GFP cells cultured on patterns of 500 μm side length superhydrophilic squares with 62.5 μm hydrophobic liquid barriers. Brightfield and GFP channel images on (a) day 0 and (b) day 7. (c) Mean (SD, $n = 4$) area fraction of cells on the hydrophobic liquid barriers versus the superhydrophilic squares after 7 days of culture.

(d) HeLa-GFP cultured on hydrophobic liquid surfaces or PEG2000 SAM surfaces and cultured for 7 days. (e) Mean (SD, $n = 4$) area fraction of cells on hydrophobic liquid surfaces and PEG surfaces. On day 5*, the cell culture medium was gently changed before imaging. On day 7*, the cells were fixed in paraformaldehyde (4% v/v in PBS) and coverslipped before imaging.

To further investigate the excellent cell-repellency of the hydrophobic liquid surfaces, we quantified cell adhesion on our hydrophobic liquid surfaces compared to that on PEG (MW 2000 g mol⁻¹) SAM surfaces for up to 7 days (Figure 6.3d,e and 6.S3). PEGylated surfaces are considered the golden standard for cell-repellent surfaces, however, long-term cell-repellency of such surfaces is still difficult to achieve. HeLa-GFP cells were observed on the hydrophobic liquid surfaces by day 1, but cells did not adhere to the PEG surfaces until day 2. When the cell culture medium was changed on day 5, the weak shear forces created during medium exchange easily removed many cells from the hydrophobic liquid surfaces. However, once cells had attached to the PEG surfaces, they did not easily detach under the same washing conditions. On day 7, the weak shear forces created during fixation and gentle washing of the cells had removed most of the cells from the hydrophobic liquid surfaces. Thus, the mean area fraction of cells on the hydrophobic liquid surfaces was $0.78 \pm 0.65\%$ compared to $27 \pm 12\%$ for the PEG surfaces on day 7* (after fixation, washing, and coverslipping). Although the cells could settle on the hydrophobic liquid surfaces, they did not firmly adhere to nor spread on the liquid surface as indicated by the rounded morphology of the cells. Any contacts that the cells make on the hydrophobic liquid layer are not anchored to a solid surface, hence the cells can be easily removed by weak shear forces. The PEG surfaces initially had good cell-repellency, but by the second day of culture the cells could firmly adhere and grow on the PEG surfaces. These results further confirm the use of hydrophobic liquid surfaces to create stable, slippery, and cell-resistant surfaces that surpass the performance of PEGylated surfaces during long-term cell culture experiments.

In addition to being able to prevent cell adhesion in specific regions, the ability to constrain migrating cells within specific areas is also important for applications such as cell microarrays and cell patterning. Thus, we compared the ability of cells to migrate across hydrophobic liquid barriers and across superhydrophobic barriers that were not infused with hydrophobic liquid. When the superhydrophilic–superhydrophobic patterned surface is immersed in an aqueous solution, the regions of superhydrophobic nanoporous polymer trap air inside the pores and within the asperities of the rough surface, exhibiting a Cassie–Baxter state (Cassie & Baxter, 1944). The trapped air within a superhydrophobic porous surface has previously been shown to reduce cell migration for at least 48 h (Geyer *et al.*, 2011). In our experiment, HEK 293 cells were

mostly confined by both the hydrophobic liquid barriers and the Cassie–Baxter air barriers one day after cell seeding (Figure 6.S4a,d). However, after 3 days of culture there was a clear difference between the two barrier types in their ability to prevent cell migration across the barrier. The hydrophobic liquid barriers effectively confined the cells and virtually no cells had migrated across the hydrophobic liquid barrier (Figure 6.S4b), whereas, the cells were clearly able to migrate across the Cassie–Baxter air barriers after 3 days in culture (Figure 6.S4e). We quantified this difference by calculating the area fraction of the cells that had migrated across the barriers after 3 days in culture, and measured an average cell area fraction of only 0.1% for the pattern with hydrophobic liquid barriers and an average cell area fraction of 15% for the pattern with Cassie–Baxter air barriers, a 150-fold difference (Figure 6.S4c,f). These results show that the micropatterns of hydrophobic liquid on the surface completely block the ability of cells to migrate across the barriers, while the air trapped within the asperities of the superhydrophobic surface loses its ability to inhibit cell migration after 3 days of culture, most likely due to a transition from the Cassie–Baxter state to the wetted Wenzel state.

For many applications, it is important to control cell adhesion without affecting cell viability. To ensure that the ability of the hydrophobic liquid barriers to confine cells within the superhydrophilic areas was not due to cytotoxicity, we tested for cell viability. We cultured HEK 293 cells on hydrophobic liquid micropatterns for 2 days and then stained the cells with Calcein, propidium iodide (PI), and Hoechst 33342. Calcein and PI are used to indicate live cells and late apoptotic cells, respectively. There was little to no cell toxicity on both hydrophobic liquid micropatterns and superhydrophobic Cassie–Baxter micropatterns, with an average of 99.9% and 99.7% Calcein-positive cells, respectively (Figure 6.S5). One should note that cells on the hydrophobic liquid barriers do not firmly adhere, so some cells may wash away during the staining procedure.

In addition to creating cell-repellent regions and confining cells using micropatterns of hydrophobic liquid as barriers, the ability to treat the clusters of cells would be useful for applications such as cell microarrays. To demonstrate the application of hydrophobic liquid arrays as cell microarrays, we performed reverse cell transfection experiments (Ziauddin & Sabatini, 2001). First, droplets of transfection mixtures containing pCS2+-GFP or pCS2+-mCherry plasmid DNA were pipetted onto the superhydrophilic spots of superhydrophilic–superhydrophobic patterned polymer surfaces. The mixtures were allowed to dry before forming the hydrophobic liquid micropatterns as described in Figure 6.1. Then, HEK 293 cells were seeded on the hydrophobic liquid micropatterns and cultured for 48 h. The average cell transfection efficiencies of the pCS2+-GFP and pCS2+-mCherry plasmid DNA were 30% and 20%, respectively (Figure 6.4). The actual transfection efficiency is a little higher due to

overlapping clusters of transfected cells being counted as one cell when individual cells were not distinguishable.

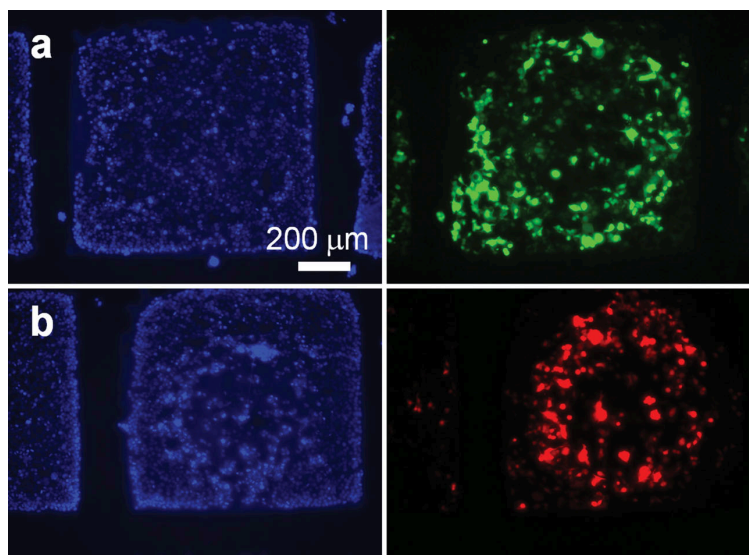


Figure 6.4 HEK 293 cells reversely transfected on hydrophobic liquid arrays

Plasmid DNA (a) pCS2+-GFP (green) and (b) pCS2+-mCherry (red) were pre-printed in the superhydrophilic spots of a patterned porous polymer with 1 mm side length squares and 100 μm barriers. HEK 293 cells were cultured on hydrophobic liquid arrays for 2 days, and then fixed and stained with Hoechst 33342 (blue).

In conclusion, we introduced a new and practical method to create precise micropatterns of hydrophobic, water immiscible liquids on porous hydrophilic–hydrophobic patterned substrates. We demonstrated the excellent stability and cell-repellency of the hydrophobic liquid micropatterns, which proved to be better than that of PEGylated or superhydrophobic surfaces during long-term experiments. To our knowledge, this is the first report regarding the use of hydrophobic liquid barriers to control eukaryotic cell adhesion and migration. Due to the relatively simple method of preparation and resulting cell-repellency surpassing the performance of most other existing surfaces, we believe that our method is useful for various applications where multiple-day cell-resistant patterns are crucial. Such applications include cell patterning, cell microarrays, or tissue engineering.

Materials and methods

Schott (Germany) Nexterion Glass B UV transparent glass slides were used as substrates for the polymer layers. All polymerizations and photografting were carried

out using an OAI Model 30 deep-UV collimated light source (San Jose, CA) fitted with an USHIO 500 W Hg-xenon lamp (Japan). Irradiation intensity was calibrated using an OAI 360 UV power meter with a 260 nm probe head. Monomers and chemicals were purchased from Sigma-Aldrich (Germany). The hydrophobic liquid we used in all of our experiments was Krytox[®] GPL 103 fluorinated oil (DuPont[™]). A UK 1115 digital camera (EHD imaging GmbH, Germany) and ImageJ software with a DropSnake plugin were used to measure the WCAs. The PEG-coated surfaces were generously provided by Linlin Xiao from the Institute of Functional Interfaces at Karlsruhe Institute of Technology. Gold-coated glass slides were immersed in a hydroxy-PEG-thiol (PEG MW 2000 g mol⁻¹, Rapp Polymere GmbH, Germany) solution (1 mM in absolute ethanol) for 48 h to form the PEG2000 SAM surfaces. Biochemicals were purchased from Life Technologies (Germany). HeLa-GFP cells were purchased from Biocat (Germany) and all other cell lines were provided by the Institute of Toxicology and Genetics at Karlsruhe Institute of Technology.

6.2 Supporting information

Formation of superhydrophilic–superhydrophobic nanoporous polymer substrates

Schott (Germany) Nexterion Glass B UV transparent glass plates were first activated in NaOH (1 M) for 1 h and then modified with 3-(trimethoxysilyl)propyl methacrylate (20% v/v in ethanol) for 1 h. Activated glass slides were fluorinated with tridecafluoro-(1,1,2,2)-tetrahydrooctyltrichlorosilane in a vacuumed desiccator. The polymerization mixture consisted of 2-hydroxyethyl methacrylate (24 wt%), ethylene dimethacrylate (16 wt%), 1-decanol (12 wt%), cyclohexanol (48 wt%), and 2,2-dimethoxy-2-phenylacetophenone (1 wt% with respect to monomers). The polymerization mixture was injected between a fluorinated and modified glass slide separated by 12.5 μm -thick strips of Teflon film (American Durafilm Co.), and irradiated for 15 min at 12 mW cm^{-2} with a 260 nm UV light to form a superhydrophilic nanoporous polymer layer. The photografting mixture consisted of 2,2,3,3,3-pentafluoropropyl methacrylate (20 wt%), ethylene dimethacrylate (1.3 wt%), 1:3 (v/v) mixture of water:*tert*-butanol (78 wt%), and benzophenone (0.33 wt%). The photografting mixture was applied to the superhydrophilic polymer substrate, covered with a fluorinated glass slide and quartz chromium photomask (Rose Fotomasken, Germany), and irradiated for 30 min at 12 mW cm^{-2} with a 260 nm UV light to obtain a superhydrophilic–superhydrophobic patterned surface. All polymerizations and photografting were carried out on an OAI Model 30 deep-UV collimated light source (San Jose, CA) fitted with an USHIO 500 W Hg-xenon lamp (Japan). Irradiation intensity was calibrated using an OAI 360 UV power meter with a 260 nm probe head. Monomers were purchased from Sigma-Aldrich (Germany). Further details can be found in our previous papers (Geyer *et al.*, 2011; Ueda *et al.*, 2012).

Measuring the width of the hydrophobic liquid barriers

Hydrophobic liquid arrays were immersed in a solution of Rhodamine 6G (0.1 mg ml^{-1} in water, Sigma, Cat. #R4127) to stain the superhydrophilic spots. Three regions on each of two substrates were imaged on a Keyence BZ-9000 fluorescence microscope (Japan), and 12 measurements per substrate of the width of the hydrophobic liquid barrier were measured using ImageJ.

Water contact angle measurements

The static, advancing, and receding WCA images were taken using a UK 1115 digital camera from EHD imaging GmbH (Germany) at ambient conditions. ImageJ software with a Dropsnake plugin was used to measure the WCA. At least 3 measurements on each of 3 substrates were made for both the hydrophobic liquid and superhydrophobic Cassie–Baxter surfaces.

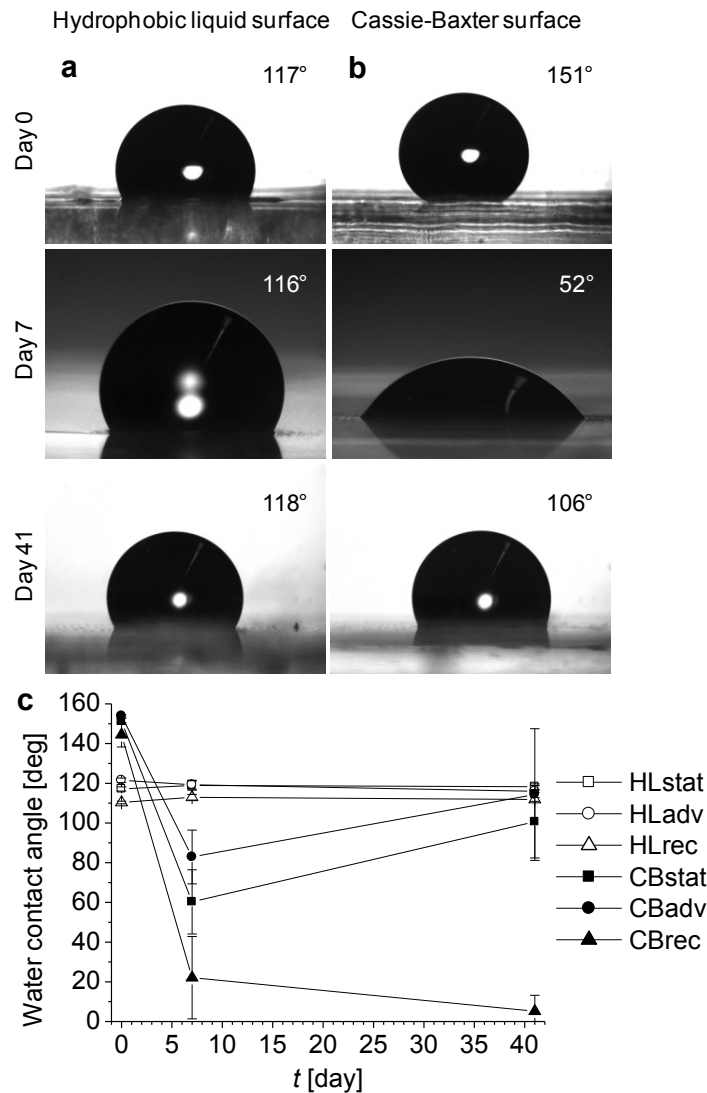


Figure 6.S1 Water contact angle measurements

Static 4 μl droplet of water on (a) hydrophobic liquid surfaces and (b) superhydrophobic Cassie–Baxter surfaces before (day 0) and after (day 7) immersion in cell culture medium for 7 days, and after storage in atmospheric conditions for an additional 34 days (day 41). (c) Mean (SD, $n = 3$) static, advancing, and receding water contact angles on hydrophobic liquid (HL) surfaces and superhydrophobic Cassie–Baxter (CB) surfaces before (day 0) and after (day 7) immersion in cell culture medium for 7 days, and after storage in atmospheric conditions for an additional 34 days (day 41).

Cells cultured on hydrophobic liquid patterns

To demonstrate the cell-repelling of the hydrophobic liquid barriers, we cultured human fibrosarcoma cells stably expressing eGFP (HT1080-eGFP), human embryonic kidney cells (HEK 293), and rat mammary carcinoma cells stably expressing eGFP (MTly-CMV-eGFP-neo) on hydrophobic liquid patterns of various geometries for 3 days (Figure 6.S2). Video S1 shows HEK 293 cells seeded at $30,000 \text{ cells cm}^{-2}$ and cultured on a hydrophobic liquid micropattern for 48 h.

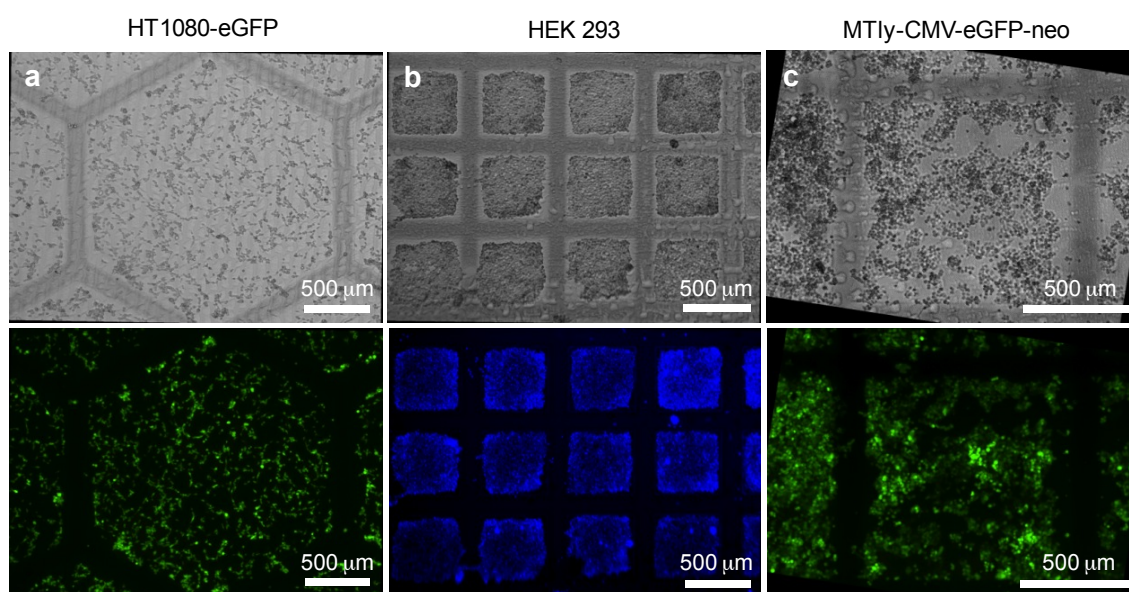


Figure 6.S2 Different hydrophobic liquid pattern geometries cultured with cells

Different hydrophobic liquid pattern geometries cultured with cells for 3 days. (a) HT1080-eGFP cells seeded at $30,000 \text{ cells cm}^{-2}$ on a 1 mm side length hexagon, 100 μm barrier hydrophobic liquid pattern. (b) DAPI-stained HEK 293 cells seeded at $30,000 \text{ cells cm}^{-2}$ on a 500 μm side length square, 100 μm barrier hydrophobic liquid micropattern. (c) MTly-CMV-eGFP cells seeded at $60,000 \text{ cells cm}^{-2}$ on a 1 mm side length square, 100 μm barrier hydrophobic liquid pattern.

Cell-repelling of hydrophobic liquid surfaces vs. PEG2000 SAM surfaces

To make the PEG2000 self-assembled monolayer (SAM) surfaces, gold-coated glass was activated under UV for 2 h, rinsed with absolute ethanol, ultrasonicated in absolute ethanol for 3 min, and then incubated in a PEG2000 thiolate solution (1 mM in absolute ethanol). The samples were removed from the solution after 48 h, rinsed with absolute

ethanol, ultrasonicated in absolute ethanol for 3 min, rinsed with absolute ethanol, and dried with nitrogen.

Hela-GFP cells (BioCat, Cat. #AKR-213) were seeded at 20,000 cells cm⁻² on hydrophobic liquid surfaces or PEG surfaces and cultured for 7 days. Cells were observed on the hydrophobic liquid surfaces by day 1, but cells did not adhere to the PEG surfaces until day 2. The cell culture medium was gently changed on day 5* and many cells on the hydrophobic liquid surfaces were easily washed away. However, once cells attached to the PEG surfaces they were not easily washed away. During fixation and gentle washing of the cells on day 7, most of the cells on the hydrophobic liquid surfaces had washed away. At least 3 images per substrate were taken using a Keyence BZ-9000 fluorescence microscope (Japan). Using ImageJ, the image threshold was adjusted and the area fraction of cells was measured.

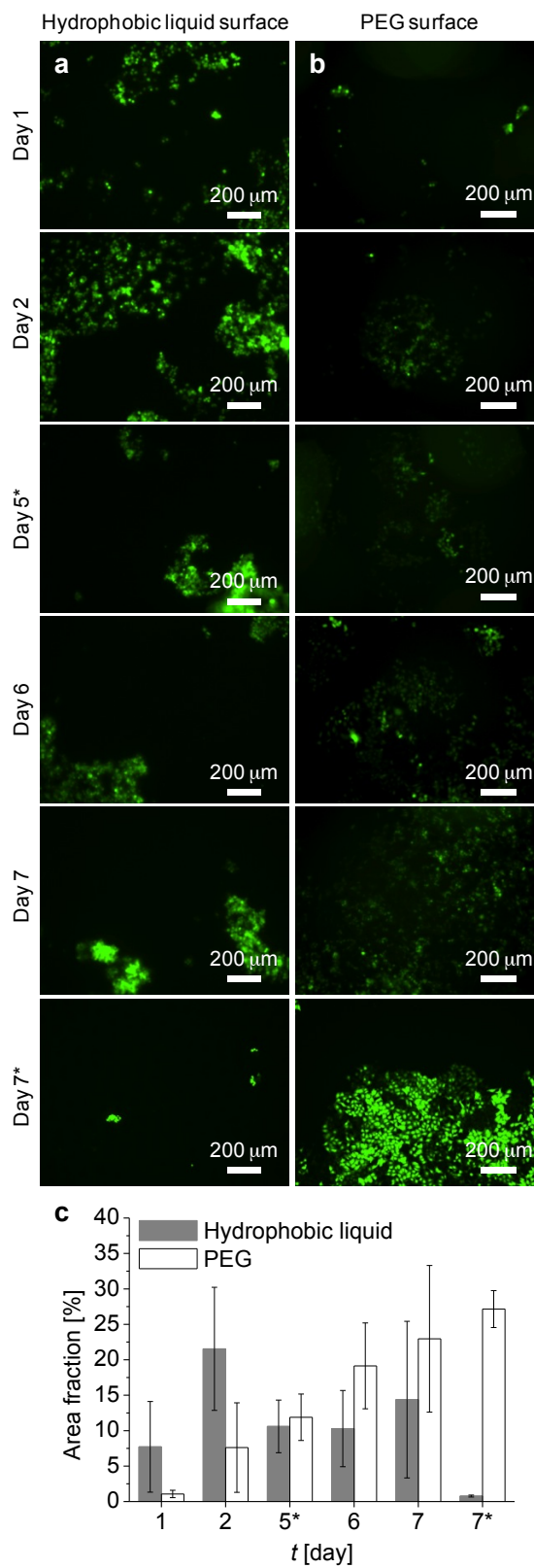


Figure 6.S3 Cells cultured on hydrophobic liquid surfaces or PEG SAM surfaces

Hela-GFP cells cultured on (a) hydrophobic liquid surfaces or (b) PEG2000 SAM surfaces for 7 days. (c) Mean (SD, n = 4) area fraction of cells growing on hydrophobic liquid surfaces and PEG surfaces. On day 5*, the cell culture medium was gently changed before imaging. On day 7*, the cells were fixed in paraformaldehyde (4% v/v in PBS) and coverslipped before imaging.

Quantification of cell migration across hydrophobic liquid barriers vs. Cassie–Baxter air barriers

A 10 μl droplet of cell suspension containing HEK 293 cells were seeded at 30,000 cells cm^{-2} in a single superhydrophilic square of 3 mm side length and 100 μm barrier width on arrays with either Cassie–Baxter air barriers or hydrophobic liquid barriers. The cells were allowed to adhere overnight, and then the droplet was aspirated to remove unadhered cells and the substrate was immersed in cell culture medium. The cell nuclei were stained with Hoechst 33342 (1 $\mu\text{g ml}^{-1}$ in HEPES Krebs Ringer solution, pH 7.4). At least 10 images were taken per substrate using a Leica DM5500 B upright microscope. The cell area fraction was obtained using ImageJ by selecting the ROI, adjusting the threshold, and measuring the area fraction.

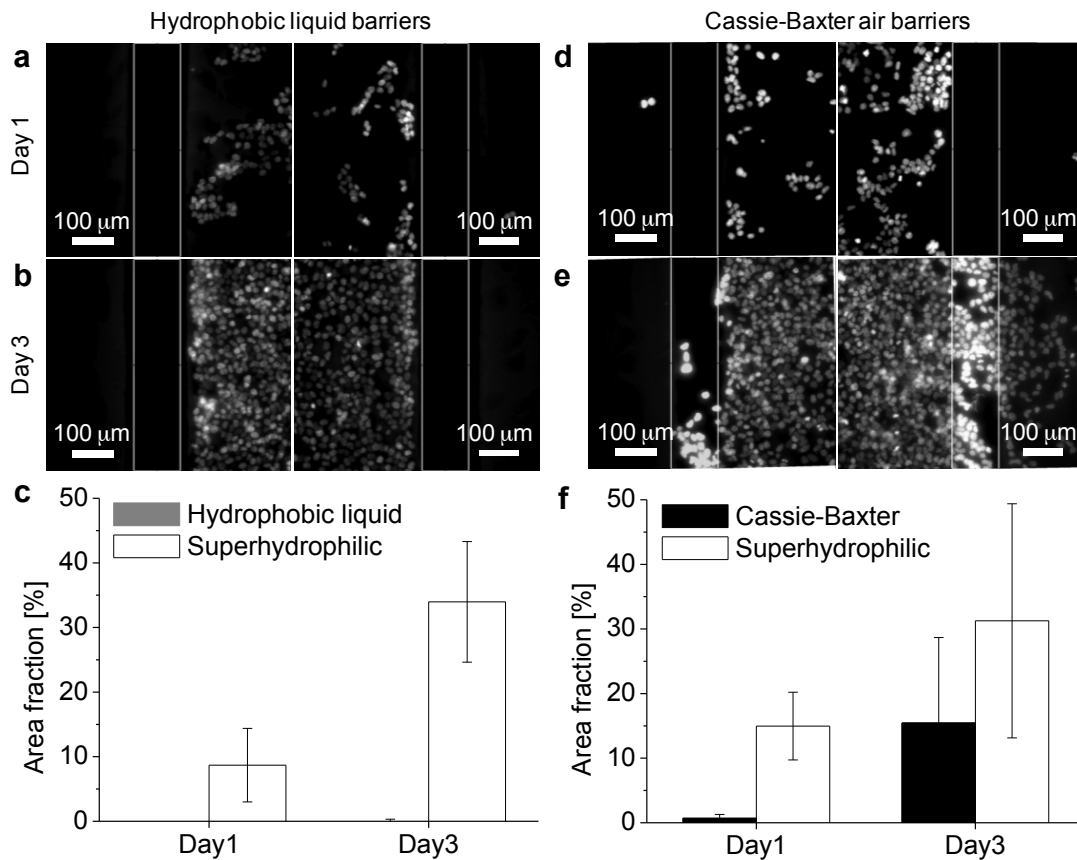


Figure 6.S4 Cell migration across hydrophobic liquid barriers and superhydrophobic Cassie–Baxter air barriers

HEK 293 cells were seeded at $30,000 \text{ cells cm}^{-2}$ in a single superhydrophilic square of 3 mm side length, $100 \mu\text{m}$ barrier and cultured for 3 days. High magnification images of representative areas used for cell area fraction quantification are shown after (a,d) 1 day and (b,e) 3 days in culture. The vertical white lines outline the edges of the barriers. The grayscale intensities of the DAPI-stained cells were enhanced for visualization. (c) Average (SD) area fraction of DAPI-stained cells on/outside the hydrophobic liquid barriers or in the superhydrophilic square on day 1 and 3. (f) Average (SD) area fraction of DAPI-stained cells on/outside the superhydrophobic Cassie–Baxter air barriers or in the superhydrophilic square on day 1 and 3.

Cytotoxicity experiment

HEK 293 cells were seeded at $20,000 \text{ cells cm}^{-2}$ on arrays with hydrophobic liquid barriers or superhydrophobic Cassie–Baxter air barriers and cultured for 2 days. The cells were stained with Calcein AM ($0.5 \mu\text{M}$, Molecular Probes, Cat. #C1430), propidium iodide (500 nM , Molecular Probes, Cat. #P3566), and Hoechst 33342 ($1 \mu\text{g}$

ml^{-1} , Molecular Probes, Cat. #H1399). At least 3 images per sample were taken using a Keyence BZ-9000 fluorescence microscope (Japan). The number of positively stained cells was quantified using the Cell Counter plugin in ImageJ to calculate the percentage of Calcein and PI-positive cells. There was little to no cell toxicity on all surfaces. For the arrays with hydrophobic liquid barriers, the percentage of Calcein and PI-positive cells was 99.9% and 0.14%, respectively. For the arrays with superhydrophobic Cassie-Baxter barriers, the percentage of Calcein and PI-positive cells was 99.7% and 0.21%, respectively.

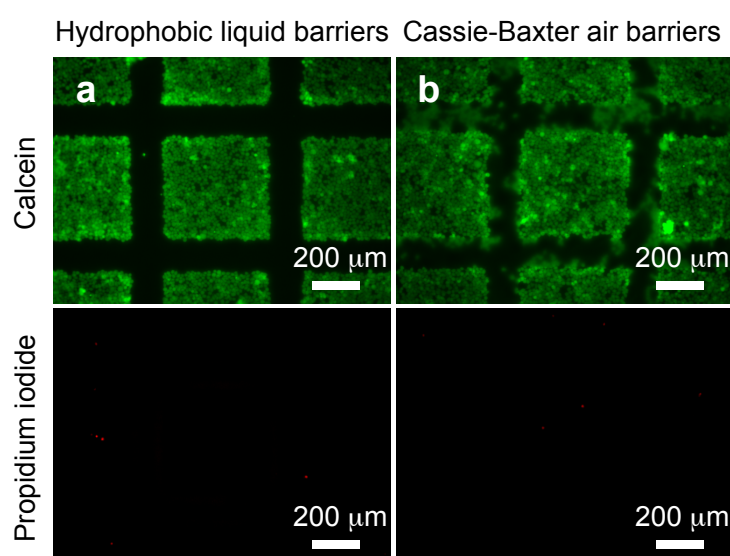


Figure 6.S5 Cell viability on hydrophobic liquid barriers and superhydrophobic Cassie–Baxter air barriers

Cell viability tests on patterns with (a) hydrophobic liquid barriers or (b) Cassie–Baxter air barriers ($500\ \mu\text{m}$ side length square, $100\ \mu\text{m}$ barrier). HEK 293 cells seeded at $20,000\ \text{cells cm}^{-2}$ and cultured for 2 days, and then stained with Calcein AM (green) and propidium iodide (PI) (red).

Reverse cell transfection experiment

$5\ \mu\text{l}$ of pCS2+-GFP or pCS2+-mCherry plasmid DNA ($0.6\ \mu\text{g}\ \mu\text{l}^{-1}$) was mixed with $7\ \mu\text{l}$ of Lipofectamine 2000 (Invitrogen) and incubated at RT for 20 min. $3\ \mu\text{l}$ of sucrose ($0.4\ \text{M}$ in RPMI) and $7.25\ \mu\text{l}$ of gelatin (0.2% w/v in water) were added. $0.5\ \mu\text{l}$ of the transfection mixture was pipetted per $1 \times 1\ \text{mm}^2$ superhydrophilic square and allowed to dry. HEK 293 cells were seeded on the surface at $20,000\ \text{cells cm}^{-2}$ and cultured for 2 days. The cells were then fixed in 4% paraformaldehyde and incubated with $1\ \mu\text{g ml}^{-1}$

Hoechst 33342. Images were taken using a Keyence BZ-9000 fluorescence microscope (Japan). The transfection efficiency was quantified using the Cell Counter plugin in ImageJ to calculate the ratio of GFP- or mCherry-expressing cells to the total number of stained nuclei.

7 Facile and multiple replication of superhydrophilic–superhydrophobic patterns using adhesive tape

Typically several substrates are needed when performing experiments to test different conditions and in replicates. Although we have already developed relatively fast and economical methods to fabricate superhydrophilic–superhydrophobic patterned substrates, we tested if we could make multiple copies of a porous polymer surface simply by transferring thin layers of the polymer onto adhesive tape. This chapter was originally published as an article in *ACS Applied Materials & Interfaces* in July 2013 and is reproduced with permission from the American Chemical Society (Auaud *et al.*, 2013).

Facile and multiple replication of superhydrophilic–superhydrophobic patterns using adhesive tape

Priscila Auaud †, Erica Ueda ‡, and Pavel A. Levkin *†§

P.A. and E.U. contributed equally to this work.

† Department of Chemical Engineering, Universidade Federal do Rio Grande do Sul, Porto Alegre, Rio Grande do Sul, 90035, Brazil

‡ Institute of Toxicology and Genetics, Karlsruhe Institute of Technology, 76021 Karlsruhe, Germany

§ Department of Applied Physical Chemistry, Heidelberg University, 69047 Heidelberg, Germany

ACS Appl. Mater. Interfaces 2013, 5, 8053–8057. DOI: 10.1021/am402135e

Author contributions:

Priscila Auad designed and performed the experiments and analysis, and contributed equally with Erica Ueda to write the manuscript.



Erica Ueda contributed Figures 7.1, 7.4, and 7.S2, designed and performed the reverse cell transfection experiments and analysis, and contributed equally with Priscila Auad to write the manuscript.



Pavel A. Levkin contributed to the original idea of the project, the experimental design, and editing of the manuscript.



7.1 Article

Abstract

Surfaces patterned with both hydrophilic and hydrophobic regions are useful in a variety of applications. For example, they can be used as surface tension-confined microchannels, in paper-based microfluidics, or for patterning cells. To create a new patterned substrate, usually the entire experimental procedure must be repeated, which can be time-consuming and laborious. In this paper, we present a simple and fast method that allows the transfer of superhydrophilic–superhydrophobic micropatterns in porous polymer films onto adhesive tape. Replicating patterns using adhesive tape is economical, as the fabrication of one patterned substrate can be used to create multiple copies of the micropatterns, which can then be used for several different experiments. We demonstrate that at least twelve consecutive copies can be made from 125 μm -thick patterned polymer films. Since the polymer film is transferred to adhesive tape, which is flexible, the copies can be used on curved surfaces and they can also be cut into different shapes and sizes. We also demonstrate an application of the replicated patterned polymer surfaces as a substrate for reverse cell transfection experiments.

Introduction

Superhydrophilic and superhydrophobic surfaces have been broadly investigated and there are many applications involved in their use (Callies & Quéré, 2005; Li *et al.*, 2012a, 2007; Ma & Hill, 2006; Quéré, 2005; Ueda & Levkin, 2013a; Ueda *et al.*, 2012; Zhang *et al.*, 2008). The difference in wettability between hydrophilic and hydrophobic surfaces can be used for patterning liquids (Jokinen *et al.*, 2008) or cells (Ueda & Levkin, 2013b) on a surface, as surface tension-confined microchannels (Hancock *et al.*, 2011a), in paper-based microfluidics (Martinez *et al.*, 2008), for studying cell-cell communication (Efremov *et al.*, 2012), and as channels for peptide separation (Han *et al.*, 2010).

In order to create a new hydrophilic–hydrophobic patterned surface, usually the entire experimental procedure must be repeated, which can be time-consuming and laborious. Although there are relatively simple methods for creating hydrophilic–hydrophobic patterns using techniques such as microcontact printing (Li *et al.*, 2012a) or hydrophobic sprays (Hancock *et al.*, 2011a), to our knowledge the possibility of making multiple copies from an already existing superhydrophilic–superhydrophobic micropatterned substrate has not been demonstrated until now. We present a simple method that allows the transfer of superhydrophilic–superhydrophobic micropatterns onto adhesive tape while maintaining the rough surface morphology that is important for the extreme wetting properties of superhydrophilicity and superhydrophobicity.

Since multiple copies of a pattern can be made from a single substrate, this results in time optimization and less reagent consumption.

Recently, Zahner et al. published a method for creating superhydrophilic patterns on a superhydrophobic surface by UV-initiated photografting (Zahner *et al.*, 2011). The micropatterns created using this method are three-dimensional because the superhydrophilic or superhydrophobic surface properties exist through the whole thickness of the porous polymer film. Therefore, separating the porous polymer film horizontally into thin slices should allow for the replication of the superhydrophilic-superhydrophobic micropatterns. In this paper, we show a simple and fast method for the transfer of such patterned surfaces using adhesive tape (Figure 7.1A). We demonstrate that by applying and then removing a flexible adhesive tape from a porous polymer film patterned with hydrophilic-hydrophobic structures, we can transfer up to twelve copies of the pattern onto the adhesive tape. Each time tape is applied to the surface, a thin layer of the porous polymer film is transferred to the tape from the original polymer surface. The method of replicating patterns using adhesive tape can be applied to most porous materials that are mechanically brittle enough to be delaminated, and can be used in numerous applications where multiple copies of the same pattern are required. In addition, the produced patterned substrates are flexible and the copies can be used on curved surfaces and cut into different shapes and sizes. The method presented here is also convenient for creating multiple copies of either superhydrophilic or superhydrophobic surfaces using adhesive tape.

Experimental methods

Fabricating porous poly(butyl methacrylate-*co*-ethylene dimethacrylate) (BMA-EDMA) films

Hydrophobic, porous BMA-EDMA films were prepared by UV-initiated radical polymerization of a prepolymer mixture containing monomers, crosslinkers, porogens, and a photoinitiator (Levkin *et al.*, 2009; Svec, 2010). The porogens in the polymerization mixture lead to phase separation once the growing crosslinked polymer chains achieve a critical size. Hence, the formation of these small polymer globules constitutes the porous structure. The mixture consisted of butyl methacrylate (BMA) (24 wt%), ethylene dimethacrylate (EDMA) (16 wt%), 1-decanol (30 wt%), cyclohexanol (30 wt%), and 2,2-dimethoxy-2-phenylacetophenone (DMPAP) (1 wt% with respect to the monomers). The prepolymer mixture was filled between two methacrylated glass plates separated by two strips of 125 μm -thick Teflon film (American Durafilm Co.), and then irradiated with UV light for 15 min. An OAI model 30 deep-UV collimated light source (San Jose, CA) fitted with a 500 W HgXe lamp was used for UV irradiation. The lamp was calibrated to 12 mW cm^{-2} at 260 nm wavelength.

Fabricating hydrophilic–hydrophobic micropatterns in the porous polymer films

To create hydrophilic patterns in the hydrophobic polymer film, the porous polymer film was wetted with a photografting mixture, and then covered with 75 μm -thick Teflon film and a photomask. Then, the polymer film was irradiated with UV light (12 mW cm^{-2} at 260 nm) for 15 min. The photografting mixture consisted of 2-acrylamido-2-methyl-1-propanesulfonic acid (AMPS) (15 wt%) and benzophenone as the initiator (0.25 wt%) in a solution of *tert*-butanol:water (3:1 v/v). All chemical reagents were purchased from Sigma-Aldrich (Germany). Further details about the procedure for fabricating the hydrophilic–hydrophobic patterned polymer films are in the Supporting Information.

Replicating porous polymer films using adhesive tape

Adhesive tape (Tesa[®], 1.5 cm-wide) based on a stable PVC backing coated with a natural rubber was adhered to the polymer surface with the help of a rubber eraser to remove air bubbles, and then the tape was peeled off. To make multiple copies, the procedure was repeated and the direction of the tape removal was alternated each time.

Scanning electron microscopy (SEM)

Samples were gold-sputtered using a Cressington sputter coater 108auto. SEM images were obtained with a LEO 1530 scanning electron microscope (Zeiss, Germany). The globule size of the polymer films was determined from the SEM images.

Measuring the radii of circular hydrophilic patterns on the copies

The hydrophilic patterns were dyed with Rhodamine 6G and images of the patterns and surfaces were taken with a Keyence BZ-9000 fluorescence microscope (Japan) and also with a digital camera (Nikon). Measurements of the radii of circular hydrophilic patterns and the fluorescent intensity were made with the software ImageJ.

Measuring water contact angles (WCAs)

A UK 1115 digital camera from EHD imaging GmbH (Germany) was used to take images of water droplets on the surfaces under ambient conditions. The static (θ_{st}), advancing (θ_{adv}), and receding (θ_{rec}) water contact angles (WCAs) on copies of a porous BMA-EDMA polymer film were measured in three different places on each sample and the average was calculated. The WCAs were determined using ImageJ software with a DropSnake plugin.

Cell experiments

To make the transfection mixture, 6 μl of 0.5 $\mu\text{g } \mu\text{l}^{-1}$ plasmid DNA (H2B-RFP) was mixed with 7 μl of Lipofectamine 2000 (Invitrogen) and incubated for 20 min at RT.

After being freshly prepared and filtered, 3 μl of 0.4 M sucrose in Roswell Park Memorial Institute (RPMI) 1640 medium (Invitrogen) and 7.25 μl of 0.2% gelatin (Sigma, Germany) in water were added to the mixture. 3.5 μl of the transfection mixture was pipetted into each of 3 hydrophilic spots (AMPS photografted, 2 mm diameter circles) on copies 1, 4, 8, and 12 from each of three BMA-AMPS patterned polymer films. The transfection mixture was allowed to dry and then each taped copy was seeded with HEK 293 cells (20,000 cells cm^{-2}) and incubated for two days. The cells were then fixed in 3.7% formaldehyde in Dulbecco's phosphate-buffered saline (PBS) for 20 min, washed 1X with PBS, incubated with 0.1% Triton X-100 in PBS for 15 min, washed 1X with PBS, incubated with 0.5 $\mu\text{g } \mu\text{l}^{-1}$ 4',6-diamidino-2-phenylindole (DAPI, Sigma-Aldrich) for 15 min, washed 2 \times with PBS, and then mounted and covered with glass coverslips. Images were taken using a Keyence BZ-9000 fluorescence microscope (Japan). ImageJ software was used to count the cells.

Results and discussion

In this paper, the fabrication, characterization, and application of replicated porous polymer surfaces are presented. The method of fabrication consists of producing a hydrophobic porous polymer film (BMA-EDMA) on a glass slide, and then modifying it by UV-initiated surface photografting^{18,19} through a photomask to create hydrophilic patterns of defined geometry. The average size of the globules in the porous polymer film was measured to be 486 ± 73 nm.

The replication procedure consists of using adhesive tape to make copies of an original hydrophilic–hydrophobic patterned porous polymer film simply by applying the adhesive tape to the polymer surface and then peeling off the tape (Figure 7.1A). This leads to the transfer of a thin, porous polymer layer (5–10 μm -thick) from the original porous film to the adhesive tape (Figure 7.S1). This method is efficient in that twelve copies of an original 125 μm -thick patterned polymer film can be made with successful transfer of the pattern to all of the copies. Complex patterns, such as channels, can be transferred to the adhesive tape, which can then be used on flat surfaces as well as on curved surfaces (Figure 7.1B, Figure 7.S2). The feature size of a pattern that can be replicated using this method will depend on several factors, such as the size of the polymer globules and the quality of the adhesive tape. The globule size depends on the type of porogen used and can be reduced to approximately 50–100 nm.

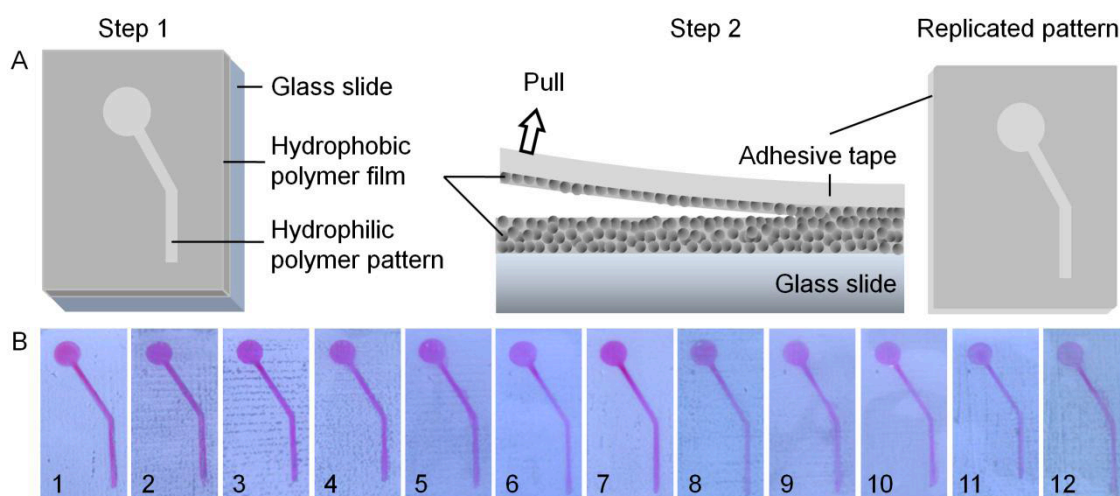


Figure 7.1 Schematic representation of the transfer of a hydrophilic–hydrophobic pattern in a polymer film onto adhesive tape

(A) Step 1: A thin, porous hydrophobic polymer film is photografted through a photomask to create a hydrophilic pattern. Step 2: Adhesive tape is firmly adhered to the surface of the polymer film and then pulled off in one motion. A thin layer of the hydrophilic–hydrophobic patterned polymer film is transferred onto the adhesive tape. (B) Photos of twelve consecutive copies of a channel pattern that was replicated onto adhesive tape and then stained with a Rhodamine 6G aqueous solution. The diameter of the circle is 2 mm.

The reproducibility of the replication procedure was demonstrated by comparing the wettability of the replicated hydrophilic pattern to that of the original patterned surface. The hydrophilic spots of twelve consecutive copies of a BMA-EDMA polymer film photografted with AMPS were filled with Rhodamine 6G aqueous solution, proving that the barriers between the hydrophobic and hydrophilic regions still existed and that the whole pattern was successfully transferred to the tape (Figure 7.2A). In the thirteenth copy, the polymer film showed irregularities and the underlying glass slide could be seen.

In order to quantify the reproducibility of the pattern transferred to the adhesive tape, we measured the defined geometry of the pattern with increasing copy number of the replicated patterned polymer film. The seven radii of the circular pattern on each of twelve replicates were measured and the average radius was calculated. As the number of the copies increased, the average radius slightly decreased (Figure 7.2B). This can be explained by the scattering of UV light during the photografting step, which reduces the photografting efficiency as the light passes through the thickness of the porous polymer film (Levkin *et al.*, 2009). The polymer layer transferred to the adhesive tape was

uniform in the first copy, but as the order of the copies increased, some regions without polymer could be seen on the adhesive tape (Figure 7.3A).

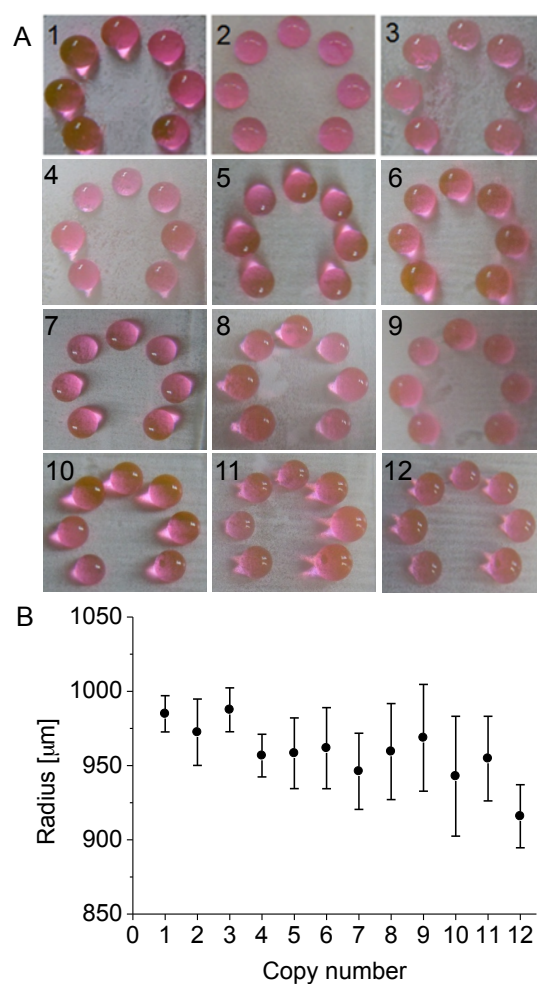


Figure 7.2 Photos of 12 consecutive copies of a patterned polymer film

(A) Photos showing the hydrophilic spots (2 mm diameter circles) of twelve consecutive copies of a patterned polymer film filled with a Rhodamine 6G aqueous solution. (B) Each point in the graph represents the average radius (SD) of the seven circles of the hydrophilic pattern for each copy.

The advantage of porous materials is that their surface properties, such as hydrophobicity, are preserved through the thickness of the porous film (Jin *et al.*, 2013). In other words, the hydrophobicity of the porous polymer film is a result of the bulk properties of the material and not just of its surface, so it should also be preserved upon the replication steps. The static (θ_{st}), advancing (θ_{adv}), and receding (θ_{rec}) water contact

angles (WCAs) of the copies of a porous BMA-EDMA polymer film were measured. The results show that both θ_{st} and θ_{adv} on the copies virtually do not change after ten consecutive copies (Figure 7.3B, Table 7.S1). However, θ_{rec} gradually decreased from 147° to 135° from the first to the tenth copy, and then dropped to 117° for the twelfth copy. The increase in WCA hysteresis after the tenth copy can be explained by the non-uniform polymer film coverage on the adhesive tape (Figure 7.3A). The number of reproducible copies is limited by the thickness of the original polymer film, thus the number of copies can be increased if a thicker polymer film is used. However, the number of reproducible copies is also limited by the mechanical damage to the original polymer film that occurs after each pattern transfer, as well as the scattering of UV light when photografting thicker layers of polymer films.

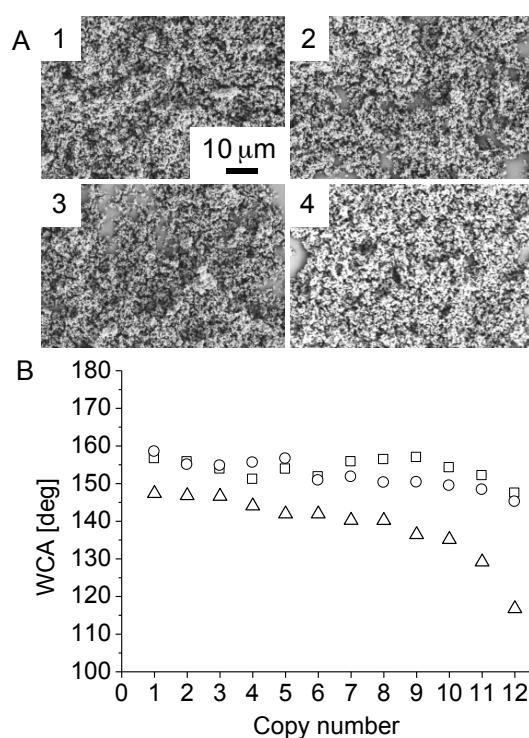


Figure 7.3 SEM images and water contact angle measurements of copies of a polymer film

(A) SEM images of the first four copies of an original BMA-EDMA polymer film. (B) Measurements of the average static (□), advancing (○), and receding (Δ) water contact angles of twelve consecutive copies of a 125 μm-thick, porous BMA-EDMA polymer film.

We have already demonstrated the ease with which multiple copies of a patterned polymer film can be replicated and subsequently used for patterning liquids. To demonstrate that the replicated polymer films are useful for a broad range of applications, including biological experiments, we used the replicates as substrates for reverse cell transfection (Ziauddin & Sabatini, 2001). Since hydrophilic-hydrophobic patterns are able to confine liquids and cells in arrays of high-density, they can be useful for high-throughput cell and chemical screening applications (Geyer *et al.*, 2011). We used copies 1, 4, 8, and 12 from BMA-AMPS patterned polymer films, and pipetted a transfection mixture containing plasmid DNA encoding for histone H2B-red fluorescent protein (pCS2+-H2B-RFP) and Lipofectamine[®] 2000 onto the hydrophilic spots (2 mm diameter circles) on the copies (Figure 7.4A). The transfection mixture was allowed to dry before seeding human embryonic kidney (HEK 293) cells on each taped copy. After two days of incubation, the cell transfection efficiency was quantified using by counting the RFP-expressing cells and dividing it by the total number of DAPI-stained cells (Figure 7.4B, 7.S5). The average transfection efficiency for all copies was approximately 40% (Figure 7.4C). This demonstrates that although there were slight changes in the morphology of the polymer film or the water contact angles as the order of the copies increased (Figure 7.3), there was no significant effect on the cell transfection efficiency. These results show that multiple copies of a patterned polymer film replicated using adhesive tape can be used to pattern bioreactive agents on a surface and perform biological experiments.

Conclusion

We introduced a new method for the facile replication of patterned polymer films using adhesive tape. Since the polymer film is transferred to adhesive tape, which is flexible, utilizing the copies is not limited to flat surfaces and they can also be cut into different shapes and sizes. We also demonstrated an application of the replicated patterned polymers as a substrate for reverse cell transfection experiments. This simple method of transferring surface properties using adhesive tape can be applied to a variety of porous polymers or aerogels (Jin *et al.*, 2013). We believe that with this novel method it is possible to significantly reduce the time and cost needed to fabricate multiple substrates composed of polymers, and that it will find numerous applications in the biological and chemical fields.

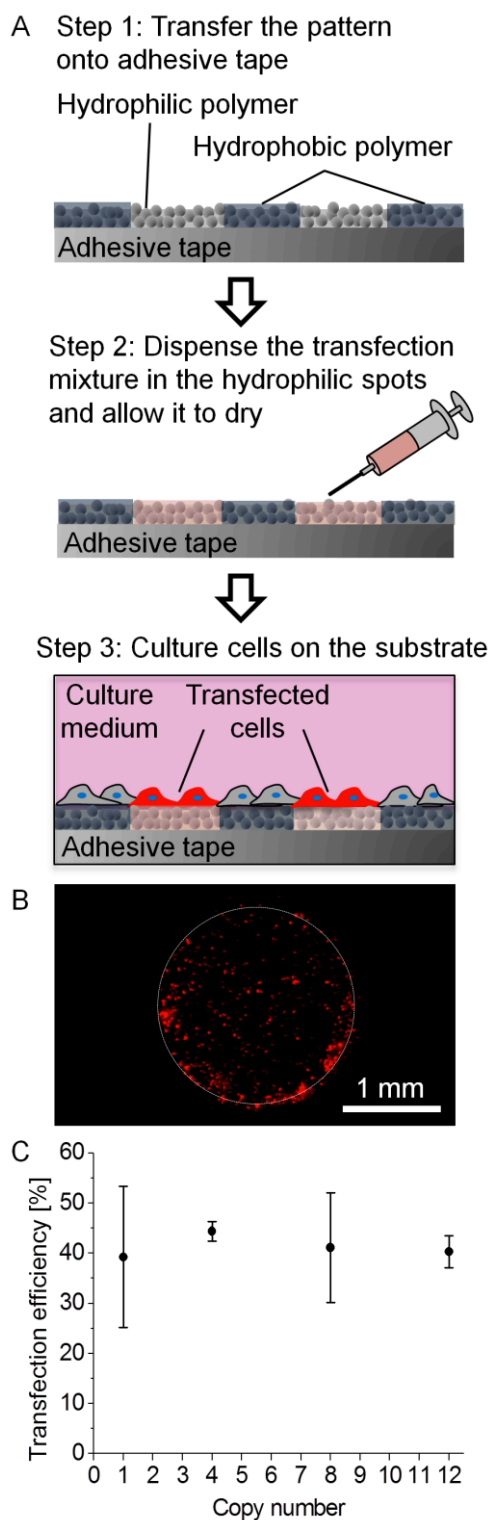


Figure 7.4 Using the copies of a patterned BMA-AMPS polymer film as substrates for reverse cell transfection

(A) Schematic of the procedure for replicating a hydrophobic–hydrophilic polymer pattern onto adhesive tape, dispensing a transfection mixture in the hydrophilic spots

and allowing it to dry, and then culturing cells on the substrate. (B) Image of red fluorescent protein-expressing cells within one hydrophilic spot (outlined in white) after two days of incubation on a copy that was printed with a transfection mixture. (C) The average (SD, $n = 3$) transfection efficiency of cells cultured on copies 1, 4, 8, and 12 that were printed with a transfection mixture.

7.2 Supporting information

Procedure for fabricating the porous polymer films

Activation of glass plates: The glass plates were immersed in a 1 M sodium hydroxide solution for 0.5 h, washed with water, and dried. After that they were immersed in a 1 M hydrochloric acid solution for 0.5 h, washed with water, and dried.

Functionalization of glass plates: The activated glass plates were functionalized with 3-(trimethoxysilyl)propyl methacrylate as an anchor group for the polymerization. A few droplets of 20 vol% 3-(trimethoxysilyl)propyl methacrylate in ethanol were applied to the activated glass plates and covered with another activated glass plate. The solution was reapplied after 30 min and retained on the glass plates for an additional 30 min. Then, the glass plates were washed with acetone and dried with a stream of air.

Making microporous BMA-EDMA films: The polymerization mixture was applied between two methacrylated glass plates, which were separated by two thin strips of a 125 μm -thick Teflon film (American Durafilm Co.). The glass slides were fixed with multiple clamps and put under the UV (12 mW cm^{-2} at 260 nm) lamp for 15 min of irradiation. After irradiation, the glass slides were carefully opened with a scalpel. The polymer film stuck to the upper glass plate, while there was only a very thin polymer layer left on the lower glass plate. The polymer was washed extensively with ethanol, immersed into ethanol for at least 1 h, and then dried with a stream of nitrogen.

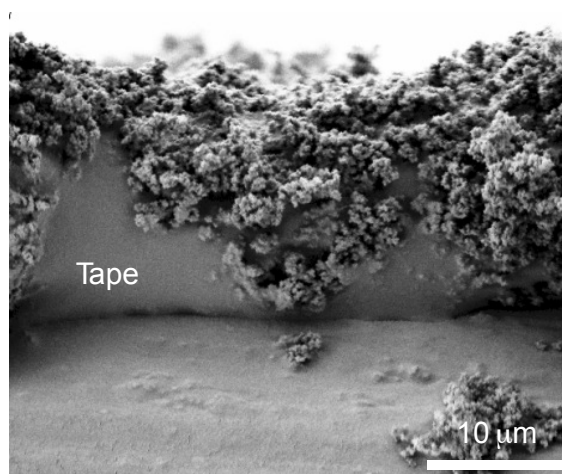


Figure 7.S1 SEM image of the cross section of a copied polymer film

SEM image of the cross section of the first copy of a BMA-EDMA polymer film replicated using adhesive tape.

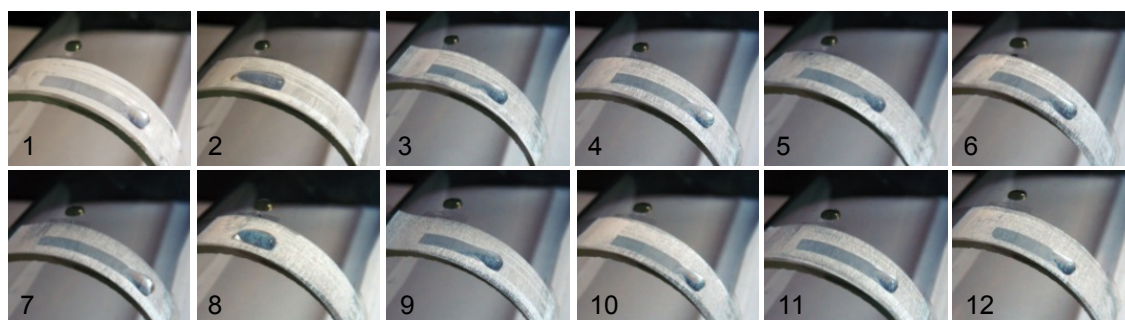


Figure 7.S2 Photos of droplets on curved copies of a patterned surface

Photos of moving water droplets confined within a rectangular channel pattern that was replicated 12 consecutive times onto adhesive tape and adhered to a curved surface using double-sided tape. The width of the channel is 5 mm.

Fluorescence analysis of the replicated patterned surfaces

In addition to replicating the hydrophilic–hydrophobic patterned polymer film, we tested whether we could also transfer to the adhesive tape a substance pre-filled and dried in the hydrophilic spots of the pattern. To test this, images of two original patterned samples, which were colored in the hydrophilic spots by a solution of Rhodamine 6G, and their subsequent copies were taken in order to compare the degree of fluorescent intensity. The original pattern was filled with the dye solution, allowed to dry before the replication process using adhesive tape was performed, and the samples were analyzed using a fluorescence microscope (Keyence BZ-9000). As shown in Figure 7.S3, as the number of the replicates increased, the degree of fluorescence decreased. The degree of fluorescence was quantified using the software ImageJ. Figure 7.S4 shows that after the seventh replicate there is almost no fluorescence.

The decreased transfer of Rhodamine 6G with increasing copy number might occur because of the low interaction between the molecules of Rhodamine 6G and the composition of the polymer film. We tried to improve the penetration of Rhodamine 6G into the polymer film by adding small amounts of gelatin to the Rhodamine 6G solution. However, there was a visual increase in the viscosity of the solution as the amount of gelatin increased, so the dye was not able to spread well through the polymer film. In other words, the dye remained predominantly on the surface of the pattern so that when the first replication was made the dye was transferred mainly to the first copy.

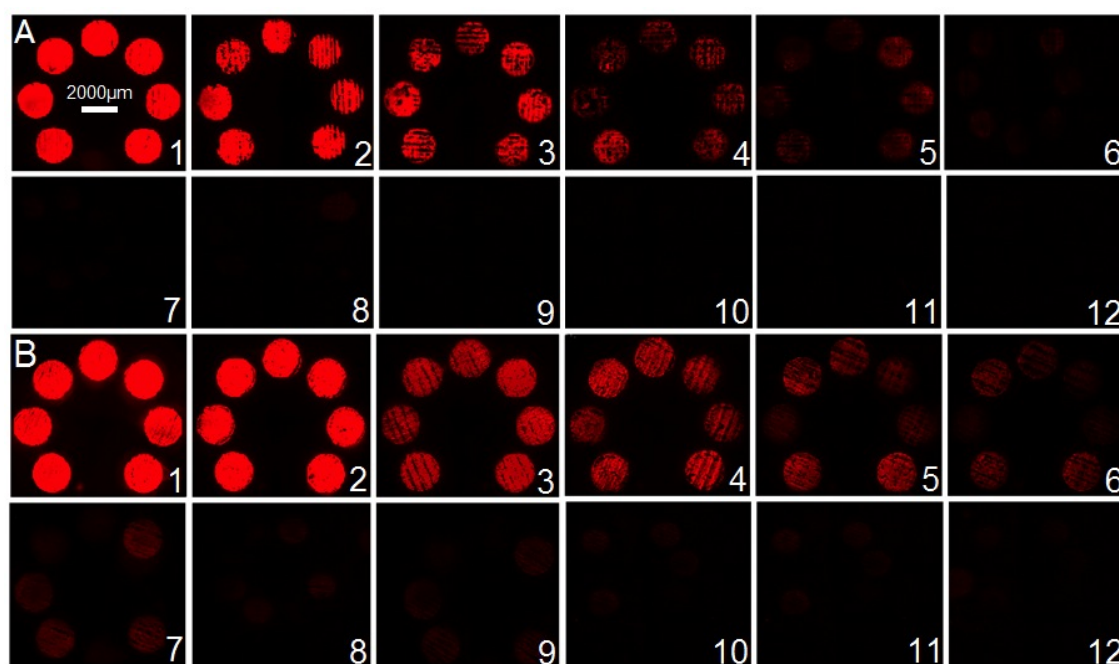


Figure 7.S3 Images of 12 copies of a patterned surface colored with dye

(A,B) Fluorescence images of two different patterns colored by a 0.1% solution of Rhodamine 6G in water and the subsequent copies of the dyed patterns. Exposure time: 1/230 s.

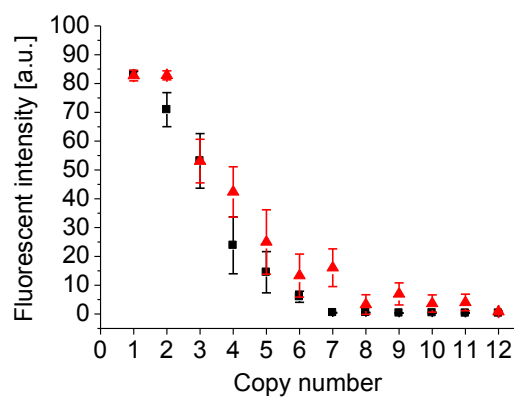


Figure 7.S4 Graph of the fluorescence intensity of 12 copies colored with dye

Intensity of fluorescence of 12 copies of a BMA-EDMA polymer film photografted with AMPS and colored by Rhodamine 6G. Two samples were imaged with an exposure time of 1/230 s.

Water contact angle measurements

Table 7.S1 Average water contact angle values of 12 copies of a polymer film

Values of the average (SD) static, advancing, and receding water contact angles of twelve copies of an original sample of a 125 μm -thick, porous BMA-EDMA polymer film calculated using the software ImageJ and the DropSnake plugin.

Copy number	Static WCA	Advancing WCA	Receding WCA
1	156.629 \pm 2.651	158.465 \pm 1.087	147.392 \pm 4.836
2	155.762 \pm 1.942	155.012 \pm 3.282	146.818 \pm 5.427
3	153.878 \pm 1.644	154.779 \pm 2.343	146.633 \pm 1.515
4	151.134 \pm 2.953	155.568 \pm 3.74	144.081 \pm 2.079
5	153.860 \pm 2.229	156.632 \pm 3.383	141.963 \pm 1.158
6	151.804 \pm 2.776	150.837 \pm 1.475	141.944 \pm 1.259
7	155.792 \pm 3.904	151.774 \pm 2.205	140.240 \pm 1.229
8	156.384 \pm 2.687	150.259 \pm 3.092	140.219 \pm 1.529
9	156.924 \pm 0.851	150.350 \pm 3.913	136.457 \pm 2.984
10	154.230 \pm 1.725	149.453 \pm 3.911	135.169 \pm 2.242
11	152.105 \pm 1.628	148.363 \pm 1.663	129.198 \pm 0.661
12	147.451 \pm 1.444	145.189 \pm 1.845	116.767 \pm 2.492

Details of the cell experiments

HEK 293 cells were cultured in DMEM (Gibco, Cat. #41966) supplemented with 10% FBS (PAA Laboratories, Cat. #A15-151) and 1% penicillin/streptomycin in a humid incubator at 37°C with 5% CO₂, and were split every two to three days.

Reverse cell transfection mixture: 6 μl of 0.5 $\mu\text{g } \mu\text{l}^{-1}$ plasmid DNA (pCS2+-H2B-RFP) was mixed with 7 μl of Lipofectamine 2000 (Invitrogen) and incubated for 20 min at RT. After being freshly prepared and filtered, 3 μl of 0.4 M sucrose in RPMI (Invitrogen) and 7.25 μl of 0.2% gelatin (Sigma) in water were added to the mixture.

3.5 μl of the transfection mixture was pipetted into each of 3 hydrophilic spots (AMPS photografted, 2 mm diameter circles) on copies 1, 4, 8, and 12 from each of three BMA-AMPS patterned polymer films. The transfection mixture was allowed to dry and then each taped copy was seeded with HEK 293 cells (20,000 cells cm^{-2}) and incubated for two days. The cells were then fixed in 3.7% formaldehyde in PBS for 20 min, washed 1 \times with PBS (Invitrogen), incubated with 0.1% Triton X-100 in PBS for 15 min, washed 1 \times with PBS, incubated with 0.5 $\mu\text{g } \mu\text{l}^{-1}$ DAPI (Sigma-Aldrich) for 15 min, washed 2 \times with PBS, and then mounted and covered with glass coverslips. Images were taken using a Keyence BZ-9000 fluorescence microscope (Japan). The cell transfection efficiency was quantified by counting the RFP-expressing cells and dividing it by the total number of DAPI-stained cells. ImageJ software was used to count the cells by converting the TIFF to 16-bit, adjusting the threshold, converting the image to binary, applying a median filter, watershedding, and analyzing the particles. The automated results were compared to several hand counted cell numbers to check the accuracy of the cell count.

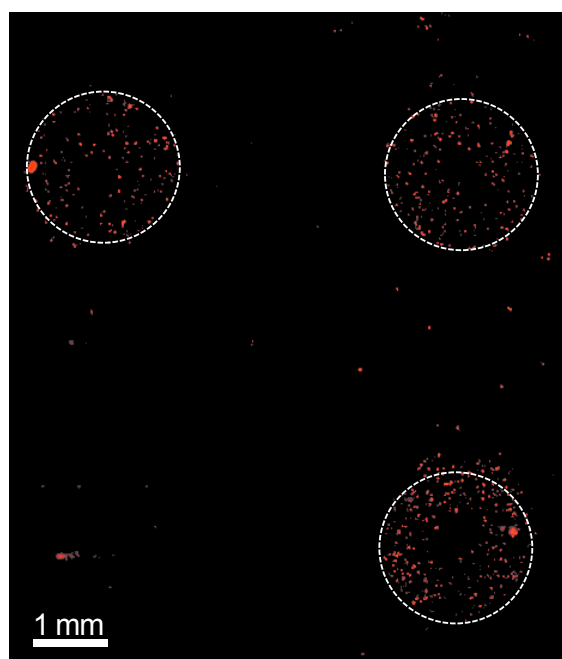


Figure 7.S5 Reverse cell transfection on a copy of a pattern

Image of red fluorescent protein-expressing cells after two days of incubation within three hydrophilic spots (outlined in white) on a copy of a pattern consisting of 2 mm diameter circles that were printed with a transfection mixture.

8 Discussion

8.1 Improving the method of fabrication for superhydrophilic–superhydrophobic patterned surfaces

Creating superhydrophilic–superhydrophobic patterned surfaces depends on surface morphology and the ability to create patterns of hydrophilic and hydrophobic functionality on the surface. During this PhD work, two methods for creating superhydrophilic–superhydrophobic patterns in porous polymer surfaces were developed for subsequent cell studies. The aim here was to develop a relatively simple yet reproducible method for creating the patterned surfaces. The first step of creating a 12.5 μm -thin, nanoporous, and superhydrophilic poly(2-hydroxyethyl methacrylate-*co*-ethylene dimethacrylate) (HEMA-EDMA) film on a glass slide by UV-initiated free radical polymerization was the same for both methods. For the second step of creating the patterned surface, either UV-initiated photografting or a UV-initiated thiol-yne click reaction was used.

During the UV-initiated photografting procedure, branched side chains composed of poly(2,2,3,3,3-pentafluoropropyl methacrylate-*co*-ethylene dimethacrylate) (PFPPMA-EDMA) were grafted to the methacrylated polymer surface. Due to the long time (30 min) needed for UV irradiation through a glass cover slide and quartz photomask in order to graft through the whole thickness of the polymer film, the high density of PFPPMA-EDMA grafted within the porous polymer layer changed the morphology of the polymer structure and resulted in reduction of the pore size and porosity (Efremov, 2014). This could reduce the hydrophobicity due to loss of the air pockets in the bulk of the polymer, which are important for maintaining the Cassie–Baxter state (Figure 8.1). For example, Rohr et al. showed that with increasing grafting time the resistance to water flow through a polymer monolith increased, indicating that the thickness of the grafted layer increased with grafting time due to the higher density and cross-linking of the grafted chains (Figure 8.2) (Rohr *et al.*, 2003). Long irradiation times also leads to oxidation or degradation of the PFPPMA-EDMA brushes, which can also reduce the hydrophobicity (Efremov, 2014). Therefore, it is challenging to find the optimal photografting conditions to achieve grafting through the whole thickness of the polymer film while minimizing the effects of over irradiating.

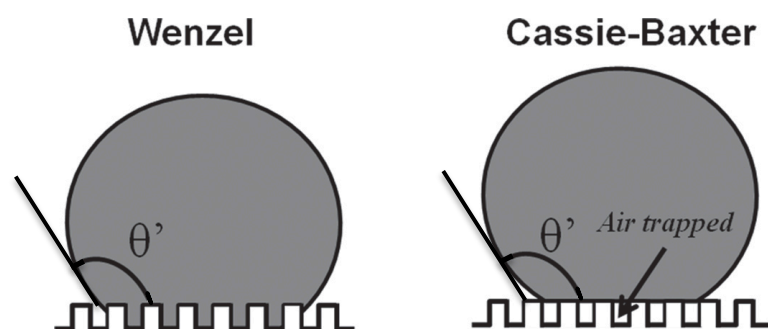


Figure 8.1 Wenzel and Cassie–Baxter states

Two typical superhydrophobic states: the Wenzel state and Cassie–Baxter state. There is always air trapped between water and the substrate in the Cassie–Baxter state but no air is trapped in the Wenzel state. Adapted with permission (Chen *et al.*, 2012). Copyright © 2012 WILEY-VCH Verlag GmbH & Co. KGaA, Weinheim.

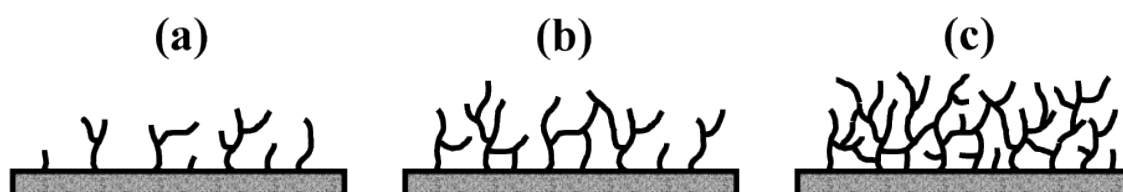


Figure 8.2 Effect of irradiation time on photografting

Schematic representation of the growing polymer chains during photografting with increasing irradiation time from (a) to (c). Reproduced with permission (Rohr *et al.*, 2003). Copyright © 2003 American Chemical Society.

The second method used to create patterned surfaces was based on thiol-yne click chemistry to functionalize the polymer surface. We found this method much more reproducible for fabricating the superhydrophilic–superhydrophobic patterned surfaces due to the modification of the polymer surface with small molecules rather than cross-linked polymer brushes, and thus we did not observe a significant change in the morphology of the polymer (Feng *et al.*, 2014). In addition, the reaction proceeded very quickly (as fast as 15 s) and could be triggered at half the UV intensity used for the photografting procedure. This method is not limited to creating only superhydrophilic–superhydrophobic patterns, but a variety of functional groups containing a terminal thiol can be covalently immobilized on the surface as we demonstrated by creating a peptide pattern (Figure 4.1G).

During polymerization of the HEMA-EDMA film on a glass substrate, a thin and smooth superficial layer forms due to the use of a fluorinated glass slide as the cover

plate during UV irradiation. When using the photografting method to create the superhydrophobic barriers, this surface layer became almost nonporous and we found that removing this superficial layer with Tesa tape to expose the underlying porous morphology and increase the surface roughness enhanced the hydrophobicity. However, this created a crater-like morphology on the surface instead of homogeneous removal of the superficial layer (Figure 2.2D), and this could affect the photografting procedure due to accumulation or diffusion of the photografting mixture in the craters during UV irradiation. This could have caused variation in the grafting density on the surface due to a higher concentration of monomers and photoinitiator in the craters. This disadvantage was overcome when using the thiol-yne click photopatterning method because the superhydrophilic–superhydrophobic patterns could be created without removal of this superficial top layer since the surface layer was still porous after modification with small molecules. In addition, the UV irradiation time was drastically reduced to just 60 s using the thiol-yne click photopatterning method versus 30 min using the photografting method.

Another advantage of the thiol-yne click photopatterning method was the ability to place the quartz photomask directly on top of the substrate without requiring a cover slide as in the photografting method. This allowed for a much sharper pattern resolution due to less scattering of the UV light at the edges (Figure 4.2). This was especially important for patterning the narrow superhydrophobic barriers such that they remained watertight through the bulk of the polymer film.

8.2 Using hydrophobicity to pattern liquids and cells

Standard glass slides are often used for high-density cell microarrays, but the cells are either cultured over the whole surface or the background is passivated such that the cells mainly adhere to the spots of interest. Instead of passivating the background with surface coatings such as poly(ethylene glycol) (PEG) (Hook *et al.*, 2009b; Ma *et al.*, 2006; Revzin *et al.*, 2003) or albumin (Arima & Iwata, 2007) to prevent cell adhesion, in this PhD work two methods based on different principles of hydrophobicity were demonstrated to be able to control the patterning of liquids and cells on surfaces. The first method was based on creating patterns of a nanoporous superhydrophobic polymer film exhibiting the Cassie–Baxter state (Figures 2.2 and 3.1), and the second method was based on infusing a hydrophobic liquid in the patterned porous polymer film (Figure 6.1).

Superhydrophilic–superhydrophobic patterned surfaces have a wide range of applications (Ueda & Levkin, 2013a), but an interesting biological application is the ability to pattern cells as well as aqueous solutions. We demonstrated that superhydrophilic–superhydrophobic micropatterns can be used to form high-density cell microarrays using micropatterns consisting of $335 \times 335 \mu\text{m}^2$ superhydrophilic squares separated by $60 \mu\text{m}$ -wide superhydrophobic barriers (Figures 2.4 and 3.3). Aqueous solutions spotted in the superhydrophilic squares wetted the microspots and were completely contained by the watertight superhydrophobic barriers. Several different cell types were cultured on the patterned surfaces and preferentially adhered and grew to confluence on the superhydrophilic microspots, while the superhydrophobic barriers prevented cell proliferation on the barriers and cell migration between neighboring spots. On the patterned surfaces fabricated using the method based on thiol-yne click chemistry, we found that no HEK 293 cells and only 1.6% of HeLa cells occupied the superhydrophobic barriers. This was an improvement in compared to when cells were cultured on the superhydrophilic–superhydrophobic patterned surfaces fabricated using UV-initiated photografting, where we calculated 13% of HEK 293 cells on the superhydrophobic barriers.

Since the superhydrophobic barriers exhibited the Cassie–Baxter state, they effectively trapped air in the surface asperities and within the pores of the polymer film, preventing the penetration of aqueous solutions in the superhydrophobic regions (Cassie & Baxter, 1944; Koishi *et al.*, 2009). Cell–surface interactions are influenced by proteins present on the surface and those that adsorb on the surface from the culture media, followed by deposition of the cell’s own extracellular matrix (ECM). Since only a small fraction of the superhydrophobic surface was in contact with the culture media, this likely reduced the number of sites available for protein adsorption and deposition of the cell’s own ECM, and subsequent focal adhesion (Ballester-Beltrán *et al.*, 2011). Even at these limited points of contact between the culture media and the

superhydrophobic surface, it has been shown in the literature that adsorbed proteins such as fibronectin showed altered conformation of the domains involved in cell adhesion (Baugh & Vogel, 2004), and reorganization or exchange of the adsorbed proteins with those deposited by the cells were significantly inhibited on superhydrophobic surfaces (Ballester-Beltrán *et al.*, 2011). These events would further discourage cell adhesion on superhydrophobic surfaces.

When the superhydrophobic barriers were transformed from the Cassie–Baxter to the Wenzel state such that the culture media was able to penetrate the pores, the ability to pattern cells was lost or severely diminished for different cell types (Figure 2.S6) (Geyer *et al.*, 2011). This suggests that although surface chemistry can be used to control cell adhesion, its effectiveness can be highly dependent on the cell type and the composition of the culture media as the original chemical pattern is obscured over time with other adsorbed proteins.

The behavior of cells on the superhydrophilic–superhydrophobic patterned surfaces developed in this work are in agreement with other published studies investigating the interaction of cells on different hydrophobic surfaces. Ishizaki *et al.* showed that cells could immediately adhere to the superhydrophilic surfaces in a highly selective manner after seeding, whereas the cells needed 24–72 h after seeding to adhere to the superhydrophobic surfaces (Ishizaki *et al.*, 2010). This difference in cell attachment was attributed to the difference in protein adsorption between the superhydrophilic and superhydrophobic surfaces. More time was needed for the cells to produce their own ECM and to form a protein layer suitable for cell attachment on the superhydrophobic surfaces. It was also demonstrated that cells were able to spontaneously migrate and recognize the superhydrophilic regions after being seeded, and coalesced there and grew to confluence after 24 h. Oliveira *et al.* showed that when patterned substrates were immersed and cultured in a suspension of SaOs-2 cells for 6 days, the superhydrophilic regions were densely populated with cells while only a few cells occupied the superhydrophobic regions (Oliveira *et al.*, 2011). Lourenço *et al.* found that less protein was adsorbed on rough and superhydrophobic surfaces, independent of the underlying surface chemistry, and attributed this to the Cassie–Baxter effect (Lourenço *et al.*, 2012). This also resulted in a lower affinity of cells to the rough superhydrophobic surfaces. Thus, superhydrophobicity can be used as a more general approach for controlling protein and cell adhesion since liquid–surface interactions are minimized, and using superhydrophobic barriers to confine cells can be an interesting and effective alternative to using physical barriers for applications such as cell patterning, cell microarrays, and lab-on-a-chip or diagnostic devices.

The second method that we explored for cell and liquid patterning was based on the idea of slippery, liquid-infused surfaces that was first introduced by the Aizenberg group (Wong *et al.*, 2011). We used the same superhydrophilic–superhydrophobic

patterned substrates described previously, and then infused the superhydrophobic barriers with a fluorinated oil called Krytox[®], a low molecular weight fluorine end-capped homopolymer of hexafluoropropylene epoxide. This replaced the non-wetting superhydrophobic Cassie–Baxter barriers with micropatterns of hydrophobic liquid barriers that were stable due to the high affinity of Krytox[®] to the porous hydrophobic polymer and its immiscibility with the surrounding aqueous solution (Figure 6.1). We demonstrated that the hydrophobic liquid micropatterns were stable underwater for at least 30 days (Figure 6.2). We also showed that the hydrophobic liquid surfaces prevented cell adhesion for at least 7 days, surpassing that of a PEGylated surface, which has long been considered the benchmark for cell-resistant surfaces (Figure 6.3). The hydrophobic liquid barriers were able to confine the different cell types tested within the superhydrophilic spots, even when the cells became very confluent. The few cells that did remain on the hydrophobic liquid barrier after 7 days in culture had a rounder morphology compared to cells on the superhydrophilic region and were easily removed by shear forces when gently washing the substrate. This suggested that the cells did not readily adhere and grow on the hydrophobic liquid even after 7 days of culture. Furthermore, the hydrophobic liquid showed no cytotoxic effects (Figure 6.S5). The slippery, water-immiscible, self-healing, and defect-free nature of the stable liquid layer formed on the hydrophobic liquid-infused porous surfaces most likely resulted in the cell-resistant behavior due to the inability of the cells to anchor to the liquid interface (Epstein *et al.*, 2012; Wong *et al.*, 2011). This phenomenon resembles the liquid-like interface of a highly hydrated PEGylated surface that is attributed to its anti-fouling properties (Jeon *et al.*, 1991; Schilp *et al.*, 2009).

As discussed previously, we demonstrated that the superhydrophobic barriers were able to confine cells within the superhydrophilic microspots and to inhibit cell migration between the neighboring microspots. However, the cell-repellent properties of the superhydrophobic barriers were less effective when cells became overly confluent during long culture times, most likely due to increasing accumulation of proteins on the surface. At the cell densities typically used in our reverse transfection experiments (30,000–35,000 cells cm⁻²), we began to observe cells on the superhydrophobic barriers after 3–4 days of culture. However, since 2 days was sufficient for our transfection experiments, we preferred to use the superhydrophilic–superhydrophilic patterned polymer surfaces since they were easier to handle for patterning cells and liquids for the reverse transfection cell microarrays. The patterned hydrophobic liquid arrays had to be kept in an aqueous environment to prevent spreading of the hydrophobic liquid over the whole area of the porous polymer substrate. Therefore, in order to print transfection mixtures or chemicals in each hydrophilic spot, they must be printed before the hydrophobic liquid is applied. As part of the procedure to make the hydrophobic liquid arrays, the excess hydrophobic liquid must be removed from the hydrophilic regions (Figure 6.1A), but this requires some shear force and occasionally we observed

spreading of the pre-printed transfection mixtures. Nevertheless, hydrophobic liquid surfaces are excellent for long-term cell repellency and they show promising potential for other applications such as anti-bacterial surfaces (Epstein *et al.*, 2012; Li *et al.*, 2013a), anti-ice/anti-frost surfaces (Kim *et al.*, 2012), and preventing marine biofouling (Xiao *et al.*, 2013).

8.3 Technical aspects of using the superhydrophilic–superhydrophobic patterned surfaces for high-density cell microarrays

8.3.1 Precise and accurate control of the volume printed

We used a Scienion S11 non-contact piezoelectric dispenser to print different solutions into each individual superhydrophilic microspot in the desired array pattern and at a specified volume. The device allowed us to select the starting position on the patterned surface using a camera mounted onto the nozzle head. Therefore, it was very important to squarely align the photomask on the substrate during pattern formation to prevent any tilt in the pattern. This avoided any errors when printing into individual hydrophilic spots across the whole slide. The motorized nozzle head allowed us to accurately and precisely print solutions into individual superhydrophilic spots without touching the surface. This was especially important for the polymer surfaces.

The device was also equipped with a camera to detect the drop volume and perform a quality control check of the droplet ejection from the nozzle before printing each sample. A single droplet was approximately 400 pl and the number of droplets required to print the desired volume was rapidly dispensed on the surface. Compared with water, printing the transfection mixtures was more challenging due to film formation at the tip of the nozzle that disturbed the formation and ejection of the subsequent drops. This problem was minimized by cleaning the nozzle tip of any debris and performing longer washing steps in between samples.

For solutions printed on glass slides, many factors affect the final concentration such as the surface properties, the surface tension and viscosity of the solution, and the temperature and humidity during printing. Solutions are often printed onto glass slides using contact printers and pins where the volume dispensed is difficult to control, so this adds another variable because the volume dispensed again depends on the surface and liquid properties, the pin design, and the printing parameters such as contact time with the surface. Therefore, it can be difficult to compare the results of cell studies because even though the starting solution is the same, the printing conditions can vary widely.

8.3.2 Controlling the relative humidity during printing

We found that controlling the relative humidity in the chamber during printing was very important for uniform distribution of the transfection mixture on the surface after drying. At less than 50% RH, a 20 nl drop printed on the surface dried relatively quickly within 15 s and we observed the so-called coffee-ring effect. This occurs when a drop on a surface is pinned at the edges and liquid evaporates faster from the edges due to the

thinner liquid layer. Particles in the solution then flow outward to replace the lost volume, causing a higher concentration of the substance at the edges (Figure 8.3) (Deegan *et al.*, 1997; Yunker *et al.*, 2011). When cells were cultured on surfaces printed with transfection mixtures at low humidity conditions, the transfected cells were located primarily around the edge of the superhydrophilic spot. When the relative humidity was set above 90% RH, a 20 nl drop took approximately 10 min to evaporate. At high relative humidity conditions during printing of the transfection mixtures, the transfected cells were located everywhere within the superhydrophilic spot. The slower evaporation rate of the drop could have allowed enough time for the lipoplexes in the solution to settle to the surface before the drop evaporated, and may have also allowed more time for evaporation to occur over the whole surface of the drop and not just at the edges. When a fluorescent dye was added to the transfection mixtures to visualize the distribution on the polymer surface, we observed a homogeneous fluorescence signal across the whole superhydrophilic spot, whereas the fluorescence signal on the uncoated glass slide was mostly concentrated at a single location as indicated by the high intensity fluorescence signal in each spot (Fig. 3.2). Therefore, we set the relative humidity above 90% when printing the transfection mixtures on the patterned polymer surfaces to achieve an even distribution of lipoplexes within the superhydrophilic spot.

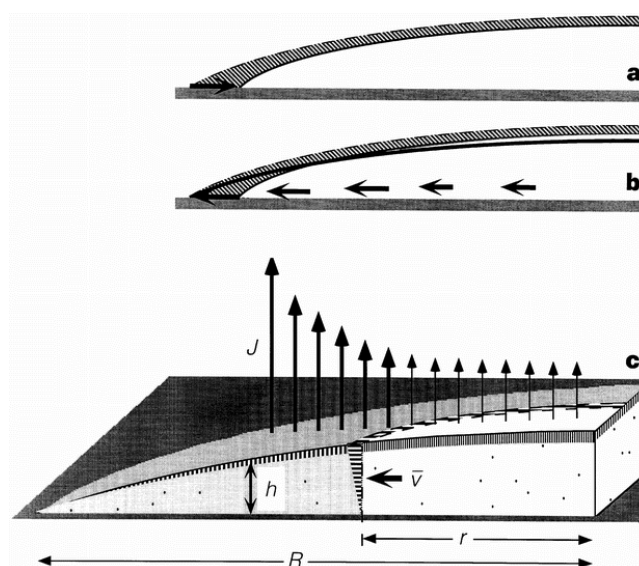


Figure 8.3 Coffee-ring effect

(a) and (b) show an increment of evaporation viewed in cross-section. (a) The result of evaporation without flow: the droplet shrinks. (b) The compensating flow needed to keep the contact line fixed. In (c), we define the quantities responsible for flow. Vapor leaves at a rate per unit area $J(r)$. The removed liquid contracts the height $h(r)$ vertically, vacating the vertically striped region in a short time Δt . The volume of this

striped region is equal to the volume removed by J . But in the shaded annular region the heavy-striped volume is smaller than the volume removed by J there (heavy arrows). Thus liquid flows outwards to supply the deficit volume: fluid at r sweeps out the horizontally striped region in time Δt . Its volume is the deficit volume; its depth-averaged speed is $\bar{v}(r)$. Reproduced with permission (Deegan *et al.*, 1997). Copyright 1997 Nature Publishing Group.

8.3.3 High density of spots without cross-contamination of liquids or cells

When glass slides or well plates are used as substrates for cell microarrays, the density of the spots is limited by the need to print at large spot-to-spot distances to reduce cross-contamination of both the printed samples on the surface and the cells growing on the spots. Typical array layouts for transfected cell microarrays are spot diameters in the range of 200–500 μm printed at a pitch of 500–1000 μm (Baghdoyan *et al.*, 2004; Mousses *et al.*, 2003; Neumann *et al.*, 2006; Rantala *et al.*, 2011). By creating densely packed 335 \times 335 μm superhydrophilic squares separated by narrow 60 μm superhydrophobic barriers, we achieved a spot density 6-fold higher than on an uncoated glass slide. At least 20 nl could be printed in neighboring hydrophilic spots without the drops merging, but on an uncoated glass slide drops of 5 nl already began to merge at the same spot pitch of 395 μm (Figure 3.2). Throughout the reverse transfection experiments, we printed 20 nl per spot to achieve the desired final concentrations of the transfection mixture. Approximately 6,000 superhydrophilic squares fit on a single slide, whereas when printing transfection mixtures on a glass slide the pitch had to be increased to 1 mm to avoid mixing of the neighboring 20 nl drops and only 950 spots could fit onto a glass slide.

More importantly, we could control the spot area of the printed mixture by confining the drop with the superhydrophobic barriers independent of the volume printed or the liquid properties of different solutions, allowing us to calculate the amount of the transfection mixture components per area for different conditions. On substrates without barriers to confine the printed solutions such as glass slides, the printed spot size depends on the drop volume, the surface properties, and the properties of the printed solution such as viscosity and surface tension due to uncontrolled spreading of the drop on the surface. For example, Delehanty *et al.* showed that with increasing surface hydrophobicity due to different surface coatings, the spot size of the printed transfection mixture decreased and the resulting amount of pDNA per area became more concentrated (Delehanty *et al.*, 2004). The higher local concentration of pDNA then correlated with increasing cell transfection. These findings demonstrate that directly comparing the transfection efficiency for different coated surfaces could be misleading if the local transfection mixture concentration is not equivalent, and it would

be difficult to distinguish the effects of the underlying substrate versus the mixture concentration.

To demonstrate that the patterned surfaces can be a useful tool for cell screening and an improvement upon conventional transfected cell arrays on glass slides, we showed that the separation of the hydrophilic spots by only 60 μm did not result in high levels of cross-contamination of the printed transfection mixtures between the neighboring spots (Figure 3.3). The percentage of cross-contamination was analyzed as the ratio of foreign (i.e. expressing the reporter gene that was not printed in that spot) to the total number of cells per spot, and it was calculated to be only 0.26% on average when HEK 293 cells were reversely transfected on the array for 2 days. This indicates that diffusion of the lipoplexes across the 60 μm superhydrophobic barriers to the neighboring spots is minimal and close-packing of the spots on the patterned substrates does not compromise the transfection results.

A major advantage of using cell microarrays versus well plates for cell screening is that the miniaturization reduces the amount of expensive chemicals needed. When comparing some typical amounts of pDNA and transfection reagent used for a single spot on the high-density patterned surfaces versus one well of a 96-well plate, we were able to reduce the amounts by 67-fold: 1.5 ng vs. 100 ng pDNA and 4 nl vs. 267 nl of transfection reagent.

8.3.4 Transparency of the polymer film

An additional advantage of the patterned substrates is the transparency of the thin nanoporous superhydrophilic polymer, which makes analysis by inverted microscopy possible. The globule size of the nanoporous structure of the polymer ranged from 100–500 nm (Geyer *et al.*, 2011), and when immersed in aqueous solutions the superhydrophilic spots are wetted, the scattering of visible light is reduced, and the transmittance of the polymer film is increased (Figure 2.S4). The superhydrophobic barriers prevented water from penetrating and did not become transparent, which helped to align the pattern when using the printing device and when using the automated high-throughput screening microscope. The dimensions of the array were designed such that a single superhydrophilic spot was maximized in the field of view when using a 20 \times objective on a high-throughput screening microscope to capture images for cell quantification.

8.4 The influence of various parameters on reverse cell transfection

For large-scale gene overexpression or knockdown studies, liposomal transfection reagents are frequently used and needed in large quantities. However, these are expensive and their efficacy is usually specific to experimental conditions such as the cell type and the nucleic acid to be transfected. There is a need for improved liposomal reagents that are highly efficient but not toxic. We used a novel liposomal transfection reagent called ScreenFect[®]A to optimize the method of reverse transfection on the superhydrophilic–superhydrophobic patterned substrates and to study the influence of various factors on transfection efficiency. In the future, libraries of biomimetic lipids recently developed by us and other groups will be screened to identify other efficient and non-toxic transfection reagents, and to ultimately understand the structure–function relationship for successful cell transfection.

8.4.1 Drying time of the printed arrays

We found that reverse transfection worked best when allowing the printed arrays sufficient time to dry at room temperature. It has been shown that residual moisture content can speed the degradation of dried lipoplexes through oxidation (Yu & Anchordoquy, 2009). When the printed arrays were dried for less than 24 h, we actually observed higher toxicity and transfected cells were spread outside of the designated printed areas. We dried the printed arrays for 2 days throughout the reverse transfection experiments. Sucrose has also been demonstrated to preserve lipoplexes in the dried state (Mannherz *et al.*, 2006) without loss of transfection efficiency after 1 week of storage (Delehanty *et al.*, 2004), which is why sucrose was added to our transfection mixtures.

It was reported that printed microarrays can be stored for up to 15 months (Erflle *et al.*, 2007). In our own experiments, we have tested arrays up to one month after printing transfection mixtures without any noticeable loss of transfection efficiency. This allows several arrays to be printed at once and the replicates of identical microarrays can be used at different time points without loss of reproducibility of the cell-based assays, allow the multiplexing of different assays on same set of arrays, or enable the testing of different cell types with the same set of arrays.

8.4.2 Cell incubation time

We cultured cells on the printed arrays for 24 or 48 h before assessing transfection, and more transfected cells were observed after 48 h. This could simply be due to the overall increase in cell number with time and more time for uptake of the lipoplexes from the polymer surface to the adhered cells. In addition, it has been shown that transfection

was enhanced in mitotic cells due to the increased chances of DNA to enter the nucleus during disassembly of the nuclear envelope, a significant barrier to transfection (Brunner *et al.*, 2000; Lechardeur & Lukacs, 2006; Ludtke *et al.*, 2002; Mortimer *et al.*, 1999; Tseng *et al.*, 1999). Starting with a lower cell density and allowing the cells to divide through multiple cell cycles to reach high confluence after 2 days could have contributed to the higher number of transfected cells after 48 h. In the future, it would be interesting to further study these effects by comparing the transfection efficiency of cells with different proliferation rates and cells at different stages of the cell cycle.

8.4.3 Cell seeding density

For transfection experiments, the initial cell seeding density was determined based on reaching high cell confluency after 2 days, but not overly confluent such that image analysis was difficult due to overlapping cells. Optimal seeding densities of 35,000 cells cm^{-2} for HEK 293 cells and 30,000 cells cm^{-2} for HeLa cells were consistently used to ensure a high cell density after 2 days of culture. Obtaining homogeneous cell coverage on the printed array was also very important to reduce variation between the replicates. We found that pipetting some media under the glass slide, pressing down firmly to prevent the cell suspension from going under the slide, and slowly flowing the cell suspension over the array resulted in even cell coverage (Figure 3.3).

8.4.4 Surface chemistry of the superhydrophilic spot

One parameter that we hypothesized might influence reverse transfection was the surface chemistry of the hydrophilic spot due to interaction of the charged lipoplexes and the functionalized polymer surface in substrate-mediated transfection. Initially, patterned surfaces with microspots functionalized with cysteamine (NH_2) were used for reverse cell transfection, but very low transfection efficiencies were observed when using ScreenFect[®]A (Figure 3.S2). However, when using microspots functionalized with 3-mercaptopropionic acid (COOH), we observed an increase in transfection efficiency for almost all of the transfection mixture combinations tested. Thus, COOH -modified surfaces were found to enhance reverse transfection compared to NH_2 -modified surfaces. This could be due to increased retention of the positively charged lipoplexes when the COOH groups on the surface become deprotonated and negatively charged, resulting in localization of the lipoplexes on the surface where the cells adhere and grow while still allowing cellular internalization.

Similarly, Pannier *et al.* showed that surface charge and hydrophilicity influenced immobilization of lipoplexes on the surface and consequently cell transfection (Pannier *et al.*, 2005). Lipoplexes formed from pDNA and Lipofectamine[®] 2000 were incubated for 2 h on self-assembled monolayers (SAMs) formed with different alkanethiols on gold, and transfection with NIH/3T3 cells were analyzed at 48 h by luciferase activity.

The highest level of transfection was measured on SAMs functionalized with 100% COOH groups and was 2.4-fold more than transfection on uncharged 100% OH-functionalized hydrophilic SAMs. The immobilization of lipoplexes was correspondingly 2-fold more on 100% COOH- versus 100% OH-modified SAMs. However, they showed that the release rate of the lipoplexes from the SAMs was not dependent on the surface chemistry, with most of total release of 70–85% of the lipoplexes occurring by 24 h. In the future, it would be interesting to study the release rate of the lipoplexes from the porous polymer surfaces to see if the lipoplexes are better retained by the charged porous surface versus a SAM.

In addition, Segura & Shea demonstrated that the immobilization and slow release of DNA complexes from a surface resulted in improved and sustained transfection compared to delivery of the DNA complexes to the media (Segura & Shea, 2002). Luo & Saltzman showed that just physically concentrating the lipoplexes near the cell surface of Chinese hamster ovarian cells increased transfection (Luo & Saltzman, 2000). The lipoplexes were complexed with dense silica nanoparticles to promote sedimentation on the surface of cells during liquid transfection. These studies further confirm that lipoplex–surface interactions and localization of the lipoplexes near the surface of cells are important for successful transfection.

It is also possible that there is more interaction of the DNA itself with the surface than originally suspected. Although it is commonly assumed that lipoplexes form a spherical complex with the DNA packed inside the lipid bilayer, this has proven to be an oversimplification. It has been demonstrated that lipoplexes actually take on different forms, such as multilayer structures in which DNA is intercalated between the lipid bilayers (Koynova, 2010; Rehman *et al.*, 2013; Ruozi *et al.*, 2003). This leaves the possibility for increased interaction of the pDNA with the functional groups on the surface.

Another possibility for the difference in transfection efficiency could be due to different cell–surface interactions on the NH₂- versus COOH-modified surfaces. We observed that when cultured on the bare surfaces without any transfection mixture, cells cultured on the NH₂-modified surfaces had a more spread cell morphology than cells on the COOH-modified surfaces that were more spindly. Although, these morphological differences were diminished when gelatin and fibronectin were printed on the surface, there could still be some effects from the underlying surface chemistry.

8.4.5 Inclusion of gelatin and fibronectin in the mixture

As part of our screening for the factors that influence reverse cell transfection, we found that the inclusion of gelatin as well as fibronectin could enhance the transfection efficiency up to 32× in HEK 293 cells. Very low levels of transfection occurred when

no gelatin or fibronectin was added to the printed mixtures (Figures 3.4 and 3.S3). This is similar to a report demonstrating that fibronectin enhanced the transfection efficiency by 40× in human mesenchymal stem cells (Yoshikawa *et al.*, 2004).

Molecules that promote cell adhesion, such as gelatin, fibronectin, and Matrigel, are often included in transfection mixtures when using glass substrates for cell microarrays (Erflle *et al.*, 2007; Rantala *et al.*, 2011; Stürzl *et al.*, 2008). These molecules are added to promote cell adhesion and growth only in the area of the printed spots since there is nothing to prevent the cells from migrating between the spots on a standard glass substrate. The inclusion of a matrix such as gelatin was also shown to help maintain the spot integrity of a printed transfection mixture after drying and to increase the transfection efficiency (Mannherz *et al.*, 2006).

Another role that cell adhesion molecules play in cell–surface interactions is to promote cell adhesion to the substrate by increased anchoring to the surface and delaying rear-retraction, which can slow cell migration or immobilize cells (Schmidt & Friedl, 2010). This can lead to cells that are more spread on the surface, which has also been shown to increase transfection (Blacklock *et al.*, 2010). We also observed this positive influence of spread cells increasing transfection especially when using the 3-mercaptopropionic acid (COOH) surfaces as microarrays. When no gelatin or fibronectin was printed on the COOH-modified superhydrophilic spots, the cells grew in circular patterns and were less spread, similar to their morphology on uncoated glass. Whereas cells cultured on the COOH-modified spots printed with gelatin/fibronectin grew in a homogeneous layer and also had a more spread morphology and larger and flatter nuclei. Increased endocytosis and uptake of the lipoplexes for cells that are more spread may be one reason why transfection is enhanced when cell spreading is induced. It would be interesting to further investigate the role of cell adhesion molecules and cell morphology in promoting efficient cell transfection. To distinguish the role of adhesion molecules as either a medium to immobilize and preserve lipoplexes on the surface or to promote cell spreading to enhance uptake of the lipoplexes during reverse transfection, we could use the method of thiol-yne click photopatterning to functionalize the hydrophilic spots with ECM-mimetic peptides instead of adding gelatin/fibronectin to the transfection mixture and compare the transfection efficiencies.

8.4.6 Ratio of pDNA to transfection reagent

In general, when the ratio of pDNA to ScreenFect[®]A was decreased, we quantified higher transfection efficiencies but this was offset by decreases in cell number, up to 47% less when compared with a blank spot. Decreasing the ratio of pDNA to transfection reagent for a given amount of pDNA means that the relative amount of transfection reagent is increased, and this could have caused some cytotoxicity as indicated by the more drastic reduction in cell number and the presence of some cells

with apoptotic bodies and condensed nuclei. These results indicate that the amount of transfection reagent relative to the pDNA is an important parameter for balancing high transfection efficiency and low cytotoxicity.

It has been shown in the literature that the ratio of nucleic acid to liposomal transfection reagent can influence the surface charge and size of the formed lipoplexes, which in turn affects cellular uptake, and is thus an important factor that determines transfection efficiency and toxicity (Bengali *et al.*, 2005; Li *et al.*, 2013b; Rehman *et al.*, 2013). The ratio of nucleic acid to transfection reagent can also affect the structure of the formed lipoplexes, which in turn can affect transfection efficiency as shown by the examples given in the Introduction regarding the screening of lipid libraries. Therefore, it would be informative to conduct further studies to determine the structure of the lipoplexes formed using ScreenFect[®]A at different ratios to pDNA, and then correlate this with the transfection efficiency.

8.4.7 Dilution buffer used during lipoplex formation

We did not find a significant difference in the reverse transfection results when different dilution buffers were used to dilute ScreenFect[®]A before lipoplex formation. Protonation of the amine head group of the lipid is an important factor for compacting the pDNA during lipoplex formation and promoting interaction with the cell surface, and it was previously demonstrated that lipoplexes with a positive zeta potential resulted in more efficient liquid phase transfection (Li *et al.*, 2012b). Therefore, an acidic buffer consisting of 50 mM NaOAc (pH 5) is usually used to dilute ScreenFect[®]A before complex formation with pDNA. Since amines are weak bases and their conjugate acids have pKa values around 10–11, they should be protonated with the pH 5 NaOAc buffers as well as Opti-MEM[®] pH 7.1–7.4 and RPMI pH 7.0–7.4. These results suggest that all of the buffers tested in the transfection mixture for lipoplex formation were suitable for reverse transfection.

8.4.8 Transfection efficiency

We achieved transfection efficiencies up to 26% when HEK 293 cells were cultured for 2 days on COOH-modified superhydrophilic spots printed with 2.1 ng of H2B-YFP-pDNA mixed with ScreenFect[®]A at a ratio of 0.375 $\mu\text{g } \mu\text{l}^{-1}$, 1.68 nmol of sucrose, 20 ng of gelatin, and 5 ng of fibronectin. At these conditions, low cell toxicity was also observed as indicated by a comparable number of cells per spot and no apparent differences in cell morphology compared to the controls. According to our results, ScreenFect[®]A was comparable in transfection efficiency with Lipofectamine[®] 2000, a commercially available and commonly used liposomal transfection reagent. The mean transfection efficiency was 27% when HEK 293 cells were cultured for 2 days on COOH-modified superhydrophilic spots printed with 1.5 ng of pCS2+-H2B-YFP

plasmid mixed with Lipofectamine[®] 2000 diluted in Opti-MEM[®] at a ratio of 0.429 $\mu\text{g } \mu\text{l}^{-1}$, 1.2 nmol of sucrose, 20 ng of gelatin, and 5 ng of fibronectin.

The transfection efficiencies obtained on the patterned surfaces were comparable to those found in the literature for transfected cell microarrays, ranging from 17–40% (Baghdoyan *et al.*, 2004; Cheng *et al.*, 2010; Delehanty *et al.*, 2004; Enomoto *et al.*, 2014; Fujita *et al.*, 2012; Pannier *et al.*, 2005). However, it is difficult to directly compare transfection efficiencies because often the exact concentration of the mixture on the surface was unknown or unreported due to inaccurate control over the volume printed and the resulting spot size, and there are also many variations of the substrate and coatings used. The method of quantifying transfection also varies. Many groups measure the activity of a luciferase reporter gene or use microarray scanners to quantify the fluorescence intensity to quantify transfection instead of directly counting the number of transfected cells. These results can be hard to compare since the fluorescence of the reporter gene usually varies from one cell to another. Also, many reports do not mention cell toxicity or variation in the number of cells for the different conditions tested.

The transfection efficiency can also depend on the plasmid used for transfection. In our case, using plasmids encoding for histone H2B versus cytoplasmic GFP as the reporter gene could result in a lower transfection efficiency compared to using a cytoplasmic reporter gene as the histone proteins have to be transported the cell nucleus, most likely through nuclear pore complexes (Mosammamarast *et al.*, 2001). We found that the amount of pDNA sufficient for efficient transfection was higher for the histone H2B nuclear reporter gene versus the cytoplasmic GFP reporter gene, approximately 2 ng/spot versus 1.5 ng/spot, respectively. We chose to use H2B as the reporter gene for quantification purposes since there was virtually no overlap of the fluorescence from neighboring cells and the cell count was more accurate when using the automated imaging software CellProfiler.

The transfection efficiency of pCS2+-GFP with ScreenFect[®] was reported to be 29% in HEK 293T cells when performing conventional liquid transfection experiments in 96-well plates (Li *et al.*, 2012b). This demonstrates that similar transfection efficiencies with ScreenFect[®] are achieved when using the method of reverse transfection compared to liquid transfection, thus the advantages of reagent and cost savings owing to the miniaturization of transfected cell microarrays make it a useful alternative for conducting screening experiments. Overall, the reverse transfection results demonstrate that the superhydrophilic–superhydrophobic patterned surfaces can be used to screen and identify efficient and non-toxic transfection reagents in a miniaturized and economical manner. In the future, we anticipate discovering other transfection reagents from the biomimetic lipid libraries synthesized in our group with the potential for successful transfection and then using this information to rationally

design lipids depending on the experimental conditions such as cell type and nuclei acid.

8.5 Culturing cells in arrays of microdroplets and hydrogels

Cell microarrays are generally limited to screening adherent cells in a 2D format, but there is also a need to perform screens with non-adherent cells, cells in 3D microenvironments, and small organisms. A potential disadvantage of 2D cell microarrays is that when the whole substrate is immersed in the same media, chemicals with fast diffusion rates or factors secreted by the cells can spread to the neighboring spots and exert an unwanted effect. We demonstrated that these limitations could be overcome by encapsulating cells and the chemical of interest within isolated droplets or hydrogels formed in each superhydrophilic spot, which are separated by the superhydrophobic barriers.

Currently, arrays of droplets or hydrogels are often formed by manually pipetting each drop, limiting the scale of spots that can be practically made at once, or require liquid dispensing robots that are not commonly available in all laboratories. We demonstrated that the superhydrophilic–superhydrophobic patterned surfaces could be used to create high-density arrays of thousands of spatially separated pico- to microliter-sized droplets, referred to as DropletMicroarrays, in one simple step (Figure 5.1) (Ueda *et al.*, 2012). We used the phenomenon of discontinuous dewetting (Butler *et al.*, 2001; Jackman *et al.*, 1998; Xia *et al.*, 2003; You *et al.*, 1997), which relies on the extreme wettability contrast between the superhydrophilic and superhydrophobic regions, to form a droplet in each superhydrophilic spot simply by moving an aqueous solution across the patterned surface. The volumes of the individually formed droplets depended on the size and geometry of the superhydrophilic spots as well as on the surface tension of the solution, and ranged between 700 pL to 3 μ L for the different conditions tested. We also demonstrated that there was low variability in the volume of the formed droplets for a given pattern size, which is important when comparing the readouts from one spot to another. The spontaneous formation of droplets on the patterned surface did not require manual pipetting or a liquid handling device, and could be used to print precious reagents or cells because thousands of spots can be filled without using a large volume of solution.

When a suspension of cells was moved across the patterned surface to form arrays of droplets encapsulating cells, no cells were present on the superhydrophobic barriers. We also demonstrated that the method of discontinuous dewetting on the patterned surfaces could be used to create arrays of crosslinked maleimide–polyvinyl alcohol hydrogels encapsulating cells (Figure 5.4b). Hydrogels were only formed within the superhydrophilic spots and immobilized the cells in these spots, and no cells were observed outside the hydrogel on the superhydrophobic barriers. The array of hydrogels can be fully immersed in cell culture medium or droplets of medium can be formed in

the superhydrophilic spots to isolate each hydrogel for further culturing. Using $500 \times 500 \mu\text{m}^2$ superhydrophilic spots, cells could be cultured for at least 18 h in individual droplets, or at least 6 days when cultured in hydrogels fully immersed in culture medium.

We also demonstrated that the superhydrophilic spots of a DropletMicroarray could be pre-filled with chemicals, and the diffusion of the chemicals was confined to the individual microdroplets and inter-spot mixing was prevented. We showed the concentration-dependent decrease in cell viability when human breast adenocarcinoma cells encapsulated in isolated MI-PVA hydrogels were exposed to increasing amounts of pre-printed doxorubicin, a chemotherapeutic drug known to induce apoptosis (Figure 5.5). This demonstrates that chemicals pre-printed on the patterned surface can diffuse into the hydrogels and exert their biological effect.

Although small pattern sizes allow high-density arrays to be achieved, the limitations of working with very small droplet volumes for culturing cells are preventing droplet evaporation and nutrient starvation. We found that storing the DropletMicroarrays in pre-humidified Petri dishes in a high humidity environment (~80% RH) greatly slowed or stopped the rate of evaporation. An important factor to consider when culturing cells in small volumes is the number of cells and the time that the cells are cultured in the droplets to avoid nutrient starvation, which can induce apoptosis or necrosis (Hwang & Lee, 2008; Mercille & Massie, 1994). One possible way to overcome this limitation could be to supplement the culture medium with additional nutrients to extend the time that cells can survive in the droplets (Han *et al.*, 2011). To also avoid toxicity due to accumulation of metabolic waste products, if the cells are adherent or are encapsulated in the hydrogels, the medium can be replaced by forming new drops of fresh culture medium in the superhydrophilic spots.

In recent experiments conducted in our group by Dr. Anna Popova, we found that cell viability, cell adherence to the surface, and the duration of culture could be improved by pre-coating cysteamine-modified superhydrophilic spots with gelatin before forming the array of cells in droplets. Adherent cells rely on adhesion promoting proteins, such as fibronectin, from the culture medium to adsorb to the surface to provide initial cell-binding sites, but it was shown in the literature that plasma proteins such as albumin adsorb much faster and in much higher amounts to surfaces (Tamada & Ikada, 1993). Therefore, for small droplet volumes it is possible that the adsorption of molecules that promote cell adhesion is too few, but this can be mediated by pre-incubation with cell adhesion molecules such as gelatin or fibronectin. Although the porous polymer surface is only $12.5 \mu\text{m}$ thin, it could act like a sponge and absorb most of the nutrients from the small droplet. Pre-incubating with gelatin could work to offset this sponge effect. To further study these effects, it would be interesting to functionalize the patterned surface with ECM-mimetic peptides using the thiol-yne click

photopatterning method (Figure 4.1G) before forming the droplets and observe if cell viability and adherence are improved. Additionally, different surface chemistries of the superhydrophilic spot should be tested since this could affect the rate and amount of nutrients absorbed from the medium.

The two-step procedure we used to form MI–PVA hydrogels encapsulating cells provides a relatively simple method for screening cells in 3D microenvironments (Figure 5.4). Culturing cells in 3D microenvironments, such as hydrogels, versus 2D cell culture gives the opportunity to study cells in an environment that more accurately resembles the *in vivo* situation (Jongpaiboonkit *et al.*, 2009; Tibbitt & Anseth, 2009). In addition, there are many ways that hydrogels can be tailored for various cell studies, such as the inclusion of cell adhesion molecules or drugs, as well as tuning of the physical properties such as stiffness and degradability (DeForest & Anseth, 2012). Even plasmids can be incorporated into the hydrogels for transfection in 3D (Lei *et al.*, 2009). High-throughput screening of cells in 3D systems is an important tool that can provide valuable information, but the methods are still being established.

In principle, the superhydrophilic–superhydrophobic patterned polymer substrates are compatible with other published methods for forming hydrogels, such as dispensing a hydrogel precursor solution that crosslinks upon UV irradiation (Jongpaiboonkit *et al.*, 2009; Nichol *et al.*, 2010) or forming alginate hydrogels by ionic crosslinking with the addition of calcium chloride (Salgado *et al.*, 2012). The DropletMicroarray can also be an alternative for growing suspension cells in microwells or in a hanging drop.

8.6 Methods to easily and cheaply produce multiple patterned substrates

To create a new patterned substrate, usually the entire experimental procedure must be repeated, which can be time-consuming and laborious. We presented a simple and fast method that allowed the transfer of superhydrophilic–superhydrophobic micropatterns in porous polymer films onto adhesive tape. We demonstrated that at least twelve copies could be made from 125 μm -thick patterned polymer films, and the hydrophobicity of the original surface was preserved up to the tenth copy. This was a very time- and cost-efficient way to create multiple copies of the micropatterns, which we then used as substrates for reverse cell transfection experiments.

One limitation of the method is that the feature size of the transferred micropattern depends on the quality of the tape. Since we used ordinary sticky tape (Tesa), as the number of copies increased the coverage of the transferred polymer on the tape became less homogeneous. We also found that chemicals that were printed and then dried in the hydrophilic spots did not transfer well to the subsequent copies. In spite of this, the method was practical for making multiple copies of patterned polymer surfaces down to a sub-millimeter pattern resolution, which can be sufficient for applications looking for an efficient way to create superhydrophilic–superhydrophobic patterns using cheap materials while still having good chemical stability. For example, another method for making cheap hydrophilic–hydrophobic patterns is the use of wax-based printing (Carrilho *et al.*, 2009; Lewis *et al.*, 2012; Vella *et al.*, 2012) or hydrophobic markers (Martinez *et al.*, 2008; Nie *et al.*, 2012) for paper-based microfluidic devices, which was first introduced by the group of Whitesides to provide affordable diagnostic devices to impoverished regions.

8.7 Outlook

Research involving superhydrophilic and superhydrophobic surfaces actively started only about a decade ago. During the last few years, a number of methods allowing for the fabrication of superhydrophilic–superhydrophobic patterned substrates were introduced, and the interest is now shifting towards the development of new applications that use the unique properties of such patterns.

Some of the advantages of such patterns are that: a) complex geometries and the positioning of liquid droplets can be easily controlled; b) micropatterns can be pre-filled with aqueous solutions; c) droplets can be positioned extremely close to each other on a surface without merging, which is useful for creating high-density arrays or for cell patterning applications; d) the existence of the Cassie–Baxter state in superhydrophobic regions creates “air-grid” patterns that can be used to control protein and cell adhesion as well as cell migration; and e) the discontinuous dewetting effect arising from the extreme difference in WCAs between the superhydrophilic and superhydrophobic regions allows passive dispensing of aqueous solutions into the superhydrophilic spots without wetting the superhydrophobic background, even for very small separation distances between the spots.

Since the adhesion of molecules and cells was surprisingly well controlled by superhydrophobic air-grid patterns, it is an interesting alternative to using physical barriers for applications such as cell patterning, cell screening using microarrays, performing bioassays, controlling the adhesion of biomolecules and cells in complex 2D or 3D architectures, tissue engineering, bioimplants, or creating high-throughput combinatorial chemical libraries. Air-grid patterning is a more general method for controlling protein and cell adhesion since interactions with the surface are minimized due to the superhydrophobic Cassie–Baxter state, which seems to be mostly independent of the protein structure or chemical composition.

A major part of this PhD work was to utilize the advantageous properties of superhydrophilic–superhydrophobic patterned surfaces to develop reverse cell transfection microarrays. Now that we have identified and tested how several important parameters influence reverse transfection, we can use the optimized conditions obtained with ScreenFect[®]A as a basis for screening the other lipids synthesized in our group. The aim would be to determine if the lipid structure correlates with high transfection efficiency and low toxicity, and if the function is specific to certain cell types or nucleic acids. A variety of cell types, as well as cells that are known to be difficult to transfect, should be tested. Since it has been shown that certain genes can enhance or suppress lipofection (Barker & Diamond, 2008), it would be interesting to screen these genes in combination with the lipid libraries.

Since we observed a significant increase in transfection efficiency when gelatin and fibronectin were added to the transfection mixtures, it would be worth further investigating the role of cell adhesion molecules and cell spreading in promoting transfection. This can be done by testing a variety of cell adhesion molecules in the mixture itself or functionalizing the patterned surface with ECM-mimetic peptides using the thiol-yne click chemistry patterning method. The transfection results could then be correlated with cell–surface interactions observed by microscopy.

Culturing cells in arrays of droplets or hydrogels opens up the possibilities of screening non-adherent cells and cells in 3D microenvironments. Although using the superhydrophilic–superhydrophobic patterned surfaces to easily create thousands of individual droplets in one simple step without requiring a liquid dispenser is convenient, the current challenges are preventing droplet evaporation and nutrient starvation in very small droplets for extended culture times. Another important issue to address is how to exchange the medium in the droplets to prevent toxicity from accumulation of metabolic waste.

Some initial results revealed that pre-coating the hydrophilic spot with gelatin increased cell viability and adhesion. To further study this effect, it would be interesting to culture cells in droplets on spots functionalized with ECM-mimetic peptides, rather than pre-coating the surface with gelatin, and observe if cell viability and adherence are still improved. Additionally, different surface chemistries of the superhydrophilic spot should be tested since this could affect the rate and amount of nutrients absorbed from the medium.

In addition to demonstrating the cell-repellent properties of superhydrophobic surfaces, we showed that hydrophobic liquid surfaces also possess excellent and long-term cell-repellent properties. The concept of hydrophobic liquid-infused porous surfaces for anti-biofouling applications was recently introduced in 2011–2012, but the mechanism of cell-repellency has not been confirmed and should be explored in detail. This information could lead to the better design of non-fouling surfaces.

References

- Akinc, A., Zumbuehl, A., Goldberg, M., Leshchiner, E. S., Busini, V., Hossain, N., Bacallado, S. A., Nguyen, D. N., Fuller, J. & other authors. (2008).** A combinatorial library of lipid-like materials for delivery of RNAi therapeutics. *Nat Biotechnol* **26**, 561–9.
- Arima, Y. & Iwata, H. (2007).** Effect of wettability and surface functional groups on protein adsorption and cell adhesion using well-defined mixed self-assembled monolayers. *Biomaterials* **28**, 3074–82.
- Auad, P., Ueda, E. & Levkin, P. A. (2013).** Facile and multiple replication of superhydrophilic-superhydrophobic patterns using adhesive tape. *ACS Appl Mater Interfaces* **5**, 8053–7.
- Baghdoyan, S., Roupioz, Y., Pitaval, A., Castel, D., Khomyakova, E., Papine, A., Soussaline, F. & Gidrol, X. (2004).** Quantitative analysis of highly parallel transfection in cell microarrays. *Nucleic Acids Res* **32**, e77–e77.
- Bailey, S. N., Sabatini, D. M. & Stockwell, B. R. (2004).** Microarrays of small molecules embedded in biodegradable polymers for use in mammalian cell-based screens. *PNAS* **101**, 16144–9.
- Balazs, D. A. & Godbey, W. (2011).** Liposomes for use in gene delivery. *J Drug Deliv.* DOI: 10.1155/2011/326497.
- Ballester-Beltrán, J., Rico, P., Moratal, D., Song, W., Mano, J. F. & Salmerón-Sánchez, M. (2011).** Role of superhydrophobicity in the biological activity of fibronectin at the cell–material interface. *Soft Matter* **7**, 10803–11.
- Barbulovic-Nad, I., Lucente, M., Sun, Y., Zhang, M., Wheeler, A. R. & Bussmann, M. (2006).** Bio-microarray fabrication techniques--a review. *Crit Rev Biotechnol* **26**, 237–59.
- Barbulovic-Nad, I., Au, S. H. & Wheeler, A. R. (2010).** A microfluidic platform for complete mammalian cell culture. *Lab Chip* **10**, 1536–42.
- Barker, G. A. & Diamond, S. L. (2008).** RNA interference screen to identify pathways that enhance or reduce nonviral gene transfer during lipofection. *Mol Ther* **16**, 1602–8.
- Barthlott, W. & Neinhuis, C. (1997).** Purity of the sacred lotus, or escape from contamination in biological surfaces. *Planta* **202**, 1–8.

-
- Baugh, L. & Vogel, V. (2004).** Structural changes of fibronectin adsorbed to model surfaces probed by fluorescence resonance energy transfer. *J Biomed Mater Res A* **69**, 525–34.
- Bengali, Z., Pannier, A. K., Segura, T., Anderson, B. C., Jang, J.-H., Mustoe, T. A. & Shea, L. D. (2005).** Gene delivery through cell culture substrate adsorbed DNA complexes. *Biotechnol Bioeng* **90**, 290–302.
- Bhairamadgi, N. S., Gangarapu, S., Caipa Campos, M. A., Paulusse, J. M. J., van Rijn, C. J. M. & Zuilhof, H. (2013).** Efficient functionalization of oxide-free silicon(111) surfaces: thiol-yne versus thiol-ene click chemistry. *Langmuir* **29**, 4535–42.
- Blacklock, J., Vetter, A., Lankenau, A., Oupický, D. & Möhwald, H. (2010).** Tuning the mechanical properties of bio-reducible multilayer films for improved cell adhesion and transfection activity. *Biomaterials* **31**, 7167–74.
- Boutros, M. & Ahringer, J. (2008).** The art and design of genetic screens: RNA interference. *Nat Rev Genet* **9**, 554–66.
- Brafman, D. A., Chien, S. & Willert, K. (2012).** Arrayed cellular microenvironments for identifying culture and differentiation conditions for stem, primary and rare cell populations. *Nat Protoc* **7**, 703–17.
- Brunner, S., Sauer, T., Carotta, S., Cotten, M., Saltik, M. & Wagner, E. (2000).** Cell cycle dependence of gene transfer by lipoplex, polyplex and recombinant adenovirus. *Gene Ther* **7**, 401–7.
- Burchak, O. N., Mughlerli, L., Ostuni, M., Lacapère, J. J. & Balakirev, M. Y. (2011).** Combinatorial discovery of fluorescent pharmacophores by multicomponent reactions in droplet arrays. *JACS* **133**, 10058–61.
- Butler, J. H., Cronin, M., Anderson, K. M., Biddison, G. M., Chatelain, F., Cummer, M., Davi, D. J., Fisher, L., Frauendorf, A. W. & other authors. (2001).** In situ synthesis of oligonucleotide arrays by using surface tension. *JACS* **123**, 8887–94.
- Callies, M. & Quéré, D. (2005).** On water repellency. *Soft Matter* **1**, 55–61.
- Cao, L., Jones, A. K., Sikka, V. K., Wu, J. & Gao, D. (2009).** Anti-icing superhydrophobic coatings. *Langmuir* **25**, 12444–8.
- Carrilho, E., Martinez, A. W. & Whitesides, G. M. (2009).** Understanding wax printing: a simple micropatterning process for paper-based microfluidics. *Anal Chem* **81**, 7091–5.

- Cassie, A. B. D. & Baxter, S. (1944).** Wettability of porous surfaces. *Trans Faraday Soc* **40**, 546–51.
- Chen, L., Yang, G. & Wang, S. (2012).** Air-grid surface patterning provided by superhydrophobic surfaces. *Small* **8**, 962–5.
- Cheng, X., Guerasimova, A., Manke, T., Rosenstiel, P., Haas, S., Warnatz, H.-J., Querfurth, R., Nietfeld, W., Vanhecke, D. & other authors. (2010).** Screening of human gene promoter activities using transfected-cell arrays. *Gene* **450**, 48–54.
- Cramer, N. B., Reddy, S. K., Cole, M., Hoyle, C. & Bowman, C. N. (2004).** Initiation and kinetics of thiol-ene photopolymerizations without photoinitiators. *J Polym Sci Part A Polym Chem* **42**, 5817–26.
- Crick, C. R. & Parkin, I. P. (2010).** Preparation and characterisation of superhydrophobic surfaces. *Chemistry (Easton)* **16**, 3568–88.
- Deegan, R. D., Bakajin, O., Dupont, T. F., Huber, G., Nagel, S. R. & Witten, T. A. (1997).** Capillary flow as the cause of ring stains from dried liquid drops. *Nature* **389**, 827–9.
- DeForest, C. A. & Anseth, K. S. (2012).** Advances in bioactive hydrogels to probe and direct cell fate. *Annu Rev Chem Biomol Eng* **3**, 421–44.
- Delehanty, J. B., Shaffer, K. M. & Lin, B. (2004).** A comparison of microscope slide substrates for use in transfected cell microarrays. *Biosens Bioelectron* **20**, 773–9.
- Deng, X., Mammen, L., Zhao, Y., Lellig, P., Müllen, K., Li, C., Butt, H.-J. & Vollmer, D. (2011).** Transparent, thermally stable and mechanically robust superhydrophobic surfaces made from porous silica capsules. *Adv Mater* **23**, 2962–5.
- Dorrer, C. & Rühle, J. (2008a).** Wetting of silicon nanograss: from superhydrophilic to superhydrophobic surfaces. *Adv Mater* **20**, 159–63.
- Dorrer, C. & Rühle, J. (2008b).** Mimicking the stenocara beetle--dewetting of drops from a patterned superhydrophobic surface. *Langmuir* **24**, 6154–8.
- Du, X., Li, J., Li, L. & Levkin, P. A. (2013).** Porous poly(2-octyl cyanoacrylate): a facile one-step preparation of superhydrophobic coatings on different substrates. *J Mater Chem* **1**, 1026–29.
- Echeverri, C. J. & Perrimon, N. (2006).** High-throughput RNAi screening in cultured cells: a user's guide. *Nat Rev Genet* **7**, 373–84.
- Efremov, A. (2014, June 26).** *Fabrication and application of hydrophilic-hydrophobic micropatterned polymer surfaces*. University of Heidelberg.

-
- Efremov, A. N., Stanganello, E., Welle, A., Scholpp, S. & Levkin, P. A. (2012).** Micropatterned superhydrophobic structures for the simultaneous culture of multiple cell types and the study of cell–cell communication. *Biomaterials* **34**, 1757–63.
- Enomoto, J., Takagi, R., Onuki-Nagasaki, R., Fujita, S. & Fukuda, J. (2014).** Reverse transfection in microchamber arrays for cell migration assays. *Sensors Actuators B Chem* **190**, 896–9.
- Epstein, A. K., Wong, T.-S., Belisle, R. A., Boggs, E. M. & Aizenberg, J. (2012).** Liquid-infused structured surfaces with exceptional anti-biofouling performance. *PNAS* **109**, 13182–7.
- Erfle, H., Neumann, B., Liebel, U., Rogers, P., Held, M., Walter, T., Ellenberg, J. & Pepperkok, R. (2007).** Reverse transfection on cell arrays for high content screening microscopy. *Nat Protoc* **2**, 392–9.
- Erfle, H., Neumann, B., Rogers, P., Bulkescher, J., Ellenberg, J. & Pepperkok, R. (2008).** Work flow for multiplexing siRNA assays by solid-phase reverse transfection in multiwell plates. *J Biomol Screen* **13**, 575–80.
- Fairbanks, B. D., Scott, T. F., Kloxin, C. J., Anseth, K. S. & Bowman, C. N. (2009).** Thiol-yne photopolymerizations: novel mechanism, kinetics, and step-growth formation of highly cross-linked networks. *Macromolecules* **42**, 211–7.
- Feldman, K., Hähner, G., Spencer, N. D., Harder, P. & Grunze, M. (1999).** Probing resistance to protein adsorption of oligo(ethylene glycol)-terminated self-assembled monolayers by scanning force microscopy. *JACS* **121**, 10134–41.
- Feng, W., Li, L., Ueda, E., Li, J., Heißler, S., Welle, A., Trapp, O. & Levkin, P. A. (2014).** Surface patterning via thiol-yne click chemistry: an extremely fast and versatile approach to superhydrophilic-superhydrophobic micropatterns. *Adv Mater Interfaces*. DOI: 10.1002/admi.201400269.
- Feng, X., Zhai, J. & Jiang, L. (2005).** The fabrication and switchable superhydrophobicity of TiO₂ nanorod films. *Angew Chemie Int Ed* **44**, 5115–8.
- Fernandes, T. G., Kwon, S., Bale, S. S., Lee, M., Diogo, M. M., Clark, D. S., Cabral, J. M. S. & Dordick, J. S. (2010).** Three-dimensional cell culture microarray for high-throughput studies of stem cell fate. *Biotechnol Bioeng* **106**, 106–18.
- Flaim, C. J., Chien, S. & Bhatia, S. N. (2005).** An extracellular matrix microarray for probing cellular differentiation. *Nat Methods* **2**, 119–25.

- Fujita, S., Onuki-Nagasaki, R., Fukuda, J., Enomoto, J., Yamaguchi, S. & Miyake, M. (2012).** Development of super-dense transfected-cell microarrays generated by piezoelectric inkjet printing. *Lab Chip* **13**, 77–80.
- Fukuda, J., Khademhosseini, A., Yeh, J., Eng, G., Cheng, J., Farokhzad, O. C. & Langer, R. (2006).** Micropatterned cell co-cultures using layer-by-layer deposition of extracellular matrix components. *Biomaterials* **27**, 1479–86.
- Galopin, E., Piret, G., Szunerits, S., Lequette, Y., Faille, C. & Boukherroub, R. (2010).** Selective adhesion of *Bacillus cereus* spores on heterogeneously wetted silicon nanowires. *Langmuir* **26**, 3479–84.
- Ganesh, V. A., Raut, H. K., Nair, A. S. & Ramakrishna, S. (2011).** A review on self-cleaning coatings. *J Mater Chem* **21**, 16304–22.
- Gao, X. & Jiang, L. (2004).** Biophysics: water-repellent legs of water striders. *Nature*. DOI: 10.1038/432036a.
- Garrod, R. P., Harris, L. G., Schofield, W. C. E., McGettrick, J., Ward, L. J., Teare, D. O. H. & Badyal, J. P. S. (2007).** Mimicking a *Stenocara* beetle's back for microcondensation using plasmachemical patterned superhydrophobic-superhydrophilic surfaces. *Langmuir* **23**, 689–93.
- Geyer, F. L., Ueda, E., Liebel, U., Grau, N. & Levkin, P. A. (2011).** Superhydrophobic-superhydrophilic micropatterning: towards genome-on-a-chip cell microarrays. *Angew Chem, Int Ed* **50**, 8424–7.
- Guerrouache, M., Mahouche-Chergui, S., Chehimi, M. M. & Carbonnier, B. (2012).** Site-specific immobilisation of gold nanoparticles on a porous monolith surface by using a thiol-yne click photopatterning approach. *Chem Commun* **48**, 7486–8.
- Guo, Z., Liu, W. & Su, B.-L. (2011).** Superhydrophobic surfaces: from natural to biomimetic to functional. *J Colloid Interface Sci* **353**, 335–55.
- Hamlett, C. a E., Shirtcliffe, N. J., Pyatt, F. B., Newton, M. I., McHale, G. & Koch, K. (2011).** Passive water control at the surface of a superhydrophobic lichen. *Planta* **234**, 1267–74.
- Han, Y., Levkin, P., Abarientos, I., Liu, H., Svec, F. & Fréchet, J. M. J. (2010).** Monolithic superhydrophobic polymer layer with photopatterned virtual channel for the separation of peptides using two-dimensional thin layer chromatography-desorption electrospray ionization mass spectrometry. *Anal Chem* **82**, 2520–8.
- Han, Y. K., Ha, T. K., Lee, S. J., Lee, J. S. & Lee, G. M. (2011).** Autophagy and apoptosis of recombinant Chinese hamster ovary cells during fed-batch culture: effect of nutrient supplementation. *Biotechnol Bioeng* **108**, 2182–92.

-
- Hancock, M. J., He, J., Mano, J. F. & Khademhosseini, A. (2011a).** Surface-tension-driven gradient generation in a fluid stripe for bench-top and microwell applications. *Small* **7**, 892–901.
- Hancock, M. J., Piraino, F., Camci-Unal, G., Rasponi, M. & Khademhosseini, A. (2011b).** Anisotropic material synthesis by capillary flow in a fluid stripe. *Biomaterials* **32**, 6493–504.
- Hancock, M. J., Yanagawa, F., Jang, Y., He, J., Kachouie, N. N., Kaji, H. & Khademhosseini, A. (2012a).** Designer hydrophilic regions regulate droplet shape for controlled surface patterning and 3D microgel synthesis. *Small* **8**, 393–403.
- Hancock, M. J., Sekeroglu, K. & Demirel, M. C. (2012b).** Bioinspired directional surfaces for adhesion, wetting, and transport. *Adv Funct Mater* **22**, 2223–34.
- Hasenbank, M. S., Edwards, T., Fu, E., Garzon, R., Kosar, T. F., Look, M., Mashadi-Hosseini, A. & Yager, P. (2008).** Demonstration of multi-analyte patterning using piezoelectric inkjet printing of multiple layers. *Anal Chim Acta* **611**, 80–8.
- Hensarling, R. M., Doughty, V. A., Chan, J. W. & Patton, D. L. (2009).** “Clicking” polymer brushes with thiol-yne chemistry: indoors and out. *JACS* **131**, 14673–5.
- Hoekstra, D., Rejman, J., Wasungu, L., Shi, F. & Zuhorn, I. (2007).** Gene delivery by cationic lipids: in and out of an endosome. *Biochem Soc Trans* **35**, 68–71.
- Hoheisel, J. D. (2006).** Microarray technology: beyond transcript profiling and genotype analysis. *Nat Rev Genet* **7**, 200–10.
- Hoogenboom, R. (2010).** Thiol-yne chemistry: a powerful tool for creating highly functional materials. *Angew Chemie, Int Ed* **49**, 3415–7.
- Hook, A. L., Voelcker, N. H. & Thissen, H. (2009a).** Patterned and switchable surfaces for biomolecular manipulation. *Acta Biomater* **5**, 2350–70.
- Hook, A. L., Thissen, H. & Voelcker, N. H. (2006).** Surface manipulation of biomolecules for cell microarray applications. *Trends Biotechnol* **24**, 471–7.
- Hook, A. L., Thissen, H. & Voelcker, N. H. (2009b).** Advanced substrate fabrication for cell microarrays. *Biomacromolecules* **10**, 573–9.
- Hu, Y.-H., Warnatz, H.-J., Vanhecke, D., Wagner, F., Fiebitz, A., Thamm, S., Kahlem, P., Lehrach, H., Yaspo, M.-L. & Janitz, M. (2006).** Cell array-based intracellular localization screening reveals novel functional features of human chromosome 21 proteins. *BMC Genomics*. DOI: 10.1186/1471-2164-7-155.

- Huebner, A., Bratton, D., Whyte, G., Yang, M., Demello, A. J., Abell, C. & Hollfelder, F. (2009).** Static microdroplet arrays: a microfluidic device for droplet trapping, incubation and release for enzymatic and cell-based assays. *Lab Chip* **9**, 692–8.
- Hwang, S. O. & Lee, G. M. (2008).** Nutrient deprivation induces autophagy as well as apoptosis in Chinese hamster ovary cell culture. *Biotechnol Bioeng* **99**, 678–85.
- Ishii, D., Yabu, H. & Shimomura, M. (2009).** Novel biomimetic surface based on a self-organized metal–polymer hybrid structure. *Chem Mater* **21**, 1799–1801.
- Ishizaki, T., Saito, N. & Takai, O. (2010).** Correlation of cell adhesive behaviors on superhydrophobic, superhydrophilic, and micropatterned superhydrophobic/superhydrophilic surfaces to their surface chemistry. *Langmuir* **26**, 8147–54.
- Jackman, R. J., Duffy, D. C., Ostuni, E., Willmore, N. D. & Whitesides, G. M. (1998).** Fabricating large arrays of microwells with arbitrary dimensions and filling them using discontinuous dewetting. *Anal Chem* **70**, 2280–7.
- Jeon, S. I., Lee, J. H., Andrade, J. D. & De Gennes, P. G. (1991).** Protein–surface interactions in the presence of polyethylene oxide. *J Colloid Interface Sci* **142**, 149–158.
- Jiang, S. & Cao, Z. (2010).** Ultralow-fouling, functionalizable, and hydrolyzable zwitterionic materials and their derivatives for biological applications. *Adv Mater* **22**, 920–32.
- Jin, H., Tian, X., Ikkala, O. & Ras, R. H. A. (2013).** Preservation of superhydrophobic and superoleophobic properties upon wear damage. *ACS Appl Mater Interfaces* **5**, 485–8.
- Jokinen, V., Sainiemi, L. & Franssila, S. (2008).** Complex droplets on chemically modified silicon nanograss. *Adv Mater* **20**, 3453–6.
- Jokinen, V., Kostianen, R. & Sikanen, T. (2012).** Multiphase designer droplets for liquid-liquid extraction. *Adv Mater* **24**, 6240–3.
- Jongpaiboonkit, L., King, W. J. & Murphy, W. L. (2009).** Screening for 3D environments that support human mesenchymal stem cell viability using hydrogel arrays. *Tissue Eng, Part A* **15**, 343–53.
- Kang, S. M., You, I., Cho, W. K., Shon, H. K., Lee, T. G., Choi, I. S., Karp, J. M. & Lee, H. (2010).** One-step modification of superhydrophobic surfaces by a mussel-inspired polymer coating. *Angew Chem, Int Ed* **49**, 9401–4.

-
- Kassner, P. D. (2008).** Discovery of novel targets with high throughput RNA interference screening. *Comb Chem High Throughput Screen* **11**, 175–84.
- Kato, S. & Sato, A. (2012).** Micro/nanotextured polymer coatings fabricated by UV curing-induced phase separation: creation of superhydrophobic surfaces. *J Mater Chem* **22**, 8613–21.
- Khademhosseini, A., Suh, K. Y., Yang, J. M., Eng, G., Yeh, J., Levenberg, S. & Langer, R. (2004).** Layer-by-layer deposition of hyaluronic acid and poly-L-lysine for patterned cell co-cultures. *Biomaterials* **25**, 3583–92.
- Kim, P., Wong, T.-S., Alvarenga, J., Kreder, M. J., Adorno-Martinez, W. E. & Aizenberg, J. (2012).** Liquid-infused nanostructured surfaces with extreme anti-ice and anti-frost performance. *ACS Nano* **6**, 6569–77.
- Kobaku, S. P. R., Kota, A. K., Lee, D. H., Mabry, J. M. & Tuteja, A. (2012).** Patterned superomniphobic-superomniphilic surfaces: templates for site-selective self-assembly. *Angew Chemie, Int Ed* **51**, 10109–13.
- Koch, K. & Barthlott, W. (2009).** Superhydrophobic and superhydrophilic plant surfaces: an inspiration for biomimetic materials. *Philos Trans R Soc* **367**, 1487–509.
- Koch, P., Opitz, T., Steinbeck, J. A., Ladewig, J. & Brüstle, O. (2009).** A rosette-type, self-renewing human ES cell-derived neural stem cell with potential for in vitro instruction and synaptic integration. *PNAS* **106**, 3225–30.
- Koishi, T., Yasuoka, K., Fujikawa, S., Ebisuzaki, T. & Zeng, X. C. (2009).** Coexistence and transition between Cassie and Wenzel state on pillared hydrophobic surface. *PNAS* **106**, 8435–40.
- Kota, A. K., Li, Y., Mabry, J. M. & Tuteja, A. (2012).** Hierarchically structured superoleophobic surfaces with ultralow contact angle hysteresis. *Adv Mater* **24**, 5838–43.
- Koynova, R. (2010).** Analysis of lipoplex structure and lipid phase changes. *Methods Mol Biol* **606**, 399–423.
- Krausz, E. (2007).** High-content siRNA screening. *Mol BioSyst* **3**, 232–40.
- Krumpfer, J. W. & McCarthy, T. J. (2011).** Dip-coating crystallization on a superhydrophobic surface: a million mounted crystals in a 1 cm² array. *JACS* **133**, 5764–6.
- Kuang, J. & Messersmith, P. B. (2012).** Universal surface-initiated polymerization of antifouling zwitterionic brushes using a mussel-mimetic peptide initiator. *Langmuir* **28**, 7258–66.

- Kwak, G., Lee, M. & Yong, K. (2010).** Chemically modified superhydrophobic WO(x) nanowire arrays and UV photopatterning. *Langmuir* **26**, 9964–7.
- Lafuma, A. & Quéré, D. (2003).** Superhydrophobic states. *Nat Mater* **2**, 457–60.
- Lai, Y., Lin, C., Wang, H., Huang, J., Zhuang, H. & Sun, L. (2008).** Superhydrophilic–superhydrophobic micropattern on TiO₂ nanotube films by photocatalytic lithography. *Electrochem Commun* **10**, 387–91.
- Lai, Y., Huang, J., Gong, J., Huang, Y., Wang, C., Chen, Z. & Lin, C. (2009).** Superhydrophilic–superhydrophobic template: a simple approach to micro- and nanostructure patterning of TiO₂ films. *J Electrochem Soc* **156**, D480–4.
- Lai, Y., Pan, F., Xu, C., Fuchs, H. & Chi, L. (2013).** In situ surface-modification-induced superhydrophobic patterns with reversible wettability and adhesion. *Adv Mater* **25**, 1682–6.
- Lechardeur, D. & Lukacs, G. L. (2006).** Nucleocytoplasmic transport of plasmid DNA: a perilous journey from the cytoplasm to the nucleus. *Hum Gene Ther* **17**, 882–9.
- Lee, A., Moon, M.-W., Lim, H., Kim, W.-D. & Kim, H.-Y. (2012a).** Water harvest via dewing. *Langmuir* **28**, 10183–91.
- Lee, M.-Y., Kumar, R. A., Sukumaran, S. M., Hogg, M. G., Clark, D. S. & Dordick, J. S. (2008).** Three-dimensional cellular microarray for high-throughput toxicology assays. *PNAS* **105**, 59–63.
- Lee, Y. Y., Narayanan, K., Gao, S. J. & Ying, J. Y. (2012b).** Elucidating drug resistance properties in scarce cancer stem cells using droplet microarray. *Nano Today* **7**, 29–34.
- Lei, P., Padmashali, R. M. & Andreadis, S. T. (2009).** Cell-controlled and spatially arrayed gene delivery from fibrin hydrogels. *Biomaterials* **30**, 3790–9.
- Levkin, P. A., Svec, F. & Fréchet, J. M. J. (2009).** Porous polymer coatings: a versatile approach to superhydrophobic surfaces. *Adv Funct Mater* **19**, 1993–8.
- Lewis, G. G., Ditucci, M. J., Baker, M. S. & Phillips, S. T. (2012).** High throughput method for prototyping three-dimensional, paper-based microfluidic devices. *Lab Chip* **12**, 2630–3.
- Li, J., Kleintschek, T., Rieder, A., Cheng, Y., Baumbach, T., Obst, U., Schwartz, T. & Levkin, P. A. (2013a).** Hydrophobic liquid-infused porous polymer surfaces for antibacterial applications. *ACS Appl Mater Interfaces* **5**, 6704–11.

-
- Li, J. S., Ueda, E., Nallapaneni, A., Li, L. X. & Levkin, P. A. (2012a).** Printable superhydrophilic-superhydrophobic micropatterns based on supported lipid layers. *Langmuir* **28**, 8286–91.
- Li, L., Zahner, D., Su, Y., Gruen, C., Davidson, G. & Levkin, P. A. (2012b).** A biomimetic lipid library for gene delivery through thiol-yne click chemistry. *Biomaterials* **33**, 8160–6.
- Li, L., Wang, F., Wu, Y., Davidson, G. & Levkin, P. A. (2013b).** Combinatorial synthesis and high-throughput screening of alkyl amines for nonviral gene delivery. *Bioconjug Chem* **24**, 1543–51.
- Li, X.-M., Reinhoudt, D. & Crego-Calama, M. (2007).** What do we need for a superhydrophobic surface? A review on the recent progress in the preparation of superhydrophobic surfaces. *Chem Soc Rev* **36**, 1350–68.
- Lindquist, R. A., Ottina, K. A., Wheeler, D. B., Hsu, P. P., Thoreen, C. C., Guertin, D. A., Ali, S. M., Sengupta, S., Shaul, Y. D. & other authors. (2011).** Genome-scale RNAi on living-cell microarrays identifies novel regulators of drosophila melanogaster TORC1–S6K pathway signaling. *Genome Res* **21**, 433–46.
- Lindström, S. & Andersson-Svahn, H. (2010).** Overview of single-cell analyses: microdevices and applications. *Lab Chip* **10**, 3363–72.
- Liu, K. & Jiang, L. (2012).** Bio-inspired self-cleaning surfaces. *Annu Rev Mater Res* **42**, 231–63.
- Liu, X., Wang, Q., Qin, J. & Lin, B. (2009).** A facile “liquid-molding” method to fabricate PDMS microdevices with 3-dimensional channel topography. *Lab Chip* **9**, 1200–5.
- Lourenço, B. N., Marchioli, G., Song, W., Reis, R. L., van Blitterswijk, C. A., Karperien, M., van Apeldoorn, A. & Mano, J. F. (2012).** Wettability influences cell behavior on superhydrophobic surfaces with different topographies. *Biointerphases* **7**, 1–11.
- Ludtke, J. J., Sebestyén, M. G. & Wolff, J. A. (2002).** The effect of cell division on the cellular dynamics of microinjected DNA and dextran. *Mol Ther* **5**, 579–88.
- Luo, D. & Saltzman, W. M. (2000).** Enhancement of transfection by physical concentration of DNA at the cell surface. *Nat Biotechnol* **18**, 893–5.
- Ma, H., Hyun, J., Stiller, P. & Chilkoti, A. (2004).** “Non-fouling” oligo(ethylene glycol)- functionalized polymer brushes synthesized by surface-initiated atom transfer radical polymerization. *Adv Mater* **16**, 338–41.

- Ma, H., Li, D., Sheng, X., Zhao, B. & Chilkoti, A. (2006).** Protein-resistant polymer coatings on silicon oxide by surface-initiated atom transfer radical polymerization. *Langmuir* **22**, 3751–6.
- Ma, M. & Hill, R. M. (2006).** Superhydrophobic surfaces. *Curr Opin Colloid Interface Sci* **11**, 193–202.
- MacKeigan, J. P., Murphy, L. O. & Blenis, J. (2005).** Sensitized RNAi screen of human kinases and phosphatases identifies new regulators of apoptosis and chemoresistance. *Nat Cell Biol* **7**, 591–600.
- Mahon, K. P., Love, K. T., Whitehead, K. A., Qin, J., Akinc, A., Leshchiner, E., Leshchiner, I., Langer, R. & Anderson, D. G. (2010).** Combinatorial approach to determine functional group effects on lipidoid-mediated siRNA delivery. *Bioconjug Chem* **21**, 1448–54.
- Manna, U., Broderick, A. H. & Lynn, D. M. (2012).** Chemical patterning and physical refinement of reactive superhydrophobic surfaces. *Adv Mater* **24**, 4291–5.
- Mannherz, O., Mertens, D., Hahn, M. & Lichter, P. (2006).** Functional screening for proapoptotic genes by reverse transfection cell array technology. *Genomics* **87**, 665–72.
- Martinez, A. W., Phillips, S. T., Wiley, B. J., Gupta, M. & Whitesides, G. M. (2008).** FLASH: a rapid method for prototyping paper-based microfluidic devices. *Lab Chip* **8**, 2146–50.
- Mercille, S. & Massie, B. (1994).** Induction of apoptosis in nutrient-deprived cultures of hybridoma and myeloma cells. *Biotechnol Bioeng* **44**, 1140–54.
- Mertaniemi, H., Jokinen, V., Sainiemi, L., Franssila, S., Marmur, A., Ikkala, O. & Ras, R. H. A. (2011).** Superhydrophobic tracks for low-friction, guided transport of water droplets. *Adv Mater* **23**, 2911–4.
- Moffat, J. & Sabatini, D. M. (2006).** Building mammalian signalling pathways with RNAi screens. *Nat Rev Mol Cell Biol* **7**, 177–87.
- Mohr, S., Bakal, C. & Perrimon, N. (2010).** Genomic screening with RNAi: results and challenges. *Annu Rev Biochem* **79**, 37–64.
- Mortimer, I., Tam, P., MacLachlan, I., Graham, R. W., Saravolac, E. G. & Joshi, P. B. (1999).** Cationic lipid-mediated transfection of cells in culture requires mitotic activity. *Gene Ther* **6**, 403–11.
- Mosammaparast, N., Jackson, K. R., Guo, Y., Brame, C. J., Shabanowitz, J., Hunt, D. F. & Pemberton, L. F. (2001).** Nuclear import of histone H2A and H2B is mediated by a network of karyopherins. *J Cell Biol* **153**, 251–62.

-
- Mousses, S., Caplen, N. J., Cornelison, R., Weaver, D., Basik, M., Hautaniemi, S., Elkahloun, A. G., Lotufo, R. A., Choudary, A. & other authors. (2003).** RNAi microarray analysis in cultured mammalian cells. *Genome Res* **13**, 2341–7.
- Mrksich, M., Chen, C. S., Xia, Y., Dike, L. E., Ingber, D. E. & Whitesides, G. M. (1996).** Controlling cell attachment on contoured surfaces with self-assembled monolayers of alkanethiolates on gold. *PNAS* **93**, 10775–8.
- Mugherli, L., Burchak, O. N., Balakireva, L. A., Thomas, A., Chatelain, F. & Balakirev, M. Y. (2009).** In situ assembly and screening of enzyme inhibitors with surface-tension microarrays. *Angew Chem, Int Ed* **48**, 7639–44.
- Mukherji, M., Bell, R., Supekova, L., Wang, Y., Orth, A. P., Batalov, S., Miraglia, L., Huesken, D., Lange, J. & other authors. (2006).** Genome-wide functional analysis of human cell-cycle regulators. *PNAS* **103**, 14819–24.
- Na, K., Jung, J., Shin, B. & Hyun, J. (2006).** Micropatterning of cell-repellent polymer on a glass substrate for the highly resolved virus microarray. *Langmuir* **22**, 10889–92.
- Nakajima, A., Fujishima, A., Hashimoto, K. & Watanabe, T. (1999).** Preparation of transparent superhydrophobic boehmite and silica films by sublimation of aluminum acetylacetonate. *Adv Mater* **11**, 1365–8.
- Nakata, K., Nishimoto, S., Yuda, Y., Ochiai, T., Murakami, T. & Fujishima, A. (2010).** Rewritable superhydrophilic-superhydrophobic patterns on a sintered titanium dioxide substrate. *Langmuir* **26**, 11628–30.
- Nelson, C. M., Raghavan, S., Tan, J. L. & Chen, C. S. (2003).** Degradation of micropatterned surfaces by cell-dependent and -independent processes. *Langmuir* **19**, 1493–9.
- Neto, A. I., Custódio, C. A., Song, W. & Mano, J. F. (2011).** High-throughput evaluation of interactions between biomaterials, proteins and cells using patterned superhydrophobic substrates. *Soft Matter* **7**, 4147–51.
- Neumann, B., Held, M., Liebel, U., Erfle, H., Rogers, P., Pepperkok, R. & Ellenberg, J. (2006).** High-throughput RNAi screening by time-lapse imaging of live human cells. *Nat Methods* **3**, 385–90.
- Neumann, B., Walter, T., Hériché, J.-K., Bulkescher, J., Erfle, H., Conrad, C., Rogers, P., Poser, I., Held, M. & other authors. (2010).** Phenotypic profiling of the human genome by time-lapse microscopy reveals cell division genes. *Nature* **464**, 721–7.

- Nichol, J. W., Koshy, S. T., Bae, H., Hwang, C. M., Yamanlar, S. & Khademhosseini, A. (2010).** Cell-laden microengineered gelatin methacrylate hydrogels. *Biomaterials* **31**, 5536–44.
- Nie, J.-F., Zhang, Y., Lin, L.-W., Zhou, C.-B., Li, S.-H., Zhang, L.-M. & Li, J.-P. (2012).** Rapid, low-cost fabrication of paper-based microfluidic devices by one-step plotting. *Anal Chem* **84**, 6331–5.
- Nishimoto, S., Sekine, H., Zhang, X., Liu, Z., Nakata, K., Murakami, T., Koide, Y. & Fujishima, A. (2009a).** Assembly of self-assembled monolayer-coated Al₂O₃ on TiO₂ thin films for the fabrication of renewable superhydrophobic-superhydrophilic structures. *Langmuir* **25**, 7226–8.
- Nishimoto, S., Kubo, A., Nohara, K., Zhang, X., Taneichi, N., Okui, T., Liu, Z., Nakata, K., Sakai, H. & other authors. (2009b).** TiO₂-based superhydrophobic-superhydrophilic patterns: Fabrication via an ink-jet technique and application in offset printing. *Appl Surf Sci* **255**, 6221–5.
- Oliveira, S. M., Song, W., Alves, N. M. & Mano, J. F. (2011).** Chemical modification of bioinspired superhydrophobic polystyrene surfaces to control cell attachment/proliferation. *Soft Matter* **7**, 8932–41.
- Ostuni, E., Chapman, R. G., Holmlin, R. E., Takayama, S. & Whitesides, G. M. (2001).** A survey of structure–property relationships of surfaces that resist the adsorption of protein. *Langmuir* **17**, 5605–20.
- Otsuka, H. (2010).** Nanofabrication of nonfouling surfaces for micropatterning of cell and microtissue. *Molecules* **15**, 5525–46.
- Pampaloni, F., Reynaud, E. G. & Stelzer, E. H. K. (2007).** The third dimension bridges the gap between cell culture and live tissue. *Nat Rev Mol Cell Biol* **8**, 839–45.
- Pannier, A. K., Anderson, B. C. & Shea, L. D. (2005).** Substrate-mediated delivery from self-assembled monolayers: effect of surface ionization, hydrophilicity, and patterning. *Acta Biomater* **1**, 511–22.
- Papadopoulou, S. K., Tsiptsias, C., Pavlou, A., Kaderides, K., Sotiriou, S. & Panayiotou, C. (2011).** Superhydrophobic surfaces from hydrophobic or hydrophilic polymers via nanophase separation or electrospinning/electrospraying. *Colloids Surf, A* **387**, 71–78.
- Parker, A. R. & Lawrence, C. R. (2001).** Water capture by a desert beetle. *Nature* **414**, 33–4.

-
- Parker, A. L., Newman, C., Briggs, S., Seymour, L. & Sheridan, P. J. (2004).** Nonviral gene delivery: techniques and implications for molecular medicine. *Expert Rev Mol Med*. DOI: 10.1017/S1462399403006562.
- Pastine, S. J., Okawa, D., Kessler, B., Rolandi, M., Llorente, M., Zettl, A. & Fréchet, J. M. J. (2008).** A facile and patternable method for the surface modification of carbon nanotube forests using perfluoroarylazides. *JACS* **130**, 4238–9.
- Pedersen, O. & Colmer, T. D. (2012).** Physical gills prevent drowning of many wetland insects, spiders and plants. *J Exp Biol* **215**, 705–9.
- Pedroso de Lima, M. C., Neves, S., Filipe, A., Düzgüneş, N. & Simões, S. (2003).** Cationic liposomes for gene delivery: from biophysics to biological applications. *Curr Med Chem* **10**, 1221–31.
- Perrimon, N. & Mathey-Prevot, B. (2007).** Applications of high-throughput RNA interference screens to problems in cell and developmental biology. *Genetics* **175**, 7–16.
- Piraino, F., Camci-Unal, G., Hancock, M. J., Rasponi, M. & Khademhosseini, A. (2012).** Multi-gradient hydrogels produced layer by layer with capillary flow and crosslinking in open microchannels. *Lab Chip* **12**, 659–61.
- Piret, G., Galopin, E., Coffinier, Y., Boukherroub, R., Legrand, D. & Slomianny, C. (2011).** Culture of mammalian cells on patterned superhydrophilic/superhydrophobic silicon nanowire arrays. *Soft Matter* **7**, 8642–9.
- Qi, H., Du, Y., Wang, L., Kaji, H., Bae, H. & Khademhosseini, A. (2010).** Patterned differentiation of individual embryoid bodies in spatially organized 3D hybrid microgels. *Adv Mater* **22**, 5276–81.
- Quéré, D. (2005).** Non-sticking drops. *Rep Prog Phys* **68**, 2495–532.
- Rajan, S., Djambazian, H., Dang, H. C. P., Sladek, R. & Hudson, T. J. (2011).** The living microarray: a high-throughput platform for measuring transcription dynamics in single cells. *BMC Genomics*. DOI: 10.1186/1471-2164-12-115.
- Rånby, B. (1992).** Surface modification of polymers by photoinitiated graft polymerization. *Macromol Chem, Macromol Symp* **63**, 55–67.
- Rantala, J. K., Mäkelä, R., Aaltola, A.-R., Laasola, P., Mpindi, J.-P., Nees, M., Saviranta, P. & Kallioniemi, O. (2011).** A cell spot microarray method for production of high density siRNA transfection microarrays. *BMC Genomics*. DOI: 10.1186/1471-2164-12-162.

- Rehman, Z. ur, Zuhorn, I. S. & Hoekstra, D. (2013).** How cationic lipids transfer nucleic acids into cells and across cellular membranes: recent advances. *J Control Release* **166**, 46–56.
- Rejman, J., Oberle, V., Zuhorn, I. S. & Hoekstra, D. (2004).** Size-dependent internalization of particles via the pathways of clathrin- and caveolae-mediated endocytosis. *Biochem J* **377**, 159–69.
- Reticker-Flynn, N. E., Malta, D. F. B., Winslow, M. M., Lamar, J. M., Xu, M. J., Underhill, G. H., Hynes, R. O., Jacks, T. E. & Bhatia, S. N. (2012).** A combinatorial extracellular matrix platform identifies cell-extracellular matrix interactions that correlate with metastasis. *Nat Commun.* DOI: 10.1038/ncomms2128.
- Revzin, A., Tompkins, R. G. & Toner, M. (2003).** Surface engineering with poly(ethylene glycol) photolithography to create high-density cell arrays on glass. *Langmuir* **19**, 9855–62.
- Reymann, J., Beil, N., Beneke, J., Kaletta, P.-P., Burkert, K. & Erfle, H. (2009).** Next-generation 9216-microwell cell arrays for high-content screening microscopy. *Biotechniques* **47**, 877–8.
- Rodriguez-Emmenegger, C., Houska, M., Alles, A. B. & Brynda, E. (2012).** Surfaces resistant to fouling from biological fluids: towards bioactive surfaces for real applications. *Macromol Biosci* **12**, 1413–22.
- Rohr, T., Hilder, E. F., Donovan, J. J., Svec, F. & Fréchet, J. M. J. (2003).** Photografting and the control of surface chemistry in three-dimensional porous polymer monoliths. *Macromolecules* **36**, 1677–84.
- Ruozi, B., Forni, F., Battini, R. & Vandelli, M. A. (2003).** Cationic liposomes for gene transfection. *J Drug Target* **11**, 407–14.
- Sainiemi, L., Jokinen, V., Shah, A., Shpak, M., Aura, S., Suvanto, P. & Franssila, S. (2011).** Non-reflecting silicon and polymer surfaces by plasma etching and replication. *Adv Mater* **23**, 122–6.
- Salgado, C. L., Oliveira, M. B. & Mano, J. F. (2012).** Combinatorial cell-3D biomaterials cytocompatibility screening for tissue engineering using bioinspired superhydrophobic substrates. *Integr Biol* **4**, 318–27.
- Schilp, S., Rosenhahn, A., Pettitt, M. E., Bowen, J., Callow, M. E., Callow, J. A. & Grunze, M. (2009).** Physicochemical properties of (ethylene glycol)-containing self-assembled monolayers relevant for protein and algal cell resistance. *Langmuir* **25**, 10077–82.

-
- Schmidt, S. & Friedl, P. (2010).** Interstitial cell migration: integrin-dependent and alternative adhesion mechanisms. *Cell Tissue Res* **339**, 83–92.
- Schmitz, C. H. J., Rowat, A. C., Köster, S. & Weitz, D. A. (2009).** Dropspots: a picoliter array in a microfluidic device. *Lab Chip* **9**, 44–9.
- Schoenfish, M. H. & Pemberton, J. E. (1998).** Air stability of alkanethiol self-assembled monolayers on silver and gold surfaces. *JACS* **120**, 4502–13.
- Segura, T. & Shea, L. D. (2002).** Surface-tethered DNA complexes for enhanced gene delivery. *Bioconjug Chem* **13**, 621–9.
- Shahsavani, H., Arunbabu, D. & Zhao, B. (2012).** Biomimetic modification of polymeric surfaces: a promising pathway for tuning of wetting and adhesion. *Macromol Mater Eng* **297**, 743–60.
- Shirtcliffe, N. J., McHale, G. & I. Newton, M. (2011).** The superhydrophobicity of polymer surfaces: Recent developments. *J Polym Sci, Part B Polym Phys* **49**, 1203–17.
- Siegrwart, D. J., Whitehead, K. A., Nuhn, L., Sahay, G., Cheng, H., Jiang, S., Ma, M., Lytton-Jean, A., Vegas, A. & other authors. (2011).** Combinatorial synthesis of chemically diverse core-shell nanoparticles for intracellular delivery. *PNAS* **108**, 12996–3001.
- Silva, J. M., Mizuno, H., Brady, A., Lucito, R. & Hannon, G. J. (2004).** RNA interference microarrays: high-throughput loss-of-function genetics in mammalian cells. *PNAS* **101**, 6548–52.
- Skardal, A., Smith, L., Bharadwaj, S., Atala, A., Soker, S. & Zhang, Y. (2012).** Tissue specific synthetic ECM hydrogels for 3-D in vitro maintenance of hepatocyte function. *Biomaterials* **33**, 4565–75.
- Soen, Y., Mori, A., Palmer, T. D. & Brown, P. O. (2006).** Exploring the regulation of human neural precursor cell differentiation using arrays of signaling microenvironments. *Mol Syst Biol*. DOI: 10.1038/msb4100076.
- Song, W., Veiga, D. D., Custódio, C. A. & Mano, J. F. (2009).** Bioinspired degradable substrates with extreme wettability properties. *Adv Mater* **21**, 1830–4.
- Song, W., Lima, A. C. & Mano, J. F. (2010).** Bioinspired methodology to fabricate hydrogel spheres for multi-applications using superhydrophobic substrates. *Soft Matter* **6**, 5868–71.
- Sriganapalan, S., Eydelnant, I. A., Simmons, C. A. & Wheeler, A. R. (2012).** A digital microfluidic platform for primary cell culture and analysis. *Lab Chip* **12**, 369–75.

- Starkuviene, V., Pepperkok, R. & Erfle, H. (2007).** Transfected cell microarrays: an efficient tool for high-throughput functional analysis. *Expert Rev Proteomics* **4**, 479–89.
- Stürzl, M., Konrad, A., Sander, G., Wies, E., Neipel, F., Naschberger, E., Reipschläger, S., Gonin-Laurent, N., Horch, R. E. & other authors. (2008).** High throughput screening of gene functions in mammalian cells using reversely transfected cell arrays: review and protocol. *Comb Chem High Throughput Screen* **11**, 159–72.
- Sun, S., Wang, M., Knupp, S. A., Soto-Feliciano, Y., Hu, X., Kaplan, D. L., Langer, R., Anderson, D. G. & Xu, Q. (2012).** Combinatorial library of lipidoids for in vitro DNA delivery. *Bioconjug Chem* **23**, 135–40.
- Svec, F. (2010).** Porous polymer monoliths: amazingly wide variety of techniques enabling their preparation. *J Chromatogr, A* **1217**, 902–24.
- Tadanaga, K., Morinaga, J., Matsuda, A. & Minami, T. (2000).** Superhydrophobic–superhydrophilic micropatterning on flowerlike alumina coating film by the sol–gel method. *Chem Mater* **12**, 590–2.
- Tamada, Y. & Ikada, Y. (1993).** Effect of preadsorbed proteins on cell adhesion to polymer surfaces. *J Colloid Interface Sci* **155**, 334–9.
- Thickett, S. C., Neto, C. & Harris, A. T. (2011).** Biomimetic surface coatings for atmospheric water capture prepared by dewetting of polymer films. *Adv Mater* **23**, 3718–22.
- Tibbitt, M. W. & Anseth, K. S. (2009).** Hydrogels as extracellular matrix mimics for 3D cell culture. *Biotechnol Bioeng* **103**, 655–63.
- Tseng, W.-C., Haselton, F. R. & Giorgio, T. D. (1999).** Mitosis enhances transgene expression of plasmid delivered by cationic liposomes. *Biochim Biophys Acta - Gene Struct Expr* **1445**, 53–64.
- Ueda, E. & Levkin, P. A. (2013a).** Emerging applications of superhydrophilic-superhydrophobic micropatterns. *Adv Mater* **25**, 1234–47.
- Ueda, E. & Levkin, P. A. (2013b).** Micropatterning hydrophobic liquid on a porous polymer surface for long-term selective cell-repellency. *Adv Healthcare Mater* **2**, 1425–9.
- Ueda, E., Geyer, F. L., Nedashkivska, V. & Levkin, P. A. (2012).** DropletMicroarray: facile formation of arrays of microdroplets and hydrogel micropads for cell screening applications. *Lab Chip* **12**, 5218–24.

-
- Vazquez, G., Alvarez, E. & Navaza, J. M. (1995).** Surface tension of alcohol water + water from 20 to 50 .degree.C. *J Chem Eng Data* **40**, 611–4.
- Vella, S. J., Beattie, P., Cademartiri, R., Laromaine, A., Martinez, A. W., Phillips, S. T., Mirica, K. A. & Whitesides, G. M. (2012).** Measuring markers of liver function using a micropatterned paper device designed for blood from a fingerstick. *Anal Chem* **84**, 2883–91.
- Vergauwe, N., Witters, D., Atalay, Y. T., Verbruggen, B., Vermeir, S., Ceyskens, F., Puers, R. & Lammertyn, J. (2011).** Controlling droplet size variability of a digital lab-on-a-chip for improved bio-assay performance. *Microfluid Nanofluidics* **11**, 25–34.
- Wang, M., Sun, S., Alberti, K. A. & Xu, Q. (2012).** A combinatorial library of unsaturated lipidoids for efficient intracellular gene delivery. *ACS Synth Biol* **1**, 403–7.
- Wang, R., Hashimoto, K., Fujishima, A., Chikuni, M., Kojima, E., Kitamura, A., Shimohigoshi, M. & Watanabe, T. (1997).** Light-induced amphiphilic surfaces. *Nature* **388**, 431–2.
- Wang, S. & Jiang, L. (2007).** Definition of superhydrophobic states. *Adv Mater* **19**, 3423–4.
- Wasungu, L. & Hoekstra, D. (2006).** Cationic lipids, lipoplexes and intracellular delivery of genes. *J Control Release* **116**, 255–64.
- Wendeln, C., Rinnen, S., Schulz, C., Arlinghaus, H. F. & Ravoo, B. J. (2010).** Photochemical microcontact printing by thiol-ene and thiol-yne click chemistry. *Langmuir* **26**, 15966–71.
- Wenzel, R. N. (1936).** Resistance of solid surfaces to wetting by water. *Ind Eng Chem* **28**, 988–94.
- Wheeler, D. B., Carpenter, A. E. & Sabatini, D. M. (2005).** Cell microarrays and RNA interference chip away at gene function. *Nat Genet* **37 Suppl**, S25–30.
- Witters, D., Vergauwe, N., Vermeir, S., Ceyskens, F., Liekens, S., Puers, R. & Lammertyn, J. (2011).** Biofunctionalization of electrowetting-on-dielectric digital microfluidic chips for miniaturized cell-based applications. *Lab Chip* **11**, 2790–4.
- Witters, D., Vergauwe, N., Ameloot, R., Vermeir, S., De Vos, D., Puers, R., Sels, B. & Lammertyn, J. (2012).** Digital microfluidic high-throughput printing of single metal-organic framework crystals. *Adv Mater* **24**, 1316–20.

- Wong, T.-S., Kang, S. H., Tang, S. K. Y., Smythe, E. J., Hatton, B. D., Grinthal, A. & Aizenberg, J. (2011).** Bioinspired self-repairing slippery surfaces with pressure-stable omniphobicity. *Nature* **477**, 443–447.
- Wood, K. C., Konieczkowski, D. J., Johannessen, C. M., Boehm, J. S., Tamayo, P., Botvinnik, O. B., Mesirov, J. P., Hahn, W. C., Root, D. E. & other authors. (2012).** MicroSCALE screening reveals genetic modifiers of therapeutic response in melanoma. *Sci Signal* **5**, rs4–rs4.
- Xia, X. & Wong, S. T. (2012).** Concise review: a high-content screening approach to stem cell research and drug discovery. *Stem Cells* **30**, 1800–7.
- Xia, Y., Yin, Y., Lu, Y. & McLellan, J. (2003).** Template-assisted self-assembly of spherical colloids into complex and controllable structures. *Adv Funct Mater* **13**, 907–18.
- Xiao, L., Li, J., Mieszkis, S., Di Fino, A., Clare, A. S., Callow, M. E., Callow, J. A., Grunze, M., Rosenhahn, A. & Levkin, P. A. (2013).** Slippery liquid-infused porous surfaces showing marine antibiofouling properties. *ACS Appl Mater Interfaces* **5**, 10074–80.
- Xing, S., Harake, R. S. & Pan, T. (2011).** Droplet-driven transports on superhydrophobic-patterned surface microfluidics. *Lab Chip* **11**, 3642–8.
- Xue, Z., Liu, M. & Jiang, L. (2012).** Recent developments in polymeric superoleophobic surfaces. *J Polym Sci, Part B Polym Phys* **50**, 1209–24.
- Yamaguchi, S., Yamahira, S., Kikuchi, K., Sumaru, K., Kanamori, T. & Nagamune, T. (2012).** Photocontrollable dynamic micropatterning of non-adherent mammalian cells using a photocleavable poly(ethylene glycol) lipid. *Angew Chem, Int Ed* **51**, 128–31.
- Yan, Y. Y., Gao, N. & Barthlott, W. (2011).** Mimicking natural superhydrophobic surfaces and grasping the wetting process: a review on recent progress in preparing superhydrophobic surfaces. *Adv Colloid Interface Sci* **169**, 80–105.
- Yao, X., Song, Y. & Jiang, L. (2011).** Applications of bio-inspired special wettable surfaces. *Adv Mater* **23**, 719–34.
- Yarmush, M. L. & King, K. R. (2009).** Living-cell microarrays. *Annu Rev Biomed Eng* **11**, 235–57.
- Yoshikawa, T., Uchimura, E., Kishi, M., Funeriu, D. P., Miyake, M. & Miyake, J. (2004).** Transfection microarray of human mesenchymal stem cells and on-chip siRNA gene knockdown. *J Control Release* **96**, 227–32.

-
- You, A. J., Jackman, R. J., Whitesides, G. M. & Schreiber, S. L. (1997).** A miniaturized arrayed assay format for detecting small molecule-protein interactions in cells. *Chem Biol* **4**, 969–75.
- Yu, J. & Anchordoquy, T. J. (2009).** Effects of moisture content on the storage stability of dried lipoplex formulations. *J Pharm Sci* **98**, 3278–89.
- Yuan, L., Yu, Q., Li, D. & Chen, H. (2011).** Surface modification to control protein/surface interactions. *Macromol Biosci* **11**, 1031–40.
- Yunker, P. J., Still, T., Lohr, M. A. & Yodh, A. G. (2011).** Suppression of the coffee-ring effect by shape-dependent capillary interactions. *Nature* **476**, 308–11.
- Yusof, A., Keegan, H., Spillane, C. D., Sheils, O. M., Martin, C. M., O’Leary, J. J., Zengerle, R. & Koltay, P. (2011).** Inkjet-like printing of single-cells. *Lab Chip* **11**, 2447–54.
- Zahner, D., Abagat, J., Svec, F., Fréchet, J. M. J. & Levkin, P. A. (2011).** A facile approach to superhydrophilic-superhydrophobic patterns in porous polymer films. *Adv Mater* **23**, 3030–4.
- Zawko, S. A. & Schmidt, C. E. (2010).** Simple benchtop patterning of hydrogel grids for living cell microarrays. *Lab Chip* **10**, 379–83.
- Zhai, L., Berg, M. C., Cebeci, F. C., Kim, Y., Milwid, J. M., Rubner, M. F. & Cohen, R. E. (2006).** Patterned superhydrophobic surfaces: toward a synthetic mimic of the Namib Desert beetle. *Nano Lett* **6**, 1213–7.
- Zhang, J. & Seeger, S. (2011a).** Polyester materials with superwetting silicone nanofilaments for oil/water separation and selective oil absorption. *Adv Funct Mater* **21**, 4699–704.
- Zhang, J. & Seeger, S. (2011b).** Superoleophobic coatings with ultralow sliding angles based on silicone nanofilaments. *Angew Chem, Int Ed* **50**, 6652–6.
- Zhang, X., Jin, M., Liu, Z., Tryk, D. A., Nishimoto, S., Murakami, T. & Fujishima, A. (2007a).** Superhydrophobic TiO₂ surfaces: preparation, photocatalytic wettability conversion, and superhydrophobic-superhydrophilic Patterning. *J Phys Chem C* **111**, 14521–9.
- Zhang, X., Shi, F., Niu, J., Jiang, Y. & Wang, Z. (2008).** Superhydrophobic surfaces: from structural control to functional application. *J Mater Chem* **18**, 621–33.
- Zhang, X., Kono, H., Liu, Z., Nishimoto, S., Tryk, D. A., Murakami, T., Sakai, H., Abe, M. & Fujishima, A. (2007b).** A transparent and photo-patternable superhydrophobic film. *Chem Commun* 4949–51.

Ziauddin, J. & Sabatini, D. M. (2001). Microarrays of cells expressing defined cDNAs. *Nature* **411**, 107–10.